UNIVERSIDADE Ð COIMBRA

Talha Bin Yaqub

OPTIMIZATION OF SPUTTERED Mo-Se-C COATINGS FOR EFFICIENT SELF-ADAPTATION DURING SLIDING IN DIVERSE ENVIRONMENTS

December 2020

FCTUC FACULDADE DE CIÊNCIAS
E TECNOLOGIA
UNIVERSIDADE DE COIMBRA

DEPARTAMENTO DE
ENGENHARIA MECÂNICA

OPTIMIZATION OF SPUTTERED Mo-Se-C COATINGS FOR EFFICIENT SELF-ADAPTATION DURING SLIDING IN DIVERSE ENVIRONMENTS

Submitted in Partial Fulfilment of the Requirements for the Degree of Doctor of Philosophy in Mechanical Engineering

Author   **Talha Bin Yaqub**

Supervisor   **Doctor Albano Augusto Cavaleiro Rodrigues de Carvalho**
Full Professor in University of Coimbra

Co-supervisor   **Doctor Stéphanie Bruyere**
Assistant Professor in University of Lorraine

In the framework of a Ph.D. in Mechanical Engineering

Coimbra,
December 2020

Dedication

"In family life, love is the oil that eases friction, the cement that binds closer together, and the music that brings harmony."

(Eva Burrows)

To my father, Muhammad Yaqub Awan and my mother, Khalida Yaqub for giving me strength & courage to show the best of my abilities, for believing in me throughout my life and making me what I am today.

To my wife and siblings for their endless support through every thick and thin.

To my uncle, Tauqeer Ahmed for always standing by my side and supporting me like a friend.

And

"To my journey, that has brought me here"

Acknowledgements

First and foremost, I am grateful to Almighty Allah for never letting my efforts go unrewarded and for the successful completion of this project. I am deeply obliged to my supervisor Professor Albano Cavaleiro (University of Coimbra, Portugal), for his unwavering support to me throughout my thesis with his patience and knowledge, while allowing me to explore on my own, however, keeping a track of my progress to provide guidance to recover when my steps faltered. You have been a wonderful mentor and a role model for me, one simply could not wish for a better and friendlier advisor. I would also like to take this opportunity to thank my co-supervisor Professor Stéphanie Bruyere (University of Lorraine, France) for her guidance and support throughout the project, especially her critical analysis on my work and confidence in me. Her comments and questions were very beneficial in the betterment of this work. In short, working under the supervision of such subject experts and wonderful human beings has been no less than an honour for me.

I would also like to extend my gratitude to the different institutions, laboratories and key persons involved in my research project, especially, Engineer Joao Paula Dias (Institute Pedro Nunes, Portugal), Professor Jeff-Francois Pierson (Institute Jean Lamour, France) and the consortium coordinator Professor Tomas Polcar (Czech Technical University, Czech Republic), who have put their knowledge and equipment at my disposal and provided me with a platform to further my research and scientific understanding. Special thanks to my colleague researchers at the University of Coimbra, particularly, Dr. Manuel Evaristo, Dr. Filipe Fernandes, and Kaushik Hebbar Kannur. I also express my special thanks to Todor Vuchkov, for helping me out at every stage of this research journey. This cannot go without thanking the technical staff at University of Coimbra, Institute Pedro Nunes, and Institute Jean Lamour.

I am off-course forever grateful to the Institute Pedro Nunes and University of Coimbra for hosting me and providing me with this research position. I am also grateful to the Marie Skłodowska-Curie Actions selection committee for awarding me the funding to undertake my research under their Research Fellowship Programme, SOLUTION-ITN (grant No. 721642).

Apart from those who supported and guided me academically, there is, of course, a long list of people in my life, who have played important roles in ensuring that I achieve this dream of mine. My sincere thanks to all of my friends, particularly Mohammad Hammad Zahid, Syed Sadiq Bokhari and Muhammad Mehtab. Last but not at the least, I am grateful for the support of my family, in particular, my parents for always being the beacons of light that guided me on my journey to this point and for always being there for me, throughout my life.

Abstract

Coatings deposited by physical vapour deposition (PVD) revolutionized the world of tribology and resolved various problems encountered in industrial domains. Magnetron sputtered carbon-alloyed transition metal dichalcogenide (TMD-C) coatings have been widely explored in the past few decades due to their self-adaptive sliding properties. The drawback is that their frictional properties are highly environmental dependent. This substantial variation of the frictional response during sliding in diverse environments, is the main hindrance behind their large-scale application. In the domain of TMD-C coatings, although very less reported, C-alloyed molybdenum diselenide (Mo-Se-C) is a promising candidate as solid lubricant coatings for aerospace and automotive industries, due to an excellent stability in both humid air and vacuum conditions. The present work is aimed at the development, investigation and optimization of magnetron sputtered Mo-Se-C coatings. The goal is to deposit coatings capable of providing highly stable and consistent tribological properties in diverse environments under different conditions, i.e., sliding distances, sliding speeds and contact stresses.

In the initial phase of the project, feasibility for development of an efficient self-adaptive lubricant system based on Mo-Se-C coatings was studied. The coatings were deposited via an industrially favourable co-sputtering (separate $MoSe_2$ and C targets) approach, utilizing direct current (DC) power supplies. A detailed parametric study of the deposition parameters and carbon content versus coatings properties was carried out. The tribological testing was done in ambient air and dry N_2 atmospheres. These coatings displayed a maximum Se/Mo ratio of 1.88, a compact morphology, an amorphous crystal structure, and a maximum hardness of 4.9 GPa. Small $MoSe_2$ platelets (< 10 nm size) were randomly oriented in an amorphous carbon matrix. The tribological testing in dry N_2 and ambient air resulted in the lowest friction coefficient (COF) values of 0.025 and 0.06, respectively. Overall, improved results as compared to literature were achieved.

The research was followed by optimization of chemical composition, structure, morphology and mechanical properties of similar coatings deposited by both DC and radio frequency (RF) power supplies in a confocal plasma sputtering unit. The characterization of these optimized coatings showed that the use of low C content as compared to literature recommendations resulted in a Se/Mo ratio of ~2 for DC coatings and ~1.9 for RF coatings. The coatings showed a highly compact morphology, presence of (002) peaks of $MoSe_2$

phase and a hardness increment up to 5.2 GPa. In the post-optimization stage, the sliding behaviour was tested in ambient air, dry N_2, and at 200 ⁰C. An in-depth investigation of the chemistry and evolution of the low friction tribolayers with the number of sliding cycles was carried out. In ambient conditions, friction coefficient and specific wear rate decreased with the number of sliding cycles. The coatings outperformed similar coatings presented in initial depositions and the literature. The coverage of the wear tracks with a $MoSe_2$ tribolayer was extended with increasing number of sliding cycles. The measured COF was almost consistent in ambient air, dry N_2 and at 200 ⁰C. These results established that the coatings were efficiently capable to be used in diverse operating environments. This was attributed to the fact that the $MoSe_2$ phase was always governing the low friction tribolayer in all environments. Thus, the coatings did not show the chameleon behaviour, disagreeing with the literature on TMD-C coatings. Further, the mechanism and routes behind the formation of low friction tribolayers were also explored. This investigation unfolded that both the transfer layer formed due to the 3rd body inside the contact and the reorientation within the coating matrix contribute to the tribolayer formation.

In the last stage, tribological testing of Mo-Se-C coatings was performed, for the first time, in both ambient air and vacuum atmospheres; under various conditions of sliding cycles, sliding speeds and contact stress regimes to confirm their applicability as universal solid lubricants. The testing resulted in no significant variations between the tribological performance (COF: 0.02-0.06).

In conclusion, the achieved optimization of self-adaptive behaviour in diverse environments demonstrated that the Mo-Se-C system is a potential universal solid lubricant for low friction in aerospace and terrestrial atmospheres.

Keywords: transition metal dichalcogenides, low friction, self-adaptive behaviour, physical vapour deposition, microstructure, sputtering.

Resumo

Os revestimentos depositados por técnicas de deposição física em fase de vapor (PVD) têm revolucionado o mundo da tribologia e resolvido problemas muito diferentes encontrados nos mais variados domínios industriais. Neste contexto, os revestimentos de dicalcogenetos de metais de transição ligados com carbono (TMD-C), depositados por pulverização catódica magnetrão, têm sido largamente explorados nas décadas recentes devido às suas propriedades auto-adaptativas durante o deslizamento. A sua principal desvantagem é que as suas propriedades tribológicas são fortemente dependentes do ambiente em que os revestimentos são utilizados. Esta variação significativa da resposta ao atrito, durante o deslizamento em diferentes ambientes, tem sido o maior obstáculo para a aplicação destes revestimentos numa larga escala industrial. No domínio dos revestimentos TMD-C, embora menos reportados na literatura, os disselenietos de molibdénio ligados com carbono (Mo-Se-C) são candidatos muito promissores para as indústrias automóvel e aerospacial, devido a uma estabilidade excelente em ambos os ambientes húmidos e em vácuo. Este trabalho de investigação tem como objetivo desenvolver, investigar e otimizar revestimentos do tipo Mo-Se-C depositados por pulverização catódica magnetrão. É pretendido depositar revestimentos capazes de providenciar propriedades tribológicas estáveis e consistentes em meios diversos sob diferentes condições de aplicação, i.e. distâncias de deslizamento, velocidades de deslizamento e tensões de contato.

Numa primeira fase do projeto, foi estudada a possibilidade de desenvolver um sistema lubrificante auto-adaptativo baseado em revestimentos do tipo Mo-Se-C. Os revestimentos foram depositados utilizando uma aproximação amigável do ponto de vista industrial, consistindo na co-pulverização de alvos separados ($MoSe_2$ e carbono) utilizando fontes de potência de corrente contínua (DC). Para tal foi efetuado um estudo detalhado da influência dos parâmetros de deposição e do teor em carbono nas propriedades dos revestimentos. Os revestimentos foram testados tribologicamente em meios ambientes húmido e seco. Os revestimentos apresentaram uma razão Se/Mo de 1,88 e uma morfologia compacta; a estrutura era amorfa e a dureza máxima alcançada foi de 4,9 GPa. A estrutura consistia em pequenas plaquetas de $MoSe_2$ embebidas numa matriz amorfa de carbono. O teste tribológico em azoto seco e ar ambiente deu valores de coeficiente de atrito (COF) de, respetivamente, 0,025 e 0,06. Em comparação com a literatura, foram alcançados resultados com melhorias acentuadas.

A investigação prosseguiu com a otimização da composição química, estrutura, morfologia e propriedades mecânicas de revestimentos semelhantes depositados por ambos os processos em DC e rádio-frequência (RF), num equipamento de pulverização catódica com plasma confocal relativamente aos cátodos. A caraterização dos revestimentos otimizados mostrou que a utilização de baixos teores de C, em comparação com as recomendações encontradas na literatura, resultou numa razão de Se/Mo de ~2, para os revestimentos DC e ~1,9 para os RF. Os revestimentos apresentavam uma morfologia muito compacta, picos (002) da fase $MoSe_2$ e um aumento de dureza para 5,2 GPa. Após esta otimização, o comportamento tribológico foi avaliado em testes em ar ambiente, azoto seco e a 200 ºC. Depois, foi efetuada uma investigação detalhada da evolução das tribocamadas de baixo atrito formadas em função do número de ciclos de deslizamento. Em condições ambiente, os coeficientes de atrito e desgaste diminuíram com o número de ciclos. Estes revestimentos ultrapassaram o desempenho tribológico daqueles depositados anteriormente e os referenciados na literatura. A cobertura da pista de desgaste com uma tribocamada de baixo atrito foi sendo formada progressivamente com a evolução do número de ciclos. Os coeficientes de atrito medidos foram muito similares independentemente das condições de teste, podendo ser concluído que estes revestimentos são adequados para os mais diversos meios de teste. Este comportamento é devido à formação duma camada da fase $MoSe_2$ que governa o deslizamento e providencia um atrito reduzido. Em consequência, estes revestimentos não mostram o tão reclamado "comportamento de camaleão", em desacordo com o referido na literatura para revestimentos do tipo TMD-C. Para além destes resultados, foram ainda explorados os mecanismos e processos que estão por trás da formação da tribocamada de baixo atrito. Esta investigação revelou que quer a transferência de uma camada do elemento antagonista do par de contacto, quer a reorientação dos cristais de $MoSe_2$ dentro da matriz amorfa de carbono, contribuem para a formação da tribocamada.

Numa última fase do trabalho, foi efetuado pela primeira vez um estudo tribológico em atmosfera ambiente e em vácuo, variando o número de ciclos de deslizamento, as velocidades de deslizamento e as tensões de contacto para confirmar a aplicabilidade dos revestimentos otimizados de Mo-Se-C como lubrificantes sólidos universais. Os testes mostraram não haver variações significativas no desempenho tribológico para todas as condições (COF = 0.02-0.06).

Resumindo, a otimização do comportamento auto-adaptativo em diferentes atmosferas, demonstrou claramente que os revestimentos Mo-Se-C são uma potencial solução para baixo atrito em aplicações terrestres e no espaço.

Palavras-chave: dicalcogenetos de metais de transição, baixo atrito, comportamento auto-adaptativo, deposição física em fase de vapor, pulverização catódica.

Table of contents

List of figures

List of tables

Nomenclature

Acronyms

AFM - atomic force microscopy

COF - coefficient of friction, friction coefficient

CVD - chemical vapour deposition

DLC - diamond like carbon

DC - direct current

DCMS - direct current magnetron sputtering

EDS - energy dispersive spectroscopy

FESEM - field emission scanning electron microscope

HiPIMS - high power impulse magnetron sputtering

HRTEM – high-resolution transmission electron microscope

PVD - physical vapour deposition

P.D. - partial delamination

RF - radio frequency

RFMS - radio frequency magnetron sputtering

RH - relative humidity

RT – room temperature

SEM - scanning electron microscope

TEM - transmission electron microscope

TMD - transition metal dichalcogenide

T.D. - total delamination

WDS - wavelength dispersive spectroscopy

XRD – x-ray diffraction

XPS - x-ray photoelectron microscope

Units

a.u. - arbitrary units

at. % - atomic percent

GPa – gigapascal

kHz – kilohertz

MPa – megapascal

mm – mili-meter

nm – nano-meter

ns – nano-second

Nm - Newton meter

Pa – pascal

s – second

V – voltage

W – watt

Elements and compounds

Ar – argon

Au – gold

Ag – silver

a-C – amorphous carbon

AlN – aluminium nitride

BaF$_2$ – barium fluoride

C - carbon

Cr – chromium

Cu – copper

C$_2$H$_2$ – acetylene

CH$_4$ – methane

CrN – chromium nitride

CrAlN – chromium aluminium nitride

CrC – chromium carbide

CrBN – chromium boron nitride

CaF$_2$ – calcium fluoride

CeF$_3$ – cesium fluoride

In – indium

Mo - molybdenum

MoS$_2$ – molybdenum disulphide

MoSe$_2$ – molybdenum diselenide

MoO$_3$ – molybdenum trioxide

N$_2$ – nitrogen

O – oxygen

Pb – lead

Pt – platinum

S – sulphur

Se – selenium

Si – silicon

SiC – silicon carbide

Ti – titanium

TiC – titanium carbide

TiN – titanium nitride

TiAlN – titanium aluminium nitride

TiBN – titanium boron nitride

V – vanadium

V$_2$O$_5$ – vanadium oxide

W - tungsten

WS$_2$ – tungsten disulphide

WSe$_2$ – tungsten diselenide

W$_2$C – tungsten carbide

WTiC – tungsten titanium carbide

WO$_3$ – tungsten oxide

WC – tungsten carbide

YSZ – yttria-stabilized zirconia

V$_2$O$_5$ – vanadium oxide

Chapter I

1. INTRODUCTION

Tribology is the field of science which deals with the macro, micro, and nano-level interactions between the contacting surfaces. This domain covers almost every field of daily life with interactions governed by both physical and chemistry perspectives. It can be said that, in our daily lives, tribology is as important as breathing. Tribo-interactions are usually quantified in terms of friction and wear [1]. Where friction is the force needed to initiate the motion between two surfaces in contact and wear is the removal of the material due to frictional force [2]. When the distance between two bodies decreases, strong attraction forces come in play, significantly enhancing the adhesion, creating unfavourable conditions for low friction and wear applications [3]. On the other hand, mechanical interlocking / adhesion between the contacting surfaces, attributed to their roughness or non-uniformities, can also act as the source of friction and wear enhancement. Anyways, in machine components that slide against each other, the energy loss due to friction and wear is a key concern- as they greatly influence the most complex assemblies of an engine component to the simplest of the parts, such as a wheel [4]. Their reductions must be considered even in the case of the smallest components of the machine, to enhance their performance. Otherwise, machine breakdowns and failures might occur due to the loss of integrity of sliding components. For instance, the main source of the decrease of the efficiency of internal combustion engines is friction, leading to the loss of performance of the engines. Degradation of sliding gears and other engine components may lead to additional friction, further adding up to the energy consumption and increased economic costs. If this situation worsens, even the whole engine can also suffer damage [5]. On the other hand, the production of effluent gases from the transportation industry can also occur due to the low tribological efficiency. This, in turn, enhances the cost of energy resources, environmental hazards, and equipment damage. Major areas where tribology plays a vital role, other than the transportation industry, include machining and cutting operations, rolling and sliding bearings, various power plant components, mechanical seals, mould casting and forming operations, electric brushes, grinding and lapping, gas turbines, railroads, and magnetic storage devices, etc [1,6]. The atmospheric conditions in each of

these applications may fluctuate between vacuum, dry, ambient air and temperature etc. Therefore, the tribological principles must be implemented properly to have a highly productive, sustainable, and friendly system which will ultimately lead to avoid unwanted work and resource wastage.

The primary solution for friction reduction is based on the use of liquid lubricants at tribo-contacts. A lot of efforts have been put in past by the lubricant industry to develop a sustainable tribological solution and overcome mechanical inefficiencies. Diverse types of fluids with varying viscosities and additives are being utilized for different applications, according to the working environment, for improving the lifetime and performance. Yet many issues need to be addressed. The main problem of the use of liquid lubricants is volatilization and degradation, leading to premature failure of the part. Liquid lubricants undergo irreversible degradation and creep with time. This not only results in machine or component failure but also increases machine downtimes, induces process disruptions, poor product quality, and economic losses. Correspondingly, the use of oils has been increasingly discouraged by increasing environmental health awareness and research on environment-friendly green solutions. Most of the lubricants contain chemical compounds that raise concerns among environment protection fraternity [7–11]. Several investigations have been carried out throughout Europe to estimate the detrimental effects of oils and other lubricating additives. Technical Committee of Petroleum Additive Manufacturers in Europe researched and analysed health and safety issues for engine lubricants in 15 different countries of Europe [7]. The studies concluded that out of the sold 2600 kilo-tonnes, 24 % is emitted through cars while 75 % is drained as waste oil, out of which 47 % is used for burning. The emission and burning of fuel are responsible for deleterious effects on the environment consequently increasing global warming. A small fraction of oil is lost as leakage as well. In total, approx. 28 % of oil is waste or dumped in water and soil causing damage to the ecosystem. Such a vast amount of dumped oil is alarming and must be taken care of to save the environment. Thus, the laws on the protection of earth and its atmosphere are pushing considerably towards the design of systems that require minimal use of the dangerous chemicals and additives in liquid lubricants. Corrosion and oxidation damage related to liquid lubricants is another important concern following environmental damage. The additives used in oils can result in ash and solid products such as lacquer, sludge, etc., and may also lead to oil thickening resulting in detrimental outcomes such as ring jamming

in engines. Moreover, volatility and oxidation of fluids result in ineffective lubrication between interfaces causing catastrophic failures. In the transportation industry, the cold start is also one of the hindrances behind efficient liquid lubrication. Additionally, efficient fluid lubrication system requires good control over fluid stability. In the same way, minor damages and carelessness can cause fluid leakage leading to severe effects on the system and environment in the form of liquid waste and pollution. Leakage may not only cause loss of costly fluid affecting economics but is also dangerous for the surrounding environment and workers [4]. Despite all the awareness and restrictions, the efforts have rendered very less effects on atmospheric pollution. The main issue is that the breakeven between the efficiency and harmful additive removal from lubricants has not yet been achieved.

To overcome the shortcomings in energy conservation, reduction of friction and wear at the tribological contacts and for the effective replacement of harmful liquid lubricants, research was directed towards green solutions. Here, the solid lubricant coatings come into play. Solid lubricants can be applied as a bulk coating or as a constituent of thin solid coatings on the cutting tools or machine components, as required. The main aim is to modify the surfaces of bulk materials. The domain of solid lubrication underwent a massive breakthrough with the advent of the latest development technologies like chemical vapour deposition, plasma-enhanced chemical vapour depositions, and magnetron sputtering for physical vapour depositions. Also, the advanced characterization techniques have rendered endless possibilities for detailed understanding and modifications of the tribological surfaces [12]. These tribological materials must meet certain criteria of stiffness, fatigue life, thermal expansion, strength, and hardness for efficient sliding performances. Developing a bulk material consisting of all these properties along with very low friction is quite tricky and becomes a tough job, practically. As discussed earlier, in any tribological contact, adhesive forces should be as minimum as possible. The real contact area at sliding interfaces is not what we see, in fact, it is very small and depends on the asperity interaction / contact. So, for low adhesion, the real contact area should be minimized. This can easily be achieved by playing with surface material properties and surface roughness during coating deposition [13]. Besides low roughness of the film surface, properties of the coating-substrate interface also affects the frictional characteristics. Substrate must have adequate hardness, toughness, and stiffness to resist such plastic deformations that can have

a negative influence on the interface conformity [14]. Bowden and Tabor [15] also emphasized that the substrate should be capable of sustaining applied normal load while keeping the real contact area small and the coating, on the other hand, has to provide easy shear properties and minimum interlocking at tribo-contacts.

Currently, in the domain of thin-film solid lubrication, scientific community has developed different type of coatings such as DLCs (diamond-like carbon) [16], tungsten carbide with carbon (WC/C) [17], molybdenum and tungsten doped films [18,19], different TMD (transition metal dichalcogenide) coatings [20–27], polymers [1,27,28] and soft metals [1,12] etc. These coatings are capable of not only reducing friction and wear but can also increase the lifespan of coated components. Such properties pave the way in the production of superior quality products along with increasing production and reducing manufacturing costs. The friction coefficient (COF) for solid lubricants has been reported to reach the low friction regime (COF between 0.1-0.3), ultralow friction regime (COF between 0.01-0.1), or even the super-low friction (COF between 0.001-0.01, usually in ultra-high vacuum conditions) [12,27,29] and some reported wear rates range from 1×10^{-7} to 1×10^{-6} (mm^3/Nm) [24,30,31]. However, low oxidation resistance and poor cyclic environment performance of the coatings result in premature failures of components coated with solid lubricants. Recently, a new concept of lubrication was proposed based on the combination of some coating systems [32] (CrN, CrAlN, TiAlN, TiN and YSZ, etc.) with specific lubricating elements (like Ag, V, Cu, Au Pb, etc.) which diffuse to the surface to form low friction tribolayers. The friction decreased, and the wear resistance improved; however, such improvements were of short durations due to the rapid release of the metal, and the consequent loss of the low-friction tribolayer after short operating periods. Thus, this domain of solid lubrication is still inefficient and needs further improvement.

On the other hand, the use of DLCs is also very common and even it has been tried on various industrial applications. DLCs also lack diverse environment applicability due to the non-performance in vacuum atmospheres. Hydrogen addition can enhance their performance in dry atmospheres but this affects the efficiency in ambient air conditions. Moreover, DLCs are not effective at temperatures slightly higher than 300 ⁰C resulting in high friction and wear [12,30,33,34]. Similarly, the solid lubricants based on polymers and soft metals also fail to provide efficient lubrication in diverse environments and can undergo degradation with temperature shifts. Also, the low heat dissipation capacity of

these materials is a major drawback [1,12,27,28]. Thus, there exists a major gap for a universal solid lubricant. Growing economic needs, urge the demand for coating operability in diverse sliding conditions, especially, in the case of satellites and aerospace applications.

To cope with such demands, various researches have been carried out, lately, on the use of transition metal dichalcogenides after being given key importance by the scientific community. TMD compounds have been under research for the past few decades. The use of TMDs for aerospace components by the National Aeronautics and Space Administration (NASA) dates back to the early '60s for dry and vacuum applications [35]. Since then, a lot of research has been conducted on these coatings. Initially, TMDs were coated on machine components by burnishing, and later they were used as an additive to oils [10,11,36]. Modern research mainly focuses on their use as dry solid lubricant coatings deposited by plasma sputtering. Sputtering provides an ease of coating´s property tuning by variations in the deposition parameters. Pure sputtered TMDs provide ultra-low friction properties when used in vacuum conditions but in moist environments, the wear and frictional performance is comparatively low. Thorough studies on the mechanisms behind this low friction of TMDs in vacuum revealed that this behaviour is governed by the formation of tribolayer having basal planes oriented in the sliding direction [37–44]. Along with low resistance to oxygen and moisture, the low hardness of TMDs is also a limitation to be used as solid lubricants for diverse environments.

As a rescue to these limitations, metal [45–53] and non-metal [25,54–57] alloying of TMDs was experimented, which showed an improved mechanical and tribological results in fluctuating environments (discussed in detail in section 2.3). Industries do not prefer the use of metal alloying as compared to non-metal doping. The latter appeared to be easier and cost-effective. Among non-metals, C-alloyed transition metal dichalcogenide (TMD-C) coatings are more common as they show a significant enhancement of the tribological performance in terrestrial environments. Most importantly, this milestone has been achieved without affecting the tribological properties in vacuum. Furthermore, almost one order of magnitude improvements in hardness has also been reported so far after C-alloying [54,58].

These enhancements in properties came at a cost of low film crystallinity and stoichiometry. Likewise, the reported TMD-C systems show large variations of the friction

and wear with changing sliding environments [24,59,60]. Thus, despite the improved stability in ambient air and vacuum conditions after C-alloying, still, a single solid lubricant system is needed for consistent tribological properties with environmental shifts. So, any coating system that is operable in both earth and space environments (in temperature ranges of 0-300 °C), coupled with consistently low wear and friction would be considered a breakthrough in the aerospace industry. Similarly, the existing literature in the domain of carbon-alloyed TMD systems, reports multiple incongruencies in the results. Literature fails to report any consistency of the behaviour of the coatings, where the achieved properties improve in some cases and lacks improvement in others. The reasons attributed to low film stoichiometry, low hardness, and nanocrystallites formation still require thorough investigation. Besides, the tribological testing in literature deals with the investigation of properties at very high contact pressures, contrary to most of the industrial requirements. Along with diverse environment sliding efficiency, the coating system must be optimized enough to show consistent properties under a range of loading conditions and sliding speeds. Moreover, none of the groups have reported a more systematic and organized study towards any domain of TMD-C coatings. Extensive research has been reported on C-alloyed tungsten disulfide (W-S-C) and C-alloyed molybdenum disulfide (Mo-S-C) coatings while other domains of TMD-C coatings that can have better resistance to moisture e.g., C-alloyed molybdenum disulfide (Mo-Se-C) have been very less explored.

These shortcomings can only be overcome by having a deeper understanding and optimization of the TMD-C coatings. The coating´s composition, compactness, crystal structure, microstructure, adhesion and hardness combine to play a significant role in defining the tribological characteristics of these films. Therefore, the basic purpose of this study is to utilize various lab-scale deposition techniques to optimize these properties of the coatings in such a way to have a highly efficient and universal TMD-C coating system. This work will deal with the Mo-Se-C coatings only, as the ambient air environment properties of MoSe$_2$ are superior to other domains of TMDs. Research will start with the first-ever deposition of these coatings using direct current magnetron sputtering (DCMS) of multiple targets to understand the sputtering behaviour and deposition parameters by this sputtering approach. This will be followed by the second deposition approach where the optimization will be carried out, in a way, to obtain highly stoichiometric, compact, adhesive coatings with improved hardness than the literature. The comparative study of the

properties of the coatings deposited by both DC and RF power supplies will also be explored during this research, to check whether the properties of optimized coatings are independent of the used power supply. Coupled together, these milestones will converge towards the development of a "universal coating system" with highly stable and consistent tribological properties. Detailed tribological testing of the optimized coatings deposited by both DC and RF power supplies will be carried out under different sliding environments, sliding cycles, sliding speeds and contact pressures. The tribological testing will be followed by an in-depth wear track analysis to unfold the mechanisms behind the formation of low friction tribolayers. The evolution and chemistry of the tribolayers as a function of sliding environment and sliding cycles will also be discussed in detail. Finally, the study will conclude by displaying Mo-Se-C coatings as a potential universal dry lubricant for aerospace and terrestrial environments, which is an achievement that will surely open new doors for researchers and industries working in the solid lubrication domain. An important remark is that the upscaling leads to heterogeneity of properties due to dimensions and 3D shaped substrates, and this can also be reduced with these coatings, once fully optimized.

1.1. Thesis organization

Besides the introductory part, the present thesis will be divided into 8 chapters. *Chapter 2* will comprise of the classification of solid lubricant coatings and later, a detailed overview of TMDs. The alloying of TMDs, especially C-alloying will be discussed in detail for different TMDs. A thorough comparison will be reported for the effects of deposition parameters, composition, mechanical properties and testing conditions on the sliding properties of Mo-S-C, W-S-C and Mo-Se-C coatings. Considering the scope of this thesis, all the literature works on Mo-Se-C coatings will be reported in greater detail. The chapter will conclude by pointing out the research gaps and thesis objectives. *Chapter 3* starts with a basic overview of sputtering and its types. Further, it elaborates substrate materials and deposition techniques that will be used in this work, along with an explanation of the main characterization setups to be utilized during analysis of the coatings. *Chapter 4* will deal with the results of the first-ever deposition of Mo-Se-C coatings deposited by (DCMS) co-sputtering of 2 targets. Detailed chemical, structural, mechanical and tribological characterization will be reported. In *chapter 5*, a novel deposition approach will be introduced along with the guidelines to achieve highly optimized compositional, structural

and mechanical properties. Deposition using both DC and RF power supplies will be reported followed by a comparison between coatings properties achieved using both power supplies. *Chapter 6* deals with the tribological testing under diverse environments and various sliding durations for the coatings discussed in chapter 5. An in-depth wear track analysis after different sliding cycles will be reported to understand the evolution and chemistry of the tribolayers. In **chapter 7**, the mechanisms behind the formation of easy shear tribolayers will be discussed to unfold the misconceptions of the literature. In the last **chapter 8**, Mo-Se-C coatings will be introduced as a universal coating system for both terrestrial and aerospace applications. The optimized coatings (of chapter 5) deposited by both DC and RF will undergo tribological testing in both ambient air and vacuum conditions, under a range of contact pressures and sliding speeds. **Chapter 9** is the conclusions and future works section of this thesis.

1.2. List of publications

- **Articles as principal author**

T. Bin Yaqub, T. Vuchkov, M. Evaristo, A. Cavaleiro, *DCMS Mo-Se-C solid lubricant coatings – Synthesis, structural, mechanical and tribological property investigation*, Surf. Coat. Technol. (2019).

T. Bin Yaqub, T. Vuchkov, P. Sanguino, T. Polcar, A. Cavaleiro, *Comparative Study of DC and RF Sputtered MoSe$_2$ Coatings Containing Carbon—An Approach to Optimize Stoichiometry, Microstructure, Crystallinity and Hardness*, Coatings. 10 (2020) 133.

T. Bin Yaqub, S. Bruyere, J. François Pierson, T. Vuchkov, A. Cavaleiro, *Insights into the wear track evolution with sliding cycles of carbon-alloyed transition metal dichalcogenide coatings,* Surf. Coat. Technol. (2020).

T. Bin Yaqub, K. Hebbar Kannur, T. Vuchkov, C. Pupier, C. Héau, A. Cavaleiro, *Molybdenum diselenide coatings as universal dry lubricants for terrestrial and aerospace applications*, Mater. Lett. 275 (2020).

T. Bin Yaqub, S. Bruyere, J. François Pierson, T. Vuchkov, A. Cavaleiro, *Mechanisms behind the tribolayer formation in TMD-C coatings* – (under process)

Reprints of the above-mentioned published papers were made and can be found in annexes.

- **Articles as Co-author on alloyed-TMDs published during this research**

T. Vuchkov, T. Bin Yaqub, M. Evaristo, A. Cavaleiro, *Synthesis, microstructural, and mechano-tribological properties of self-lubricating W-s-C(H) thin films deposited by different RF magnetron sputtering procedures*, Coatings. 10 (2020).

T. Vuchkov, M. Evaristo, T. Bin Yaqub, T. Polcar, A. Cavaleiro, *Synthesis, microstructure and mechanical properties of W–S–C self-lubricant thin films deposited by magnetron sputtering*, Tribol. Int. 150 (2020)

T. Vuchkov, M. Evaristo, T. Bin Yaqub, A. Cavaleiro, *The effect of substrate location on the composition, microstructure and mechano-tribological properties of W-S-C coatings deposited by magnetron sputtering*, Surf. Coatings Technol. 386 (2020)

T. Vuchkov, T. Bin Yaqub, M. Evaristo, A. Cavaleiro, *Synthesis, microstructural and mechanical properties of self-lubricating Mo-Se-C coatings deposited by closed-field unbalanced magnetron sputtering*, Surf. Coatings Technol. 394 (2020) 125889.

K.H. Kannur, T. Bin Yaqub, T. Huminiuc, T. Polcar, C. Pupier, C. Héau, A. Cavaleiro, *Synthesis and structural properties of Mo-S-N sputtered coatings*, Appl. Surf. Sci. 527 (2020) 146790.

K. Hebbar Kannur, T. Bin Yaqub, C. Pupier, C.Héau, A. Cavaleiro, *Mechanical properties and vacuum tribological performance of Mo-S-N sputtered coatings*, ACS Applied Materials & Interfaces (2020).

T. Vuchkov, T. Bin Yaqub, A. Cavaleiro, *The influence of the deposition pressure on the composition and the mechanical properties of W-S-C coatings deposited by magnetron sputtering in semi-industrial conditions*, Vacuum (2020).

Chapter II

2. STATE OF THE ART

This chapter starts with a brief overview of the classification of solid lubricant coatings which is followed by a general introduction to TMDs, the mechanisms behind the low friction of TMDs and the problems arising with the use of pure TMD coatings. In the next part, metal-alloying in TMDs are reported briefly. Finally, this chapter deals with a detailed walkthrough of carbon-alloyed TMDs.

2.1. Classification of solid lubricant coatings

Solid lubricant coatings have been under research for decades with the main aim of the effective replacement of liquid lubricants and the mitigation of extra economical costs, especially in automobiles and aerospace applications. Currently, the developed solid lubricant coatings can be divided into four generations as described below:

2.1.1. Single component coatings

Most of the industrially applicable single layer coatings deposited by techniques like physical vapour deposition (PVD) and chemical vapour deposition (CVD) are known as monolithic coatings and consist of one to two components. Due to the low cost of production, they are still in demand and, industrially they are considered very favourable. These coatings include CrN, CrC, WC/C, W_2C, DLC, TiN, TiC, MoS_2, diamond, soft metals and some polymers. The lack of efficient friction and wear resistance of single component coatings have largely compensated the economic constraints leading to the development of multilayer and multicomponent complex coatings [1].

2.1.2. Multicomponent coatings

Coatings made up of two or more components are referred to as multicomponent coatings. Different phases / components may be present in the form of fibres or particles. Generally, materials described in single component coatings are combined to achieve this

class of lubricant coatings e.g., TiAlN, TiN/AlN, CrBN, TiBN, WTiC etc. If a periodic repetition of each of the component structures is carried out, multilayers coatings are deposited. In cases where the individual layer is in the nm range, the coatings are referred to as superlattice. The combinations of different materials are intended for achieving very specific properties like high temperature performance, diffusion barrier, low friction, control of the excessive divergence between the substrate and working coating, resistance to crack propagation, reduced stresses, hardness enhancement by resistance to dislocation propagation, etc. Such coatings and their industrial applicability experienced a breakthrough after the introduction of vacuum and hybrid deposition technologies [61]. However, the performance of these coatings is highly dependent on the application parameters and environmental conditions.

2.1.3. Gradient, super-lattice and nanostructured coatings

With the increased demand for compositional and structural control of the coatings, grading and nanostructuring approaches were introduced. Various hard and soft phases like TiAlN plus MoS_2 can be combined through the manipulation of the deposition processes to achieve coating with a graded composition variation of MoS_2 in a TiAlN matrix [62]. The adhesion to the substrate is also improved through gradient layers to overcome the drastic hardness variation between the coating and the substrate, e.g. underlayers of Ti, Cr or TiC are often used to accomplish this objective [63]. The other domain of these coatings consists of nanosized grains embedded in amorphous phases as an extension of the multi-component coatings to the nanometer range. A particular field in multilayer coatings are the superlattice coatings (with individual layer up to 50 nm), specifically developed to improve the fracture toughness, hardness and adhesion [64]. Currently, research is being carried out to deposit nanoscale coatings that are thermally stable and can avoid phase transformations and outwards elemental diffusion [65].

2.1.4. Smart (adaptative or chameleon) coatings

The chameleon behaviour corresponds to the ability of some coatings to retain their properties in fluctuating environments during their effective lifecycle. These coatings are

known as smart or chameleon coatings. The W-S-C composite coatings developed by Voevodin et al. [66] holds great importance in this domain. WS and WC nanograins embedded in a diamond like carbon matrix showed an excellent practical example of the chameleon concept. Generally, the chameleon behaviour is associated with a self-adaptive concept which, in the case of this coating system, is related to the possibility to create a different tribolayer according to the working environment. These coatings were explored for aerospace applications and, in those cases, the self-adaptation occurs by either the WS_2 reorientation / crystallization or the graphitization of the amorphous DLC. During cyclic environments, as in space simulation tests, the synergistic effects of WS_2 in vacuum conditions and DLC, in the ambient air atmosphere, played their respective roles for low friction. The main hindrance to the industrial applicability of smart materials is still the large variation of the tribological properties with the sliding environments and conditions.

It can be said that the solid lubricants fall into either extrinsic lubricants that require the influence of an additive from the surrounding to activate the low shear mechanism (e.g. humidity with some sort of DLCs) [67], or intrinsic lubricants which have easily shearing of the atomic structure such as soft metals and MoS_2 [24]. The most widely used solid lubricants in the industry are MoS_2, graphite, and boron nitride which possess easy-shearing lamellar structures resulting in low friction coefficient. Most solid lubricants perform best in a narrow range of operating conditions. For instance, graphite, transition metal dichalcogenides, DLCs, and polymers lose their lubricating properties at temperatures exceeding 350 °C, due to their rapid oxidation [24,68]. TMDs are excellent lubricants in dry air environments or vacuum but degrade quickly in moist air. Graphite is the lubricant of choice for applications in ambient air but cannot provide satisfactory results in vacuum. Polymers can only work in moderate temperature regimes. Fluorides (e.g. BaF_2, CaF_2, and CeF_3), soft metals (such as Cu, Ag, Pb, In, and Au), and some metal oxides (e.g. WO_3, V_2O_5) provide lubrication by forming easily shearing tribolayer at high temperatures. However, these lubricants are not efficient at low temperatures. Oxides lack lubricating characteristics at relatively low temperatures because they are typically brittle, form abrasive wear debris, which leads to high friction [69]. Fluorides become highly prone to cracking, when used at low temperatures and transform to glass-like substances after

melting at high temperatures. Thus, the challenge lies in the development of coatings for effective and stable low friction properties working under multiple reversible environmental cycles.

Pure TMDs and alloyed TMDs will be discussed in greater details in the following sections as per the objective of the thesis. The main focus will be on C-alloyed TMD coatings.

2.2. Transition metal dichalcogenides (TMDs)

TMDs have X-M-X lamellar structure in which M is a transition metal atom while Xs are the chalcogenide atoms. In a typical TMD structure, each metal atom is surrounded by 6 chalcogenide atoms and each chalcogenide is linked to 3 metal atoms. Bonding structure of TMDs is unique with strong covalent-based bonding within X-M-X sandwich while, between sandwiches, there are weak Van der Waals bonds that determine some beneficial properties [58,70]. Such bonding makes the structure highly anisotropic and, thus, TMDs are widely used in different electrical and tribological applications [70]. The most common use of TMDs targeted their electrical properties. These are among the most capable materials for the next generation of electronic devices to replace silicon. The most promising applications in the domain of electronics include sensors, memory devices, and field-effect transistors while, in some cases, the whole electronic circuit could be replaced by TMDs in combination with graphene layers. Despite many advantages, significant improvements have to be reached directed towards the coating reliability concerning the performance. Doping TMDs can help in the modification of the electronic structure [71].

Few decades ago, various studies were initiated on the application of TMDs as lubricating materials. The motivation was the lamellar and low friction structure of these materials, similar to graphite [72]. Transition metal dichalcogenides is a quite big family of materials including WS_2, MoS_2, WSe_2, $MoSe_2$ and $MoTe_2$ as the key ones. They have filled outer d-orbital, providing good and easy shear properties. Out of these, WS_2 and MoS_2 have been widely explored for tribological applications [73]. Excellent lubricating properties of TMDs in vacuum arise from the hexagonal structure with inter-mechanical

weakness, as the weakly bonded layers can slip easily under the applied shear forces, reducing the friction.

After thorough studies on the reasons behind low friction of TMDs in vacuum conditions, several authors [74,75] concluded that the formation of tribofilms / tribolayers at the sliding contact with the basal planes of the TMD phases oriented parallel to the sliding direction was the main mechanism. These lamellar tribolayers, with strong covalent bonds within the layer and weakly bonded planes, are easy to slip, during shearing [30]. The tribolayers in many cases are pure TMD phases, relatively softer than the coating and the substrate material. If the structure of the original coating is carefully tailored to get the TMD in a hard matrix, this adaptive process makes an ideal combination of a hard material covered by a soft tribolayer. However, the phenomenon is entirely dependent on the ability of the coating to allow the reorientation of the planes and / or the transfer of coating material to the counter body during sliding [76].

The formation of tribolayers is not instantaneous and requires sufficient time for the process. This time is associated with the running-in time. The running-in time is a function of the surface roughness, applied load, temperature, humidity, number of laps and sliding speed. As soon as the tribolayer is formed, it accommodates the sliding by itself. The sliding should always occur along the least shear strength plane in the tribolayer, which is not easily distinguishable. Once the sliding and the tribolayer formation starts, it is not possible to distinguish to which surface of the contact pair these easy shear planes belong. The system becomes analogous to the fluid / liquid lubricants only knowing that the surfaces are separated by a lubricious layer allowing the easy sliding of a material over the other. The presence of these low bonding planes parallel to the sliding direction makes TMDs capable of achieving friction lower than the one with liquid lubricants. For example, in boundary lubrication, friction as low as 0.05-0.2 has been reported in liquid lubrication, which is higher than what can be achieved with fully functional and ideally operating WS_2 coatings. Although in some cases, hydrodynamic lubrication can reach friction values around 0.001-0.01, solid lubricant coatings overpower them by overcoming issues like cold starts (especially in engine and cutting tools), thermal fluctuations and high-speed

requirements [73]. Fully formed tribolayers are very stable, long-lasting, and capable of bearing high loads and cycles, thus, providing low wear as well.

As above referred, the key for low friction is to have the (002) basal planes parallel to the sliding direction. During the depositions, however, TMD crystals are deposited with those planes randomly oriented. Then, reorientation of those crystals or (re)crystallization with the (002) planes parallel to the sliding direction is necessary for the low friction. Until the formation of the tribolayer, the coatings wear out and the wear debris can form a transfer layer on the counter body which, itself, can also transform / crystallize being part of the tribolayer. The wear and the material transfer to the counter body decrease when the steady-state tribolayer formation is reached [12]. The thickness of the fully formed tribolayers does not vary much and, therefore, the wear is restricted within the tribolayers, protecting the coating underneath. Another interesting feature of TMD-based coatings is the regeneration and replenishing of worn-out areas, keeping the wear low. During sliding, the transfer film attached to the counter body can help in replenishing the worn-out zones. [77].

Among all TMDs, WS_2 and MoS_2 are the most studied ones. Initial focus was on molybdenum disulfide (MoS_2) based thin coatings. It is used as a lubricant for a long time, with first published patent dating back to 1927 and its vacuum application dates back to the 1940s [79]. MoS_2 can be used as a powder for lubrication or as an additive in different oils [80]. Considering that MoS_2 is an excellent lubricant in dry and vacuum conditions, NASA started its research in the early '60s [81] with the aim of its application in space instruments and devices. In vacuum applications, MoS_2 could not be implemented as an oil additive; therefore, powder brushing (on components) was used as an alternative technique. Researchers at NASA studied the frictional behaviour of MoS_2 in various environments. They concluded that in dry air, COF and wear were lower as compared to ambient air. MoS_2 tested in dry argon exhibited the lowest values out of all the three environments [82]. Similarly, in NASA laboratories, the deposition of MoS_2 coating for aerospace components was carried out through the electrodeposition of MoO_3 followed by annealing in H_2S atmosphere. Nevertheless, later it was found that the finest way for MoS_2 coating

deposition was to utilize magnetron sputtering, owing to its advantages on the coating property control [20].

Although MoS_2 has been widely studied during the initial research phase on TMDs, later, tungsten disulfide (WS_2) became the core research domain [83]. WS_2 has better temperature stability and higher oxidation resistance [84] than the former. Selenides (Se_2), on the other hand, were rarely studied. Irrespective of the incipient exploration, it was shown by Kubart et al. [42] that they have a better resistance to humidity than other TMDs, along with an excellent lubrication capability in dry air or vacuum environment. In the study, they tested the tribological performance of DC magnetron sputtered $MoSe_2$ and MoS_2 coatings in different humidity ranges and temperatures. $MoSe_2$ coatings display better tribological properties than MoS_2 coatings, in almost every testing conditions. Likewise, the influence of changing environmental conditions was less prominent for $MoSe_2$ coatings as compared to the MoS_2 coatings. Another core advantage of $MoSe_2$, is its higher chalcogen atom / metal atom ratio, closer to stoichiometric value (2), than other TMDs [85]. One of the possible reasons for the low exploration of $MoSe_2$ is its high wear in dry atmospheres, as compared to MoS_2 [42,86]. Another possibility can be its non-availability as a natural mineral, unlike MoS_2. Similarly, S is more abundant in nature than Se. This puts an extra burden on the cost perspective of $MoSe_2$. However, despite this issue, it seems (from the above-mentioned reasons) that a properly optimized $MoSe_2$ coating might have a greater potential as solid lubricant material.

No matter what TMD is used, these coatings have some basic and common issues that hinder their long-term sliding properties. The TMD coatings provided very low COF (typically around 0.001) [74] in ultra-high vacuum environments while COF increases in the presence of moisture and oxygen (COF = 0.1-0.2) [87]. This means that the shift of the sliding environment from dry to ambient air adversely affects the easy shear properties of TMDs. A key focus in determining the best possible solution for excellent tribological properties was on the study of the mechanisms behind oxidation and moisture effects. In TMDs, the defects or voids at the dangling bonds result in high energy sites vulnerable to atmospheric attacks. Sulfur or selenium in the TMD structure can combine with water

molecules, resulting in a modified chemical structure due to the formation of strong hydrogen bonds. Then, mutual attraction, instead of repulsion, occurs between the layers [77]. Similarly, oxygen and water vapours from ambient air environments can form respective oxides (e.g. WO_3 and MoO_3), affecting the bond structure and thus, again resulting in mutual attraction between the layers [86]. Serpini [21] introduced another theory, based on the adsorption of H_2O between the TMD layers, thus increasing the shearing forces. No matter what the reason is, this instability in ambient air atmospheric conditions is a major drawback of TMD coatings, especially for the machine components that have to work in fluctuating environments. Elisabetta et al. [21] suggested that the adverse effects of moisture can be overcome by heating to a temperature that can sufficiently remove the moisture but, this solution cannot be applied in every case / area. Therefore, a permanent self-sustaining solution is needed. Along with the low resistance to oxygen and moisture, the low mechanical strength of TMD is also a primary issue. The low bonding energy between the planes is good for the low friction but gives rise to very soft materials. Moreover, when sputtered, pure TMD coatings are highly porous which even result in low hardness, weak adhesion to the substrates, and low load-bearing capacity. This all makes them inappropriate for most applications submitted to high contact loads [68,88–91]. The high temperature performance of pure sputtered TMDs is also very limited [86].

With the advancements in the research capacity and the development of coating deposition methods, associated with the increasing demands for robust and economic industrial solution for low friction applications, it is mandatory to have an environmentally suitable, dynamic, and applicable solid lubrication coating system that can efficiently work in cyclic environments [31]. Alloying TMD coatings is a possibility to overcome their drawbacks, what has been achieved by combining them with various metals, non-metals, and compounds [24]. The next section sums up the effects of metals and non-metals alloying on the performance of TMD-based coatings. Main focus will be given to the carbon-alloying reported in the literature, along with the research gap that needs to be solved.

2.2.1. Alloying of TMDs

2.2.1.1. Metal alloying of TMDs

Metal alloying has been reported by various researchers. Titanium is the most widely studied alloying metal for both MoS_2 and WS_2 coatings [45–47,92–95]. Ti-alloyed MoS_2 coatings known as MOST were the most famous, so far [45]. Other metallic elements used for alloying TMD coatings include, Au [48,49,96,97], Pb [96,98], Cr [92,99,100], Zr [51,101], Ta [102], Fe [97] and Ni [96,97,103]. Despite some acceptable results related to the tribological performance in vacuum environments after metal alloying, the frictional properties vary considerably with environmental changes, even within the same metal-alloyed coatings. Also, most of the testing was carried out for a short number of sliding cycles. Likewise, metal alloying is not favourable (especially in industries) due to: (i) the operating costs can increase significantly (e.g. in case of Au), (ii) the improvement on the tribological performance in relation to pure TMD is not attractive or long-lasting for the main part of applications, (iii) the potential oxidation of some metals (e.g. in case of Ti), is one more drawback with negative impact for long-term stable tribological performance and industrial applicability; oxidation can result in abrasive particles and such particles, if stuck in the wear tracks, can result in high wear and, in some cases, coating failures, (iv) metals hinder efficient tribolayer formation and, (v) the recommended alloying contents in literature of different metals (e.g., for Ti, Cr) have to be low, which impacts on a higher porous and columnar structure. This leads to poor tribological performance and low load-bearing capability, far from the one that could be reached with higher metal contents procedure. Finally, the literature lacks systematic values of an in-depth tribological investigation in vacuum, dry, ambient air and high temperature environments in relation to almost all the metal alloyed TMD coatings reported so far.

Next section will be solely dedicated towards carbon-alloyed TMD coatings, to further converge the literature review towards the aim of the project.

2.2.1.2. Non-metal alloying

Carbon alloyed TMD films

C-alloyed TMD coatings have been widely explored in the past few decades, owing to their attractive mechanical and tribological properties both in terrestrial and non-terrestrial environments. In this section, the background of the main subsets of C-alloyed TMDs will be discussed briefly with respect to the deposition method, chemical composition, hardness, and tribological properties. Although literature reports considerable work on various subsets of TMDs, this section will focus on the most interesting and relevant results achieved with coatings deposited by magnetron sputtered PVD techniques. The deposition approaches based on RF and DC power supplies coupled with different target combinations (composite targets, co-sputtering of multiple targets and reactive or non-reactive atmosphere) will be under discussion.

- *Mo-S-C and W-S-C*

C-alloying was introduced to improve the mechanical, chemical and sliding properties of the MoS_2 coatings, envisaging their application in a great diversity of environments [22]. The idea was to use the combined advantages of DLC and MoS_2. So, the past few decades have been marked by an extensive investigation of Mo-S-C coatings deposited by magnetron sputtering. These studies have concluded that the optimum properties can be achieved through a nanocomposite structure of MoS_2 and a-C. a-C provides the load-bearing capability while MoS_2 enhances the sliding properties in the contact region. The next two tables summarize the notorious and most important research carried out on PVD magnetron sputtered Mo-S-C coatings. An effort has been made to cover most of the data that can be helpful to have a detailed overview of the literature with respect to the deposition method, the targets utilized and their configuration, the C content, the composition, the hardness, and the tribo-testing details (testing equipment, sliding environment, sliding mechanism, sliding durations, counter body). Finally, the achieved COF in different environments is reported to compare the effects of different deposition conditions and chemical composition on the mechanical properties and sliding test results.

Table 2-1: Main deposition parameters and characterization results of PVD magnetron sputtered Mo-S-C coatings reported in the literature

Deposition and Basic Characterization Details					
System	**Deposition Method**	**Target Details**	**C content (at. %)**	**S/Mo**	**Hardness (GPa)**
MoSC-1 [104]	RF (multilayer)	Co-sputtering: MoS_2 (1)* and C (1)	–	–	6.5-14
MoSC-2 [105]	DC and RF	Reactive sputtering: RF-CH_4, DC-MoS_2 (1)	74	0.9	NA
MoSC-3 [106]	RF	Co-sputtering: MoS_2 (1) and C (1)	13-55	1.25-1.75	0.7-4
MoSC-4 [107]	Medium frequency	Co-sputtering: C (2) and MoS_2 (1)	84-96	1.34-1.55	2.5-5.2
MoSC-5 [108]	Medium frequency	Reactive co-sputtering with CH_4, MoS_2 (1) and C (2)	85-93	0.91-1.96	2.5-5
MoSC-6 [109]	medium frequency (multilayer)	Reactive co-sputtering with CH_4 gas, MoS_2 (1), C (2)	–	–	1.3-2.8
MoSC-7 [110]	DC	Composite target: MoS_2 pellets on C	41-73	1-1.1	7-10.8
MoSC-8 [111]	RF (multilayer)	Co-sputtering: MoS_2 (1) and C (1)	qualitative reported	given (multilayer)	1.37
MoSC-9 [112]	RF	Co-sputtering: MoS_2 (1) and C (1)	25-40	1.53-1.89	0.3-2.3
MoSC-10 [113]	DC and medium frequency, probably multilayer	Co-sputtering: MoS_2 (1) and C (3)- not fully clear	qualitative reported	qualitative reported	3.55 original
MoSC-11 [114]	DC	Composite target: MoS_2 pellets on C	45-84	1.45-1.7	7-8.7
MoSC-12 [115]	DC	Co-sputtering: MoS_2 (1) and C (1)	38-75	1-1.3	-
MoSC-13 [116]	RF	Co-sputtering: MoS_2 (2) and C (1)	19-41	1.71-1.81	1.96
MoSC-14 [117]	DC	Co-sputtering: MoS_2 (2) and C (2)	40	1.65	5
*Numbers in parentheses represent number of targets.					

Table 2-2: Tribological testing parameters and friction coefficients of PVD magnetron sputtered Mo-S-C coatings reported in Table 2-1

Tribological Properties						
Ambient Air Performance						
System	**Tribometer configuration**	**Applied load**	**Test duration**	**COF**	**Counter body**	**Relative Humidity (RH)**
MoSC-1	Pin-on-disc tribometer-rotating	5 N	6000 cycles	0.025-0.17	440C	30% RH
MoSC-3	Pin-on-disc tribometer-rotating	5-30 N	5000 cycles	0.04-0.3	100Cr6	30% RH
MoSC-4	Pin-on-disc tribometer-rotating	5 N	3600 sec	0.035	GCr15	45% RH
MoSC-5	Pin-on-disc tribometer-rotating	5 N	3600 sec	0.05-0.08	GCr6	-
MoSC-6	Pin-on-disc tribometer-rotating	5 N	720 m	0.056	GCr15	45% RH
MoSC-7	Pin-on-disc tribometer-reciprocating	5 N	3000 sec	0.08-0.095	GCr15	50% RH
MoSC-8	Pin-on-disc tribometer rotating	3 N	40000	0.08	GCr15	35% RH
MoSC-9	Pin-on-disc tribometer-rotating	3 N	60000 cycles	0.05-0.25	GCr15	35% RH
MoSC-11	Pin-on-disc tribometer-reciprocating	10 N	7000 sec	0.05-0.1	GCr15	35% RH
MoSC-12	Pin-on-disc tribometer-rotating	1 N	-	0.45-0.5 (FKM substrate), 0.2-0.4 (NBR), 0.2-0.6 (HNBR), 0.4-0.6 (TPU)	100Cr6	50% RH
MoSC-13	Pin-on-disc tribometer rotating	3N	15000	0.08	GCr15	25% RH
MoSC-14	Pin-on-disc tribometer-reciprocating	5N	20000 cycles	0.24	GCr15	78% RH
Vacuum Performance						
System	**Tribometer configuration**	**Applied load**	**Test duration**	**COF**	**Counter body**	**Relative Humidity (RH)**

System	Tribometer configuration	Applied load	Test duration	COF	Counter body	Relative Humidity (RH)
MoSC-2	Pin-on-disc tribometer rotating	2 N	2500 cycles	0.8	SiC	-
MoSC-4	Pin-on-disc tribometer-rotating	5 N	3600 sec	0.008-0.03, 0.008 till 600 sec	GCr15	-
MoSC-5	Pin-on-disc tribometer-rotating	5 N	3600 sec	0.002 (only 1 coating survived)	GCr6	-
MoSC-6	Pin-on-disc tribometer-rotating	5 N	720 m and 10000 m	0.019-0.025	GCr15	-
MoSC-8	Pin-on-disc tribometer-rotating	3 N	150000 cycles	0.07 Low vacuum, 0.05 High vacuum	GCr15	-
MoSC-9	Pin-on-disc tribometer-rotating	3 N	60000 cycles	0.04-0.07	GCr15	-
MoSC-10	Pin-on-disc tribometer-rotating	5 N	3600 sec	0.04	GCr6	-
MoSC-13	Pin-on-disc tribometer-rotating	3N	110000 cycles	0.05	GCr15	-
MoSC-14	Pin-on-disc tribometer-reciprocating	5 N	20000 cycles	0.07	GCr15	-
Dry Nitrogen Performance						
System	**Tribometer configuration**	**Applied load**	**Test duration**	**COF**	**Counter body**	**Relative Humidity (RH)**
MoSC-3	Pin-on-disc tribometer rotating		5000 Cycles	0.015-0.02	100Cr6	-
MoSC-4	Pin-on-disc tribometer rotating	5 N	3600 sec	0.03	GCr15	-
MoSC-6	Pin-on-disc tribometer-rotating	5 N	720 m	0.04	GCr15	-

The C-alloying of WS_2 was first introduced by Voevodin [66], to improve the tribological properties for applicability in the aerospace industry. The study found quite interesting results regarding sliding in diverse atmospheres and the above referred "chameleon behaviour" was observed for the composite coatings. Following his work, intensive research was carried out by other authors on the microstructure, crystal structure, mechanical and tribological properties of W-S-C systems. The tribological properties have been analysed in various sliding conditions. The following tables summarize the research carried out on PVD magnetron sputtered W-S-C coatings. An effort has been made to cover

most of the data available in the literature. Henceforth, the first table deals with the information on the deposition method, the targets used, and their configuration in the apparatus, the chemical composition, and the hardness. The second table, for the same coatings, deals with the tribo-testing details (testing equipment, sliding environment, sliding mechanism, sliding durations, counter body) and the COF results. The idea is to compare and correlate the COF with the parameters shown in Table 2-3 as well as with the sliding test parameters and approaches shown in Table 2-4.

Table 2-3: Main deposition parameters and characterization results of PVD magnetron sputtered W-S-C coatings reported in the literature

Deposition and Basic Characterization Details					
System	**Deposition Method**	**Target Details**	**C content (at. %)**	**S/Mo**	**Hardness (GPa)**
WSC-1 [118]	RF	Reactive sputtering with CH_4, WS_2 (1)	15-62	1.1-1.2	2-5.5
WSC-2 [70]	RF	Reactive sputtering with CH_4, WS_2 (1)	13-64	1-1.6	0.8-5.4
WSC-3 [119]	RF	Reactive sputtering with CH_4, WS_2 (1)	50	-	5.4
WSC-4 [104]	RF (multilayer)	Co-sputtering: WS_2 (1) and C (1)	-	-	11-17
WSC-5 [120]	RF	Reactive sputtering with CH_4, and WS_2 (1)	15-72	0.9-1.5	0.5-13
WSC-6 [120]	RF	Co-sputtering: WS_2 (1) and C (1)	34-63	1.6-1.8	3-7
WSC-7 [121]	RF	Composite target: WS_2 pellets on C	29-70	1.2-1.45	4-10
WSC-8 [122]	RF	Composite target: WS_2 pellets on C	29-70	1.2-1.5	4-10
WSC-9 [123]	RF	Composite target: WS_2 pellets on C	29-70	1.2-1.45	4-10
WSC-10 [74]	RF	Co-sputtering: WS_2 (1) and C (1)	42	1.7	6
WSC-11 [74]	RF	Composite target: WS_2 pellets on C	42	1.2	10
WSC-12 [124]	RF	Reactive sputtering with CH_4, and WS_2 (1)	13-69	0.98-1.57	1.5-5
WSC-13 [125]	RF	Composite target: WS_2 pellets on C	42	1.26	4.9
WSC-14 [125]	RF	Composite target: WS_2 pellets on C	42	1.26	4.9
WSC-15 [126]	DC	Co-sputtering: WS_2 (1) and C (1)	39	1.3	9
WSC-16 [126]	DC	Co-sputtering: WS_2 (1) and C (1)	39	1.3	9
WSC-17 [127]	DC	Co-sputtering: WS_2 (1) and C (1), one coating with substrate heating 300 ºC	16-32	0.75-0.84	4.1-6.9

WSC-18 [128]	DC	Co-sputtering: WS$_2$ (1) and C (1)	18-41	0.7-0.9	-
WSC-19 [128]	DC	Co-sputtering: WS$_2$ (1) and C (1)	18-41	0.7-0.9	-
WSC-20 [129]	RF	Composite target: WS$_2$ pellets on C	42	1.26	4.9
WSC-21 [130]	RF	Reactive sputtering with CH$_4$, WS$_2$ (1)	14-69	1-1.54	-
WSC-22 [19]	DC	WS$_2$, C, W	57-76	1.3-0.5	6.5-14.0
WSC-23 [131]	DC	Co-sputtering: WS$_2$ (1) and C (2)	22-28	0.55-0.97	4.9-7.6
WSC-24 [55]	DC and pulsed-DC	Co-sputtering: WS$_2$ (2) pulsed-DC and C (1) DC	17-64	1.33-1.79	5.4-10.6
WSC-25 [55]	DC and pulsed-DC	Co-sputtering: WS$_2$ (2) pulsed-DC and C (1) DC	17-64	1.33-1.79	5.4-10.6
WSC-26 [132]	DC and pulsed-DC	Co-sputtering: WS$_2$ (2) pulsed-DC and C (1) DC	16	1.73	-
WSC-27 [132]	DC and pulsed-DC	Co-sputtering: WS$_2$ (2) pulsed-DC and C (1) DC	16	1.73	-
WSC-28 [56]	DC and pulsed-DC	Co-sputtering: WS$_2$ (2) pulsed-DC and C (1) DC	16-27	0.5-1.7	5.4-12
WSC-29 [56]	DC and pulsed-DC	Co-sputtering: WS$_2$ (2) pulsed-DC and C (1) DC	16-27	0.5-1.7	5.4-12
WSC-30 [56]	DC and pulsed-DC	Reactive sputtering with C$_2$H$_2$ and WS$_2$ (2)	25-70	0.8-1.89	4.3-11
WSC-31 [56]	DC and pulsed-DC	Reactive sputtering with C$_2$H$_2$ and WS$_2$ (2)	25-70	0.8-1.89	4.3-11
WSC-32 [133]	DC and pulsed-DC	Co-sputtering: WS$_2$ (2) pulsed-DC and C (1) DC	-	-	-

*Numbers in parentheses represent number of targets.

Table 2-4: Tribological testing parameters and friction coefficients of PVD magnetron sputtered W-S-C coatings reported in Table 2-3

Tribological Properties						
Ambient air Performance						
System	Tribometer configuration	Applied load	Test duration	COF	Counter body	Relative Humidity (RH)
WSC-1	Pin-on-disc tribometer-reciprocating	10 N	-	0.18-0.23	100Cr6	-
WSC-2	Pin-on-disc tribometer-reciprocating	5-10 N	-	0.07-0.22	100Cr6	60% RH

WSC-3	Pin-on-disc tribometer-rotating	10 N	1000 m	0.2	100Cr6	60% RH
WSC-4	Pin-on-disc tribometer-rotating	5 N	6000 cycles	0.05-0.15	440C	30% RH
WSC-5	Pin-on-disc-tribometer-rotating	10 N	5000 cycles	0.1-0.3	100Cr6	40% RH
WSC-6	Pin-on-disc tribometer-rotating	10 N	5000 cycles	0.1-0.4	100Cr6	40% RH
WSC-7	Pin-on-disc tribometer-rotating	5 N	1500 cycles	0.2-0.3	100Cr6	30% RH
WSC-8	Pin-on-disc tribometer-rotating	5-47 N	5000 cycles	0.06-0.23	100Cr6	30% RH
WSC-9	Pin-on-disc tribometer-rotating	5 N	1500 cycles	0.03-0.3	100Cr6	5-70% RH
WSC-10	Pin-on-disc tribometer-reciprocating	20-1000 N	24000 cycles	0.04-0.15 (20 N=0.15)	100Cr6	40% RH
WSC-11	Pin-on-disc tribometer-reciprocating	20-1000 N	24000 cycles	0.11-0.24(20 N=0.24)	100Cr6	40% RH
WSC-12	Nano-scratch tribology	0.5-4 mN	25 micron	0.07-0.15	-	30% RH
WSC-13	Pin-on-disc tribometer-rotating	1-15 N	5000 cycles	0.07-0.27	100Cr6	34% RH
WSC-14	Pin-on-disc tribometer-rotating	10 N	10000 cycles	0.035	100Cr6	1% RH
WSC-15	Pin-on-disc tribometer-rotating	1-50.8 N	-	0.04-0.2	100Cr6	30% RH
WSC-16	Pin-on-disc tribometer-rotating	5 N	500-50000 cycles	0.08-0.12	100Cr6	30% RH
WSC-17	Pin-on-disc tribometer-rotating	5 N	1000 cycles	0.02-0.03	100Cr6	5% RH
WSC-18	Pin-on-disc tribometer-rotating	5 N	10000 cycles/160 m	0.02-0.03	100Cr6	5% RH
WSC-19	Pin-on-disc tribometer-rotating	5 N	-	0.1-0.15	100Cr6	50% RH
WSC-20	Nano (AFM) tribology	0-80 nN	1 micron	0.03-0.18	-	-
WSC-21	Micro (AFM) tribology	25-50 mN	2000 cycles/8 m	0.2-0.4	-	40% RH
WSC-22	Pin-on-disc tribometer-rotating	5 N	60000 cycles/3000 m	0.15-0.3	E52100 steel	50-60% RH
WSC-23	Nano (AFM) tribology	0.5-300 nN	4 micron	0.01-0.08	-	-

System	Tribometer configuration	Applied load	Test duration	COF	Counter body	Relative Humidity (RH)
WSC-24	Pin-on-disc tribometer-rotating	5 N	1000 m	0.02-0.03	100Cr6	5% RH
WSC-25	Pin-on-disc tribometer-rotating	5 N	1000 m	0.1-0.17	100Cr6	55% RH
WSC-26	Pin-on-disc tribometer-rotating	5 N	10000 cycles	0.02	100Cr6	5% RH
WSC-27	Pin-on-disc tribometer-rotating	5 N	10000 cycles	0.1	100Cr6	55% RH
WSC-28	Pin-on-disc tribometer-rotating	5 N	10000 cycles	0.02-0.15	100Cr6	5% RH
WSC-29	Pin-on-disc tribometer-rotating	5 N	10000 cycles	0.1-0.23	100Cr6	55% RH
WSC-30	Pin-on-disc tribometer-rotating	5 N	10000 cycles	0.03-0.12	100Cr6	5% RH
WSC-31	Pin-on-disc tribometer-rotating	5 N	10000 cycles	0.22-0.5	100Cr6	55% RH
WSC-32	Pin-on-disc tribometer-rotating	NA	10000 cycles	0.027	100Cr6	5-7% RH
Dry Nitrogen Performance						
System	**Tribometer configuration**	**Applied load**	**Test duration**	**COF**	**Counter body**	**Relative Humidity (RH)**
WSC-3	Pin-on-disc tribometer-rotating	10 N	1000 m	0.07	100Cr6	**-**
WSC-7	Pin-on-disc tribometer-rotating	5 N	1500 cycles	0.06-0.12	100Cr6	-
WSC-10	Pin-on-disc tribometer-reciprocating	20-500 N	24000 cycles	0.02-0.045	100Cr6	-
WSC-11	Pin-on-disc tribometer-reciprocating	20-500 N	24000 cycles	0.04-0.08	100Cr6	-
WSC-22	Pin-on-disc tribometer-rotating	5 N	3000 m (60000 cycles)	0.02-0.05	E52100 steel	-
High Temperature Performance						
System	**Tribometer configuration**	**Applied load**	**Test duration**	**COF**	**Counter body**	**Relative Humidity (RH)**
WSC-7	Pin-on-disc tribometer-rotating	5 N	1500 cycles	0.04-0.1	100Cr6	**-**

From the analysis of Tables 2-1 and 2-3, it can be concluded that W-S-C and Mo-S-C coatings can be deposited by reactive and non-reactive processes. Reactive sputtering

needs a carrier gas to be utilized (e.g. CH_4 or C_2H_2), which can result in hydrogen incorporation in the final coating. It is evident from the tables that this deposition approach leads to large variations in S/Mo or S/W ratios. The deposition species can be sputtered from either a composite target (C target with TMD pellets) or a combination of targets (multiple targets of C and TMD). With the composite target use, it is difficult / impossible to study the high TMD contents since C will be always present in the coatings. Moreover, controlling and varying the chemical composition is trickier since any variation of the number of TMD pellets in the target requires an arrangement of the pellets over the surface. Contrarily, the co-sputtering of multiple targets is more favourable as it provides the leverage to control both TMD and C targets individually. So, any C or TMD contents can be easily achieved from 0 up to 100 at. %. The mechanical properties do not show any specific trend and it seems that they can be correlated as per the need of the compactness and the chemical composition of the coatings. To improve the adhesion, different types of gradient layers can be deposited; when multicathode equipment is being used, the interlayer can be tailored by playing with the individual target power among the TMD-C targets and the metallic ones (e.g. Cr, Ti), used for the adhesion layer. In relation to the power supplies connected to the sputtering targets, the DC one is more favourable for companies due to the much higher deposition rates and lower cost of operation. Despite the higher plasma density provided, the RF power supply needs a matching box that, potentially, adds cost to the sputtering process. The chalcogen / metal atom ratios are closer to stoichiometry for DC magnetron sputtered coatings.

A glimpse at the tribological results of PVD magnetron sputtered Mo-S-C and W-S-C coatings reported in literature allows us to find a lacuna concerning the high temperature tribological analysis of the Mo-S-C coatings as well as the vacuum tribological results for W-S-C coatings. Additionally, for both systems, the performance in dry N_2 has only been superficially explored when compared to ambient air studies. No specific trend can be observed between the C content and the COF but, in most of the cases (except composite target sputtering), increasing C content results in a decrease of the S/Mo or S/W ratios, which are in the basis of an increase in the COF. Moreover, the selection of an appropriate load, associated with a convenient adhesion of the coating to the substrate, is a

prime requirement for optimizing the sliding performance. Generally, against the typical Amonton principle [134,135], increasing the applied load results in a decrease in the COF in traditional tribological testing; however, in the case of nano / micro tribological testing, an inverse trend is observed. The increment in the applied load cannot be tested beyond a threshold value; in fact, it can have an adverse effect, since the coatings with poor adhesive characteristics fail under high loads. The comparison of the coating´s performance is a cumbersome task due to these specific behaviours. For example, even for the same applied loads, the COF can significantly change, which is probably related to the different deposition approaches and conditions which directly influence the properties of the coating.

One of the most important conclusions from the analysis of the tables is the large variation in the tribological properties of the coatings by changing the sliding environments from dry or vacuum atmosphere to ambient air conditions. Even in the ambient air atmosphere, the increments in humidity led to an increase in the friction. In other words, the environment plays a dominant role in defining the COF of Mo-S-C and W-S-C systems, which is determinant for the durability of a machine component that has to work in fluctuating environments. Irrespective of the loads and the sliding environments, in the literature, most of the results refer to a low number of cycles sliding tests, which are not a true representation of the durability of the coatings. Lastly, the tribological performance, reported in the tables above, concerns tests performed with initial applied contact stresses higher than ~500-600 MPa, which may not be the case in many industrial conditions.

Summarizing, previous literature reports considerable work in the field of Mo-S-C and W-S-C coatings, but an organized and systematic study involving all processing conditions and testing environments is absent. Moreover, the optimization of a single deposition approach is missing and the work seems to be more scattered then converging towards a specific direction. For example, WSC-10 and WSC-11 coatings were deposited by co-sputtering and composite target, respectively, using a C content of 42 at. %. The S/W ratio and COF of co-sputtered coating out-performed the composite one while, hardness was higher of the latter. The approach should have been to optimize the co-sputtered coatings. However, later, the composite target approach was again reported, where the

hardness decreased from 10 GPa (WSC-11) to 4.9 GPa (WSC-13). Thus, there is a need to optimize a single deposition approach (for both W-S-C and Mo-S-C coatings), preferably co-sputtering as: (i) it displayed better results, (ii) is more user friendly and, (iii) is a more favourable approach for upscaling. For developing an environmental independent coating system, either the high temperature and vacuum sliding performance of W-S-C coatings, or the dry nitrogen and high temperature sliding performance of Mo-S-C coatings, need thorough investigation. Sliding performance at low contact stresses and for long sliding duration must be explored for these coatings to be industrially accepted and upscaled. Lastly, one of the most important research gaps in previous reports of W-S-C and Mo-S-C coatings i.e., the large variations in the COF with changing sliding conditions. This cannot be overcome without performing thorough studies on the chemistry, evolution, and mechanism of the tribolayer formation, with changing the sliding conditions. The literature conflicts about the role of C and TMD phases on the tribolayer formation under ambient air conditions should be dismissed. The current urgent need is to overcome these gaps, being a universal solid lubricant desired.

- *Mo-Se-C*

In the recent past, our research group explored the C-alloying of $MoSe_2$ coatings for the first time. Until now, no other works have been reported on Mo-Se-C coatings. For Mo-Se-C coatings deposited till now, some improved properties could be observed as compared to other TMD-C coatings. Polcar et al. [136], investigated the deposition of RF sputtered Mo-Se-C coatings (from composite carbon target having $MoSe_2$ pellets) with respect to their mechanical and (micro)structural properties. The Se/Mo ratio was reported to increase with increasing carbon content (from 29 at. % up to 68 at. %) being the highest ratio 2.0, the stoichiometric value. Low C coatings were columnar but less porous than pure $MoSe_2$ coatings. Above 50 at. % C, the coatings were compact and amorphous with no columns. The hardness increased up to 4.1 GPa as compared to 0.7 GPa of pure $MoSe_2$. Considering the X-ray diffraction (XRD) results, authors claimed the formation of $MoSe_2$ nanograins in an amorphous carbon matrix, but no (002) peak was detected, meaning that basal planes are not oriented parallel to the surface. In view of previous literature, the

authors proposed that such microstructure, crystal structure, and hardness improvements could provide excellent lubrication in the ambient air atmosphere.

Thus, the ambient air (RH = 35 %) tribological properties of Mo-Se-C coatings were evaluated [137]. Before tribotesting, the coatings, for the first time, were analysed by transmission electron microscope (TEM), which allowed to demonstrate the presence of $MoSe_2$ platelets whose size decreased with increasing C content. The tribological analysis was performed in a rotating pin-on-disk tribometer using a 100Cr6 steel ball as a counter body. The wear and friction decreased with the applied load; 0.14 at 5 N to 0.04 at 47 N. Tests with 500, 2000 and 20000 laps using 5 and 33 N applied loads were also carried out. AFM analysis of the wear track tested with 33 N showed abrasion of the surface after a low number of laps while, with increasing number of laps, the replenishing of the worn-out surfaces occurred. AES depth profiles showed an absence of carbon in the first top layers, increasing with depth thereafter. TEM clearly showed a tribolayer comprising of $MoSe_2$ basal planes parallel to the surface in the wear track that resulted in the lower frictional properties.

Owing to the excellent tribo-performance in ambient air under increasing loads, our group further extended the research to analyse the sliding behaviour of the same coatings in varying humidity levels (RH = 5 % to 70 %) and under different temperatures (RT to 500 °C) [138]. The tests were carried out for 1000 laps in a rotating pin-on-disk tribometer using a 100Cr6 steel ball as a counter body. At 5 % humidity, the COF values were 0.02 and 0.03 for 58 and 68 at. % C coatings, respectively, which at 70 % humidity, increased to 0.14 and 0.08, respectively. A wear track depth of 100-500 nm and a wear rate as low as 5 x 10^{-7} m^3/Nm were reported, both decreasing with relative humidity and C content. The high temperature tests demonstrated the limit temperature of the coatings to be 250 ⁰C with a COF in the range of 0.01-0.04. Only the coatings with C content higher than 50 at. % survived the whole test duration at this temperature. The running-in period of the coatings decreased with increasing temperature. The wear rate also decreased at the higher temperatures. In high humidity tests, the centre of the wear track was covered by $MoSe_2$ but a 2nd layer of a mixture of $MoSe_2$ and graphitic carbon was also detected at various

locations, meaning that C also could play a role. The presence of C is against the previous report by the same authors [137]. As there is no passivation of carbon dangling bonds at higher temperatures, the MoSe$_2$ tribolayer played the key role in the friction reduction.

The tribological analysis was expanded by testing Mo-Se-C coatings in different sliding environments, in a rotating pin-on-disk tribometer using 100Cr6 steel ball as a counter body [78]. C-alloying of 47 and 61 at. % were used in this study. Three different applied loads i.e., 2, 5, and 10 N were used for a total sliding duration of 1000 cycles, in each case. In dry Ar, dry nitrogen, dry air (RH < 1 %) and ambient air (RH= 55-60 %) the achieved COF values were in the ranges of 0.01-0.05, 0.02-0.05, 0.02-0.05 and 0.05-0.1, respectively. As expected, the COF decreased with increasing applied loads. The low COF was attributed to the reorientation of MoSe$_2$ platelets and the tribolayer formation inside the contact zone.

Previous literature explains the deposition and tribological performance of Mo-Se-C coatings deposited by RF sputtering of composite target but DC sputtering is yet to be investigated. The reactive and the co-sputtering from individual targets have never been explored at all. Tribological performances under longer duration and low applied contact stresses is also missing. The available research on Mo-Se-C demonstrates that the influence of environmental fluctuations is considerably lower compared to other TMD-C systems, which can be attributed to its higher stability in ambient air atmospheres. Also, their tribological properties in vacuum and dry environments are quite similar. The chalcogen / metal atom ratio for MoSe$_2$ is higher than for all the other TMD-C coatings. The microstructure of Mo-Se-C coatings displayed MoSe$_2$ crystals / platelets dispersed in an a-C matrix which provides additional benefits for easy shear properties. Contrarily, the hardness of Mo-Se-C coatings is comparatively lower in relation to other TMD-C systems, needing, then, to be enhanced. Moreover, to get a higher Se/Mo ratio, higher C-alloying is necessary which is also an inverse trend to other TMD-C systems when deposited by co-sputtering.

Considering, (i) the improved performance in diverse environments, (ii) the much higher Se/Mo ratios than with other TMDs, (iii) the much favourable microstructure, and,

(iv) the less probability of formation of hard carbides (due to the higher Se/Mo ratio), the Mo-Se-C system must be explored in detail. The synthesis should be carried out using the more industrially favourable DC sputtering. As explained earlier, the co-sputtering of individual targets provides easier and greater control over the deposition parameters, so, this approach must be preferred. In short, by the combination of the intrinsic properties of the Mo-Se-C system with a proper deposition approach, these coatings can be optimized for actual industrial needs in diverse environments.

2.3. Research gap

The development of a coating system applicable in all ambient air, dry, and vacuum conditions, at room and high temperatures, by providing highly stable long-term low friction and wear properties is a continuous updated need. Furthermore, considering only space applications, the coatings must be capable of sustaining cyclic environments, as satellites for example, since they remain in coastal regions before their launch. From the literature analysis, C-alloyed TMDs can be suitable candidates for such a coating system. Although the existing research on TMD-C systems is vast, it lacks an organized structure. A detailed analysis has been reported on the W-S-C system. The other TMD-C researches, however, also require an organized investigation, in particular the $MoSe_2$ subset, which remained unmapped to a considerable extent. The literature reports many incongruencies in relation to the microstructure, stoichiometry, compactness, hardness, and COF for the reported TMD-C coatings, as can be assessed in the above summarizing tables, even when the same deposition conditions and testing techniques are used. Thus, the analysis of the reasons, for an unsuitable tribological performance of TMD-C coatings, attributed to the low coating stoichiometry, the low hardness, and the complex nanocrystalline (micro)structure must also be performed before the optimization of any coating system. For instance, the low friction and wear are related to TMD platelets formation and their reorientation but the literature is lacking knowledge regarding the mechanism behind the formation of these platelets which, thus, requires a thorough examination. Likewise, it must be kept in mind that the low stoichiometry, if overcome, can potentially enhance the tribological performance of the coatings, as in some cases, the low friction tribolayer may

not form due to the low chalcogen content. The long duration sliding efficiency can only be known by testing coatings for higher sliding distances, a critical point mostly ignored in the literature. The science behind the tribolayer evolution with the number of sliding cycles and the chemistry in the wear track also needs to be explored for a better understanding of the long-term industrial applicability.

Another important point missing in the literature is the mechanism of the tribolayer formation. An in-depth study should be performed to understand if the widely accepted theory of tribolayer formation based on the TMD crystallization / reorientation, inside the coating material near the contact zone, is the only one governing the frictional behaviour or if other mechanisms can be present. Such knowledge may further help in the development of a highly optimized TMD-C system. Another very crucial and majorly ignored issue is the tribological testing at low contact pressures (Hertzian contact stress < 150 MPa). As per the actual industrial requirements, the testing at low contact pressures needs to be carried out to be representative of those situations. Overcoming these deficiencies and proceed to the coating optimization will act as the main steps towards the upscaling and the industrial implementation of the coatings. As already mentioned, the less explored Mo-Se-C coatings have the potential to overcome many drawbacks of the Mo-S-C and W-S-C coatings; therefore, this research will focus on a comprehensive study of the Mo-Se-C system only.

2.4. Aims and objectives

PVD is a technique of selection to produce lubricious coatings due to the easy control of the deposition parameters which can, then, tailor the chemical composition, microstructure, crystal structure, and mechanical properties which, in turn, play a vital role in determining the tribological performance of these coatings. The deposition and the lab-scale optimization, utilizing PVD magnetron sputtering, as well as a very detailed characterization of the C-alloyed $MoSe_2$ coatings, will be the basis of this research. The optimization will be targeted to make the coatings capable of an efficient low friction performance in diverse sliding conditions of atmosphere, applied contact pressures, number of sliding cycles, sliding speeds, etc. The literature suggests that the low friction

can be achieved by an envisaged nanostructure consisting of TMDs nanocrystals embedded in an amorphous carbon matrix. Thus, the coatings will be optimized at lab scale to achieve dense, compact, and close to stoichiometry and, finally, low friction using a systematic study. DC sputtering of Mo-Se-C has never been explored, even if it is a more industrially favourable way of depositing coatings; thus, this method will be preferentially adopted for the development. Alternatively, RF sputtering will also be applied for comparison purposes. Co-sputtering of multi targets will be utilized to achieve better control over the sputtered material. The step-wise division of the objectives and tasks is as follows:

- First-ever trial for depositing Mo-Se-C coatings using DC magnetron sputtering from 2 separate targets to study the influence of this deposition approach and the C content on the Se/Mo ratio, crystal structure, microstructure, adhesion to the substrate, hardness, and tribological properties. The effects of the substrate bias on all the above-mentioned properties will also be studied. The tribological analysis will be carried out in ambient air and dry N_2 atmospheres.

- Based on the results achieved in the first trial, a comparative study between DC and RF magnetron sputtered Mo-Se-C optimized coatings will be carried out to further enhance the Se/Mo ratio, compactness, structure, and hardness. Low C-alloying will be utilized to achieve higher Se/Mo ratios and higher $MoSe_2$ crystallinity. Emphasis will be given to the achievement of a microstructure consisting of nanoparticles or platelets of $MoSe_2$ embedded in an amorphous carbon matrix. The literature states that this nanostructure if achieved is ideal for low friction sliding properties. The absence of research studies referring to the mechanism behind the formation of TMD platelets / crystals in the C matrix is also a motivation for the current study. To check the microstructure, the coatings will be characterized using XRD and TEM.

- After optimization, the tribological analysis will be carried out in diverse sliding environments. Most of the TMD-C coatings do not perform well in ambient air conditions; so, this part will get deep attention. The achieved results will, then, be compared to the sliding behaviour in dry nitrogen and high temperature, to check the coating efficiency under diverse environmental conditions. The ambient air tribological testing will be carried out at different number of sliding cycles for long-

term stability analysis. The evolution of the tribolayer with an increasing number of sliding cycles and C content will be explored. There have been some incongruencies about the role of TMD in ambient air sliding conditions; therefore, to unfold the role of C or $MoSe_2$ during sliding, the wear tracks will be investigated. For this, exhaustive TEM studies will be carried out. The analysis of the mechanisms behind the tribolayer formation will also be explored.

- Finally, to check the applicability of this system as a universal solid lubricant, the tribological analysis will be carried out under various conditions including high and low contact pressures, ambient air and vacuum environments, high and low sliding speeds, and shorter and longer sliding duration testing.

Achievements of the above-mentioned milestones are expected to overcome the hindrances of a stable and efficient industrially applicable solid lubricant. These distinct objectives will converge towards sorting out the optimum parameters for the Mo-Se-C system deposition creating the conditions for its upscaling for industrial applications.

Chapter III

3. MATERIALS AND METHODS

This chapter is focused on the experimental details related to the deposition and characterization of Mo-Se-C coatings. The substrate materials, the deposition setups, and procedures adopted for the production of the coatings will be discussed. Due to the deep discussion of the importance of the deposition conditions on the properties of the coatings in the chapters of results, an overview of the sputtering technique will also be presented in this section. Finally, a brief description of the characterization techniques and the conditions utilized for the analysis of the coatings is included.

3.1. An overview of sputtering

Sputtering is a deposition technique where high energy particles (positive ions) are bombarding a target surface, in a vacuum, to eject atoms or ions from the target material. The ejected material is then transported in the deposition chamber and deposited over the substrates. The process is not as simple as it seems. Several parameters must be met to achieve the required sputter efficiency. The efficiency of the sputtering process, as a deposition technique, is related to the deposition rate, i.e. the number of depositing species arriving at the substrate. This rate depends on 3 different efficiencies, (i) the sputtering rate at the target i.e. the number of atoms ejected from the target per ion bombardment, (ii) the transport of the species from the target to the substrate, which depends on the number and intensity of the collisions occurring in the interelectrode spacing and, (iii) the adsorption of the depositing species to the growing film. In any of these processes, there is an unfindable number of parameters influencing directly each one. For example, for (i) the voltage and current at the target, the intensity of the magnetic field, the electrical characteristics of the target material, the type of applied current (DC, pulsed-DC, RF, HiPIMS), etc, for (ii) the discharge pressure, the interelectrode distance, the mean free path of the species, the charge of the sputtered species, etc, for (iii) the substrate temperature, the substrate bias, the rotation of the substrate holder, etc [139]. All these parameters not only affect the deposition efficiency but also have an enormous effect on the final properties of the coatings.

Sputtering was first observed in the 1850s but was scarcely explored until the 1940s when diode sputtering was used for commercial coating deposition. The low deposition rates made it with less economical interest. Then, the researchers were compelled to find alternative approaches that could increase significantly the deposition rate. Magnetron sputtering was introduced in 1970 and provides higher deposition rates for metals, alloys, and compounds. A magnetic field is applied to the target material such that electrons can be entrapped in the magnetic field lines creating drift currents. The localized trapping of electrons near the target surface creates an endless racetrack, increasing the chances of ionizing gas atom collisions. The higher ionization efficiency increases the number of ions available, leading to the decrease of the plasma impedance and reducing the magnetron operating voltages compared to conventional diode sputtering (600 V vs several kV, respectively). Consequently, the target erosion rate increases due to the higher ionization which leads to an increased ion current density on the target [139,140]. Therefore, magnetron sputtering offers various advantages over diode sputtering including:

- higher deposition rates
- excellent coverage of steps and valleys
- higher uniformity in the coated surfaces
- higher purity coatings
- better coating adhesion
- easier sputtering of metals, alloys, and compounds.

There are several variants of the magnetron sputtering method depending on the power supply used for the targets. Each variant possesses its pros and cons. The use of each power supply depends on the intended properties required for the final product. As the work is focused on RF and DC magnetron sputtered TMD-C coatings, a brief introduction to both types is presented below.

The simplest of the magnetron deposition techniques is the DC one which is mainly used for the deposition of metallic materials and / or non-metallic compounds if a reactive atmosphere is used. DC power supplies are simpler to manufacture, so they contribute to make the cheapest magnetron sputtering setups. In DC magnetron sputtering, the target is directly connected to a DC electric current; therefore, it preferentially has to be an electric conductor to make available an electrical field to the chamber. During DC sputtering, the

working gas is ionized. As a result, many positive ions are accelerated towards the target by the electric field, bombarding it, and producing sputtered species. Simultaneously, secondary electrons are emitted from the target which will be necessary for keeping the ionization in the gas discharge. In the case of metallic materials, deposition rates of several thousand nanometres per minute can be achieved. DC magnetron sputtering provides to the coatings, good adhesion to the substrate, minimal defect density, good uniformity, and thickness control of the deposited coatings. The application areas include microelectronics, metallurgical coatings, decorative coatings among others.

To overcome the drawbacks of DC magnetron sputtering, especially the inability to sputter from insulating or semi-conductor targets, RF sputtering is used. Alternating current at high frequency (13.56 MHz) is used in RF magnetron sputtering. During the negative electric field cycle, the positive ions are accelerated to the target and sputter it while, during the positive field, the charged positive ions on the surface of the target are neutralized by the attracted electrons. Therefore, along with metals and insulators, dielectric materials can also be sputtered. During the application of RF power to the target, it is capacitively coupled and a DC (sheath) potential is developed on the surface. Due to the capacitive coupling, the electrode material can be an insulator, semiconductor, or metal. Due to the difference in the masses, ions and electrons travel different distances during every half cycle, but no net charge can be transferred to the electrode; then, an excess negative charge on the surface of the target biases negatively the electrode. This results in a net DC negative voltage on the target surface causing the bombardment to occur similarly to the DC magnetron sputtering. The main difference is that the oscillation of the electrodes in the plasma due to the alternating field increases the plasma density which may affect the final characteristics of the coatings. RF sputtering can be used for depositing superconductive coatings, dielectrics for the semiconductor industry, insulative coatings, hard and wear resistant coatings, and polymeric coatings. In the past few decades, low friction and wear coatings from compound materials are widely being manufactured using RF sputtering which exhibits good adhesion, uniformity, and homogeneity. Despite several advantages, RF sputtering is not cost-effective, involving complex matching networks setups and generators. Furthermore, the heat generated during the deposition of non-conducting materials requires special cooling systems for the targets. The sputter yield for ionic and

covalent materials is much less than metallic materials, leading to lower deposition rates when compared to the ones of metallic sputtering with DC currents [140,141].

3.2. Substrate materials

Three different kinds of substrates, polished high-speed steel (AISI M2, Ø20 x 3 mm), 100Cr6 steel (Ø25 x 7 mm), and monocrystalline Si (111) were used as substrates, allowing different types of coatings characterization (Table 3-1). The main properties of the substrates are presented in Table 3-2. Steel substrates were first ground in steps using emery papers from 180 up to 1200 grit sizes and then polished using diamond suspension (6, 3, and 1 microns respectively). Polishing results normally in a roughness (Ra) less than 0.02 µm. Before placement in the chamber, ultrasonic cleaning of all substrates was carried out in acetone and ethanol for 15 minutes each, to remove impurities on the surface.

Table 3-1: Characterization techniques and list of substrates used

Characterization	Substrate
Chemical Composition, Chemical Bonding, Morphology, Thickness, Crystal Structure, Hardness	Silicon
Critical Adhesion Loads, Unidirectional pin-on-disk	M2 Steel
Reciprocating pin-on-disk	100Cr6 Steel

3.3. Deposition techniques

As discussed earlier, Mo-Se-C coatings were never deposited either from separated $MoSe_2$ and C targets (co-sputtering) or by DC magnetron sputtering. So, the first step was to try the deposition using a simple 2 targets set up in a Hartec® deposition chamber. The coatings were thoroughly characterized to establish the properties correlation with the literature on TMD-C coatings. Later, the depositions were moved for an ATC-Orion 8 (AJA International) apparatus, which was equipped with 4 targets. This chamber was selected to overcome the drawbacks encountered for the $MoSe_2$ deposition in the Hartec® chamber, which are as follows: (i) to allow to deposit an adhesion interlayer, (ii) to overcome the low sputtering yield of carbon, (iii) to reduce the reflected Ar neutrals growing film bombardment, and, (iv) to increase the overall coating deposition rate by

continuous confocal plasma sputtering. The details of the coatings deposition in each case are presented in the next subsections.

Table 3-2: Main properties of the substrates

100Cr6 steel - Composition	
Element	**Content (at. %)**
Iron, Fe	Balance
Chromium, Cr	1.30 - 1.60
Carbon, C	0.98 - 1.10
Manganese, Mn	0.250 - 0.45
Silicon, Si	0.150 - 0.30
Molybdenum, Mo	≤ 0.10
Aluminum	≤ 0.05
Copper, Cu	≤ 0.30
Sulfur, S	≤ 0.025
100Cr6 steel – Mechanical properties	
Elastic modulus	190 - 210 GPa
Hardness	62 - 65 HRC
M2 steel - Composition	
Element	Content (at. %)
Iron, Fe	Balance
Chromium, Cr	3.75 – 4.50
Carbon, C	0.78 – 0.88
Manganese, Mn	0.15 – 0.40
Vanadium, V	1.75 – 2.20
Molybdenum, Mo	4.50 – 5.50
Tungsten, W	5.50 – 6.75
Silicon, Si	0.20-0.45
Sulfur, S	≤ 0.03
M2 steel - Mechanical properties	
Elastic modulus	190-210 GPa
Hardness	62-65 HRC

3.3.1. Mo-Se-C sputtering using 2 targets (Hartec® chamber)
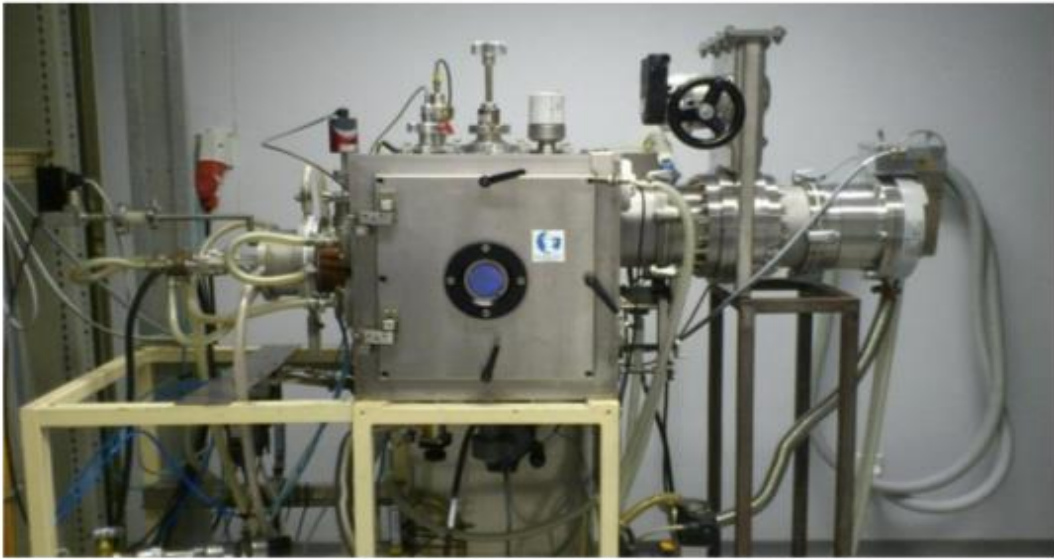
Figure 3-1: Hartec® deposition chamber

DC magnetron sputtered Mo-Se-C coatings were deposited in the Ar gas atmosphere in a Hartec® deposition unit (Fig. 3-1), equipped with 2 targets, graphite (150 mm x 150 mm, 99.99 % purity) and $MoSe_2$ (139 mm x 139 mm, 99.99 % purity). The samples were placed on a rotating substrate holder (18 rev/min) positioned at 100 mm from each target. The substrate holder was parallel to the surface of the target and passed, alternatively in front of each target. It means that the sputtered material arrived at the growing film was intermittent. The schematic is shown in figure 3-2.

Figure 3-2: Top-view schematic of the targets (cathode 1: graphite, cathode 2: $MoSe_2$) and substrate arrangements in Hartec® chamber

Before the depositions, systematic sputter cleaning of the substrates and targets was carried out in the Ar gas atmosphere by maintaining a pressure of 0.5 Pa. At first $MoSe_2$ target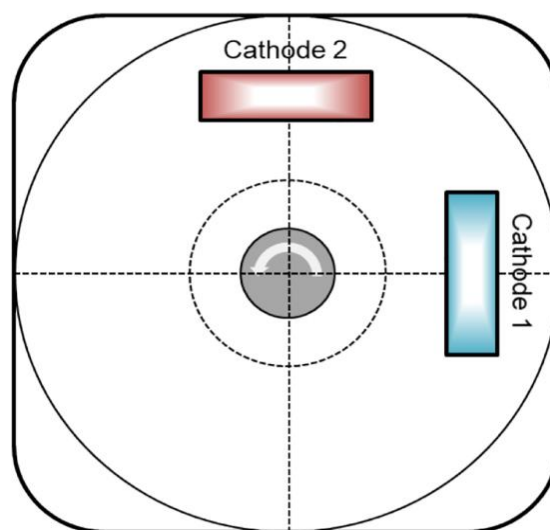 was sputter cleaned for 15 minutes with a DC power (P=200 W) with a shutter in front, to avoid cross-contamination. Meanwhile, the etching of the substrates was also performed, by applying pulsed DC power, V= 400 V, f= 250 kHz, and pulse-on time= 1600 ns. The power on the $MoSe_2$ target was turned off after 15 mins and the DC power to C was switched on (P= 150 W). The shutter was moved in front of the C target. The conditions for the substrate etching were kept the same. After more 15 mins, the sputter cleaning of C and the etching of the substrates were terminated. After cleaning, the depositions were carried out at the same pressure of 0.5 Pa. The power to $MoSe_2$ target was kept constant for all depositions while the power applied to C target was varied to achieve a series of depositions with different C contents. The effects of DC and pulsed DC substrate bias on the coating properties were also studied by depositing a set of coatings with different applied substrate bias voltage, coatings were compared to the ones deposited without substrate bias. A list of all deposited coatings, as well as the main deposition parameters are shown in Table 3-3. From now onwards, the coatings will be named as presented in Table 3-3.

Table 3-3: Main Deposition parameters used for depositing Mo-Se-C Coatings using 2 targets

Coatings	MoSe₂ Power (W)	Carbon Power (W)	Bias (V)	Time (min)
Pure MoSe₂	200	-	-	60
330C	200	330	-	90
400C	200	400	-	90
500C	200	500	-	120
400C(50V)	200	400	50	120
400C(70V)	200	400	70	120
400C(90V)	200	400	90	120
400C Pulsed 90V	200	400	p-90	120

3.3.2. Mo-Se-C sputtering using 4 targets (ATC-Orion 8 chamber)

Figure 3-3: ATC-Orion 8 (AJA International) deposition chamber

The Mo-Se-C solid lubricant coatings were deposited by balanced magnetron sputtering using an ATC-Orion 8 (AJA International) deposition chamber (Fig. 3-3) equipped with 4 targets. Two different setups of targets and power supplies were used. In case 1, the DC power supply was connected to two carbon targets (99.99%) and one $MoSe_2$ target (99.99%) while, the fourth target was powered by RF power supply and was assigned to Cr (99.99%). In case 2, the DC power supply was connected to two carbon targets (99.99%) and one Cr target (99.99%) while, RF power supply target was assigned to the $MoSe_2$ target (99.99%). This combination was used to see if the RF sputtering of $MoSe_2$ can further enhance the properties of the Mo-Se-C system. In both cases, two carbon targets were selected since carbon has a very low sputtering yield. The Cr target was used for the deposition of an interlayer and gradient layers to enhance the adhesion of the coatings. Each target had a diameter of 50.2 mm. The target to substrate distance was ~80 mm and the targets were tilted 30 º with respect to the substrate normal (Fig. 3-4) to enhance the deposition rate, homogeneity of coatings and to provide continuous sputtering on to the

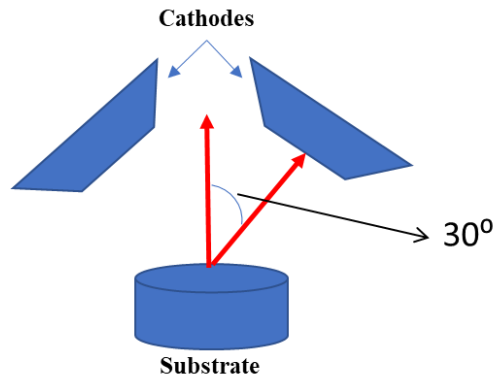substrates. The substrate holder was rotated at a speed of 10 rpm to enhance the homogeneity in the coatings.

After placing cleaned substrates, the chamber was pumped down to a base pressure of 5×10^{-5} Pa. Before deposition, sputter cleaning of the targets and etching of the substrates was carried out in Ar atmosphere, for 30 minutes, by maintaining an overall chamber pressure of 1.33 Pa, with shutters in front of the targets. A power of 250 W was applied to carbon, $MoSe_2$, and Cr targets for cleaning while 40 W RF power was used for substrate etching. After cleaning, the pressure was decreased to 0.5 Pa for underlayers and final coating deposition. The total time for the interlayer, gradient layer, and final Mo-Se-C coating deposition for cases 1 and 2 was 110 and 210 mins, respectively, to achieve a coating thickness close to 2 µm. The power applied to the $MoSe_2$ target was kept constant in all cases, while the composition was varied by applying different powers to the carbon targets. In the case of the interlayer, 250 W power was applied to the Cr target for 10 minutes and, then, for the next 10 minutes, the Cr target power was gradually decreased to 0 W, while the power to each carbon target was progressively increased up to 250 W. For the last 5 minutes of the gradient layer, the power to $MoSe_2$ was also progressively increased up to 250 W. Then, the power to the Cr target was turned off and the power to the other targets was adjusted as shown in Table 3-4. For the coatings deposited with substrate bias, an RF voltage of -50 V was applied. In the case of DC and RF sputtered pure $MoSe_2$ coatings, the deposition time was 60 mins and 120 mins, respectively, since the sputtering rate with the RF power supply is lower. For pure coatings, Cr interlayers were not deposited. Instead, the substrate bias was applied initially for 2 mins, in order to have a Mo rich interlayer. The coatings will be denominated as shown in Table 3-4.

Table 3-4: Main deposition parameters used for depositing Mo-Se-C coatings using 4 targets

Coating	MoSe$_2$ Power (W)	Carbon Power (W)	Bias (V)	Time (min)
Case 1 - DC sputtering of MoSe$_2$				
DC Pure MoSe$_2$	270	-	-	60
DC324	270	324	-	110
DC540	270	540	-	110
DC676	270	675	-	110
DC540(50V)	270	540	50	110
Case 2 - RF sputtering of MoSe$_2$				
RF Pure MoSe$_2$	270	-	-	120
RF170	270	170	-	170
RF270	270	270	-	210
RF340	270	340	-	170
RF270(50V)	270	270	50	170

3.4. Fundamental characterization of the coatings

The main characterization techniques implemented during the investigation of the coatings of this thesis are:

3.4.1. Chemical composition

Wavelength dispersive spectroscopy (WDS-Oxford Instruments) operated through INCA software was used to determine the chemical composition of the coatings. The detector was attached to the field emission scanning electron microscope (FESEM, SEM-Zeiss Merlin). The known composition standards acquired from Micro Analysis Consultants were used for the calibration. An accelerating voltage of 15 kV was selected for the analysis.

3.4.2. Coating morphology and thickness

The surface and fractured cross-sectional morphologies were analysed using FESEM (SEM-Zeiss Merlin). The top surface was observed as it is while for cross-sections, a freshly cut surface was analysed. For imaging, 25 kx and 50 kx magnifications were selected. The coating thickness was measured by FESEM from the cross-sectional images.

3.4.3. Structural analysis

X-ray diffraction (XRD-X´ Pert Pro MPD diffractometer) operated in grazing (3⁰) mode utilizing copper $K_{\alpha 1}$ radiation (λ=1.5406 Å), was used for the crystal structure analysis and to check the presence of $MoSe_2$ and Mo-C nanocrystals in the C matrix.

3.4.4. Microstructural analysis

High-resolution transmission electron microscopy (HRTEM) images were acquired for the thin films deposited on copper TEM grids. The deposition time for thin films was set to 1.5 min to achieve a thickness of 25-40 nm. The observation was performed in a Jeol JEM 2100 using 200 kV excitation voltage.

3.4.5. Chemical bonding analysis

Raman and X-ray photoelectron spectroscopies (XPS) were used for the chemical bonding analysis. Raman spectroscopy was performed in a wavenumber range of 100 to 1800 cm^{-1}, using 532 nm laser (XploRA, Horiba) and 488 nm laser (LabRam HR Horiba Jobin Yvon). Care was taken in selecting the laser power and acquisition time to avoid coating damage.

XPS was performed using Kratos Axis Ultra HAS with monochromatic Al Kα X-rays (hν= 1486.6 eV). The power of the X-ray source was set to 90 W and a charge neutralizer was used during measurements. The survey spectra were obtained by setting the pass energy at 80 eV with a step of 1 eV and a dwell time of 200 ms. The high-resolution spectra of the regions of interest were obtained using a pass energy of 40 eV with a step of 0.1 eV and a dwell time of 600 ms. Sputter etching was performed using an Ar$^+$ ion gun operated at 2.2 keV and a current density of 2.2 μA/cm^2. The data acquisition was done at pressures lower than 10^{-6} Pa. The data analysis was done using the CasaXPS software. The

baselines of the spectra were obtained using the Shirley method and peak fitting was done using Gaussian-Lorentzian functions.

3.4.6. Mechanical property investigation

The hardness measurements were performed by nanoindentation (Micro Materials Nano Test platform), with a Berkovich diamond indenter. The load (5 mN) was selected to avoid the influence of the substrate since indentation depth remained less than 10 % of the coating thickness. A total of 32 indentations were performed at two different positions and the average was calculated.

The coating adhesion on the M2 steel substrates was evaluated in a scratch-testing apparatus (CSM Revetest). The specimens were scratched as the normal force was progressively increased from 2-50 N, using a Rockwell indenter (tip radius=0.2 mm), a scratch speed of 10 mm/min, and a loading rate of 100 N/min. The critical loads were determined by analysing the scratches in an optical microscope. The coating adhesive properties were quantified using the critical load value corresponding to the load for which the first exposure of the underlying layers occurred.

3.5. Tribological testing and wear track investigation:

3.5.1. For 2 target depositions

For the coatings deposited using 2 targets (Hartec® Chamber), the tribological testing was performed in an Optimol SRV friction and wear equipment under reciprocating sliding conditions against a 100Cr6 steel ball of 10 mm diameter. Before testing, both disc and ball were ultrasonically cleaned in acetone for 15 minutes. The tests were performed at 25 °C in an ambient air atmosphere (RH 0 ~35-45 %) as well as in dry nitrogen atmosphere. The reciprocating frequency and stroke length were set to 25 Hz and 2 mm, respectively, resulting in a sliding speed of 0.1 m/s under 30 N applied load. In any contact pair, the initial Hertzian contact stress was higher than 1.2 GPa. The test duration was set at the maximum sliding distance of 180 m, resulting in 90000 cycles. The experiments were repeated twice to ensure repeatability. The wear profiles were then taken by stylus profilometer (Surftest SJ-500) and the wear track images and elemental maps were acquired using energy dispersive spectroscopy (EDS) detector (Oxford Instruments X-

Max) attached to FESEM (SEM-Zeiss Merlin). Here, the data acquisition was carried out using Aztec software (Oxford Instruments). The specific wear rates were later calculated using the wear volume, applied load, and sliding distance.

3.5.2. For 4 target depositions

For the DCMS coatings deposited using 4 targets (ATC-Orion 8- AJA International chamber), the detailed tribological studies were performed in ambient air, dry nitrogen, and at 200 ⁰C, against 100Cr6 steel counter body. The unidirectional tribological tests were performed using the CSM pin-on-disk tribometer. The tests were performed at room temperature in relative humidity of 35-45 %. A load of 10 N and a sliding speed of 0.1 m/s was used. In any contact pair, the initial Hertzian contact stress was higher than 1 GPa. The tests were performed at three different numbers of cycles (5000, 25000 and 100000 cycles) to: (i) observe the difference between the running-in and the steady-state; (ii) check if the coatings are capable of a long duration sliding; (iii) analyse if they can be upscaled to industrial components requiring low friction and high wear resistance and, (iv) to understand the evolution of the tribolayers with the sliding cycles. The experiments were repeated three times (except for 100000 cycle tests, for which two repetitions were performed) to check repeatability. The wear track profiles of the coatings were taken using a stylus profilometer (Surftest SJ-500) and, the specific wear rates were calculated. To calculate the specific wear rates of the counter body, the profiles of the scars were measured using a 3D optical profilometer (Alicona Infinite Focus). All the coatings wear tracks and the counter body wear scars were observed using optical microscopy (DM4000 M LED). The wear tracks of selected coating samples were analysed in FESEM (SEM-Zeiss Merlin). Elemental mapping of the wear track was also carried out using an EDS detector (Oxford Instruments X-Max) attached to FESEM (SEM-Zeiss Merlin), to check for any possible delamination. Raman spectroscopy was performed to check: (i) the presence of different phases in the wear tracks and the wear debris, (ii) the distribution of $MoSe_2$ or C in different regions of the wear track and in the tribolayer, and, (iii) the evolution of the composition of the tribolayer with the sliding cycles. For the HRTEM analysis of the wear track in cross-section (to access the sliding contact interface), lamellae were prepared by focused ion beam (SEM-FIB, Helios Nanolab 600i) using Ga+ ions. To protect the surface from damage during ion etching, a protective layer of Pt and C was first deposited. The ion beam energy was varied from 3 kV to 30 kV for thinning various regions; in the end, an energy

of 1 kV was used to minimize the sample damage. For HRTEM imaging and scanning TEM (STEM) EDS mapping, a JEOL ARM 200F (cold FEG) was used. The beam size in STEM mode was less than 1 nm.

Further, to analyse the sliding behaviour in different atmospheres, reciprocating sliding tests (Optimol SRV friction and wear equipment) on selected specimens were performed in ambient air (relative humidity ~35-45 %), dry nitrogen (relative humidity less than 5 %), and at high temperatures (200 ⁰C). The tests were carried out for 25000 cycles under 10 N applied load and 0.1 m/s sliding speed. In any contact pair, the initial Hertzian contact stress was higher than 1 GPa. The wear tracks were observed in FESEM (SEM-Zeiss Merlin). The wear profiles of the coatings and the counter body scar were analyzed taken using a 3D optical profilometer (Alicona Infinite Focus), and later the specific wear rates were calculated.

3.5.3. Universal sliding behaviour analysis of the coatings

The coatings deposited in the 4-target setup (ATC-Orion 8- AJA International chamber) were also tested at low contact pressures, low sliding speeds, and in vacuum environment to analyse whether the coatings show consistent frictional properties under variable conditions. For ambient air and vacuum tribological testing, a reciprocating tribometer with a 100Cr6 steel cylinder (10 mm x Ø10 mm) on flat arrangement was used. A 5 mm stroke length and a 2 mm/s sliding speed were selected as the parts move much slower in space [143]. A high vacuum condition (10^{-6} mbar) was used for the vacuum tests. Although the initial contact pressure mostly reported in the literature is above 500-600 MPa (with a claim that coatings are good for aerospace applications), in actual industrial applications the pressure can vary from those high values down to less than 100 MPa [27,144]. So, a contact pressure of ~85 MPa was used for low contact pressure studies. To further simulate the earth environment tests, for parts that operate at high contact pressure (e.g. ball bearings), unidirectional ball on disk sliding tests were carried out in ambient air, under ~1010 MPa contact pressure and 0.1 m/s sliding speed, against 100Cr6 steel ball (Ø10 mm). The low contact pressure tests were carried out up to 10000 cycles while 25000 and 100000 cycles were selected for high contact pressure tests. In the latter case, the idea was to examine the coating stability for longer sliding durations. In all tests, the coatings were sliding until the steady-state regime was reached. In short, these tests not only

replicated the actual industrial needs (especially aerospace industry) but also confirmed these coatings as a universal solid lubricant for terrestrial and non-terrestrial sliding conditions.

Chapter IV

4. DEPOSITION OF Mo-Se-C COATINGS USING 2 TARGETS BY DCMS

4.1. Introduction

This chapter is dedicated to the first-ever deposition of Mo-Se-C coatings using direct current magnetron sputtering of 2 separate targets, in a conventional deposition chamber (Hartec® chamber). The use of 2 targets is a more industrially acceptable way of depositing thin coatings by sputtering. The main advantage is the easy control of the coating composition by varying the applied power to both targets. DC magnetron sputtering of low friction Mo-Se-C coatings as well as the co-sputtering of 2 individual targets (by any power supply) has not been carried out yet.

In this chapter, the effects of the carbon concentration and substrate bias on the properties of Mo-Se-C coatings will be presented. The main objective is to shed some light on the interrelation between the deposition parameters and the chemical composition, microstructure, crystal structure, chemical bonding, and mechanical properties of the Mo-Se-C coatings. The section also includes the tribological performance of the coatings in ambient air and dry nitrogen atmospheres. Special attention has been paid to the effects of the substrate bias on the coating properties and performance. This work is a first step towards the understanding of the processing and the properties of DC sputtered Mo-Se-C coatings for sliding in both inert and ambient air atmospheres.

The details about the deposition procedure and the fundamental characterization of these coatings were discussed already in sections 3.3.1 and 3.4, respectively. The tribological testing approach was described in section 3.5.1. This chapter is supported by the publication attached in annex A.

4.2. Results and discussion

4.2.1. Chemical composition and deposition rate

The chemical composition of the deposited coatings measured by WDS is shown in Table 4-1, along with the Se/Mo ratio, thickness, and deposition rate. All coatings presented a small amount of residual oxygen that may have accumulated in growing coatings from either the residual atmosphere of the chamber or the contamination in the porous $MoSe_2$ target [78,145]. With the increase in the power applied to the C target, the percentage of C in the coatings increased.

The pure $MoSe_2$ coating displayed the highest deposition rate of ~38 nm/min (Table 4-1) due to its highly porous and columnar morphology (see Fig. 4-1). When the C target was sputtered in the chamber, to deposit Mo-Se-C nanocomposite coatings, the deposition rate decreased to ~18 nm/min for 330C coating (330 W power), as compared to the pure $MoSe_2$ coating. This decrease is related to the higher compactness and the lower porosity of the coating. With increasing C target power, the additional sputtered C atoms made the deposition rate to increase up to ~21.1 nm/min. Further increase in the power to 500 W (for 500C coating) resulted in a small decrease of the deposition rate down to ~20.8 nm/min which may be related to the increase in the voltage on the C target from 530 V for 400C coating to 560 V for 500C coating. With this increase in the voltage, more energetic Ar neutrals are produced and, thus, enhancement of the re-sputtering of atoms from the growing coating can occur.

The carbon content around 50 at. % (400C coating) was selected to deposit the coatings with negative substrate bias. With the application of substrate bias, there was no specific trend for the carbon percentage in the coatings. The deposition rate showed a decrease after the application of the substrate bias, which may be related to the re-sputtering of atoms from the growing coatings due to the progressive increase of their Ar ions bombardment. The substrate bias also helps to increase the compactness due to an easier ad-atom mobility effect [146]. The increased ion bombardment resulted in a decrease of the Se/Mo ratio (see Table 4-1). The Se/Mo ratio decreased from 1.88 in the coating without substrate bias (400C) down to 1.44 in the 90 V pulsed bias one. The lower Se/Mo ratio can also be related to the preferential re-sputtering of Se from the growing coating as explained in literature for different TMDs. When sputtering a compound, the lighter element, here

Se, is preferentially sputtered [78]. The effect of ion bombardment on the Se/Mo ratio was enhanced in the pulsed substrate bias deposition. With pulsed DC 90 V, the plasma was more confined near the substrate enhancing the ion bombardment and thus leading to higher re-sputtering of Se. However, overall, the Se/Mo ratio was much closer to the $MoSe_2$ stoichiometry as compared to other TMD-C nanocomposite coatings reported, in particular WS_2, WSe_2, and MoS_2 [25,43,147,148]. In all these compounds the atomic mass of the elements is much more different than in $MoSe_2$, increasing the preferential sputtering rate of the lighter element [149].

In our previous work on Mo-Se-C coatings deposited by RF sputtering from composite C target with $MoSe_2$ pellets, we have reported a Se/Mo ratio of around 1.45 for a coating with 50 at. % C [78,136], as compared to 1.88 achieved in this study for the same carbon content (400C coating), both coatings were deposited without substrate bias. Again, this result can be understood by the higher plasma density close to the substrate existing in RF discharges [2,150]. Therefore, by DC co-sputtering of separate $MoSe_2$ and C targets, it is easier to keep the Se/Mo ratio close to stoichiometry, with the consequent advantages of either allowing to use higher bombardment of the growing coating (more compact coatings) or having higher Se/Mo ratios, known to induce a better friction behaviour [24].

Table 4-1: Chemical composition, adhesion critical loads, thickness and deposition rates of the deposited coatings

Coatings	C (at. %)	Mo (at. %)	Se (at. %)	O (at. %)	Se/Mo	Lc$_3$ – Critical Load (N)	Thickness (μm)	Deposition Rate (nm/min)
Pure MoSe$_2$	5±0.2	29±0.1	64±0.3	2±0.1	2.2	-	2.3	38.3
330C	44±0.6	19±0.2	34±0.3	3±0.1	1.79	9.2±0.4	1.6	17.8
400C	50±0.4	16±0.3	30±0.3	4±0.2	1.88	13±0	1.9	21.1
500C	60±0.3	13±0.2	24±0.2	3±0.1	1.85	17±0	2.5	20.8
400C(50V)	55±0.3	15±0.4	25±0.5	5±0.3	1.67	19.2±0.4	2.0	16.7
400C(70V)	51±0.5	17±0.1	28±0.3	4±0.1	1.64	12.5±0.7	1.8	15.0
400C(90V)	51±0.2	18±0.2	28±0.2	3±0.1	1.56	23±0.4	2.2	18.3
400C(p-90V)	55±0.4	18±0.2	26±0.2	1±0.2	1.44	16±0.4	2.3	19.2

4.2.2. Cross-section and surface morphology

The surface and fractured cross-sectional morphologies were analysed by FESEM. Selected cross-sectional and surface morphology micrographs are displayed in figure 4-1. The pure $MoSe_2$ depicted a columnar cross-sectional morphology with significant porosity, which is a typical feature of sputtered pure TMD coatings. Their sponge-like and highly porous surface morphology agrees with the cross-section. With the introduction of C, the columnar structure persisted but with a fairly dense morphology (Fig. 4-1 c)).
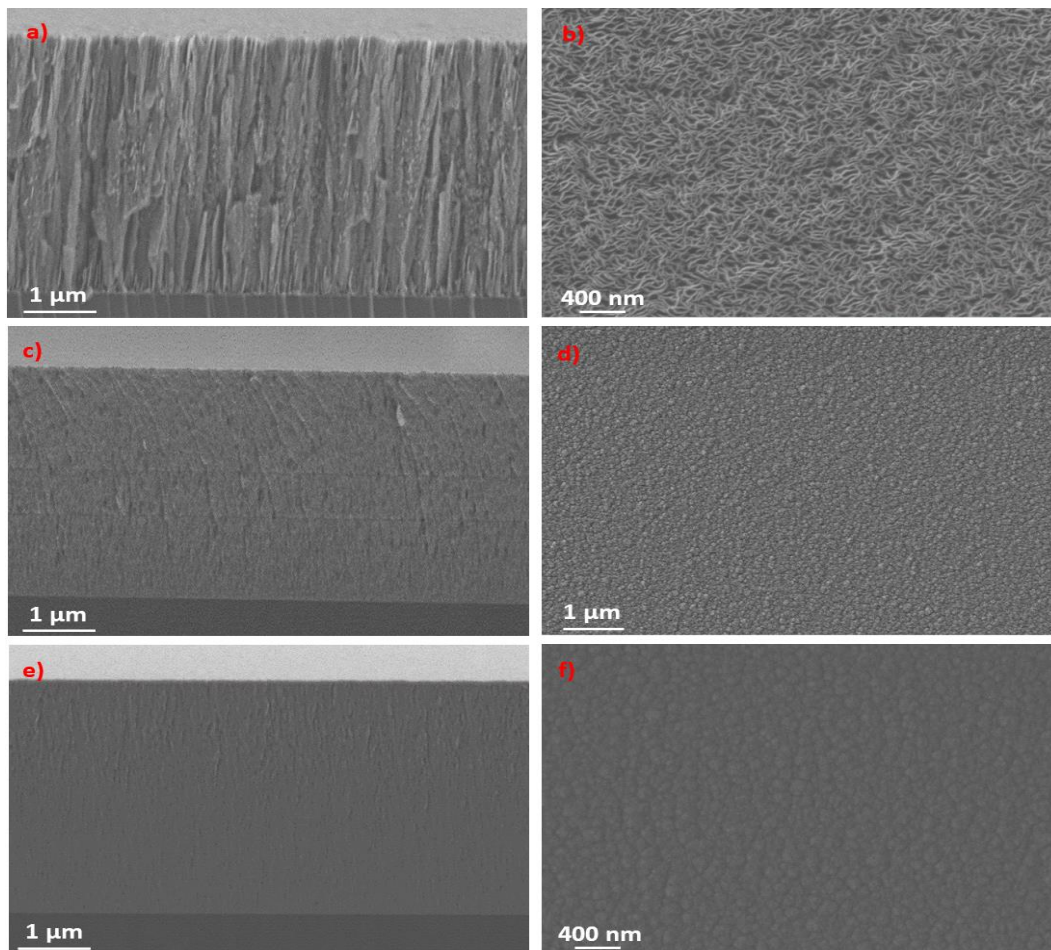

Figure 4-1: SEM cross-section images- a) Pure MoSe₂, c) 400C, e) 400(90V bias) and surface morphology images- b) Pure MoSe₂, d) 400C, f) 400(90V bias) of the coatings

The length of the columns decreased as well, and the growth occurred in a dendritic way. The surface of this coating showed fine grains with compact morphology (Fig. 4-1 d)). Further increase of the C content led to an increase of the compactness with less amount of spaces between the columns up to negligible voids and porosity are left. This is in accordance with previous literature on C-alloyed TMD nanocomposite coatings [24].

With the application of substrate bias to the 400C coating (50 at. % C), the compactness further increased with the 400C(50V) coating having a dense structure with small contributions of dendritic grain growth up to morphology with very less columns for the -70 V substrate bias coating. The coatings with -90 V (Fig. 4-1 e)) and pulsed -90 V substrate bias were the densest and the smoothest ones. With the application of the substrate bias, progressively more and more ions collide with the growing coating with higher energies resulting in the removal of impurities and more atomic coverage. The surface morphology was granular cauliflower-like for -50 V substrate bias coating and displayed no significant features with further increase of the substrate bias (Fig. 4-1 f)). As expected, the surface roughness decreased with the application of the substrate bias and the topographical details almost disappeared. The literature states that the densification and compactness of the coatings improve the adhesion, the mechanical properties, the resistance to environmental attacks, and the sliding properties [24,25].

4.2.3. Crystal structure

XRD patterns of the deposited coatings in grazing incidence angle mode are shown in figure 4-2. Only selected patterns have been displayed as all other coatings (with and without substrate bias) showed similar patterns. Pure $MoSe_2$ displayed peaks related to the typical sputtered and crystalline TMD coating structure (ICCD nº 087-2419). The broad peak at $2\Theta = 30\text{-}40^\circ$ corresponds to a turbostrating stacking of 10L planes (L=1,2,3….) as explained by Weise et al. [147]. The combined peaks at $2\Theta = 55\text{-}55.5^\circ$ correspond to (110) peak of $MoSe_2$ and Si (311) peak from the substrate as denoted in figure 4-2. The (002) peak at $2\Theta = 13^\circ$ related to nearly parallel orientation of the basal planes of $MoSe_2$ crystals showed very low intensity.

With the introduction of C, the crystallinity of the coatings decreased, displaying only broad peaks (except $2\Theta = 55^\circ$ peak corresponding to Si (311) substrate). XRD of DC and pulsed DC substrate bias coatings gave rise to a pattern similar to those of the coatings without substrate bias (see 400C(90V) as an example in Fig. 4-2). These coatings, highly compact, as observed by SEM, are X-ray amorphous in nature. No evidence of the presence of nanocrystals of Mo-C was found. Although XRD has limitations with phases having very low grain sizes, if existing, nanograins should be very small to be detected by XRD analysis. Similarly, the patterns, on one hand, clearly correspond to amorphous carbon but

the coatings have very small nanocrystals of MoSe$_2$ (in broad peak region) whose presence is evident from HRTEM and Raman spectroscopy studies.
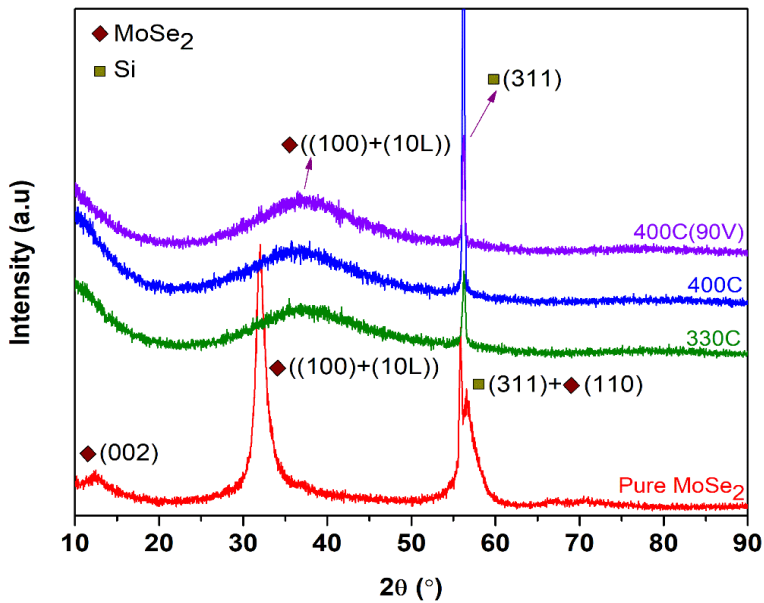

Figure 4-2: XRD patterns of the coatings

4.2.4. Microstructure

An HRTEM micrograph of the 400C coating is shown in figure 4-3 (left). Platelets/nanograins of the (002) basal planes of MoSe$_2$ phase in an amorphous carbon matrix can be seen. The platelets are randomly oriented in the matrix resembling wires [137]. The length of the platelets and distance between the (002) planes were measured at various areas; an average value less than 10 nm and 0.65-0.7 nm, respectively, were calculated. The platelets were small in size and not properly grown as an ordered structure. When MoSe$_2$ and C were sputtered together, C restricts the growth and ordering of crystalline MoSe$_2$, thus decreasing the platelet length and increasing the distance between the planes. This smaller size and the random orientation of the platelets may be the reasons why MoSe$_2$ peaks were not detected in XRD analysis.
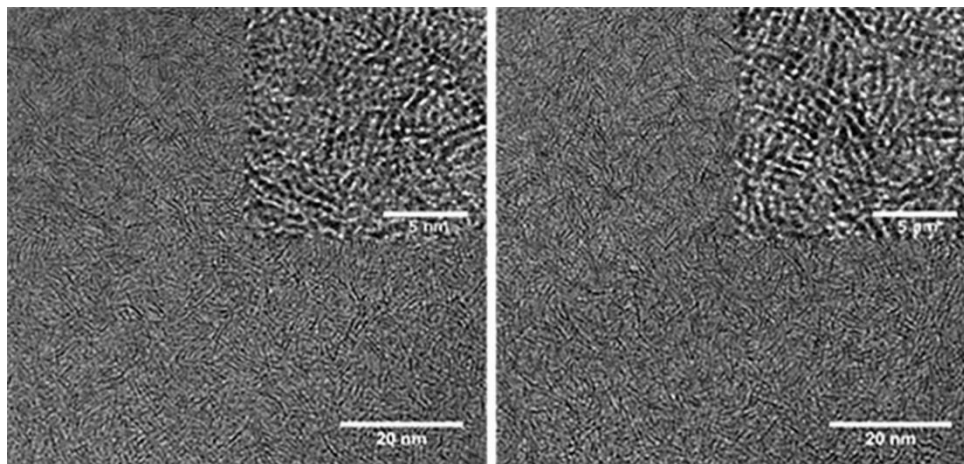
Figure 4-3: HRTEM images of the coatings: 400C - left and 400C(90V) - right

Figure 4-3 (right), shows that, although the application of substrate bias makes the compactness (section 4.2.2) and the hardness (section 4.2.6) of the coating to increase, the microstructure remained almost the same; thus, no major difference in the easy shear properties of the coatings is expected. (002) planes interplanar distance was in the range of 0.6-0.7 nm.

4.2.5. Chemical bonding

XPS spectra were obtained for the coating with ~50 at. % of carbon deposited with and without substrate bias (400C and 400C(90V)). Due to the presence of C in the coatings, charge correction for the binding energies was carried out using the oxygen O1s peak originating from MoO_3. After the charge correction, the $Mo3d_{5/2}$ peak originating from Mo-O bonds in MoO_3 (not shown) was identified at BE (binding energy) of 232.5 eV which is in good agreement with the literature [151,152]. The high-resolution XPS spectra of the regions of interest, obtained after sputter cleaning are shown in figure 4-4. The presence of Se 3s photoemission peak at binding energy of 232 eV (Mo3d region of interest) and LMM Auger lines at 287 eV (C1s region of interest) [153] can complicate the interpretation of the Mo and C spectra. To better understand the effect of these features, high-resolution XPS spectra were also obtained from a selenium pellet (99.9 % purity, Testbourne Ltd) sputter cleaned for 60 minutes in the spectrometer. The same acquisition parameters were used as for the coatings analysed. The spectra obtained from the selenium pellet are shown in figure 4-5. The Se 3s photoemission peak was observed at BE of 231 eV (see Fig. 4-5 a)). Considering a chemical shift of ~1 eV towards lower binding energy, as a result of the

existing Se-Mo bonding, a contribution of this photoemission peak at ~230 eV is expected in the spectra of the coatings. The scan done for the pure Se pellet, at the C1s region of interest (Fig. 4-5 b)) showed the $L_3M_{33}M_{45}$ (^1P) and $L_3M_{33}M_{45}$ (^3P) Se Auger lines at ~297.7 and ~285.5 eV, respectively. The position of the Auger lines at 285.5 eV can clearly contribute towards the intensity of the C1s spectra from the coating as its position is close to the location of the binding energies for C-C bonding of sp2 (BE = 284.5 eV) and sp3 type (BE = 285.4 eV) [154]. Considering these features, no reasonable fitting could be achieved for the Mo3d and C1s regions of interest. Partial fitting was done for the Mo3d peaks with a focus on the strongest features of the spectra and no fitting was attempted for the C1s region.
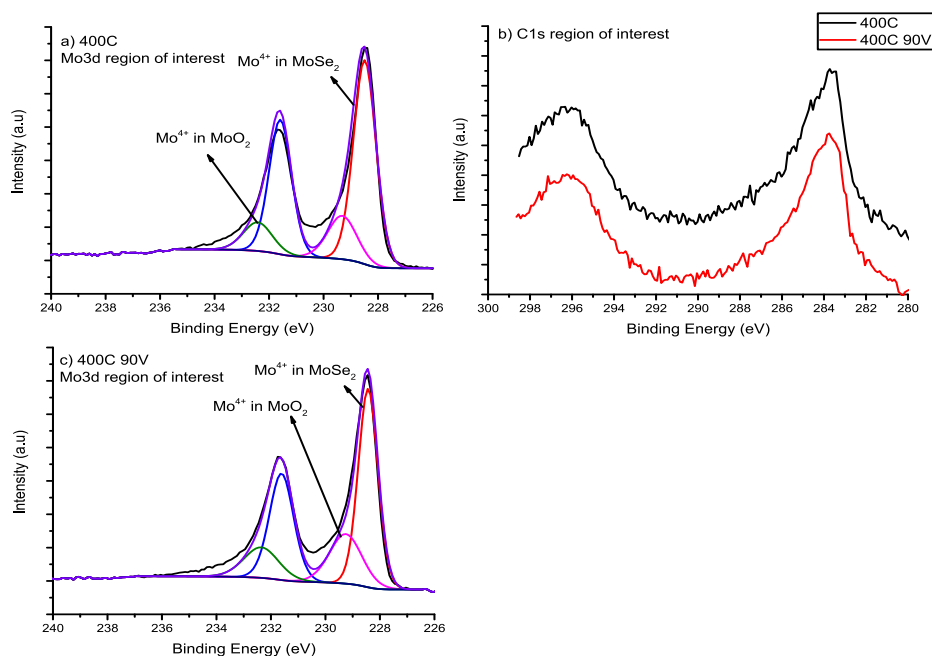

Figure 4-4: XPS spectra acquired after sputter cleaning a) Mo3d region of interest for 400C b) C1s region of interest for 400C and 400C(90V) c) Mo3d region of interest for 400C(90V)

The Mo3d spectra of the coatings 400C and 400C 90V after etching are shown in figures 4-4 a) and 4-4 c), respectively. The peaks were fitted using separation of the binding energies between the $Mo3d_{5/2}$ and $Mo3d_{3/2}$ peaks set to 3.1 eV with their peak area ratios set to 3/2 [153]. As Se and C have the same electronegativity (2.55), the identification of Mo-C bonds from the Mo3d spectra can be very difficult. The $Mo3d_{5/2}$ BE location for Mo-C bonds presented in the literature is in the range 228.2-228.7 eV [155] which is at the same location as Mo-Se bonding identified in MoSe2 which is located at 228.4-228.7 eV [156]. Fitting of the spectra before etching (not shown) was performed using 4 doublets.

The first doublet was located at 228.5 eV for the coating deposited without substrate bias and 228.3 eV for the coating deposited with substrate bias, values which represent Mo-Se bonding in $MoSe_2$ and are in agreement with the literature [156]. The slightly lower value obtained for the coating deposited with substrate bias can be the result of a lower Se/Mo ratio. The additional doublets used for fitting were located at the same positions for both coatings and they were identified as Mo-O bonds where Mo has different oxidation state (see Fig. 4-4). The Mo3d spectrum after Ar^+ ion etching has shown narrower main peaks and fitting was done using 2 doublets which were located at the same location for both coatings. The first doublet was positioned at 228.5 ($Mo3d_{5/2}$) which is considered to represent Mo-Se bonds in $MoSe_2$. The second doublet was located at BE of 229.2 eV and is representing Mo 4+ oxidation state in MoO_2. The Se 3d peaks obtained after etching showed no significant difference compared to the spectra obtained on the as deposited coatings. The peaks were fitted using a separation of 0.86 eV between the binding energies of the $3d_{5/2}$ and $3d_{3/2}$ peaks. Fitting of the Se3d spectra before and after sputter cleaning was performed with 2 doublets for both the coatings. The first doublet was located at $3d_{5/2}$ BE of 54.2 eV representing Se-Mo bonding which is in good agreement with previous studies and reference values [153,156]. The second doublet needed to complete the fitting was positioned at 55.2 eV (not shown) and this peak was assigned to Se-Se bonding [153].
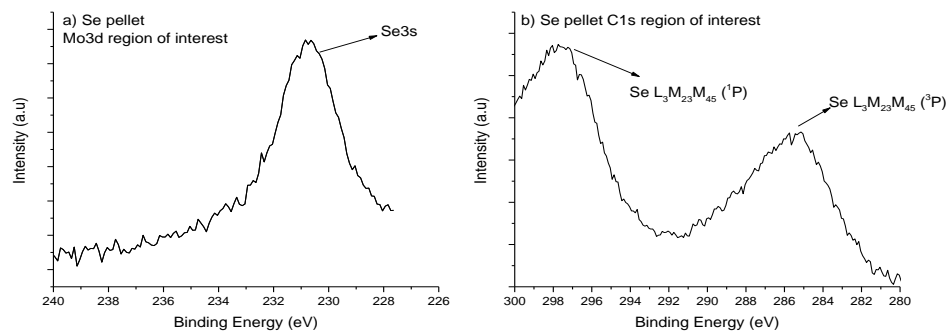

Figure 4-5: XPS spectra of the Se pellet: a) Mo3d region of interest, b) C1s region of interest

C1s photoelectron spectra is shown in figure 4-4 b). Considering the presence of the Se $L_3M_{23}M_{45}$ (^3P) Auger line (compare Fig. 4-4 b) and Fig. 4-5 b), fitting of the spectra was not attempted. However, the main peak from these spectra has the same location for both coatings with no significant difference between them. From the XPS measurements done, no significant difference could be observed for the coatings deposited with and

without substrate bias. The Mo3d spectra revealed Mo-O bonds, indicating oxidation of the pristine coating surfaces. Nevertheless, these features disappeared after the sputter cleaning process for both coatings. Depiction of Mo-C bonds, which would be indicative of the existence of nanocrystals of Mo-C was very difficult. The chemical shifts in the Mo spectra are very similar for both Mo-Se and Mo-C bonding types. On the other hand, it was shown that there is severe interference between the C1s and Se Auger LMM peak, making the identification of the bonding types from the C1s peak unreliable.

The Raman spectra of pure $MoSe_2$, 400C and 400C(90V) coatings analysed using 512 nm laser are presented in figure 4-6. The spectrum for these coatings can be divided into three main regions.

I. A group of sharp $MoSe_2$ peaks around 200 cm^{-1}

II. Mo-O peaks at 700-900 cm^{-1} region

III. D and G peaks belonging to amorphous carbon (1300-1600 cm^{-1}).

The group of peaks belonging to crystalline $MoSe_2$ is due to the splitting of E_{1g}, A_{1g} and E_{2g} modes (correspond to different in-plane and out of plane phase shifts whenever more than one $MoSe_2$ layer is present in the sample). The detail can be found in references [157,158]. The important thing to be noted is that for 400C and 400C(90V) coatings, the spectra depict narrow peaks showing the existence of crystalline $MoSe_2$, in the amorphous carbon matrix, in agreement with TEM observations. It is observed that the sharpness and intensity of the peaks decreased in the Mo-Se-C coatings in comparison with pure $MoSe_2$. The introduction of carbon in the coatings disturbs the growing of $MoSe_2$ crystals promoting the formation of these platelet-shaped crystals with just one to two layers thickness, the reason why $MoSe_2$ crystallinity is not detected by XRD analysis, where only a broad peak is displayed. The low-intensity broad peaks were identified as oxides, in particular MoO_3 [159] which can come either from the contamination during the deposition or the exposure to the atmosphere. D and G peaks clearly show the amorphous nature of the C, in accordance with X-ray and TEM results, and thus, confirming the establishment of a nanocomposite structure of $MoSe_2$ platelets embedded in an amorphous C matrix. For the analysis of D and G peaks of carbon, deconvolution was performed using a Breit-Winger-Fano asymmetric line for G-peak and Lorentz line for D-peak [160]. For 400C coating, D and G peaks were located at 1389 and 1563 cm^{-1}, respectively while for

400C(90V), the peak centres moved to 1387 and 1560 cm^{-1}, respectively. ID/IG ratios calculated using peak heights were 1.22 and 1.34 for 400C and 400C(90V), respectively. No significant quantity of sp3 C-C bonds is expected in the coatings due to the high ID/IG ratios [136]. Despite 90 % filter application, strong oxide peaks, as well as the D and G peaks, have been observed for pure MoSe$_2$ coating due to the high sensitivity of the coating to the laser. The laser power density, laser filter and exposure time to laser beam strongly affects the resulting spectrum for pure MoSe$_2$ coatings.
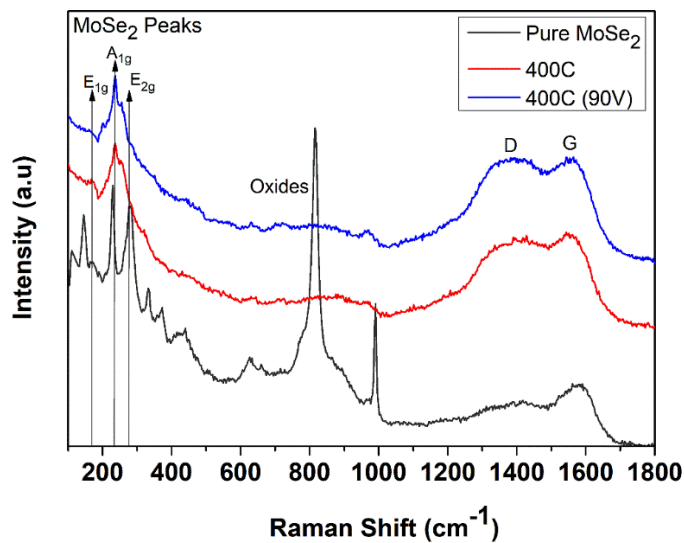

Figure 4-6: Raman spectra of the pure MoSe$_2$, 400C and 400C (90V) coatings

4.2.6. Hardness and adhesion

The hardness of deposited Mo-Se-C coatings was measured by nano-indentation and the results are shown in figure 4-7. Owing to the porous morphology, pure MoSe$_2$ coating showed a very low hardness of 0.2 GPa. As it has already been discussed, the density and compactness of Mo-Se-C coatings increased with C, thus more than one order of magnitude increase of the hardness for C-containing coatings has been observed. The increase in hardness of Mo-Se-C coatings, as compared to the pure MoSe$_2$ coating, can be explained by the increase in compactness and the decrease in the porosity. On the other hand, the nanocomposite structure, i.e., a combination of softer crystalline MoSe$_2$ nanoparticles embedded in amorphous carbon matrix can also contribute to that increase. C-based coatings deposited in similar conditions by magnetron sputtering show hardness much higher than the pure MoSe$_2$ (typically higher than 10 GPa). Therefore, knowing that

an important part of the coatings is the amorphous C hardness, a significant increase in the hardness for Mo-Se-C coatings should be expected, as in fact was observed.

330C, 400C and 500C coatings showed almost identical hardness. The hardness value in this work for the coating with 50 at. % was superior to that achieved in previous studies for RF sputtered Mo-Se-C coatings, even if Se/Mo is higher [78,136]. With the application of substrate bias, the coatings show even better mechanical properties due to either the enhanced density and compactness (as explained above) or the lower Se/Mo ratio.
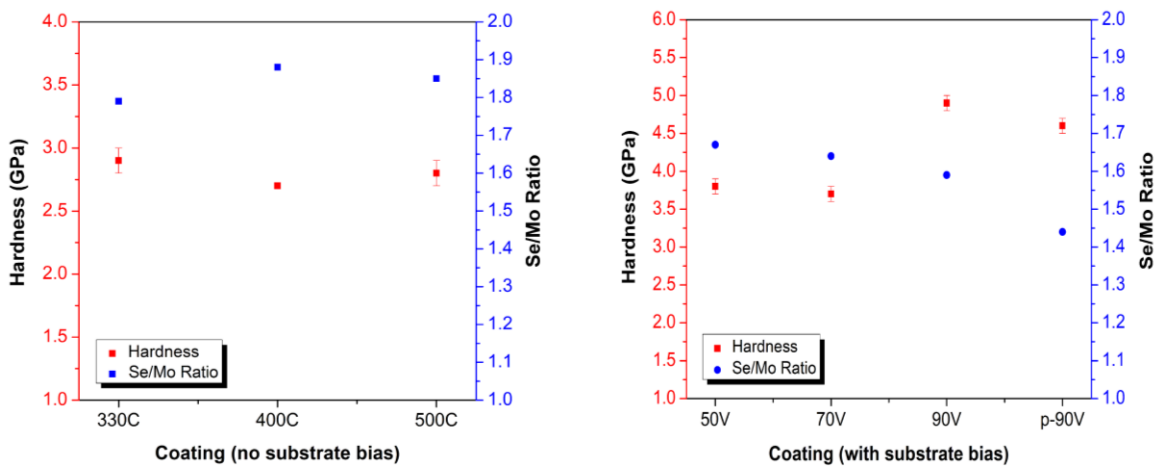

Figure 4-7: Hardness and Se/Mo ratios as a function of carbon power and applied substrate bias

It can be noted from figure 4-7, the higher the Se/Mo, the lower is the hardness, confirming the importance of this ratio on the overall mechanical behaviour of these types of coatings. Same was observed for Mo-S-C coatings in literature [110]. Other studies also suggested that the presence of hard metal-C nanocrystals, which can also be related with a lower chalcogenide/transition metal ratio, could contribute for the hardness of TMD-C sputtered coatings [130], but no clear evidences of Mo-C bonds have been observed in this work. Maximum hardness was observed for 400C(90V) DC substrate bias coating (4.9 GPa) which is better than the values reported in the literature for Mo-Se-C coatings, irrespective of the C percentage.

The coating adhesion to the steel substrates was evaluated by scratch-test (see Table 4-1). The 330C coating showed the lowest adhesion critical load value with Lc_3 around 9 N. The 400C coatings deposited with 90 V DC substrate bias, out-performed others and showed Lc_3 of 23 N. All coatings were found to fail by Lc_3 failure mode.

4.2.7. Tribological behaviour

The experimental details of the tribological testing of coatings in this chapter is already presented in section 3.5.1. The literature for TMD-C coatings reports that coatings displayed best tribological properties with ~50 at. % carbon content [24]. Tribological tests were performed on 400C coating displaying 50 at. % C and the maximum Se/Mo ratio, while, 400C(90V) was selected as it displayed the best mechanical properties. Figure 4-8 shows the friction curves for tests performed in both ambient air and dry nitrogen atmospheres. For 400C coating, the COF started with a lower value of 0.06 and after ~16200 cycles, the coating failed. This can be related to the lower hardness of the coatings, leading to high wear. Specific wear rate calculated was ~3.0 x 10^{-6} mm^3/Nm. On the other hand, when 400C(90V) coating was tested, a steady drop of the friction coefficient was observed during the first 30000 cycles, which can be related to the running-in period consisting of asperity deformation and formation of an easy shear tribolayer. A steady-state behaviour with COF of around 0.06 was observed during the remaining time of the test. Periodic drops and increments of the friction coefficient to values closer to 0.05 and 0.07 respectively, were observed. The wear of this coating was very less with the specific wear rate close to ~2.65 x 10^{-7} mm^3/Nm. The coating displayed an average COF value of 0.065 which is similar to 400C coating. Overall, the frictional response of 400C(90V) was quite stable throughout the selected test duration/cycles (unlike 400C coating).

When the same coatings were tested in dry nitrogen, much improved tribological results were achieved owing to the absence of moisture affecting MoSe$_2$ properties. 400C coating displayed an initial COF of 0.03, slightly increasing thereafter and fluctuating around 0.04 until ~50000 cycles were reached. Close to this value, the COF increased instantaneously and the coating failed. Unlike tests in ambient air, the coating survived for longer number of cycles with a specific wear rate of ~5.1 x 10^{-7} mm^3/Nm. On the other hand, for the 400C(90V) coating, the COF displayed a maximum value of 0.05 at ~5000 cycles and then decreased as the test progressed. This running-in period can be related to the formation of a MoSe$_2$ tribolayer. From ~15000 cycles until the end of the test, the COF was highly stable with an average value of 0.025. Unlike ambient air test, no peaks or fluctuations were observed after reaching the steady-state, revealing the harmful effect of moisture on the friction performance of these coatings. 400C(90V) coating again displayed

long-term stability. The average COF of the whole test was 0.027 and the wear was also very low with a specific wear rate of ~2.4 x 10^{-8} mm^3/Nm.

The application of substrate bias not only improved compactness, hardness and adhesion but also contributed for improvement of tribological properties. These coatings show COF and specific wear rates better than the previous studies on the Mo-Se-C system in ambient air and dry nitrogen environments. In ambient air, Polcar et al. [137] reported COF of 0.05 and the specific wear rate of 2.6 x 10^{-6} mm^3/Nm for 51 at. % carbon under 30 N applied load and 500 cycles. In dry nitrogen, the literature reports tests performed under 2 N, 5 N and 10 N loads and 157 m sliding distance for a coating containing 47 at. % C. The lowest COF was 0.04 and the wear rate 2.5 x 10^{-7} mm^3/Nm in case of test performed under 10 N applied load, values underperforming those we achieved in this work [78].
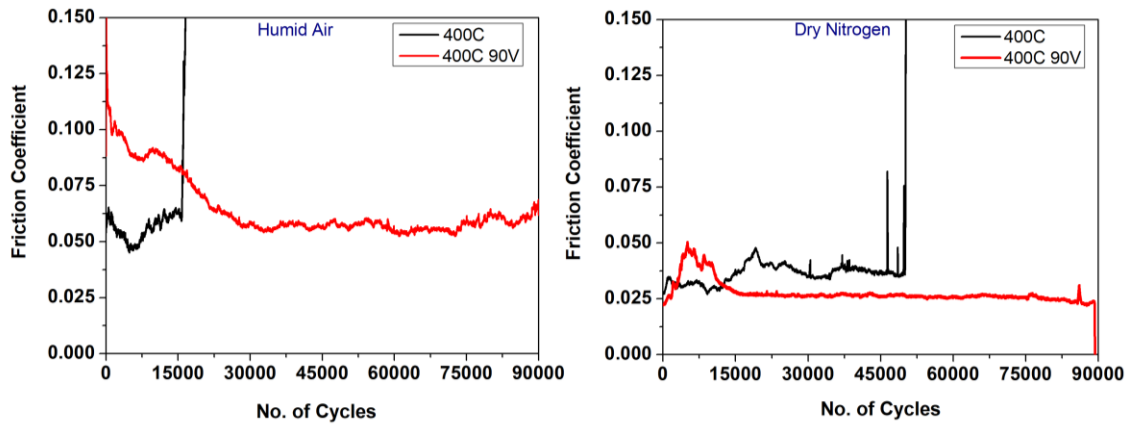

Figure 4-8: Tribological behaviour of reciprocating tests performed in ambient air and dry nitrogen atmospheres

The wear tracks of the coatings deposited with substrate bias were analysed in SEM. In ambient air, there are delaminated parts but such trend is not observed in dry nitrogen tests, looking the coating smooth and intact (Fig. 4-9 a) and b) respectively), which can justify its better performance. Figure 4-9 c) shows the elemental maps of the wear scar in ambient air test. No significant changes in the intensities of the elements can be observed inside and outside of the wear track, excepting the detection of Fe and O in the central part, which can indicate that substrate was reached in that zone. As it was demonstrated before [78], and based on the low COF obtained, the low friction performance can be attributed to the formation of a thin MoSe$_2$ tribolayer at the top contact during sliding, which occurs

when randomly distributed $MoSe_2$ platelets reorient parallel to the sliding, under the applied load.

For the harder coating (400C(90V)), the friction and wear responses are much better than for the softer coating (400C), although the latter has more $MoSe_2$ content. High hardness contributes for a higher wear resistance retarding the material loss. On the other hand, the harder coating also has a higher Young´s modulus (70.6 GPa against 57.5 GPa for 400C coating). Therefore, the contact area will be lower and, for the same applied normal load, the contact stresses are higher. The reorientation process of the $MoSe_2$ platelets is facilitated with higher shear stresses and, so, the formation of tribolayer is easier with the consequent beneficial effect on the frictional behaviour. Once the tribolayer is formed after aggregation of smaller $MoSe_2$ crystals into larger ones, it provides easy shear properties and low COF persists. The tribolayer thus dominates the sliding role.
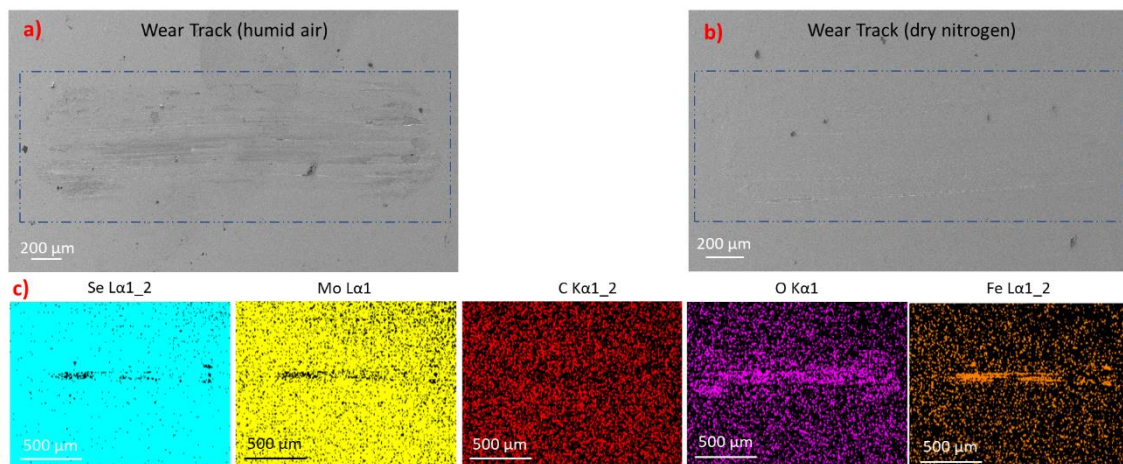

Figure 4-9: 400C(90V) coating reciprocating test wear track: a) and b) SEM images of sliding in ambient air and dry nitrogen respectively, while c) the elemental map distribution of wear track after sliding in ambient air

4.3. Conclusions

DC magnetron sputtered Mo-Se-C coatings were deposited first time using two separate targets of graphite and $MoSe_2$. Increasing carbon power led to an increase in the carbon content of the coatings in the range from 44 at. % to 60 at. % while the Se/Mo ratio decreased. The maximum Se/Mo ratio of 1.88 was achieved for coating deposited without bias and the ratio decreased as the substrate bias was increased. Pure $MoSe_2$ coating was highly porous and columnar while adding carbon or / and increasing the substrate bias led

to a more compact morphology. Pure MoSe$_2$ coating showed a crystalline structure while all the other coatings were X-ray amorphous. No strong sign of the presence of Mo-C nanocrystals was evident from the X-ray diffraction studies. However, TEM analysis showed the presence of MoSe$_2$ platelets with (002) basal planes randomly dispersed in an amorphous carbon matrix. XPS analysis of C1s spectrum was not conclusive about evidence of Mo-C bonds and Raman spectra displayed clear peaks of MoSe$_2$ nanocrystals. The hardness of all coatings without substrate bias was almost similar but by applying substrate bias an increase in the hardness of the coatings was observed. The coatings containing ~50 at. % carbon deposited with DC 90 V substrate bias displayed hardness results better than those reported in literature. This hardness increase can be related to their higher compactness with the application of substrate bias voltage. The Mo-Se-C coating deposited with 90 V substrate bias showed excellent sliding properties in dry N$_2$ while the lack of adhesion needs to be improved for ambient air atmospheres. The tribological results achieved with sputtering of two targets are quite impressive. The current study proved that the Mo-Se-C coatings can be a future for the components sliding in inert and ambient air atmospheres but an optimization of compositional, "micro"structure and mechanical properties is required.

Chapter V

5. OPTIMIZATION OF DC AND RF SPUTTERED Mo-Se-C COATINGS

5.1. Introduction

In the previous chapter, the first deposition of Mo-Se-C coatings using two separate targets by DCMS was discussed. The coatings displayed the ability to provide improved properties in relation to those in the literature. However, the coatings were non-stoichiometric and a quite high C content was required to achieve compact morphologies. This increase in the carbon content led to a chalcogen atom depletion which affected the crystallinity of $MoSe_2$. For TMDs, the closer the Se/Mo ratio to the stoichiometry of the $MoSe_2$ compound, the higher the crystallinity and the better is the frictional response of the coatings. Besides, an adhesion problem was also observed and the coatings failed in ambient air. The low hardness of Mo-Se-C coatings was still an issue since the combination of a lower hardness with a higher Se/Mo ratio results in a higher wear of the coatings. The application of substrate bias improved the hardness but, again, it had an adverse effect on the Se/Mo ratio [161]. Due to these reasons, the Mo-Se-C coatings needed further improvements to be developed as a universal coating system.

Therefore, this chapter is focused on the optimization of the deposition of Mo-Se-C coatings to achieve a microstructure having highly crystalline $MoSe_2$ with an optimal Se/Mo ratio, high compactness and high hardness. Mo-Se-C coatings are deposited by confocal plasma sputtering in an ATC-Orion 8 (from AJA INTERNATIONAL, US) chamber. This apparatus is equipped with 4 cathodes. Additional cathodes (4 instead of 2) provided the freedom of introducing Cr-based gradient layers for adhesion enhancement. Also, two C targets could be used to overcome the low sputtering yield of C and the excess of reflected Ar neutrals. Two different target-power supply combinations (DC and RF) are used to check if RF power can provide any significant advantage in $MoSe_2$ sputtering, and enhancement of the coating properties in relation to DC. The details about the deposition procedure and the characterization of the coatings are already discussed in sections 3.3.2 and 3.4, respectively. The next section will be dedicated to the results of this deposition

approach. The work presented in chapter 5 was published in Coatings Journal and is attached in annex B.

5.2. Results and discussion

5.2.1. Chemical composition, deposition rate and thickness

Table 5-1 shows the chemical composition of the deposited coatings measured by WDS. As expected, the application of power to carbon targets resulted in an increase of the carbon content in the coatings and a very small decrease in the Se/Mo ratio. The carbon content is almost similar, for corresponding coatings, in cases 1 and 2, but Se/Mo ratios are different since RF sputtering produces higher plasma density near the substrate [2,150]. Thus, a higher bombardment of Ar ions can be expected, increasing the preferential re-sputtering of the chalcogen atoms. In both cases, the application of substrate bias led to a significant drop of the Se/Mo ratio. The application of substrate bias results in an increased ion bombardment leading to higher preferential re-sputtering of the lighter Se element. The ratio decreased from 1.96 (DC540) to 1.77 (DC540 (50V)) for case 1 and, similarly, from 1.81 (RF270) to 1.07 (RF270(50V)) for case 2; the latter has the highest sub-stoichiometry (1.07) of all coatings. Overall, for the DC coatings without the substrate bias, the achieved Se/Mo ratio was ~2, unlike previous studies on other TMD-C coatings [25,43,147,148], which were sub-stochiometric. Although the preferential sputtering rate of chalcogen atoms is very low in $MoSe_2$, due to the small atomic mass difference [162] when compared to other TMDs such as MoS_2 or WS_2, there is an additional reason for the improvement: the carbon content was kept only up to 25 at. %. In other studies, the carbon content was much higher and thus led to a decrease in the stoichiometry. This occurs since increasing the carbon target power (for higher carbon content), the current and voltage on the target also increase. As a consequence, the energy and number of the Ar neutrals reflected at the target are higher. Reflected neutrals additionally bombard the growing coating, causing further preferential re-sputtering of the lighter Se element. Even in this study, any additional increments of carbon beyond 25 at. % would further reduce the Se/Mo ratio as suggested by the small, but noticeable, decrease in the Se/Mo ratio with increasing carbon content from 0 to 25 at. %. Previously, the effort was focused on high carbon content films to achieve denser microstructures. The carbon content of 50 at. % was considered as an

optimum compromise between the mechanical properties and the solid lubrication [25]. We will show later that we can achieve enhanced mechanical properties without compromising the stoichiometry. The oxygen content measured by WDS was negligible, arising from the unavoidable residual contamination of the chamber atmosphere and the porosity of $MoSe_2$ target [145].

Table 5-1: Chemical composition, Se/Mo ratio, thickness and deposition rates of the deposited coatings

Coatings	C (at. %)	Mo (at. %)	Se (at. %)	O (at. %)	Se/Mo	Thickness (μm)	Deposition Rate (nm/min)
Case 1							
DC324	17.7±0.4	27.1±0.2	54.2±0.3	1.0±0.2	2.00	2.4	22
DC540	21.4±0.3	26.2±0.1	51.3±0.2	1.1±0.1	1.96	2.3	21
DC676	25.1±0.5	25.2±0.2	48.4±0.4	1.3±0.1	1.92	2.6	24
DC540(50V)	27.2±0.4	26.1±0.5	46.2±0.5	0.5±0.1	1.77	2.2	20
Case 2							
RF170	17.9±0.3	28.2±0.2	52.4±0.4	1.5±0.1	1.86	2.5	15
RF270	21.7±0.3	27.3±0.1	49.4±0.2	1.6±0.1	1.81	2.6	13
RF340	24.7±0.4	26.6±0.2	47.7±0.2	1.0±0.2	1.79	2.6	15
RF270(50V)	35.2±0.6	30.9±0.4	33.1±0.6	0.8±0.2	1.07	1.9	11

The deposition rate and the thickness of the coatings are also shown in table 5-1. In both cases, pure $MoSe_2$ was highly porous; the deposition rate calculated as the thickness per time is, thus, the highest. The RF sputtered pure coating displayed lower deposition rates (19 nm/min vs 32 nm/min for DC sputtered $MoSe_2$), which is in agreement with the literature [2,140]. With the introduction of carbon in the chamber, more sputtered species are available for forming the coating, but the deposition rate for Mo-Se-C coatings (in both cases) decreased when compared to the pure $MoSe_2$ coatings. Such behaviour is attributed

to the improved compactness of the coatings with the addition of carbon (Fig. 5-1 and 5-2).

Considering only Mo-Se-C coatings, the deposition rate increased a little with increasing the carbon power but overall, there was not so much difference. Within each case, the deposition time was kept almost constant for all the Mo-Se-C coatings deposited with or without substrate bias. The deposition rate with bias was always lower due to the enhanced Ar^+ ion bombardment resulting in a higher material removal from the growing coating along with a higher density and compactness. DC sputtered Mo-Se-C coatings also show higher deposition rates than those deposited in our previous work [161], due to the confocal sputtering resulting in the continuous arrival of sputtered species onto the substrates. In previous work, the arrival was intermittent as the substrates were passing in front of the targets one by one.

5.2.2. Fractured cross-section and surface morphology

Figures 5-1 and 5-2 show the fractured cross-section and the surface morphologies of cases 1 and 2 coatings analysed by SEM. For $MoSe_2$ coatings, Cr interlayers were not applied. The denser region near the substrate corresponds to the initial few minutes of deposition with the substrate bias leading to high preferential re-sputtering of Se and an increased Mo content in this compact adhesion layer. In case 1 (Fig. 5-1), the sputtered $MoSe_2$ coating displayed a columnar and porous cross-sectional morphology, with the columns extending down to the Mo-rich layer. The porous nature of the $MoSe_2$ coating was also evident from the sponge-like surface morphology. When carbon was co-sputtered, the coatings became compact and the columns disappeared (Fig. 5-1: DC324). The surface morphology micrographs corroborate the cross-sectional results: the sponge-like and porous surface features were replaced by a compact cauliflower type morphology, after carbon addition, due to the limited surface mobility influencing the coating growth. No changes in the top and cross-sectional surface morphologies were observed after a further increase in the carbon content. The substrate bias contributed to a slight smoothening of the surface (Fig. 5-1: DC540(50V)), due to the increased bombardment of the growing coatings and, thus, providing an increased adatom mobility and a higher atomic coverage. The higher adatom mobility and, in turn, the increase of compactness is also facilitated by the elevated temperature at the surface of the growing film due to the substrate bias.
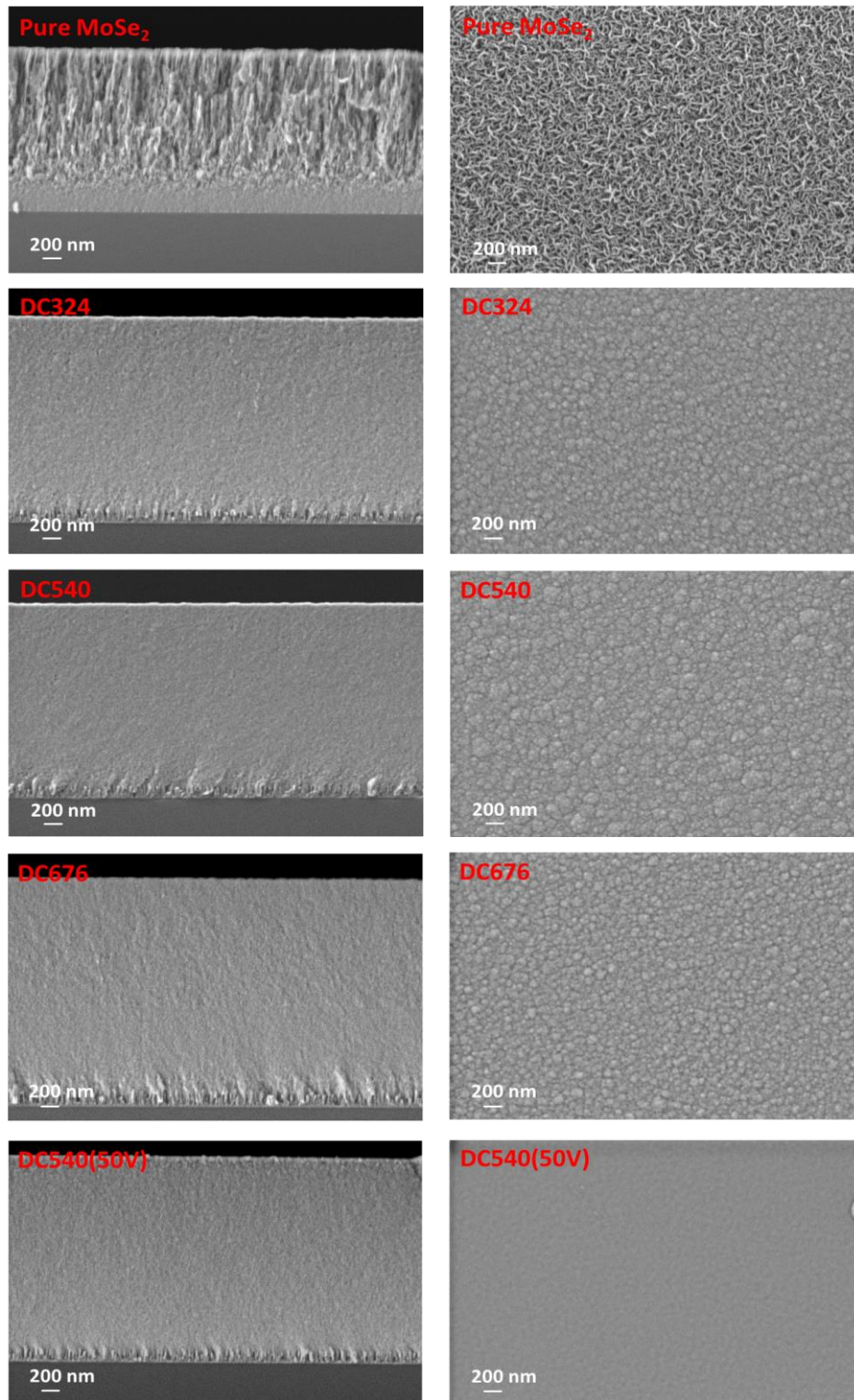
Figure 5-1: SEM micrographs of the cross-section morphologies (left) and the surface morphologies (right) of the respective coatings of case 1.
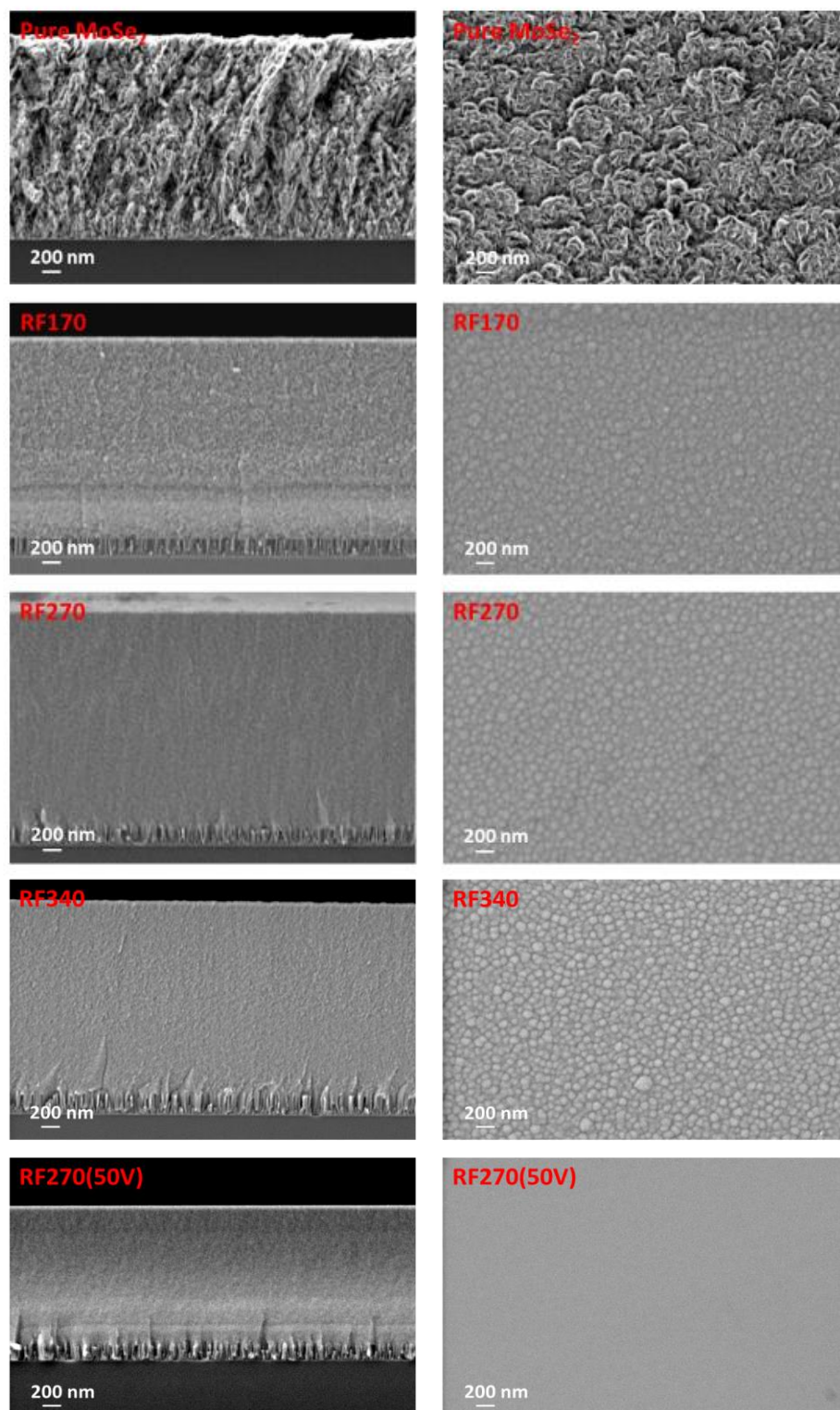
Figure 5-2: SEM micrographs of the cross-section morphologies (left) and the surface morphologies (right) of the respective coatings of case 2

In case 2 (Fig. 5-2), the MoSe$_2$ coating was again porous but the surface morphology did not show sponge-like features; instead, much wider features and grown-

up crystals were observed. This is related to the higher atomic mobility and the low deposition rate of RF sputtering, thus, allowing more time for the grains to nucleate at favourable sites and grow in size [163]. As expected, the addition of carbon led to an increase in the compactness and a decrease of the porosity similar to the case 1 coatings. For RF170, the sudden decrease of the power to the carbon targets, after the gradient layer deposition (500 W to 170 W), resulted in the formation of a visible layer in the fractured cross-section image. For the biased coating, smoothening of the surface was also observed as in case 1 coatings (Fig. 5-2: RF270(50V)).

Our previous works [74,161], showed small contributions of columns / dendrites in the Mo-Se-C coatings. In this study, the lack thereof is related to the higher achieved homogeneity, very likely due to the continuously optimal bombardment of the growing coating by the energetic particles. Furthermore, the continuous confocal sputtering enhanced the substrate temperature which is also contributing to the densification of the coatings [139]. With these conditions, even low carbon content addition to TMD coatings can give rise to a compact morphology (without columns). Globally comparing both DC and RF deposited coatings, similar morphologies and compactness were displayed. Based on the experience and reported literature [24,25], the enhanced compactness with high Se/Mo ratios achieved in this study can be ideal for the mechanical and tribological properties.

5.2.3. Crystal structure

Grazing incidence X-ray diffraction analysis was used to assess the crystal structure of the coatings. Well defined crystalline peaks typical of pure sputtered TMDs were visible in both XRD patterns for the pure $MoSe_2$ coatings – ICCD nº 087-2419 (Fig. 5-3). Working in grazing incidence (3º), the peaks detected at ~13º correspond to the (002) planes inclined 5º in relation to the surface, which are closely parallel to the surface. These planes play a vital role in the easy shear properties of TMDs during sliding. At 30º-50º, peaks with an extended shoulder related to the (100) and (10L) planes were observed. This feature was reported by Weise et al. [147] and is related to the turbostratic stacking of the (10L) planes (L=1,2,3,4,…). The TMD peaks at ~13º and ~30-50º were sharper and more well-defined in pure RF $MoSe_2$ coating than for DC one, showing the higher degree of crystallinity of the former. In RF $MoSe_2$ coating, (002) basal planes were dominant compared to (100) and

(10L) while, in DC, the inverse was observed. The only main differences in the deposition of both coatings were the low deposition rates and the more ions impinging the growing coating in RF deposition - more time, enhanced adatom mobility and surface diffusion. Then, the atoms are allowed to relax at more favourable sites, i.e. (002) preferential orientation [163]. More (002) contribution in RF sputtered $MoSe_2$ is also in agreement with the work of Muratore [26], who explained for MoS_2 that: the deposition rates of ~15 nm/min are required for achieving (002) basal planes and, despite the low desorption energies of (002) than (100), the former orientation can be achieved if there is some energetic ion bombardment (as it is in RF sputtering). It was further reported that a deposition rate close to 15 nm/min provides an increased burial rate of the 2nd layer, as compared to the desorption rates of the first layer, thus, promoting the (002) orientation. In both cases, the carbon addition leads to structural changes and a reduced crystallinity. Therefore, a broad peak at ~30-50º, related to (100) and (10L) planes of $MoSe_2$ nanocrystals (< 10 nm), appeared. Unlike other works on TMD-C coatings [24], the (002) peaks were also detected for Mo-Se-C coatings, which can tentatively be explained by the lower percentage of carbon content and the higher Se/Mo ratio. Mutafov [164] claimed in his work on WSN coatings that (002) peaks were observed due to a very low (i.e. less than 1.2) S/W ratio, but our results contradict that finding, the decrease in Se/Mo ratio resulted in the vanishing of (002) peak (RF270(50V). Anyway, these peaks reveal the interesting presence of (002) planes with the potentially possible positive impact on the tribological behaviour of the coatings.
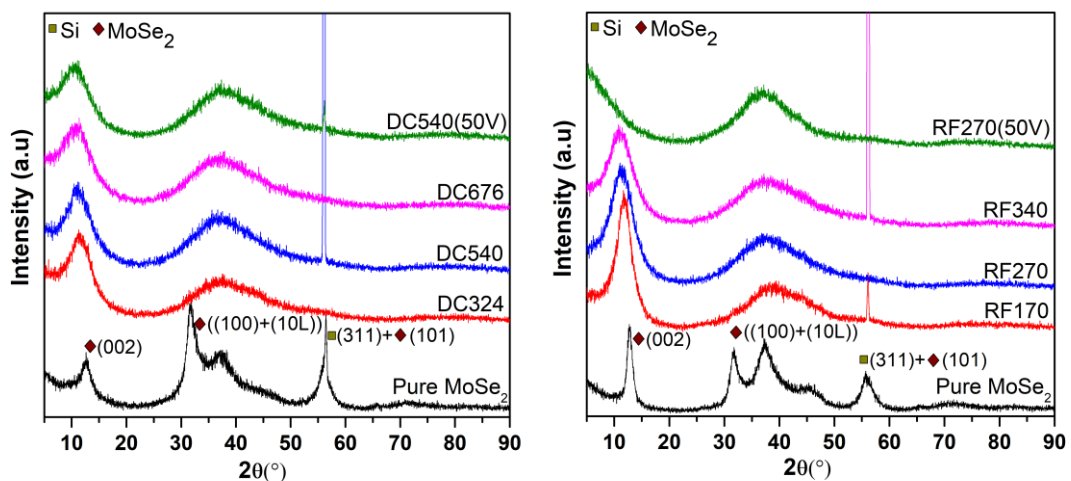

Figure 5-3: XRD patterns of the coatings (case 1-left and case 2-right)

As compared to pure coatings, the (002) peak in Mo-Se-C coatings is broader (in both cases) suggesting smaller sizes of $MoSe_2$ crystallites (in agreement with TEM results, shown later). The carbon disturbs the growth and impedes the formation of well-defined $MoSe_2$ crystals. The addition of carbon also results in an increase in the interplanar distance, as confirmed by the (002) peak shift to lower angles (the shift is more evident in the case 1 coatings). The decrease in Se/Mo ratio cannot explain the peaks shifts to a lower angle; however, carbon can get entrapped in the basal planes [165], causing the c lattice constant to increase. The increase in the interplanar distances, due to the incorporation of a 3rd element in the lattice has been reported by Rasamani [165] and Panigrahi [166], in agreement with our observations. The interplanar distances calculated from the XRD diffractograms increased from ~0.69 nm (DC $MoSe_2$) to ~0.75 nm (DC324) and from ~0.67 nm (RF $MoSe_2$) to ~0.73 (RF170) in cases 1 and 2, respectively. Furthermore, the increase in the carbon content enhanced this broadening of the peaks, the shifts in (002) peaks position to lower angles and the increase in the interplanar distances. The latter may reduce the Van der Waals forces between the basal planes and add a positive impact on the easy shearing properties of $MoSe_2$. With the application of substrate bias, no effect on the X-ray diffraction patterns was observed in case 1 coatings. In case 2, (002) peaks were absent, very likely due to the very low Se/Mo ratios (1.77 for DC540(50V) vs 1.07 for RF270(50V)).

Just like pure $MoSe_2$ coatings, by similar reasons, the (002) peaks are more intense and sharper in C-based $MoSe_2$ (Mo-Se-C) RF coatings than in DC Mo-Se-C coatings, despite their lower Se/Mo ratio.

5.2.4. Microstructure

Transmission electron microscopy analysis was performed to investigate the shape and size of $MoSe_2$ structures embedded in the carbon matrix (Fig. 5-4). Although only selected HRTEM images are shown for both cases, they are representative of all the coatings. Additionally, the HRTEM image of the pure $MoSe_2$ coating has been shown for microstructural comparison. The pure coatings depicted well-defined crystals of $MoSe_2$ having long-range ordering with crystal sizes much greater than for C-containing coatings. The planes having orientation other than (002) were also detected, agreeing with XRD results. After the introduction of carbon, the micrographs in both cases showed $MoSe_2$

nanoplatelets / nanograins randomly dispersed in the form of wires, separated by an amorphous phase. A total of 20 readings were taken for each sample at different places to measure the average distance between the planes and the average number of stacked planes. The average distances were 0.691±0.007 nm and 0.689±0.009 nm for DC540 and RF270 coatings, respectively (a bit lower than the one from XRD, i.e. 0.76 nm), which corresponds to the (002) planes of MoSe$_2$ phase. Similarly, the average number of stacked planes were 4.6±0.2 for DC540 coating and 4.0±0.3 for RF270 coating, respectively. The length of the nanoplatelets was calculated at various regions with an average value of less than 10 nm, unlike the pure coatings. Such small dimensions reflect the structural disturbance induced by the carbon incorporation in the pure coatings, hindering a suitable organization of the atoms during the growth. TEM results are in agreement with XRD observation concerning the small size of the crystals, which was the reason for the (002) XRD peak broadening for Mo-Se-C coatings. The interplanar distances measured from XRD and TEM are slightly different which can be probably explained by the very low thickness of TEM samples (25-30 nm) when compared to those analysed by XRD (~2 µm), leading to less stresses in the TEM samples as compared to the XRD ones.
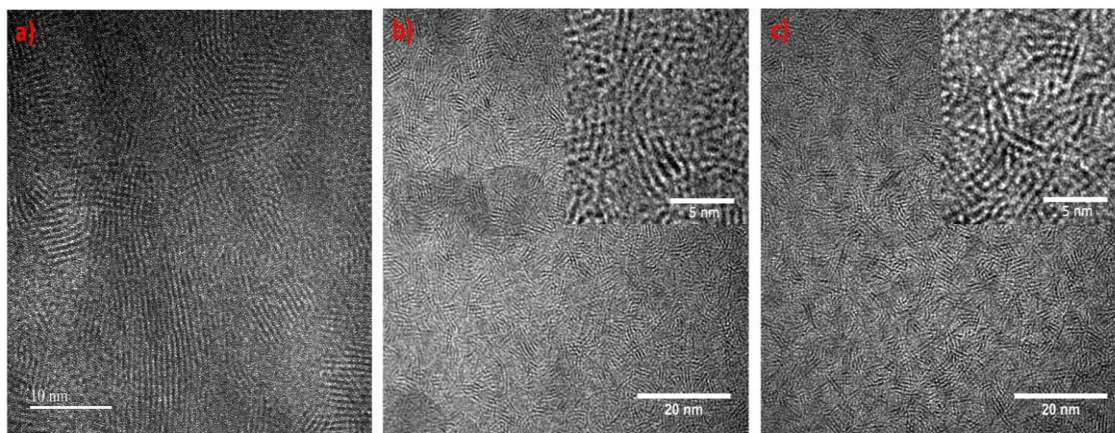

Figure 5-4: TEM images of the a) Pure MoSe$_2$, b) DC540 and c) RF270 coatings

5.2.5. Chemical bonding

Raman spectroscopy was performed on samples from cases 1 and 2 (Fig. 5-5) to further study the phases present in the coatings, especially carbon. A 512 nm laser was used. Well-defined peaks in positions typical of MoSe$_2$ were obtained in all coatings, confirming XRD and TEM results. Furthermore, as expected, the addition of carbon resulted in a decrease in the intensity and an increase in the broadness of MoSe$_2$ peaks.

Generally, for MoSe$_2$ coatings, different in-plane (E$_{1g}$ and E$_{2g}$) and out of the plane (A$_{1g}$) vibrational modes appear [158]. In the deposited pure coatings, the E$_{2g}$ mode was significantly higher than in the carbon-containing coatings. The E$_{2g}$ mode became Raman inactive and the peak disappeared with the increments of carbon, due to the structural disturbance and the decrease of the crystallite size of MoSe$_2$. These observations agreed with the XRD and TEM results where the (100) and (10L) peaks disappeared and the crystallite sizes decreased. Moreover, the carbon addition also restricted the MoSe$_2$ bond vibrations due to the increased compactness of the coating (section 5.2.2), thus influencing the Raman response. Some other broad and barely visible peaks around ~350 cm^{-1} and ~445 cm^{-1} corresponding to MoSe$_2$ peaks were also observed. The E$_{2g}$ peak was also overlapping with the oxides (Mo-oxide) positioned at ~289 cm^{-1} [78,167].
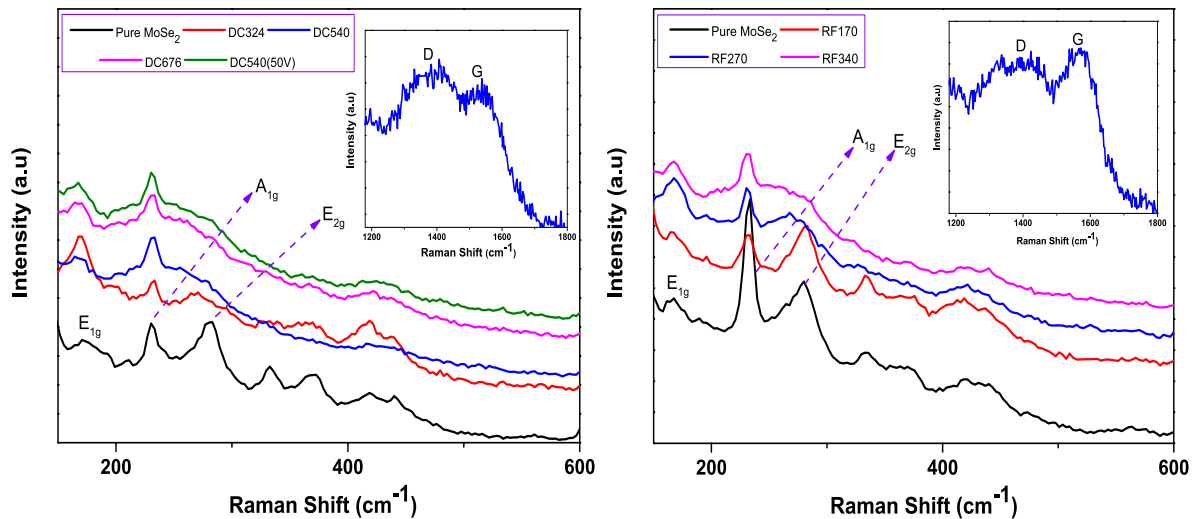

Figure 5-5: Raman spectra of coatings from case 1 (left) and case 2 (right)-inset in each figure is showing D and G peaks

Finally, the nature of the carbon phase was observed by analysing D and G peaks. D peak was deconvoluted using the Lorentz line while for G peak Breit-Winger-Fano asymmetric line was used [160]. The peak positions after deconvolution indicated the presence of an amorphous carbon phase. It was also observed that the increase of carbon and decrease of Se/Mo ratio increased the intensity of the peaks related to amorphous carbon. ID/IG increased from 0.57 to 1.24 for DC324 to DC676 coatings, respectively and from 0.45 to 1.23 for RF170 to RF340 coatings, respectively. Only DC540(50V) was analysed to study the influence of the substrate bias on the ID/IG ratio and peak positions;

minor differences were observed. D and G peaks of only one Raman spectra from each case (having 22 at. % C) has been shown as a representative of all coatings.

5.2.6. Mechanical properties

The hardness and reduced modulus (E*) values of the coatings are shown in figure 5-6. DC and RF pure $MoSe_2$ coatings displayed hardness values of 1.4 GPa and 1.0 GPa, respectively. After carbon addition, all the coatings show higher hardness than $MoSe_2$ due to the denser morphology, the increased compactness and the presence of the carbon phase. Generally, in this study, the case 1 sputtered coatings outperformed case 2 ones due to more (002) crystallinity of the latter. The presence of a higher number (002) planes, in the case 2 coatings, resulted in easy shearing properties and low hardness. Anyway, despite the lower carbon content, all coatings showed higher hardness values than those achieved in previous works [24,136,161]. A hardness of ~3.2 GPa was reported for the single target RF sputtered $MoSe_2$ coatings deposited with 61 at. % of carbon [136], while, here, a hardness of 4.6 GPa and 4.3 GPa was achieved for case 1 (DC676) and case 2 (RF340) coatings, respectively, with only ~25 at. % of carbon. In our first study with separate target DC sputtering (chapter 4), ~2.8 GPa was reported for 50 at. % C coating deposited without substrate bias [161]. Moreover, the application of RF substrate bias resulted in the reduction of the Se/Mo ratio and the enhancement of the density and compactness, which resulted in the highest hardness (i.e. 5.2 GPa) for both DC540(50V) and RF270(50V) coatings. However, it should be noted that the latter had very low Se/Mo ratio which is not desirable.
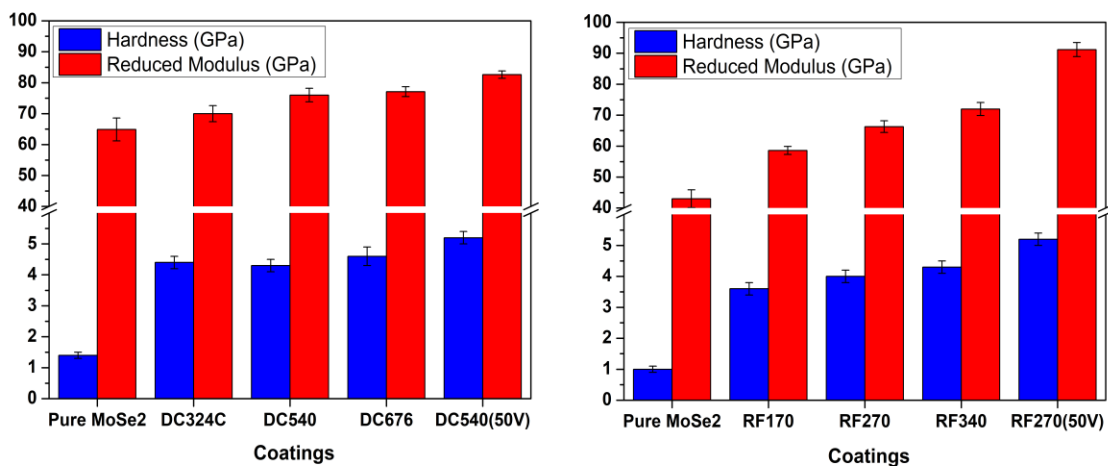

Figure 5-6: Hardness and reduced modulus of the coatings (case 1-left and case 2-right)

It should be remarked that the higher hardness values were achieved despite a much higher Se/Mo ratio (more contribution of the softer phase). An opposite trend was found in all works, i.e., the higher contribution of the softer phase reduces the hardness. The achieved results negate the claims of the literature [74,121], that ~50 at. % C is required for superior mechanical properties. The results also do not support the hypothesis of Mutafov et al. [164] which states that the presence of (002) planes parallel to the surface enhances the hardness since the indenter applies load perpendicular to the parallel planes. If this would be true, case 1 coatings should not show higher hardness than case 2 ones, since the latter presents higher crystallinity and higher (002) preferential orientation. We suggest that the high hardness is predominantly due to the higher compactness, the absence of columnar morphology and the homogeneity of the coatings.

In both cases, the reduced elastic modulus followed similar trends as the hardness i.e. the values increase for higher carbon contents. Parameters related to the elastic strain to failure H/E^* [64] and fracture toughness H^3/E^{*2} [168] are shown in figure 5-7. These values are often related to the elastic energy storage and the wear resistance of the materials, with higher values considered to be beneficial for the final tribological performance [169].
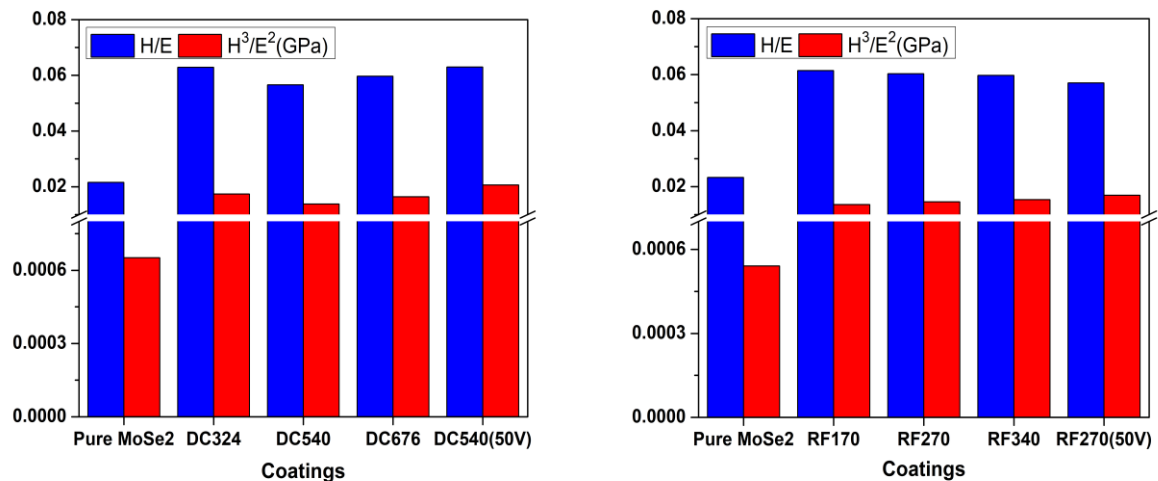

Figure 5-7: H/E* and H3/E*2 of the coatings (case 1-left and case 2-right)

5.3. Conclusions

This chapter provides guidelines to optimize and enhance the synthesis and properties of Mo-Se-C coatings. Magnetron sputtered Mo-Se-C solid lubricant coatings were deposited by using different combinations of DC and RF magnetron sputtering. Low

carbon content (~18 at. % to ~25 at. %), resulted in stoichiometric coatings i.e., Se/Mo close to 2. The carbon addition and the application of substrate bias resulted in a slight reduction of the Se/Mo ratio. Only in case of pure $MoSe_2$, differences in the morphology of DC and RF coatings were achieved; with the addition of carbon and the application of substrate bias, both cases showed similar morphologies with a significant increase of the compactness and density. Unlike previous studies, due to the continuous confocal sputtering, no columns or dendrites were observed in any of the Mo-Se-C coating. Also, differently from literature, the (002) basal planes of $MoSe_2$ phase were observed in the XRD diffractograms, even after carbon additions. The addition of carbon increased the (002) interplanar distances, which are expected to decrease the Van der Waals forces and enhance the easy shearing properties of $MoSe_2$. HRTEM images showed the presence of $MoSe_2$ nanocrystals, with a dimension lower than 10 nm, embedded in an amorphous phase. Raman analysis confirmed the presence of $MoSe_2$ crystalline material and detected the amorphous carbon phase. The mechanical properties of the coatings were enhanced after carbon additions and the values surpassed the literature.

In short, the results achieved with this deposition approach were much better than the literature and solved the issues of achieving a combination of near-stoichiometry, high crystallinity, high hardness and microstructure optimization for TMD-C solid lubricant coatings.

Chapter VI

6. TRIBOLOGICAL PROPERTIES OF Mo-Se-C COATINGS IN DIVERSE ENVIRONMENTS

6.1. Introduction

After optimizing the deposition procedure, the selected coatings were deposited, using DCMS (as discussed in chapter 5), for a thorough tribological testing. Only the DCMS technique was selected as this approach resulted in better deposition rates, stoichiometry and mechanical properties than RFMS. Moreover, the higher deposition rates and the use of DCMS are also favoured by industrial companies.

The role of sliding cycles on the evolution of the wear track composition, tribolayer formation and long-term applicability of TMD-C coatings needs an in-depth study. Most of the studies only deal with short duration tests and they are not the true indication of the long-term performance. In other cases, the detailed reasons behind the decrease of the COF with increasing sliding cycles and the study of the tribolayer evolution with sliding cycles has never been reported. The environmental conditions change abruptly from one region of the world to another- it is expected that the systems developed till now can be a good solution for a specific environment, but not for parts / machines that have to operate in fluctuating environmental conditions. Hence, the coatings which can provide a constant COF, irrespective of the sliding conditions (humidity, temperature etc.) can be a major advancement in solid lubrication.

In this chapter, a detailed tribological testing is reported under different sliding cycles and sliding environments. The effects of the deposition approach, stoichiometry, microstructure and compactness on the sliding behaviour of the coatings will be studied. The detailed analysis of the wear track and the tribolayer evolution, as a function of the C content and the sliding cycles, is also discussed based on Raman, SEM and exhaustive HRTEM results. The long-term applicability of these TMD-C coatings in ambient air and the role of $MoSe_2$ or C in the wear track is thoroughly explored. Finally, the sliding performance of the coatings in diverse environments is studied to check whether the Mo-

Se-C coatings display chameleon character and similar COF in diverse environments (ambient air, dry N_2 and 200 ºC).

The details of the experimental techniques utilized for deposition, fundamental characterization and tribological testing of these coatings were already presented in sections 3.3.2, 3.4 and 3.5.2, respectively. The following section briefly describes the main characterization results followed by a detailed explanation of the tribological performance of the coatings. Although the coatings were deposited according to the same deposition procedure as explained in section 3.3.2, the nomenclature was modified in accordance to the published article. Table 6-1 explains the revised nomenclature. The research reported in this chapter was published in the journal of Surface & Coatings Technology and is attached in annex C.

Table 6-1: Main Deposition parameters used for depositing Mo-Se-C Coatings

Coatings (New name/Old name)	MoSe$_2$ Power (W)	Carbon Power (W)	Bias (V)	Time (min)	Thickness (μm)	Deposition Rate (nm/min)
C1/DC Pure MoSe$_2$	270	-	-	60	1.9	32
C2/DC324	270	324	-	110	2.4	22
C3/DC540	270	540	-	110	2.3	21
C4/DC540(50V)	270	540	50	110	2.2	20

6.2. Results and discussion

6.2.1. Main characteristics of the deposited coatings

The chemical composition in figure 6-1 d) shows that the Se/Mo ratio achieved by this deposition procedure was almost stoichiometric (Se/Mo approx. equals to 2). Se/Mo ratio decreases linearly with increasing the carbon content in the coatings, unlike RF sputtering of Mo-Se-C from a composite target [138]. The substrate bias further decreased the Se/Mo ratio due to the enhanced re-sputtering of the chalcogen atoms from the growing coating. The reported maximum achieved values (of Se/Mo) for Mo-Se-C coatings are not more than 1.88 for DC magnetron sputtering [161]. So, the deposition approach resulted in

coatings with Se/Mo ratio closer to the stoichiometric value. The columnar and porous cross-section as well as the surface morphologies of the pure coating (Fig. 6-1 a)) became very compact and dense with the addition of carbon (C3 coating-Fig. 6-1 b)) or the application of substrate bias (Fig. 6-1 c)). The XRD diffractogram of pure $MoSe_2$ coating displayed peaks almost similar to the typical sputtered TMDs (Fig. 6-1 e)) [161]. The well-defined XRD peaks at ~30-45⁰ in pure coating were replaced by broad amorphous peaks after carbon additions but unlike other TMDs and also studies on Mo-Se-C coatings, the (002) peaks were still observed. These planes are expected to contribute for achieving low COF. The small shift of (002) peak position to lower angles is related to the increase in the interplanar distances of the basal planes due to carbon entrapment/incorporation in the lattice as explained in a previous chapter and ref [165]. Along with the presence of (002) planes, the increase in d-spacing can further facilitate the sliding of $MoSe_2$ crystals by reducing the Van der Waals forces of attraction. It is important to remark that the presence of a broad peak at ~30-45⁰ is also indicative of the presence of $MoSe_2$ crystals less than 10 nm in size [161]. With the application of substrate bias (C4), no effect on the structure was discernible, being the X-ray patterns similar to the coatings deposited without substrate bias. The hardness of pure $MoSe_2$ coating (C1) was 1.4 GPa which increased with increasing carbon contents. The coating deposited with substrate bias (C4) displayed the maximum hardness of 5.2 GPa.
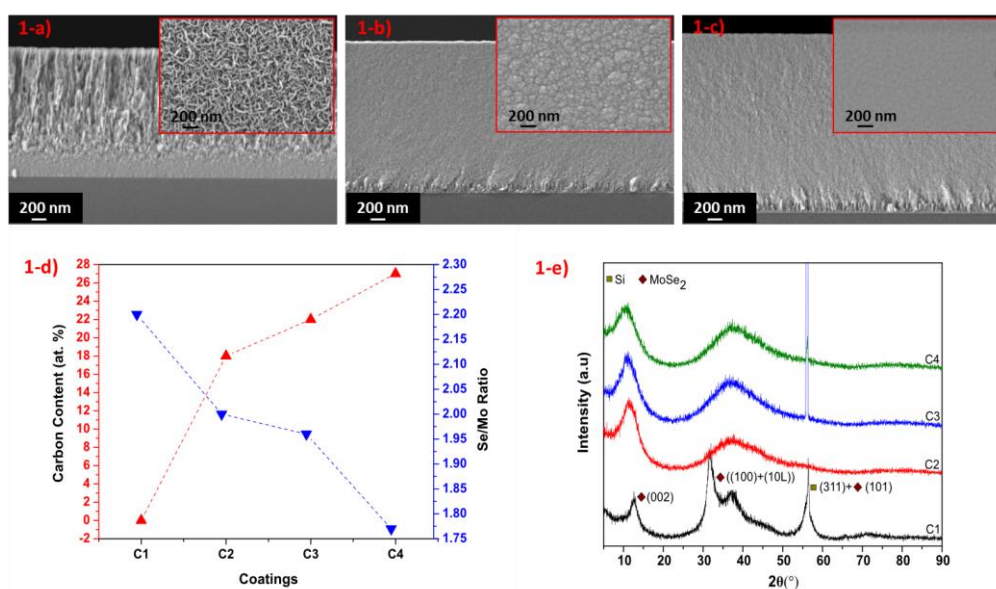

Figure 6-1: SEM cross-section and surface morphology (inset) micrographs (1-a) C1(Pure $MoSe_2$), 1-b) C2(18 %C), 1-c) C4 (27 %C, 50V bias), Carbon content vs. Se/Mo ratios (1-d)) and X-ray diffraction patterns (1-e)) of the coatings

XRD showed the presence of crystalline $MoSe_2$ in the coatings but the nature of the C phase was not clear. So, Raman spectroscopy analysis was performed to analyze the phases present in the coatings using 488 nm Ar laser. The group of bands related to $MoSe_2$ was present at 150 to 450 cm^{-1} (Fig. 6-2 (left)). In pure coating (C1), the crystalline $MoSe_2$ bands were evident due to different in-plane (E_{1g} ~160 cm^{-1} and E_{2g} ~285 cm^{-1}) and out of plane (A_{1g} ~240 cm^{-1}) phase bands [157,158]. Besides, some additional broad and barely evident $MoSe_2$ bands at ~350 cm^{-1} and ~445 cm^{-1} were also observed. Agreeing with XRD observations, the carbon addition restricted the highly ordered growth of $MoSe_2$ crystals, and thus the intensity and sharpness of the $MoSe_2$ bands were reduced. The analysis of the D and G bands of the carbon (shown in figure 6-2 (right)) confirmed its amorphous nature.
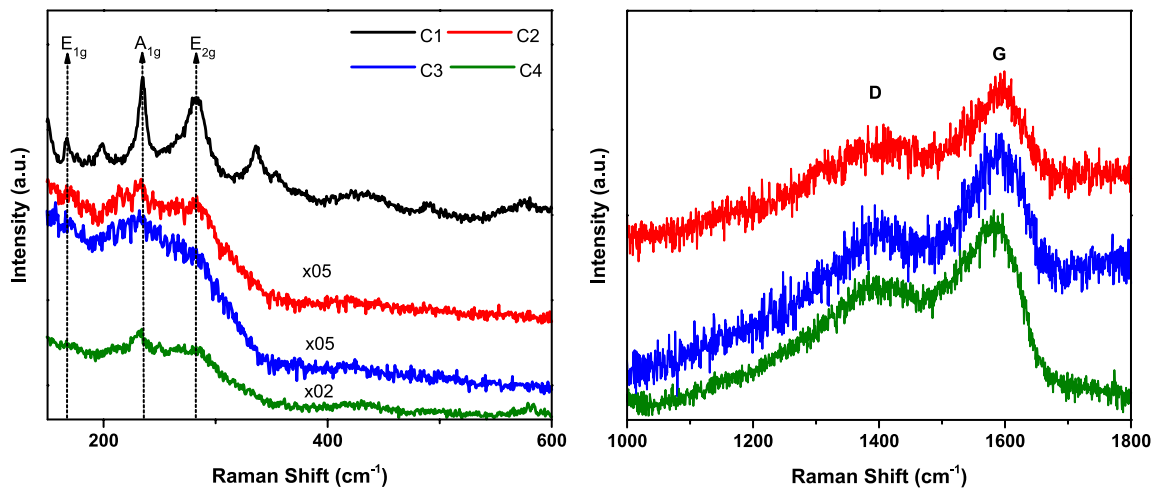

Figure 6-2: Raman spectroscopy results of the as-deposited coatings

6.2.2. Ambient air unidirectional tribological tests

Three different sets of tribological tests with varying number of sliding cycles were performed in ambient air (35-45 % RH). Shorter tests of 5000 cycles were carried out to observe the effects of carbon content, Se/Mo ratio and substrate bias on the running-in period. Afterwards, the number of cycles was increased to 25000 in the 2nd set of tests. The objective was to analyse the differences in the COF and specific wear rates during the running-in versus the steady-state sliding conditions. Finally, tests were performed with a much longer number of cycles of 100000 to assess the tribological endurance of the coatings for applications involving longer working hours between the maintenance

operations. These different cycles tests allowed to understand how the tribolayer formation evolves during the sliding.
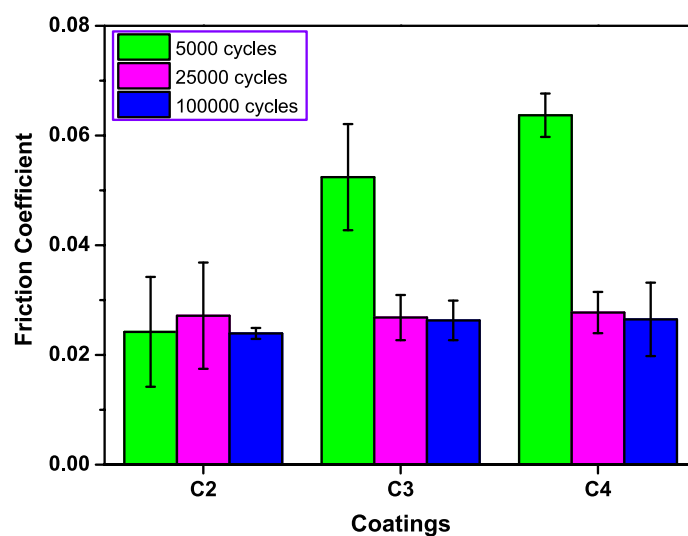

Figure 6-3: Unidirectional sliding COF results of all coatings at different cycles

6.2.2.1. Short duration tests

For the tests performed for 5000 cycles, the pure coating (C1) failed after a few hundred cycles with extensive delamination, probably due to its low load-bearing capacity, attributed to the columnar and porous morphology [24]. For all other coatings, a progressive increase in the COF was observed with increasing C content (Fig. 6-3), from an average value of 0.025 for the lowest C content coating (C2), up to 0.064 for C4 coating deposited with the application of substrate bias. In the latter two coatings (C3 and C4), the steady-state region was not reached until the end of this test. The increase in the running-in period with C content can be explained by the increased difficulty in forming the tribolayer which will be responsible for the low friction, as it will be shown and discussed later. The higher mechanical strength of the coatings (increase of the hardness), due to either the higher content of the C-phase or the increase in the density and compactness of the coatings, makes the tribolayer formation process more difficult. Moreover, it is expected that the low friction tribolayer is mainly composed of (002) aligned $MoSe_2$ crystals, the lower amount of this phase, with increasing C content, enlarges the running-in period. The mechanical strength seems also directly related to the specific wear rates (Fig. 6-4). The C2 coating displayed much higher wear rates than the C3 and C4 coatings, due to the excess of the softer $MoSe_2$ phase and the lower hardness. The softer phase could

not resist the rapid material removal during the initial stages of sliding processes and, therefore, some delaminated regions were also observed in this coating (Fig. 6-5 b)). The other coatings resisted the wear efficiently due to their high compactness and hardness. Furthermore, they also have higher Young´s modulus (C3= 75 GPa, C4= 82 GPa). A combination of high hardness and high Young´s modulus contributes to a higher wear resistance, thus, increasing the running-in and the cycles / duration for the tribolayer formation.

The specific wear rates of the counter bodies were very low, more than two orders of magnitude lower than those from the disk (Fig. 6-4). No detectable wear was observed on C2 coating as its lower hardness gives rise to a lot of material transfer to the counter body from the beginning of the test, protecting it from wear. The counter bodies tested against the other coatings displayed minor specific wear rates.
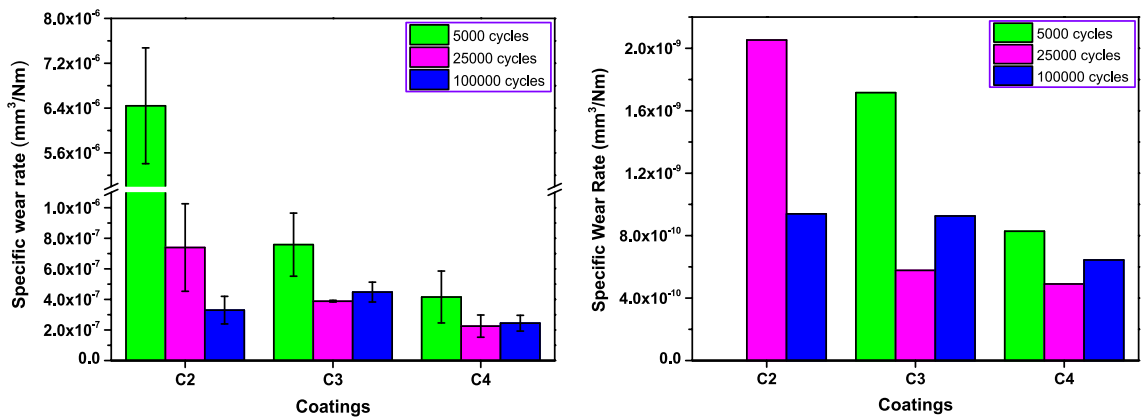

Figure 6-4: Specific wear rates of the disk/coatings (left) and counter bodies (right) at different sliding cycles

6.2.2.2. Medium duration tests

By increasing the testing cycles from 5000 to 25000 the running-in period was overcome and all coatings reached the steady-state sliding condition with the formation of tribolayers which were easily detected in the wear tracks (Fig. 6-5). As it would be expected, the lowest C content coating (C2) displayed minor changes in COF, since the tribolayer formation was already achieved; the steady-state average value was ~0.028. For the C3 and C4 coatings, the steady-state was reached with an average COF of ~0.026 and ~0.027, respectively. Such behaviour suggests that, also for these coatings, the low friction tribolayer was formed.

All coatings displayed a decrease in the disk specific wear rate, more substantial for the low C coating, to account for the much higher wear during the running-in period. It is important to remark that C2 coating showed less zones of delamination in this test (Fig. 6-5: d)), suggesting that replenishing of those zones occurred with the wear debris created in the sliding contact and transfer layer of the counter body. This might have contributed to the very minor increments in COF (i.e., 0.004) for this coating.

For the test with 25000 cycles, wear was then observed for C2 coating´s counter body (Fig. 6-4). The irregularities created by the delamination acted as abrasive features for the ball which decreased the transferred material and the protection of the counter body, with the consequent formation of a wear scar. Specific wear rates of the other counter bodies decreased since the coatings were sliding in the steady-state condition under the influence of the tribolayer, which protects both elements of the sliding pair from wear. C4 coating and its counter body outperformed the rest in terms of COF and specific wear rates in this test.
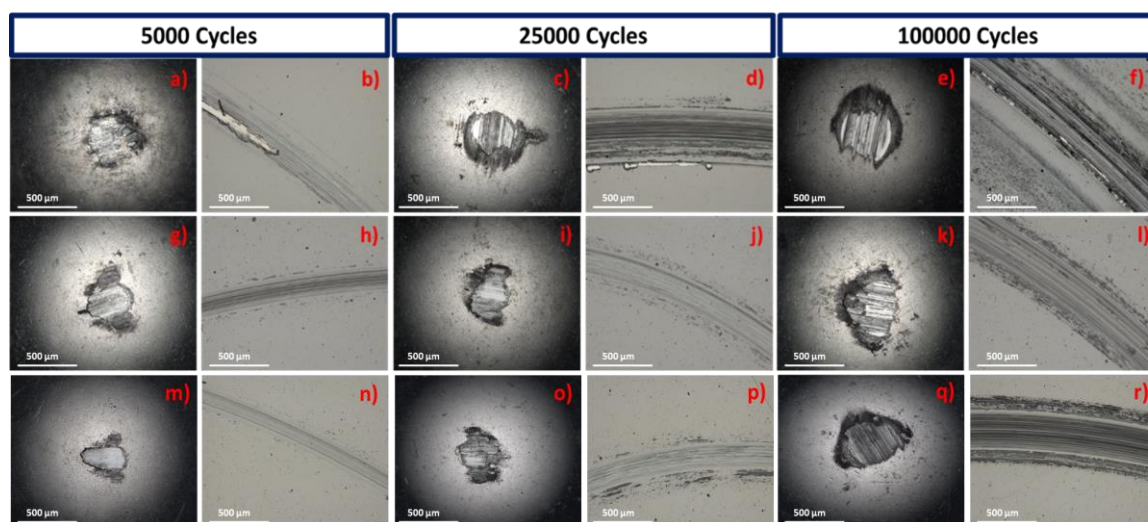

Figure 6-5: Optical microscopy images of the wear tracks and counter bodies after 5000 cycles: a) and b)-C2 coating, g) and h)-C3 coating, m) and n)-C4 coating; 25000 cycles: c) and d)-C2 coating, i) and j)-C3 coating, o) and p)-C4 coating; 100000 cycles: e) and f)-C2 coating, k) and l)-C3 coating, q) and r)-C4 coating

6.2.2.3. Long duration tests

As the sliding cycles were increased to 100000, stable friction curves were obtained despite the minor delaminated zones observable in some wear tracks. As per figure 3, all coatings showed similar COF values, suggesting that the sliding mechanism is similar in

all of them. When the specific wear rates were calculated for both the balls and the disks (Fig. 6-4), no significant differences in the values were found among the tested samples. C4 film showed a little smaller value, particularly due to its slightly better mechanical strength. These lower values were achieved since either the tribolayer in the wear track or the protective transferred layer to the ball support the sliding in the steady-state region, avoiding material removal.

After considering COF and specific wear rates of the coatings and the counter bodies in all tests, C4 displayed slightly superior results than the other coatings.

6.2.2.4. Wear track analysis

Although with some differences, the global tribological behaviour of all C-containing coatings is very similar. Therefore, a detailed analysis of the wear tracks was performed just in one of them. Since C4 coating was the one presenting the best combination of high hardness, low friction and high wear resistance for both the coating and the counter body, it was selected for the analysis. The wear tracks were first observed in SEM (Fig. 6-6). After 5000 cycles test, the wear tracks were quite smooth, with very small regions comprising of thin patches. Increasing the number of cycles to 25000 resulted in broad patchy regions separated by valleys. For the 100000 cycles test, almost the whole of the track was covered with patches with very minor valleys in between.
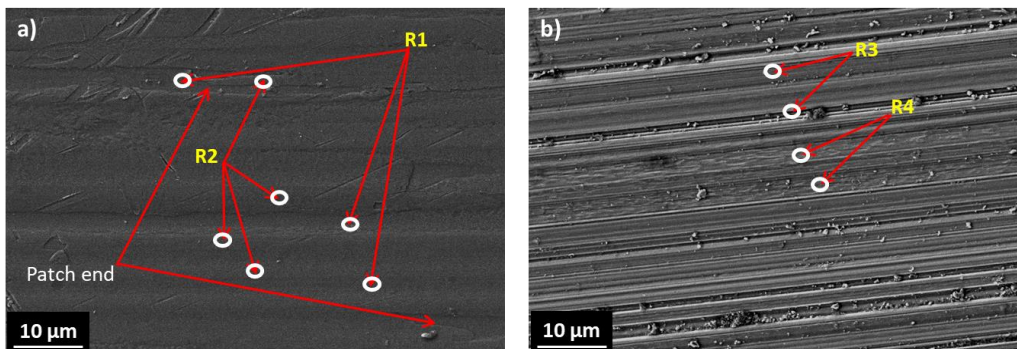

Figure 6-6: SEM micrographs of the wear tracks: a) 25000 cycles and b) 100000 cycles

Raman spectra of the regions highlighted in figure 6-6 are shown in the figure 6-7. The results showed that the wear tracks have regions corresponding to tribolayer of $MoSe_2$ (R2) and as-deposited regions (R1) after 25000 cycles while a completely covered $MoSe_2$ transformed layer was observed after 100000 cycles (R3 and R4). Despite the topographical features on the wear track surface due to the sliding, no vestiges of as-deposited regions or

patches without MoSe$_2$ tribolayer were detected. Raman showed the presence of crystalline MoSe$_2$ and a high contribution of Mo-oxides in the wear debris. Although not shown here, quite a high contribution of C was detected in the wear debris and not in the R2, R3 and R4 regions. The observed decrease of COF with the increasing number of sliding cycles can be understood by the progressively more availability and coverage of the wear tracks with TMD tribolayers, as observed by SEM and Raman analysis.
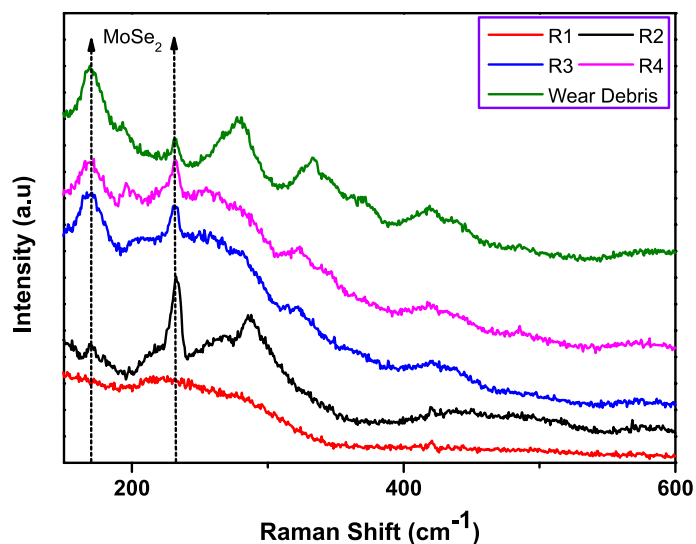

Figure 6-7: Raman spectra obtained from different regions of C4 coating´s wear track after 25000 and 100000 cycles tests – the regions are highlighted in Fig. 6-6

Additionally, elemental mapping for the highest duration test wear track, i.e. after 100000 cycles, is shown in figure 6-8. Except for some dispersed wear debris containing high contents of C or O, the wear track surface was quite uniform and no delamination was observed, in agreement with the optical microscopy results.
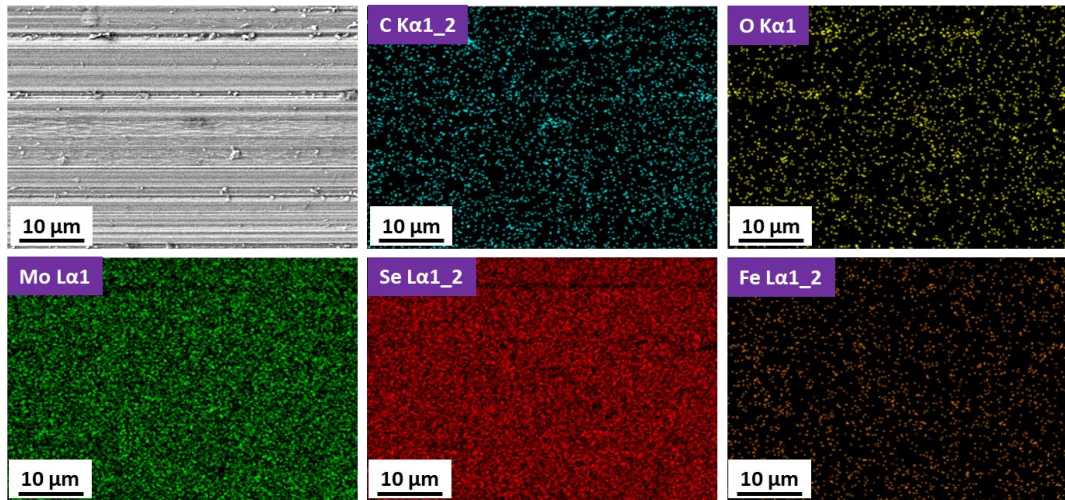
Figure 6-8: EDS elemental maps for C4 coating´s wear track after 100000 cycles test

To confirm the formation and importance of the tribolayer, FIB lamellas were prepared from the wear tracks in cross-section and, then, analysed by transmission electron microscopy. The cross-sections were cut perpendicular to the sliding direction. Only selected HRTEM images, representative of most of the wear track after 25000 cycles and 100000 cycles test are shown in figure 6-9. The observations show that the crystallization of the coatings occurred with planes well-aligned parallel to the sliding direction. The average interplanar distance calculated from various regions was ~0.64 nm, agreeing well with (002) $MoSe_2$ basal planes. So, TEM analysis of the wear tracks also confirmed that $MoSe_2$ tribolayers are the reason behind the low COF achieved. After 25000 cycles test, the tribolayer was patchy i.e., showed both as-deposited and oriented material zones (Fig. 6-9 a)) and not covering the whole wear track. Regions resembling as-deposited coatings, without tribolayer were evident (Fig. 6-9 b)). On the other hand, the tribolayer after 100000 cycles test (Fig. 6-9 c)) was dense and covered the whole wear track, without any vestiges of as-deposited regions. TEM results agreed well with SEM and Raman observations.
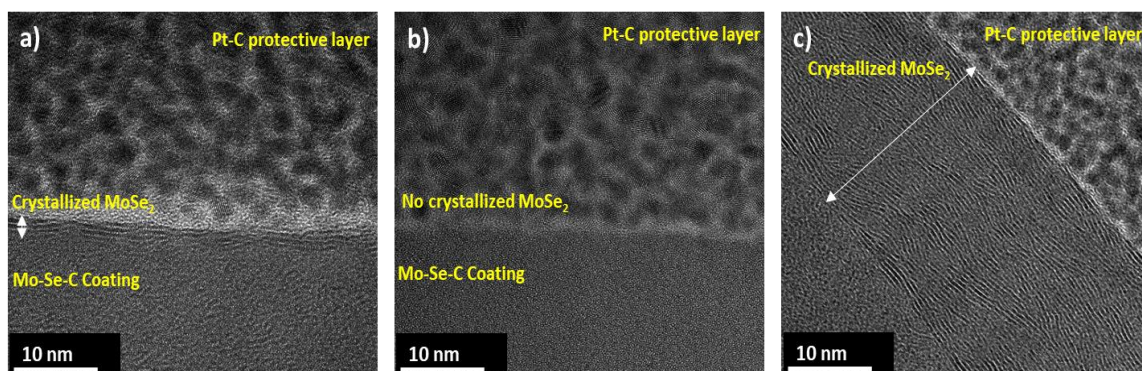
Figure 6-9: HRTEM micrographs of the wear tracks after sliding tests: a) 25000 cycles with tribolayer b) 25000 cycles with no indication of tribolayer and c) 100000 cycles

Another important remark which showed that the tribolayer is mainly formed by a well-crystallized $MoSe_2$ phase is the better stoichiometry of the $MoSe_2$ phase in the tribolayer. Figure 6-10 shows the STEM-EDS elemental maps from a lamella of the wear track cross-section. The edge of the arrowhead in the bright field images shows the start of the tribolayer. Clearly, an increase of the Se/Mo ratio in the tribolayer can be observed from the map. Besides, a compositional analysis was also performed in both zones (as-deposited and tribolayer): the tribolayer presented composition closer to the stoichiometry of $MoSe_2$ (Se/Mo = ~2 in tribolayer vs. ~1.8 in the coating), showing that the tribolayer was mainly composed of this phase.
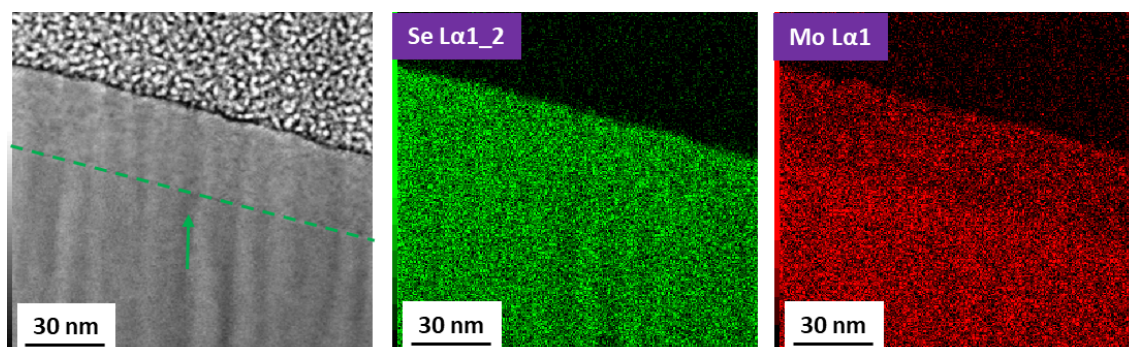

Figure 6-10: STEM-EDS elemental maps of wear track after 100000 cycles test

To summarize the results of ambient air unidirectional pin-on-disk tests in this work, it can be said that the achieved values are superior to those of other TMD-C coatings (tested in ambient air) with respect to COF, specific wear rates, and sliding cycles. For instance, the literature reports that under 10 N applied load, COF ~0.15 and specific wear rate of ~10^{-6} have been achieved for W-S-C coatings tested under 50 % relative humidity [58]. Polcar et. al [24] reported sliding results of W-S-C, W-Se-C, Mo-S-C and Mo-Se-C

coatings (under 10 N applied load): the COF was ~0.07 for W-Se-C and Mo-S-C while W-S-C and Mo-Se-C coating systems showed ~0.1. Moreover, COF of 0.12 and 0.08 have been reported, at 35-40 % relative humidity, for Mo-Se-C coatings with 29 at. % C and 68 at. % C, respectively [138]. In another study [78], a Mo-Se-C coating with 47 at. % C displayed ~0.1 COF and ~2.5 x 10^{-6} mm^3/Nm specific wear rate, under 10 N load at 55 % relative humidity. The values decreased to ~0.05 COF and ~2 x 10^{-7} mm^3/Nm specific wear rate when the C content was increased to 61 at. %. In these studies, the trend was to use higher C contents to increase the compactness and the hardness of the coatings to achieve sufficient environmental resistance for improved tribological properties. In the present study, we have found COF lower than 0.03 for coatings with only 18 at. % of C. Angled delivery and multiple target use provided continuous and optimized sputtering while low C permitted a higher contribution of the softer phases for tribolayer formation. So, it has been concluded that if the deposition procedure is properly optimized: higher Se/Mo ratio, compactness, hardness, lower COF and specific wear rate than literature, can be achieved, despite a maximum C content of ~27 at. % as compared to 50 at. % (advised by literature) [24]. It is even expected that the deposited coatings, especially C4 coating, might run for much longer durations than tested.

In short, these unidirectional tribological tests and in-depth wear track studies are a big advancement towards clarifying many ambiguities about ambient air tribological performance of less explored C-alloyed MoSe$_2$ coatings and also the role of C and MoSe$_2$ in the wear tracks. It is expected that the excellent ambient air stability will open new domains for the research and implementation of MoSe$_2$ coatings in industries as a replacement of other TMDs (like MoS$_2$) which show considerably high friction and wear in ambient air conditions.

6.2.3. Diverse environment reciprocating tribological tests

The tribological analysis was further extended by testing the performance of C3 (no substrate bias) and C4 (biased) coatings in different environments, due to their excellent performance in unidirectional pin-on-disk tests. Reciprocating sliding tests in ambient air (RH ~35-45 %), dry nitrogen (RH < 5%) and high temperature (200 ºC, ambient air) were performed. The reciprocating tests were selected as an alternative to the unidirectional pin-on-disk since this equipment was not able to provide a controlled environment. The

standard ambient air tests were repeated for a better comparison between results. The COF and the specific wear rate in all three environments are shown in figures 6-11 and 6-12, respectively.
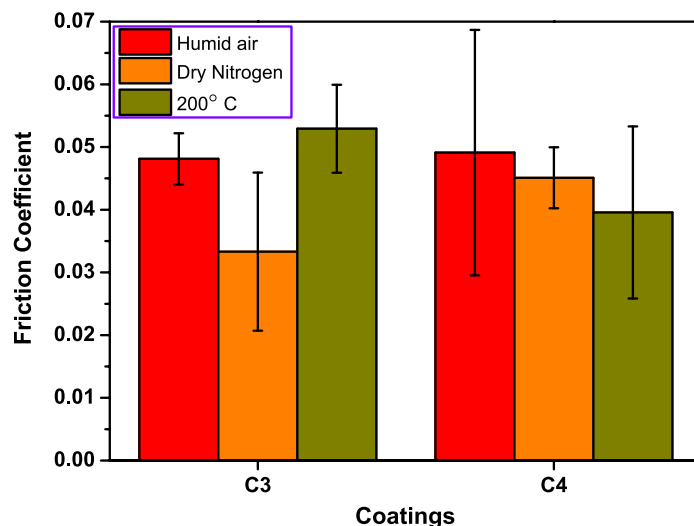

Figure 6-11: Reciprocating sliding COF values of 540C and 540C(50V) coatings in diverse environments

For ambient air sliding, the steady-state COF was ~0.05 for both C3 and C4 coatings, with wear tracks showing minor delaminated areas (Fig. 6-13). Based on the EDS mapping, the coatings delaminated in the interface between the Cr interlayer and the coating since an increased Cr signal was observed in the delaminated zones (Fig. 6-14). As previously discussed, a lower hardness can be associated with a higher wear rate, as it is confirmed in figure 6-12 where C3 coating shows a higher wear rate compared to the C4 coating due to its low hardness. On the other hand, this difference in the hardness of both coatings is reflected in the wear rate of the counter body which, when sliding against the C3 coating, showed less wear compared to the one sliding against the C4 coating. Overall, the observed trends of COF and specific wear rates of reciprocating sliding tests were similar to the unidirectional sliding tests. The slightly higher measured values can be explained since the SRV device calculates the average COF of cycles, then integrating the higher friction during stroke reversal [170].
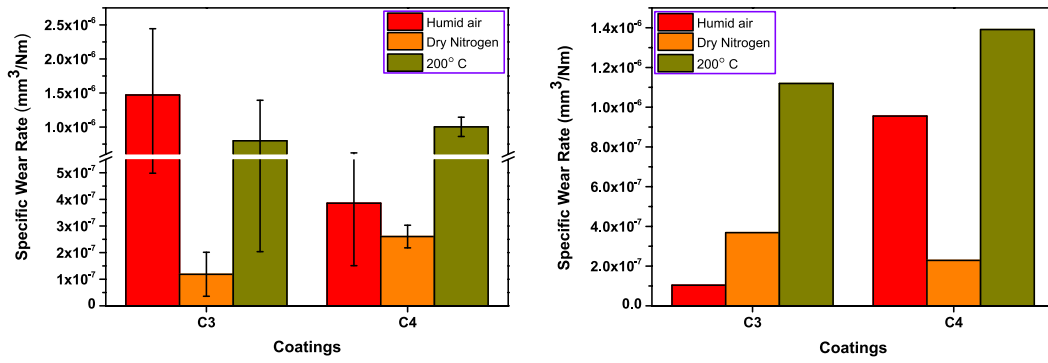
Figure 6-12: Reciprocating sliding specific wear rates of C3 and C4 disk/coating (left) and (right) counter bodies in diverse environments

Predictably, due to sliding in an inert environment, the COF and specific wear rates decreased slightly in relation to the values achieved in room conditions. The steady-state average COF was ~0.033 and ~0.045 for C3 and C4 coatings, respectively. It is well known that TMDs perform better in dry and vacuum atmospheres [87,171]. C3 coating with a high Se/Mo ratio performed slightly better when compared to C4 coating, which had lower Se/Mo ratio, behaviour which can be attributed to the easier formation of the low shear strength tribolayer responsible for the low friction behaviour of these types of coatings.
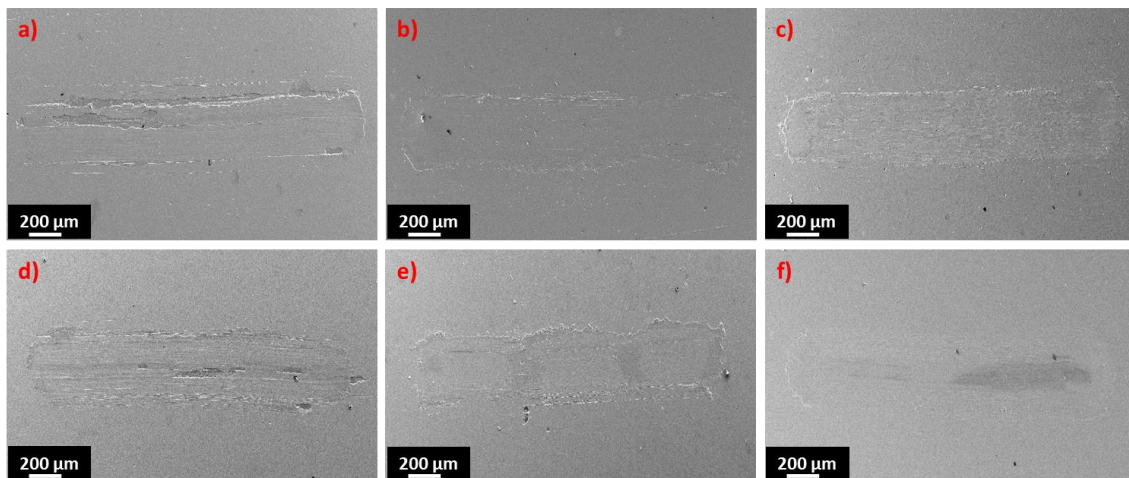

Figure 6-13: SEM wear track images after reciprocating sliding tests in diverse environment – C3: a) ambient air, b) dry nitrogen, c) 200° C and C4: d) ambient air, e) dry nitrogen, f) 200 °C

For tests performed at 200 °C, the COF showed minor changes for both C3 and C4 coatings, as compared to ambient air and dry nitrogen tests, although in opposite directions i.e., increasing for the former and decreasing for the latter. With the increase of the temperature, moisture is removed from the atmosphere surrounding the sample but, on the other hand, the probability of oxidation of $MoSe_2$ above 150 °C is enhanced [138].

Therefore, the higher Se/Mo ratio in C3 coating promotes its likelihood for high-temperature oxidation, resulting in higher COF compared to the C4 coating. In terms of specific wear rates, the values were comparable to the ones obtained for the C3 coating during sliding in ambient air atmosphere.
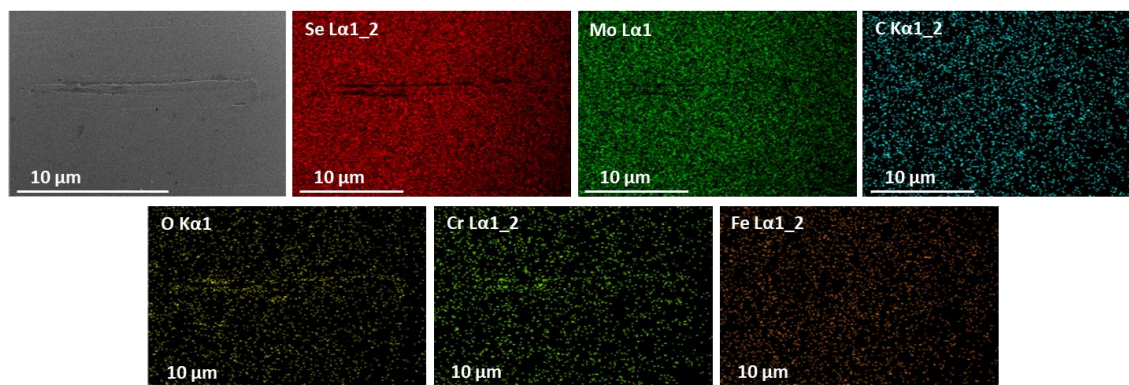

Figure 6-14: EDS elemental maps for C3 coating wear track after reciprocating sliding in ambient air

Globally speaking, minor fluctuations in COF were observed by changing the sliding environments. If the range of error values is considered in all tests, the differences are even less important. Therefore, the performance of these coatings can be affirmed as environmental independent which is not the case in any other TMD-C systems. Such a common behaviour suggests that the mechanism controlling the friction performance should be similar, i.e., as above discussed, the formation of a lubricious phase based on a stacking of basal planes of $MoSe_2$ is responsible for the friction and wear reduction. C only played a role towards the improvement of the mechanical properties, as non-hydrogenated carbon phases are unable to provide friction reduction in inert environments like dry nitrogen [34]. Therefore, we could prove that neither these coatings show chameleon behaviour, frequently reported in the literature, nor all TMD-C systems should behave as chameleon coatings.

The ability of Mo-Se-C coatings to display consistent COF irrespective of the sliding environments reported here seems to be a potential solution for applications requiring diverse environment sliding. So, as mentioned in the summary of the previous section, $MoSe_2$ based coatings can be a suitable option to be explored by industries.

6.3. Conclusions

Stoichiometric and highly compact Mo-Se-C coatings were deposited by the confocal DCMS technique. Low C contents, in the range form ~18 up to ~27 at. % were used to reduce the stoichiometric degradation of $MoSe_2$. The low C content and Se/Mo values close to stoichiometry resulted in a microstructure with the presence of (002) $MoSe_2$ basal planes, which played a vital role in the easy shearing properties during sliding. Raman spectroscopy confirmed the structural results from XRD analysis. Unidirectional tribological tests in ambient air showed COF and specific wear rates much improved then literature on TMD-C coatings, with values as low as ~0.027 and 2 x 10^{-7} mm^3/Nm, respectively. As a general trend, increasing C resulted in an increase of the running-in period while increasing number of cycles decreased the COF since the coatings entered from running-in to steady-state sliding regime. Optical microscopy showed a tribolayer formed in the wear tracks and counter bodies of all tested samples. SEM and Raman showed that a $MoSe_2$ tribolayer forms initially in patches and partially covers the wear track, but with the increase in sliding cycles, it covers the whole wear track. TEM cross-sections also confirmed that the tribolayer solely consists of well-oriented $MoSe_2$. EDS maps from SEM and STEM further reinforced these observations and, no significant amount of C was found in the tribolayer. COF and specific wear rates only showed minor fluctuations when the sliding environment was changed, unlike other TMD coatings referred in the literature. Considering the very low COF values, $MoSe_2$ was playing the dominant role in the wear track to reduce the friction and wear in all environments. This allowed to conclude that these Mo-Se-C coatings do not show chameleon behaviour. Furthermore, the deposited coatings possess excellent ability to replenish worn out regions (as observed for C2 coating after 5000 and 25000 cycles), which can be an advantage for industrial applications where catastrophic failure should not occur. The coatings display excellent ability to be used as solid-lubricant in diverse environments and for equipment that needs longer durations between inspections, like satellites.

In short, the optimization of the Mo-Se-C coatings with respect to compositional, morphological, structural and mechanical properties reported in chapter 5 led to enhanced tribological properties in diverse environment sliding. Fortunately, the idea of going against the reported literature regarding C content resulted in fruitful results and the achieved properties played a very vital role in the tribological performance of the coatings.

Chapter VII

7. MECHANISM OF TRIBOLAYER FORMATION IN TMD-C COATINGS

7.1. Introduction

The formation of a tribolayer (of TMDs) at the contact interface, and its ability to easily slide under the applied load, are the main reasons behind the excellent low friction properties of pure and alloyed TMD coatings [58,128,132,172]. However, the mechanism behind this formation in C-alloyed TMD coatings was not completely understood. Different tribolayer formation mechanisms were reported in [73], suggesting the reorientation of TMD crystals as the main reason for that event. It is widely accepted that under applied loads, this reorientation of TMD crystals solely occurs in the coating near the contact interface i.e., in a very thin layer in the top surface of the coating. During the reorientation, the (002) basal planes are aligned parallel to the sliding direction which, due to the weak Van der Waals bonding, slide easily to provide lubrication. It is also believed that this transformation / reorientation increases with the applied loads and the number of sliding cycles with the consequent decrease of the COF [24,25,57,58,75,122].

This chapter mainly focuses on the detailed study of the governing mechanisms of these tribolayers formation in Mo-Se-C coatings. For these purposes, an in-depth investigation of the wear tracks was carried out using Raman spectroscopy and TEM. Firstly, the wear tracks of C4 coating tested in chapter 6 (see figure 6-6) were studied. Raman spectroscopy was performed on both the as-deposited and various wear track regions to identify zones having different $MoSe_2$ crystallinity. Then, based on the Raman results, FIB cuts were performed in the wear tracks in specific locations to cover all the details and the morphological differences caused by the sliding. The FIB lamellae prepared from the as-deposited coating, the cross-sections of the wear tracks, after 25000 and 100000 cycles, and the wear debris were later analysed by TEM.

Additionally, a new test was designed in which a 100Cr6 steel ball was slide in a straight line against a stationary disk (the schema is shown in Fig. 7-1). The ball was fixed, being the only movement allowed was the horizontal direction. One lap was of 22 mm

distance (straight line) and, after each lap, the test was repeated over the same track but the ball was rotated to change the contact point. The idea was to use a new contact surface of the ball, keeping the same material in the coating´s wear track. This method excludes the effect of the worn material (wear debris) and any possible transfer film formed at the ball on the frictional process. Two tests were performed at 10 laps and 20 laps, resulting in total sliding distances of 220 mm and 440 mm, respectively. Both tests were performed under an applied load of 100 N (Hertzian contact pressure = ~2.2 GPa), to induce high contact stresses for the reorientation, despite the small sliding distance. Later, Raman spectroscopy was performed at different points in the wear track to study $MoSe_2$ bands, to analyse the reorientation of TMDs in the coating.
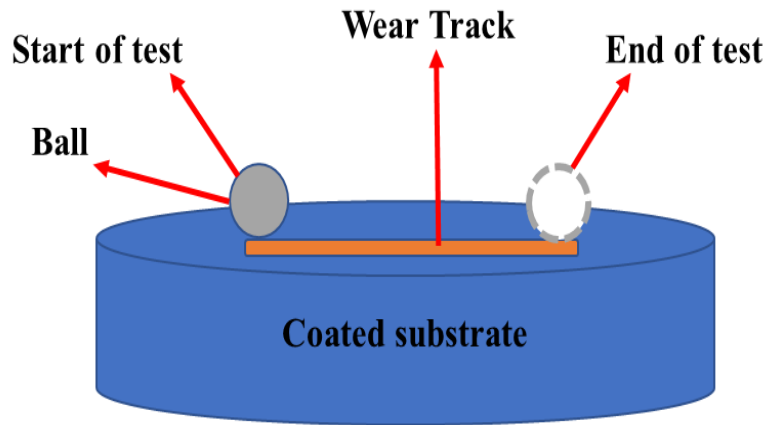

Figure 7-1: Schematic of the novel test setup used to remove the influence of transfer film

7.2. Results and discussion

As already presented in figure 6-6, different morphological regions were observed in the wear tracks after 25000 and 100000 cycles tests. Raman spectroscopy results of either the as-deposited coating or various zones marked on the wear tracks in figure 6-6 were shown in figure 6-7. The valleys and peaks shown in the SEM micrographs of the wear tracks after 25000 cycles, give rise to different $MoSe_2$ signals. These signals were related to different levels of crystallinity (crystallization / reorientations). The valleys resembled as-deposited coatings (points R1 of figure 6-6), while the protrusions showed highly crystalline $MoSe_2$ Raman peaks (points R2), suggesting the occurrence of crystalline tribolayers. The tribolayers are not homogeneously covering the wear track and are separated by as-deposited regions, and some discontinuities / break could also be observed.

The endpoints of these irregularities were also marked in the wear track in figure 6-6. After 100000 cycles, the wear tracks displayed very minor zones of the valleys. Raman analysis performed in any region on this wear track displayed sharp signals of $MoSe_2$ peaks, clearly showing highly crystalline material. To further investigate these characteristic regions, TEM studies were carried out and the results representative of the wear tracks are reported here. The FIB cross-section areas of selected regions of the as-deposited surface, 25000 cycles and 100000 cycles wear tracks are shown in figures 7-2 a), c) and e), respectively. The as-deposited coating (Fig. 7-2 b)) is structurally homogeneous both in the bulk and close to the surface, without any traces of oriented planes parallel to the surface. Only a small number of $MoSe_2$ platelets are randomly distributed throughout the coating. For the 25000 cycles wear track, the post-test analysis of the contact interface shows evidence of the occurrence of a reorientation /crystallization process, but only in some zones. In some regions, the tribolayer is clearly detected (Fig. 7-2 d)), whereas in other regions, the tribolayer is absent (inset Fig. 7-2 d)). Thus, in agreement with SEM and Raman results, the tribolayers are not covering homogeneously the wear track. On the other hand, similar analysis from the 100000 cycles wear track show a well-aligned and oriented tribolayer, covering all the surface but, again, not morphologically homogeneous with its thickness varying from point to point. Figure 7-2 f) shows highly thick regions of $MoSe_2$ tribolayer while the inset of figure 7-2 f) shows thinner oriented planes.

TEM observations confirmed that a reorientation / crystallization process is occurring leading to a tribolayer formation in the sliding interface. In literature [24,126,132], the most usual explanation for the formation of this tribolayer involves a reorientation (crystallization in case of amorphous coatings) mechanism occurring inside the coating close to the contact surface. However, a different interpretation can also be suggested based on the detailed analysis of the cross-section TEM results, as follows:

(i)   During sliding, wear of the coating occurs, resulting in the detachment of material from the coating. This detached material goes either in front of the counter body (ball in this case), to which it can stick or to the sides of wear track. Eventually, most of the harder carbon is transferred to the sides of the wear track under the influence of the load and the softer $MoSe_2$ can stick to the counter body. As the sliding continues, the material stuck to the ball can be transferred back. In fact, this material is trapped between the wear track and the counter body, like a 3rd body, being able to adhere to any of these

elements of the sliding pair. Due to the applied pressure on this $MoSe_2$-containing 3rd body, it becomes aligned and forms a well-oriented tribolayer parallel to the sliding. The tribolayer formed by this mechanism should be called as a "transfer layer" and not a "reoriented layer".
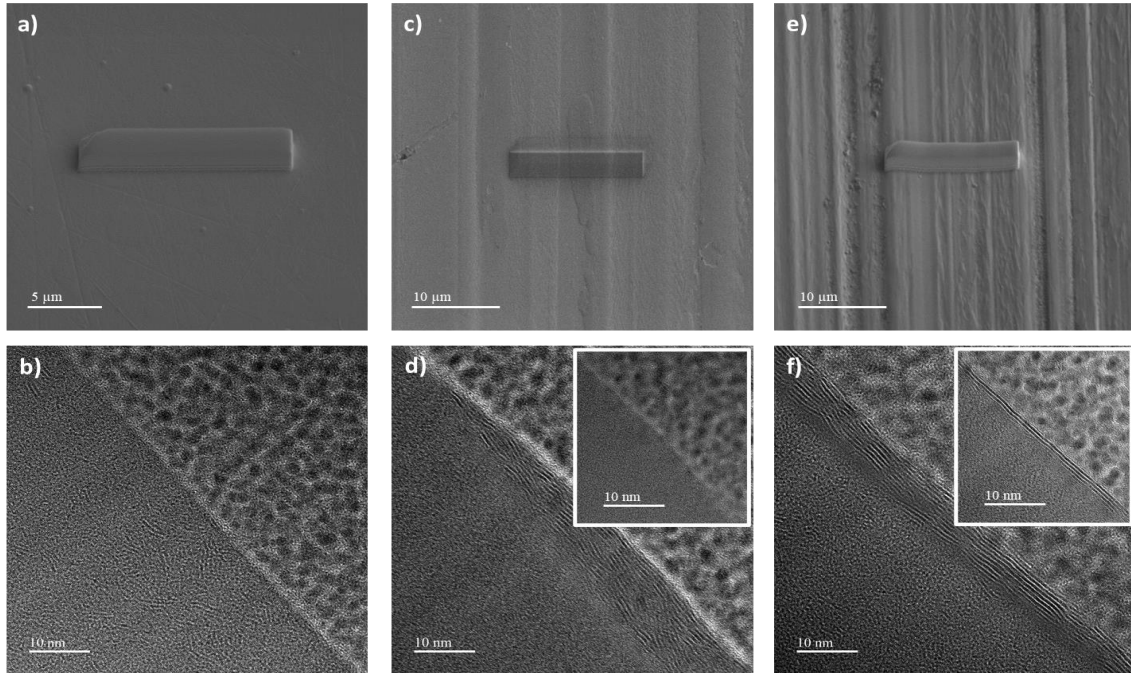

Figure 7-2: SEM images of the cross-section areas selected for FIB: a) as-deposited surface, c) wear track after 25000 cycles test, e) wear track after 100000 cycles test and the HRTEM micrographs: b) as-deposited surface, d) wear track after 25000 cycles test, f) wear track after 100000 cycles test

(ii) TEM analysis showed that there were regions in the wear track where the tribolayer consist of well-aligned $MoSe_2$ planes parallel to the surface along with amorphous zones (Fig. 7-3 a), b) and c)). As can be observed in these pictures, the aligned planes can be either in the contact surface or in the interface between the tribolayer and the coating. In any of the three shown cases, it is clear that the amorphous layer (in one case this layer is rich with O, suggesting the formation of an oxide) can only be there if adhered from the outside as a transfer layer. Such an arrangement discloses any possibility that the tribolayer is formed exclusively by reorientation / recrystallization of the top layer of the coating. Then, the reorientation / crystallization of the transfer film can occur either near the coating interface or at the counter body, creating a mixture of amorphous zone and parallel planes. A broader picture of the transfer film and all the zones discussed above is summarized in figure 7-3 d). The end of the

transferred film patch, marked in the top right inset, is a good evidence that this tribolayer is of transfer type as if it was "glued" there.
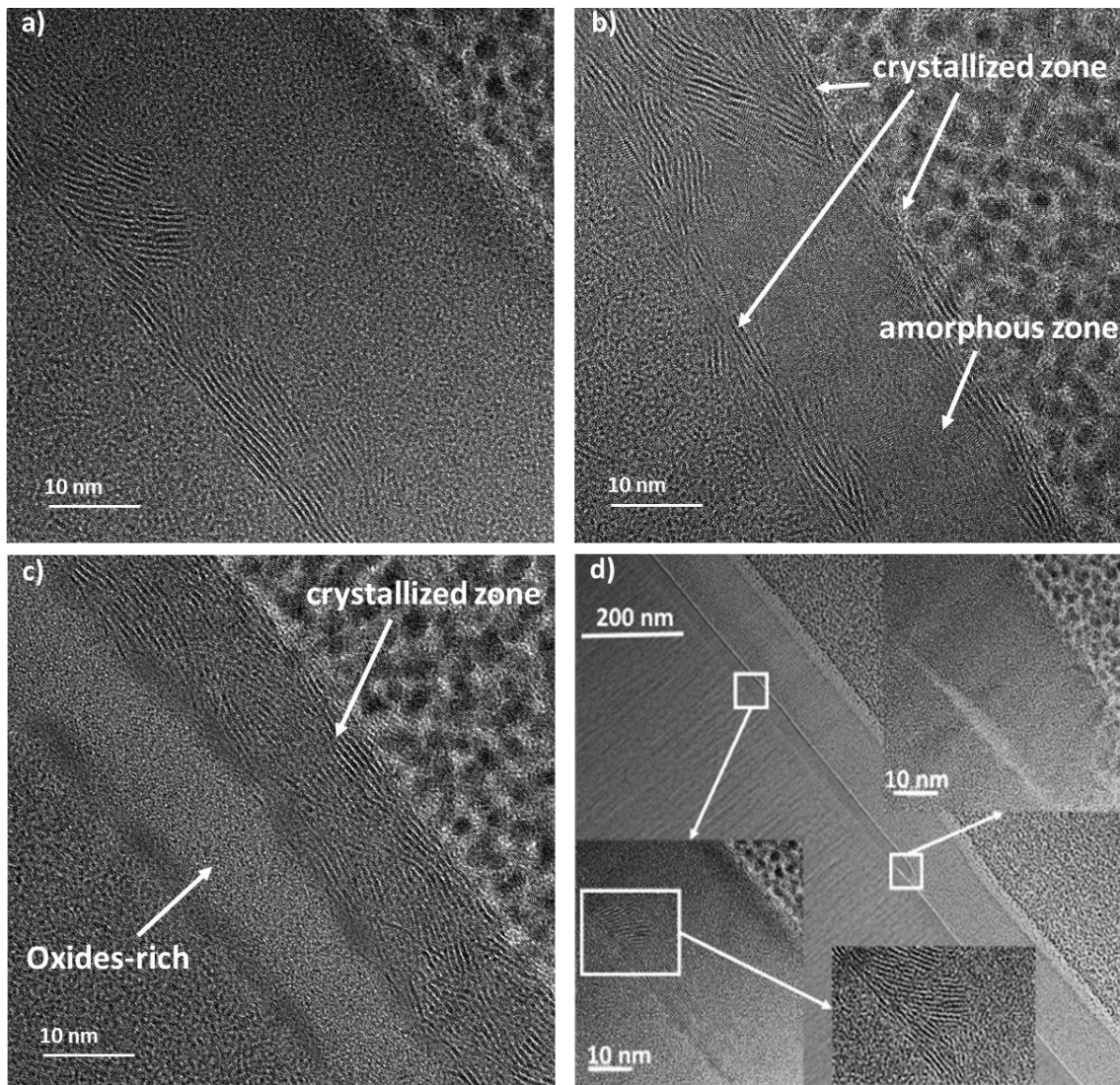

Figure 7-3: HRTEM images showing various zones observed in the tribolayer

(iii) Similar TEM micrographs were reported in literature [24,128], but none explained that the reorientation actually occurs outside the coating, being this material transferred from the counter body to the wear track. For example, in literature, it is reported that, for W-S-C coatings, the amorphous zones between the well-aligned regions corresponded to oxides (ref [128]) arising from the oxidation of W by the residual O in the coating. However, STEM analysis in the present study shows that the oxides merely appear in some regions of the wear track in the bottom part of the transfer film i.e., between the oriented layer and the as-deposited coating. For example, the light

grey region in figure 7-3 c) is rich in oxygen and a similar picture has also been reported in ref [125]. The presence of these oxides in the tribolayer is due to the oxidation of the wear debris detached from the coating.

(iv) In agreement with Gustavsson [73], the initially formed tribolayer grows and becomes thicker but a fully formed tribolayer cannot grow beyond a specific thickness. After reaching a critical thickness, it can delaminate through any basal plane due to the low Van der Waals bonding. The excess material can either be attached to the ball or move to the sides of the wear track, contributing to be a part of wear debris. HRTEM image of lamellae prepared from wear debris (Fig. 7-4 a)), shows the presence of oriented $MoSe_2$ planes from the tribolayer. This is the reason why the wear of the coating occurs despite the formation of the tribolayers. The analysis of the wear debris also displayed some Mo based oxides marked in figure 7-4 a); their morphology is in agreement with the literature [128].

(v) Finally, another indirect proof that the transfer film mechanism acts in these materials is that in literature, several times TMD-C coatings are said to possess excellent capability to replenish the worn-out regions [75]. This is only possible if the detachment of coating particles coupled with the transfer film mechanism plays its role in sliding, as mentioned above.
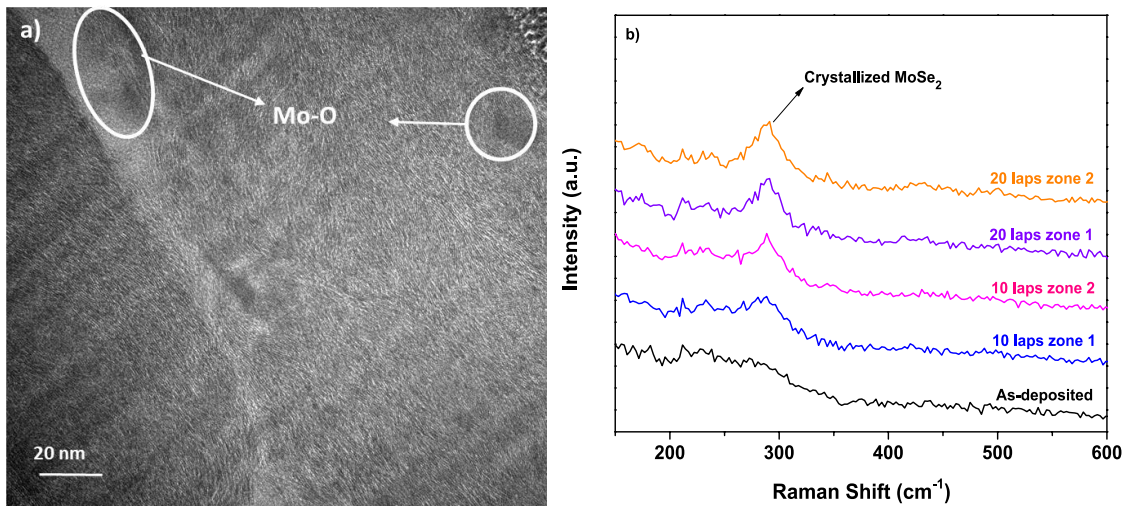

Figure 7-4: a) HRTEM image of the wear debris, b) Raman spectroscopy plots from the wear tracks obtained the novel tribo tests (zones 1 and 2 correspond to scans made at different positions in the track)

In fact, a simple test shows that the steady-state friction coefficient can be reached with the action of the transfer layer, as follows: a test in room conditions was performed on the as-deposited coating vs. a new steel ball. The initial COF in the running-in stage was 0.065. After 25000 cycles, the test was stopped and the used ball (having a built $MoSe_2$-containing transfer layer adhered) was tested against a new track in the as-deposited coating. The frictional curve in both cases followed similar trends but the COF was less with used ball, particularly in the running-in period which is, typically, 0.042. Such a low value, similar to the one achieved in steady-state, can only be possible by the action of the $MoSe_2$ tribolayer being transferred from the used ball to the coating and provided lubrication.

The question now is to know if the tribolayer can exclusively be formed by a transfer mechanism. To check if the reorientation mechanism in the contact interface can also contribute to the decrease of the COF, the coating was studied in the newly designed tribological test. It should be remarked, again, that after every lap, a new region of the ball was slide against the same wear track, thus avoiding any possible layer to be transferred from the ball. Raman analysis was performed on tracks and the results are shown in figure 7-4 b). Signals of crystalline $MoSe_2$ were observed after the tests, confirming the presence of the oriented crystalline tribolayer at the coating interface. Very minor $MoSe_2$ signals were observed after 10 laps which became quite sharp and pronounced after increasing the number of laps to 20.

Thus, based on all the above-mentioned observations, it can be said that both the reorientation within the coating matrix and the transfer film from a 3rd body play a role in the tribolayer formation. These synergetic mechanisms behind the tribolayer formation make part of a new interpretation which complements the accepted literature reports (on TMD-C coatings), where only reorientation is considered to govern the tribolayer formation.

7.3. Conclusions

To understand the mechanisms for the formation of TMD tribolayers, a detailed investigation of the wear tracks was carried out using Raman spectroscopy and transmission electron microscopy. Wear tracks, after tribological testing by unidirectional

pin-on-disk and a novel designed process, were thoroughly studied. It has been concluded that an important part of the reorientation / crystallization of TMDs occurs outside the coating, between the contact zone of the sliding bodies and not merely inside the coating. The detachment of as-deposited coatings particles during sliding, their insertion in the contact zone, and later transfer of the film from the counter body to the coating is one of the reasons behind the formation of these tribolayers. This claim was supported by the presence of oxygen-containing amorphous zones beneath the tribolayer at some points, which can only occur if the adhered material is originated from either a 3rd body or the counter body. On the other hand, it was proved that the reorientation within the coating also plays a part in the overall tribolayer formation. This chapter negates the widely accepted claims of literature that reorientation of TMDs within the coatings (of TMD-C system) is the only mechanism of easy shear tribolayers formation.

Chapter VIII

8. Mo-Se-C: UNIVERSAL DRY LUBRICANTS FOR TERRESTRIAL AND AEROSPACE APPLICATIONS

8.1. Introduction

As mentioned earlier, whether pure or combined with other elements or compounds, all the TMD-C coatings displayed very low COF in vacuum / dry atmospheres (COF < 0.03), but, as soon as the sliding environment changes to room conditions, the COF increased very significantly to 0.1-0.15 or even more [24,59,60]. These large performance discrepancies are also the major hindrance to their application in the aerospace industry, especially for satellites that endure coastal climate before being launched.

In chapter 6, Mo-Se-C coatings were shown as a good candidate for diverse environments sliding. This chapter deals with further advancements in the tribological testing of these coatings under multiple conditions. The aim is to unfold the amazing capability of the optimized Mo-Se-C coatings to act as a universal solid lubricant for both terrestrial and aerospace applications. Some novel and remarkable results for Mo-Se-C coatings are reported in this part of the thesis.

To simulate the industrial requirements, DC and RF sputtered coatings are tribologically tested, for the first time, under various contact pressure regimes, vacuum and ambient air conditions, short and long sliding cycles, and sliding speeds. The key features tested / reported in this chapter are:

1. Testing in vacuum atmospheres at low contact pressures, and ambient air at both low and high contact pressures – to date, no study can be found on the performance of Mo-Se-C coatings in vacuum and also at low contact pressures in any environment.

2. The vacuum, contact pressure, and sliding speeds were selected to replicate the actual industrial conditions in diverse environments [27,143,144].

3. Finally, for the first time, COF comparison for $MoSe_2$ (in combination with C) sputtered with DCMS vs. RFMS has been reported, for both environments.

The detailed deposition procedure and the tribological testing conditions can be found in sections 3.3.2 and 3.5.3, respectively. This chapter is supported by the publication attached in annex D.

8.2. Results and discussion

Pure MoSe$_2$ coatings were highly porous irrespective of DC or RF power supplies. The coatings names are related to their C content as: DC324-18% C, DC676-25% C, RF170-18% C, and RF340-25% C. With the addition of C, the coatings became compact in both cases with a minor decrease in the Se/Mo composition. XRD, TEM, and Raman spectroscopy showed that the coatings were polycrystalline with MoSe$_2$ embedded in amorphous carbon. The hardness increased with C, showing a maximum of 4.6 GPa for DC25 coating. For further details about the properties of these coatings, see chapter 5. The results of all tribological tests performed in this work are shown in table 8-1.

Table 8-1: Tribological results of the coatings under different testing conditions

Coatings	Low contact pressure (Applied load 5 N, Hertzian contact stress 85 MPa)				High contact pressure (Applied load 10 N, Hertzian contact stress 1010 MPa)			
	Ambient air		Vacuum		Ambient air			
	COF	Specific wear rate mm^3/Nm	COF	Specific wear rate mm^3/Nm	COF (25000 cycles)	Specific wear rate mm^3/Nm	COF (100000 cycles)	Specific wear rate mm^3/Nm
DC MoSe$_2$	0.03-0.05	2-3 E-6	0.02-0.04	2-3 E-6	Failed-T.D.	NA	Failed-T.D.	NA
DC324	0.04-0.05	2-4 E-6	0.03-0.04	2-4 E-6	0.01-0.02	3-5 E-7	0.01-0.03	2-4 E-7
DC676	0.04-0.06	3-5 E-6	0.04-0.06	2-3 E-6	0.03-0.04	1-2 E-6	0.02-0.04	1-2 E-6
RF MoSe$_2$	0.06-0.07	1-2 E-5 (P.D.)	0.02-0.03	1-3 E-6	0.02-0.04	1-3 E-6 (P.D.)	0.02-0.03	7-10 E-7 (P.D.)
RF170	0.05-0.07	2-4 E-6	0.04-0.06	1-4 E-6	0.03-0.04	4-6 E-7	0.03-0.04	3-6 E-7
RF340	0.05-0.06	4-6 E-6	0.04-0.06	2-4 E-6	0.02-0.03	2-5 E-7	0.02-0.04	1-4 E-7
**P.D. - Partial delamination, T.D. - Total delamination								

The ranges of the resulting mean values have been reported based on the repeatability of the tests and for better comparison among all tribological testing conditions. The main tribological results are described as follows:

8.2.1. Low contact pressure tests

COF evolution of the coatings after low contact pressure tests are shown in figure 8-1. When analyzed in a global way, the friction curves have similar trends and values for all coatings, independently of the deposition technique and the environmental conditions. In the case of testing in ambient air, some coatings show a longer running-in period, which can be related to the time for the formation of the tribolayer [24]. However, the final values of all the low contact pressure tests in all environments are remarkably very similar i.e., in the range of 0.02–0.06 for ambient air while, 0.02-0.07 for vacuum conditions. A significant deviation was observed for pure RF in vacuum to ambient air sliding. In ambient air, this coating also shows a COF value higher than 0.06 when sliding in room conditions, which should be related to the partial delamination observed (Fig. 8-2).
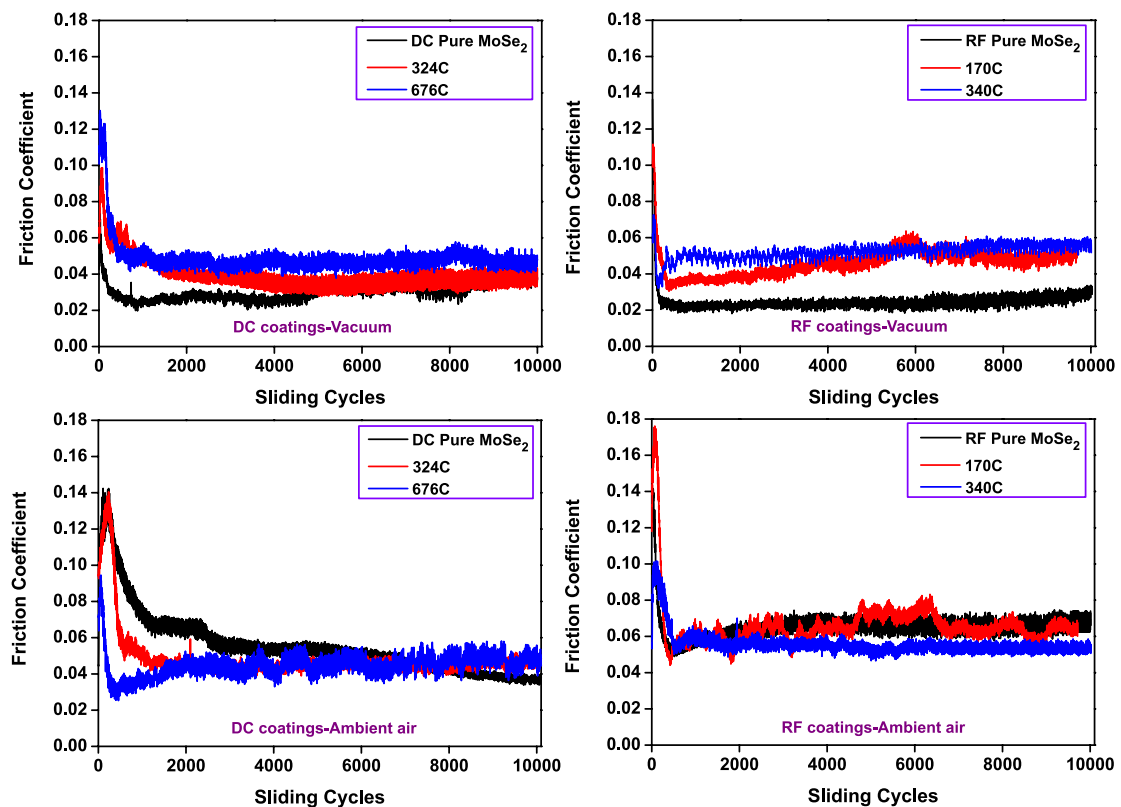

Figure 8-1: Friction curves after vacuum and ambient air tests at low contact pressure

The analysis of table 8-1 also allows us to draw very similar conclusions about the wear rates. All coatings show approximately the same wear rates independently of the power supply used for the deposition as well as the testing environment (in the range [2-4 x10^{-6} mm^3/Nm]) being the only exception, again, the pure RF coating in ambient air, due

to the observed delamination. Therefore, globally it is possible to conclude that, differently from what can be found in the literature for other TMD-based coatings, the friction and wear behaviour of Mo-Se-C coatings reported here are much less influenced by the deposition technique, C content, and testing environment.
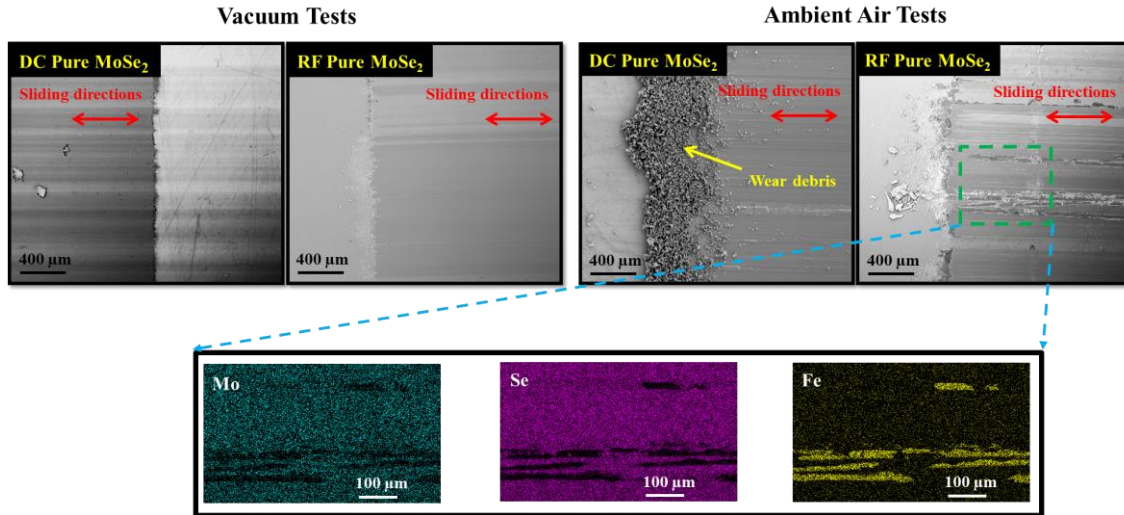

Figure 8-2: Wear track morphologies of pure MoSe$_2$ coatings of Low contact pressure

8.2.2. High contact pressure tests

COF evolution curves of the coatings after high contact pressure tests are shown in figure 8-3. Despite the different conditions in both tribological tests (low vs. high contact pressure), the trends are very similar. The friction values in all cases are very close, in the range [0.01 – 0.04]. These values are remarkably low in comparison with the literature for pin-on-disk tests of TMD-based coatings tested in ambient air conditions [24,59,60]. Very often, values as high as 0.1 - 0.15 are referred [59,60,173]. As it would be expected, the friction curves for 25000 and 100000 cycles are almost similar, since the material and testing conditions are the same. This result clearly shows that the steady-state for 25000 cycles test is kept constant for much higher duration tests and the coatings are very stable. Similar results occur for the wear rates. All coatings show values in the range [2-6 x10^{-7} mm^3/Nm], except DC676 and pure MoSe$_2$ deposited films. The DC pure coating completely failed with its total destruction during testing, whereas partial delamination is observed in RF sputtered film which gives rise to the higher measured values of the wear rate. The slightly lower COF and specific wear rates in high-pressure tests can be attributed to the non-Amonton response of TMDs (as the applied load in these tests was higher) and

the difference in the sliding mechanisms between unidirectional and reciprocating tests [24,170]. However, globally, the values are very close to each other and within the same range of COF achieved for low contact pressure in diverse environments.
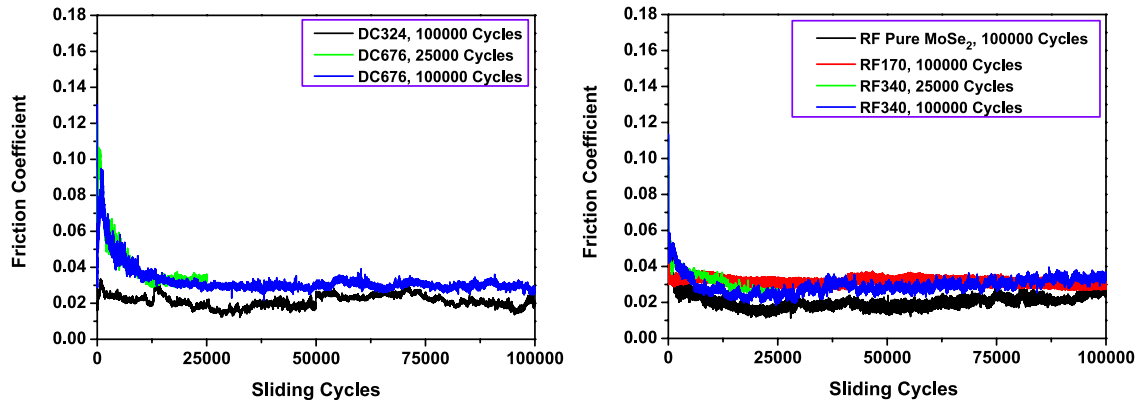

Figure 8-3: Friction curves after 25000 and 100000 sliding cycles in ambient air at high contact pressure. 25000 cycles curves of only selected coatings are shown for reference

Considering the reported contact pressure used in industrial journal and ball bearings [27,144], our study shows COF and wear rate as optimum for such applications, irrespective of the sliding environment. Moreover, it is known that atomic oxygen adversely affects the properties of MoS_2 coatings in space machinery due to the re-sputtering of S and the resulting MoO_3 formation [27]. This problem can be overcome using $MoSe_2$ due to a lower re-sputtering of Se, as compared to S [174], avoiding, then, the oxidation and degradation processes. Finally, the deposition by DC sputtering was shown to be similar to RF, the technique that has been used for the deposition of the Mo-Se-C system. The use of DC sputtering is more industrially favourable and the results perfectly align with this demand.

8.3. Conclusions

Pure and carbon-alloyed $MoSe_2$ coatings were deposited by both DC and RF sputtering. For mimicking terrestrial and space applications, the coatings were tribologically tested in vacuum and ambient air atmospheres under different contact pressure (85 MPa and 1010 MPa) and sliding speeds (0.1 m/s and 2 mm/s). When shifting from low contact to extreme loading conditions, low to high sliding speeds, vacuum to ambient air atmospheres, or DC to RF power sources, consistent low COF and wear rates

were achieved, a breakthrough that has not been reported earlier for any solid lubricant system. Hence, Mo-Se-C coatings are of high importance for applications that demand solid lubricants for working independently of the surrounding environment and loading conditions. This part of the thesis validates Mo-Se-C coating as a universal solid lubricant and can guide towards resolving sustainable solid lubrication issues for aerospace and terrestrial machine components.

Chapter IX

9. CONCLUSIONS AND FUTURE WORKS

In this thesis, a systematic approach was used to enhance the tribological performance of less explored Mo-Se-C coatings. A detailed study of the deposition procedures and properties of the coatings was made to optimize the self-adaptive tribological behaviour of Mo-Se-C coatings in diverse sliding environments and conditions.

As a first step towards this goal, the coatings were deposited using separate C and $MoSe_2$ targets (co-sputtering). During this first-ever deposition of Mo-Se-C coatings using DCMS and multiple targets setup, the effects of the C content and the substrate bias on the composition, structure, mechanical and tribological properties were explored. Carbon contents of 44 to 60 at. % and a negative substrate bias of 50, 70, and 90 V DC voltage were used. Maximum Se/Mo ratio of 1.88 was evaluated by WDS analysis, a value higher than the literature on other TMD-C systems. With the application of substrate bias, the deposition rates and Se/Mo ratios decreased but much compact coatings were observed by SEM. Mo-Se-C coatings displayed broad amorphous XRD patterns, with no signs of (002) peaks of the hexagonal $MoSe_2$ phase. HRTEM showed $MoSe_2$ platelets randomly oriented in an amorphous carbon matrix. Raman analysis showed the presence of $MoSe_2$ crystalline peaks. Nano-indentation tests showed an increase in the hardness of the coatings deposited under negative substrate bias. In reciprocating sliding, the 90 V bias coating displayed the lowest COF of 0.025 in dry nitrogen, while a value of 0.06 was recorded in ambient air.

After having the idea of the performance of coatings made by co-sputtering and deposition parameters, the next step was the optimization of the chemical composition to be as close as possible to the stoichiometry of $MoSe_2$ (Se/Mo ~2), high crystallinity, and high mechanical strength. At this stage, Mo-Se-C coatings were deposited using co-sputtering under confocal plasma. To enhance the crystallinity of $MoSe_2$ in the coatings, the depositions were carried out with a lower carbon content (< 30 at. %). Two different approaches were used; $MoSe_2$ target powered by either DC or RF magnetron sputtering. WDS displayed Se/Mo ratio of ~2 for DC coatings, values higher than the literature. The

Se/Mo ratio for RF deposited coatings was lower than the DC ones. SEM showed that irrespective of the low carbon additions, the Mo-Se-C coatings were highly compact with no vestiges of columnar growth. The application of substrate bias further improved the compactness at the expense of a lower Se/Mo ratio. XRD, HRTEM, and Raman spectroscopy confirmed the presence of $MoSe_2$ crystals. Even with very low carbon additions, an improvement of the hardness of the coatings could be reached in comparison to the previous approach. A comparison between RF and DC sputtering of Mo-Se-C coatings was also studied.

The next phase was aimed towards a thorough analysis of the diverse environment tribological performance of the optimized Mo-Se-C coatings with an emphasis on the ambient air sliding. The detailed analysis of the wear track and the tribolayer evolution as a function of the C content and the number of sliding cycles were discussed. In unidirectional tests, under ambient conditions, the increase of the sliding cycles resulted in a decrease in the COF and wear rates. This is attributed to an increased coverage of wear tracks with the low friction tribolayer of $MoSe_2$ by increasing the number of sliding cycles. After 100000 cycles, the wear track was fully covered by a thick $MoSe_2$ tribolayer. The achieved values in unidirectional humid air sliding tests were superior to the literature and previous deposition approach. Under reciprocating sliding tests in diverse environments, the coatings hindered the wear in ambient air but an enhanced tribological performance was achieved in dry N_2 and at elevated temperature (200 ºC). In all environments, the low friction tribolayer was solely composed of the $MoSe_2$ phase. Thus, the Mo-Se-C coatings did not show the chameleon behaviour, claimed in literature for TMD-C coatings. The coatings displayed excellent ability to be used as solid-lubricant in diverse operating environments.

Next, the mechanism governing the formation of the easy shear tribolayers in TMD-C coatings was investigated. Optimized Mo-Se-C coatings deposited using DC magnetron sputtering were tested under: (i) unidirectional rotating tribological tests and (ii) unidirectional test that eliminated the effects of wear debris and transfer layers. The idea was to understand the role of transfer layers and reorientation inside the coating matrix, in the formation of tribolayers. HRTEM and Raman spectroscopy studies were performed on as-deposited coating and wear scars. The research unfolded the misconceptions of literature regarding the routes for the tribolayer formation. It was observed that both the transfer layer

formed due to the 3rd body in the contact zone and the reorientation / crystallization within the coating matrix play their parts in the tribolayer formation.

Lastly, DC and RF sputtered coatings were tribologically tested, for the first time, under various contact stress regimes, vacuum and ambient air conditions, short and long sliding cycles, and different sliding speeds to simulate industrial requirements. The tribological properties were almost consistent, irrespective of the sliding conditions. In all cases, nearly consistent friction coefficient range (0.02-0.06), and long-term endurance show that these coatings can be an ideal universal solid lubricant for low friction in the aerospace and terrestrial environments.

In future works, although the most important thing is to replicate these coatings according to the optimized deposition conditions and properties, in an industrial chamber to start the upscaling. Industries working in collaboration with our group will be contacted regarding the depositions in an industrial chamber, as well as, on the actual industrial components. But before this step, the deposition and characterization of coatings at different substrate to target distance and on 3D parts needs to be explored. The coatings should also be tested for much longer sliding durations and under highly humid conditions, to further investigate the endurance limit. Moreover, the sliding properties of Mo-Se-C coatings against rubber should be explored for applications like molds for tyre manufacturing. Lastly, it can be a good possibility to study the alloying of $MoSe_2$ with nitrogen for mechanical property enhancement, as nitrogen´s adverse effects on the chalcogen / metal atom ratio will be most probably less in $MoSe_2$ as compared to other TMDs. Similarly, the formation of nitrides is a possibility that can make the coatings applicable in the cutting industry.

BIBLIOGRAPHY

[1]   Erdemir A, BHUSHAN B. Modern Tribology Handbook. CRC Press; 2001.

[2]   P.M. Martin. Handbook of deposition technologies for films and coatings: science, applications and technology. Elsevier Inc.; 2009.

[3]   Tabor D. Friction—The Present State of Our Understanding. J Tribol 1981;103:169. doi:10.1115/1.3251622.

[4]   E. C. Fitch. Fluid Chemical Stability. Proactive Maint. Mech. Syst., U.K: Elsevier; 1992, p. 99–126. doi:10.1016/B978-1-85617-166-3.50005-6.

[5]   Kennedy M, Hoppe S, Esser J. Piston Ring Coating Reduces Gasoline Engine Friction. MTZ Worldw 2012;73:40–3. doi:10.1007/s38313-012-0174-x.

[6]   Bhushan B. Introduction to tribology. vol. 17. Second Edi. New York: John Wiley & Sons. Ltd; 2013.

[7]   Technical Committee of Petroleum Additive Manufacturers in Europe. Lubricant Additives and the Environment. Atc 2007;49.

[8]   Kalin M, Velkavrh I, Vižintin J, Ožbolt L. Review of boundary lubrication mechanisms of DLC coatings used in mechanical applications. Meccanica 2008;43:623–37. doi:10.1007/s11012-008-9149-z.

[9]   Vetter J. Surface Treatments for Automotive Applications. Coat. Technol. Veh. Appl., Springer; 2015, p. 91–132.

[10]   Rapoport L, Leshchinky V, Volovik Y, Lvovsky M, Nepomnyashchy O, Feldman Y, et al. Modification of contact surfaces by fullerine-like solid lubricant nanoparticles. Surf Coatings Technol 2003;163–164:405–12. doi:10.1016/S0257-8972(02)00729-6.

[11]   Lansdown AR. Molybdenum Disulphide Lubrication. Elsevier; 1999. doi:10.1108/ilt.2000.01852aae.001.

[12]   Scharf TW, Prasad S V. Solid lubricants: a review. J Mater Sci 2013;48:511–31. doi:10.1007/s10853-012-7038-2.

[13]   Prasad S V., Michael JR, Christenson TR. EBSD studies on wear-induced

subsurface regions in LIGA nickel. Scr Mater 2003;48:255–60. doi:10.1016/S1359-6462(02)00376-7.

[14] Bower AF, Johnson KL. The influence of strain hardening on cumulative plastic deformaiton in rolling and sliding line contact. J Mech Phys Solids 1989;37:471–93. doi:10.1016/0022-5096(89)90025-2.

[15] Bowden FP, Tabor D. The Friction and Lubrication of Solids. Oxford: Oxford University Press; 1986.

[16] Grill A. Diamond-like carbon: state of the art. Diam Relat Mater 1999;8:428–34. doi:10.1016/S0925-9635(98)00262-3.

[17] Esteve J, Zambrano G, Rincon C, Martinez E, Galindo H, Prieto P. Mechanical and tribological properties of tungsten carbide sputtered coatings. Thin Solid Films 2000;373:282–6. doi:10.1016/S0040-6090(00)01108-1.

[18] Ji L, Li H, Zhao F, Chen J, Zhou H. Microstructure and mechanical properties of Mo/DLC nanocomposite films. Diam Relat Mater 2008;17:1949–54. doi:10.1016/J.DIAMOND.2008.04.018.

[19] Dai MJ, Wei CB, Zhou KS, Zhu M, Hou HJ, Lin SS, et al. Properties of W/DLC/W-S-C composite films fabricated by magnetron sputtering. Trans Nonferrous Met Soc China (English Ed 2015;25:3002–11. doi:10.1016/S1003-6326(15)63927-9.

[20] Roberts EW. Towards an Optimised Sputtered MoS2 Lubricant Film. 20th Aerosp Symp 1986:103–19.

[21] Serpini E, Rota A, Ballestrazzi A, Marchetto D, Gualtieri E, Valeri S. The role of humidity and oxygen on MoS2 thin films deposited by RF PVD magnetron sputtering. Surf Coatings Technol 2017;319:345–52. doi:10.1016/j.surfcoat.2017.04.006.

[22] Hilton MR, Bauer R, Didziulis S V., Dugger MT, Keem JM, Scholhamer J. Structural and tribological studies of MoS2 solid lubricant films having tailored metal-multilayer nanostructures. Surf Coatings Technol 1992;53:13–23. doi:10.1016/0257-8972(92)90099-V.

[23] Prasad S V., Zabinski JS. Tribology of tungsten disulphide (WS2): characterization of wear-induced transfer films. J Mater Sci Lett 1993;12:1413–5. doi:10.1007/BF00591592.

[24] Polcar T, Cavaleiro A. Review on self-lubricant transition metal dichalcogenide nanocomposite coatings alloyed with carbon. Surf Coat Technol 2011;206:686–95. doi:10.1016/j.surfcoat.2011.03.004.

[25] Polcar T, Cavaleiro A. Self-adaptive low friction coatings based on transition metal dichalcogenides. Thin Solid Films 2011;519:4037–44. doi:10.1016/j.tsf.2011.01.180.

[26] Muratore C, Voevodin AA. Control of molybdenum disulfide basal plane orientation during coating growth in pulsed magnetron sputtering discharges. Thin Solid Films 2009;517:5605–10. doi:10.1016/j.tsf.2009.01.190.

[27] Roberts EW. Thin solid lubricant films in space. Tribol Int 1990;23.2:95–104. doi:10.1016/0301-679X(90)90042-N.

[28] Briscoe BJ, Tabor D. The effect of pressure on the frictional properties of polymers. Wear 1975;34:29–38. doi:10.1016/0043-1648(75)90306-3.

[29] Martin JM. Superlubricity of molybdenum disulfide. Superlubricity, 2007, p. 207–25. doi:10.1016/B978-044452772-1/50044-5.

[30] Donnet C, Erdemir A, Robertson J. Tribology of diamond-like carbon films : Fundamentals and applications 2008.

[31] Scharf TW, Kotula PG, Prasad S V. Friction and wear mechanisms in MoS2Sb2O2Au nanocomposite coatings. Acta Mater 2010;58:4100–9. doi:10.1016/j.actamat.2010.03.040.

[32] Subramanian C, Strafford KN. Review of multicomponent and multilayer coatings for tribological applications. Wear 1993;165:85–95. doi:10.1016/0043-1648(93)90376-W.

[33] Xia L, Li G. The frictional behavior of DLC films against bearing steel balls and Si3N4 balls in different humid air and vacuum environments. Wear 2008;264:1077–84. doi:10.1016/j.wear.2007.08.010.

[34] Andersson J, Erck RA, Erdemir A. Friction of diamond-like carbon films in different atmospheres. Wear 2003;254:1070–5. doi:10.1016/S0043-1648(03)00336-3.

[35] Fusaro RL. Effect of substrate surface finish on the lubrication and failure mechanisms of molybdenum disulfide films. ASLE Trans 1982;25:141–56. doi:10.1080/05698198208983076.

[36] Waghray H, Lee TS, Tatarchuk BJ. A study of the tribological and electrical properties of sputtered and burnished transition metal dichalcogenide films. Surf Coatings Technol 1995;76–77:415–20. doi:10.1016/0257-8972(95)02564-2.

[37] Prasad S V., Zabinski IS, McDevitt NT. Friction behavior of pulsed laser deposited tungsten disulfide films. Tribol Trans 1995;38:57–62. doi:10.1080/10402009508983380.

[38] Fayeulle S, Ehni PD, Singer IL. Paper V (ii) Role of transfer films in wear of MoS2 coatings. Tribol Ser 1990;17:129–38. doi:10.1016/S0167-8922(08)70249-9.

[39] Lancaster JK. A review of the influence of environmental humidity and water on friction, lubrication and wear. Tribol Int 1990;23:371–89. doi:10.1016/0301-679X(90)90053-R.

[40] Wahl KJ, Singer IL. Quantification of a lubricant transfer process that enhances the sliding life of a MoS2 coating. Tribol Lett 1995;1:59–66. doi:10.1007/BF00157976.

[41] Donnet C, Martin JM, Le Mogne T, Belin M. The origin of super-low friction coefficient of MoS2 coatings in various environments. Tribol Ser 1994;27:277–84. doi:10.1016/S0167-8922(08)70317-1.

[42] Kubart T, Polcar T, Kopecký L, Novák R, Nováková D. Temperature dependence of tribological properties of MoS2 and MoSe2 coatings. Surf Coat Technol 2005;193:230–3. doi:10.1016/j.surfcoat.2004.08.146.

[43] Dominguez-Meister S, Justo A, Sanchez-Lopez JC. Synthesis and tribological properties of WSex films prepared by magnetron sputtering. Mater Chem Phys 2013;142:186–94. doi:10.1016/j.matchemphys.2013.07.004.

[44] Singer IL, Fayeulle S, Ehni PD. Wear behavior of triode-sputtered MoS2 coatings in dry sliding contact with steel and ceramics. Wear 1996;195:7–20. doi:10.1016/0043-1648(95)06661-6.

[45] Renevier NMU, Hamphire J, Fox VC, Witts J, Allen T, Teer DG. Advantages of using self-lubricating , hard , wear-resistant MoS 2 -based coatings. Surf Coat Technol 2001:67–77. doi:10.1016/S0257-8972(01)01108-2.

[46] Savan A, Simmonds MC, Huang Y, Constable CP. Effects of temperature on the chemistry and tribology of co-sputtered MoSx -Ti composite thin films. Thin Solid Films 2007;489:137–44. doi:10.1016/j.tsf.2005.04.078.

[47] Scharf TW, Rajendran A, Banerjee R, Sequeda F. Growth, structure and friction behavior of titanium doped tungsten disulphide (Ti-WS2) nanocomposite thin films. Thin Solid Films 2009;517:5666–75. doi:10.1016/j.tsf.2009.02.103.

[48] Chien H, Ma K, Vattikuti SVP, Kuo C, Huo C, Chao C. Tribological behaviour of MoS2/Au coatings. Thin Solid Films 2010;518:7532–4. doi:10.1016/j.tsf.2010.05.040.

[49] Lince JR. Tribology of co-sputtered nanocomposite Au/MoS2 solid lubricant films over a wide contact stress range. Tribol Lett 2004;17:419–28. doi:10.1023/B:TRIL.0000044490.03462.6e.

[50] Wahl KJ, Dunn DN, Singer IL. Wear behavior of Pb – Mo – S solid lubricating coatings. Wear 1999:175–83. doi:10.1016/S0043-1648(99)00100-3.

[51] Ye M, Zhang G, Ba Y, Wang T, Wang X, Liu Z. Microstructure and tribological properties of MoS 2 + Zr composite coatings in high humidity environment. Appl Surf Sci 2016;367:140–6. doi:10.1016/j.apsusc.2016.01.163.

[52] Deepthi B, Barshilia HC, Rajam KS, Konchady MS, Pai DM, Sankar J, et al. Structure, morphology and chemical composition of sputter deposited nanostructured Cr-WS2 solid lubricant coatings. Surf Coat Technol 2010;205:565–74. doi:10.1016/j.surfcoat.2010.07.050.

[53] Rigato V, Maggioni G, Boscarino D, Sangaletti L, Depero L, Fox VC, et al. A study of the structural and mechanical properties of Ti-MoS2 coatings deposited by closed field unbalanced magnetron sputter ion plating. Surf Coat Technol

Talha bin Yaqub

1999;116–119:176–83. doi:10.1016/S0257-8972(99)00312-6.

[54] Voevodin AA, O'Neill JP, Zabinski JS. Nanocomposite tribological coatings for aerospace applications. Surf Coatings Technol 1999;116–119:36–45. doi:10.1016/S0257-8972(99)00228-5.

[55] Cao H, De Hosson JTM, Pei Y. Effect of carbon concentration and argon flow rate on the microstructure and triboperformance of magnetron sputtered WS2/a-C coatings. Surf Coatings Technol 2017;332:142–52. doi:10.1016/J.SURFCOAT.2017.06.087.

[56] Cao H, Wen F, Kumar S, Rudolf P, De Hosson JTM, Pei Y. On the S/W stoichiometry and triboperformance of WSxC(H) coatings deposited by magnetron sputtering. Surf Coatings Technol 2018. doi:10.1016/J.SURFCOAT.2018.04.040.

[57] Hudec T, Mikula M, Satrapinskyy L, Roch T, Truchlý M, Švec Jr P, et al. Structure, mechanical and tribological properties of Mo-S-N solid lubricant coatings. Appl Surf Sci 2019;486:1–14. doi:10.1016/j.apsusc.2019.03.294.

[58] Polcar T, Nossa A, Evaristo M, Cavaleiro A. Nanocomposite coatings of carbon-based and transition metal dichalcogenides phases: A review. Rev Adv Mater Sci 2007;15:118–26.

[59] Donnet C, Erdemir A. Historical developments and new trends in tribological and solid lubricant coatings. Surf Coat Technol 2004;181:76–84. doi:10.1016/j.surfcoat.2003.10.022.

[60] Voevodin AA, Neill JPO, Zabinski JS. WC/DLC/WS2 nanocomposite coatings for aerospace tribology. Tribol Lett 1999;6:75–8.

[61] Jehn HA. Multicomponent and multiphase hard coatings for tribological applications. Surf Coat Technol 2000;131:433–40. doi:10.1016/S0257-8972(00)00783-0.

[62] Savan A, Pflüger E, Goller R, Gissler W. Use of nanoscaled multilayer and compound films to realize a soft lubrication phase within a hard, wear-resistant matrix. Surf Coatings Technol 2000;126:159–65. doi:10.1016/S0257-8972(00)00542-9.

[63] Voevodin AA, Walck SD, Zabinski JS. Architecture of multilayer nanocomposite coatings with super-hard diamond-like carbon layers for wear protection at high contact loads. Wear 1997;203–204:516–27. doi:10.1016/S0043-1648(96)07425-X.

[64] Leyland A, Matthews A. On the significance of the H/E ratio in wear control: A nanocomposite coating approach to optimised tribological behaviour. Wear 2000;246:1–11. doi:10.1016/S0043-1648(00)00488-9.

[65] Vepřek S. The search for novel, superhard materials. J Vac Sci Technol A Vacuum, Surfaces, Film 1999;17:2401–20. doi:10.1116/1.581977.

[66] Voevodin AA, O'Neill JP, Zabinski JS. WC/DLC/WS2 nanocomposite coatings for aerospace tribology. Tribol Lett 1999;6:75–8. doi:10.1023/A:1019163707747.

[67] Berman D, Erdemir A, Sumant A V. Graphene: A new emerging lubricant. Mater Today 2014;17:31–42. doi:10.1016/j.mattod.2013.12.003.

[68] Voevodin AA, Muratore C, Aouadi SM. Hard coatings with high temperature adaptive lubrication and contact thermal management: Review. Surf Coat Technol 2014;257:247–65. doi:10.1016/j.surfcoat.2014.04.046.

[69] Sanders J, Zabinski J, Nainaparampil J, Prasad S. Lubrication using a microstructurally engineered oxide: performance and mechanisms. Tribol Lett 2000;8:103–16. doi:10.1023/A:1019187202237.

[70] Nossa A, Cavaleiro A. Mechanical behaviour of W-S-N and W-S-C sputtered coatings deposited with a Ti interlayer. Surf Coatings Technol 2003;163–164:552–60. doi:10.1016/S0257-8972(02)00622-9.

[71] Onofrio N, Guzman D, Strachan A. Novel doping alternatives for single-layer transition metal dichalcogenides. Appl Phys 2017;122:1–25. doi:10.1063/1.4994997.

[72] Braithwaite E. Solid Lubricants and Surfaces. Oxford: Clarendon Press; 1964.

[73] Gustavsson F, Jacobson S. Diverse mechanisms of friction induced self-organisation into a low-friction material - An overview of WS2 tribofilm formation. Tribol Int 2016;101:340–7. doi:10.1016/0040-6090(84)90117-2.

[74] Polcar T, Evaristo M, Cavaleiro A. Comparative study of the tribological behavior

Talha bin Yaqub

of self-lubricating W-S-C and Mo-Se-C sputtered coatings. Wear 2009;266:388–92. doi:10.1016/j.wear.2008.04.011.

[75] Pimentel J V., Danek M, Polcar T, Cavaleiro A. Effect of rough surface patterning on the tribology of W-S-C-Cr self-lubricant coatings. Tribol Int 2014;69:77–83. doi:10.1016/j.triboint.2013.09.004.

[76] Singer IL, Dvorak SD, Wahl KJ, Scharf TW. Role of third bodies in friction and wear of protective coatings. J Vac Sci Technol A Vacuum, Surfaces, Film 2003;21:S232–40. doi:10.1116/1.1599869.

[77] Fleischauer PD, Lince JR, Bertrand PA, Bauer R. Electronic Structure and Lubrication Properties of MoS2: A Qualitative Molecular Orbital Approach. Langmuir 1989;5:1009–15. doi:10.1021/la00088a022.

[78] Gustavsson F, Jacobson S, Cavaleiro A, Polcar T. Frictional behavior of self-adaptive nanostructural Mo-Se-C coatings in different sliding conditions. Wear 2013;303:286–96. doi:10.1016/j.wear.2013.03.032.

[79] Serpini E. Friction Mechanisms of MoS2 Surfaces with Different Crystallographic Order 2017.

[80] Salomon G, De Gee AWJ, Zaat JH. Mechano-chemical factors in MoS2-film lubrication. Wear 1964;7:87–101. doi:10.1016/0043-1648(64)90081-X.

[81] Fusaro RL. Lubrication and Failure Mechanisms 1978.

[82] Pritchard C, Midgley JW. The Effect of Humidity on the Friction and Life of Unbonded Molybdnum Disulphide Films. Wear 1968;13:39–50. doi:10.1016/0043-1648(69)90430-X.

[83] Hirano M, Miyake S. Sliding life enhancement of a WS2 sputtered film by ion beam mixing. Appl Phys Lett 1985;47:683–5. doi:10.1063/1.96057.

[84] Zabinski JS, Donley MS, Prasad S V. Synthesis and Characterization of Tungsten Disulfide Films Grown By Pulsed-Laser Deposition. J Mater Sci 1994;29:4834–9. doi:10.1007/bf00356530.

[85] Bichsel R, Levy F. Morphological and Compositional Properties of MoSe2 Films Prepared by R.F Magnetron Sputtering 1984;116:367–72.

[86] Brainard WA. The thermal stability and friction of the disulfides, diselenides, and ditellurides of molybdenum and tungsten in vaccum (10-9 to 10-6 TORR). NASA Tech Note D-5141 1968:1–26.

[87] Voevodin AA, Zabinski JS. Nanocomposite and nanostructured tribological materials for space applications. Compos Sci Technol 2005;65:741–8. doi:10.1016/j.compscitech.2004.10.008.

[88] Hilton MR. Fracture in MoS2 solid lubricant films. Surf Coat Technol 1994;68–69:407–15. doi:10.1016/0257-8972(94)90194-5.

[89] Wang D-Y, Chang C-L, Ho W-Y. Microstructure analysis of MoS2 deposited on diamond-like carbon films for wear improvement. Surf Coat Technol 1999;111:123–7. doi:10.1016/S0257-8972(98)00712-9.

[90] Fleischauer PD, Lince JR. Comparison of oxidation and oxygen substitution in MoS2 solid film lubricants. Tribol Int 1999;32:627–36. doi:10.1016/S0301-679X(99)00088-2.

[91] Prasad S V., McDevitt NT, Zabinski JS. Tribology of tungsten disulfide-nanocrystalline zinc oxide adaptive lubricant films from ambient to 500°C. Wear 2000;237:186–96. doi:10.1016/S0043-1648(99)00329-4.

[92] Ding XZ, Zeng XT, He XY, Chen Z. Tribological properties of Cr- and Ti-doped MoS2 composite coatings under different humidity atmosphere. Surf Coatings Technol 2010;205:224–31. doi:10.1016/j.surfcoat.2010.06.041.

[93] Bülbül F, Efeoğlu İ. Synergistic effect of bias and target currents for magnetron sputtered MoS2-Ti composite films. Mater Test 2016;58:471–4. doi:10.3139/120.110870.

[94] Qin X, Ke P, Wang A, Kim KH. Microstructure, mechanical and tribological behaviors of MoS2-Ti composite coatings deposited by a hybrid HIPIMS method. Surf Coatings Technol 2013;228:275–81. doi:10.1016/j.surfcoat.2013.04.040.

[95] Rigato V, Maggioni G, Patelli A, Boscarino D, Renevier NM, Teer DG. Properties of sputter-deposited MoS2/metal composite coatings deposited by closed field unbalanced magnetron sputter ion plating. Surf Coatings Technol 2000;131:206–10. doi:https://doi.org/10.1016/S0257-8972(00)00797-0.

Talha bin Yaqub

[96]   Mikhailov S, Savan A, Pflüger E, Knoblauch L, Hauert R, Simmonds M, et al. Morphology and tribological properties of metal (oxide)–MoS2 nanostructured multilayer coatings. Surf Coatings Technol 1998;105:175–83. doi:10.1016/S0257-8972(98)00483-6.

[97]   Zabinski JS, Donley MS, Walck SD, Schneider TR, Mcdevitt NT. The Effects of Dopants on the Chemistry and Tribology of Sputter-Deposited MoS2 Films. Tribol Trans 1995;38:894–904. doi:10.1080/10402009508983486.

[98]   Li H, Zhang G, Wang L. Low humidity-sensitivity of MoS2/Pb nanocomposite coatings. Wear 2016;350–351:1–9. doi:10.1016/j.wear.2015.12.008.

[99]   Simmonds MC, Savan A, Pflüger E, Van Swygenhoven H. Mechanical and tribological performance of MoS2 co-sputtered composites. Surf Coatings Technol 2000;126:15–24. doi:10.1016/S0257-8972(00)00521-1.

[100]   Kao WH. Tribological properties and high speed drilling application of MoS2-Cr coatings. Wear 2005;258:812–25. doi:10.1016/j.wear.2004.09.045.

[101]   Jianxin D, Wenlong S, Hui Z, Jinlong Z. Performance of PVD MoS2/Zr-coated carbide in cutting processes. Int J Mach Tools Manuf 2008;48:1546–52. doi:10.1016/j.ijmachtools.2008.06.009.

[102]   Liu X, Ma GJ, Sun G, Duan YP, Liu SH. MoSx-Ta composite coatings on steel by d.c magnetron sputtering. Vacuum 2013;89:203–8. doi:10.1016/j.vacuum.2012.05.013.

[103]   Nainaparampil JJ, Phani AR, Krzanowski JE, Zabinski JS. Pulsed laser-ablated MoS2-Al films: friction and wear in humid conditions. Surf Coatings Technol 2004;187:326–35. doi:10.1016/j.surfcoat.2004.02.043.

[104]   Noshiro J, Watanabe S, Sakurai T, Miyake S. Friction properties of co-sputtered sulfide/DLC solid lubricating films. Surf Coatings Technol 2006;200:5849–54. doi:10.1016/j.surfcoat.2005.08.147.

[105]   Takeno T, Abe S, Adachi K, Miki H, Takagi T. Deposition and structural analyses of molybdenum-disulfide (MoS2)-amorphous hydrogenated carbon (a-C:H) composite coatings. Diam Relat Mater 2010;19:548–52.

doi:10.1016/j.diamond.2009.10.028.

[106] Pimentel J V., Polcar T, Cavaleiro A. Structural, mechanical and tribological properties of Mo-S-C solid lubricant coating. Surf Coatings Technol 2011;205:3274–9. doi:10.1016/j.surfcoat.2010.11.043.

[107] Wu Y, Li H, Ji L, Ye Y, Chen J, Zhou H. Preparation and properties of MoS2/a-C films for space tribology. J Phys D Appl Phys 2013;46. doi:10.1088/0022-3727/46/42/425301.

[108] Wu Y, Li H, Ji L, Liu L, Ye Y, Chen J, et al. Structure, mechanical, and tribological properties of MoS2/a-C:H composite films. Tribol Lett 2013;52:371–80. doi:10.1007/s11249-013-0216-9.

[109] Wu Y, Li H, Ji L, Ye Y, Chen J, Zhou H. A long-lifetime MoS2/a-C:H nanoscale multilayer film with extremely low internal stress. Surf Coatings Technol 2013;236:438–43. doi:10.1016/j.surfcoat.2013.10.021.

[110] Gu L, Ke P, Zou Y, Li X, Wang A. Amorphous self-lubricant MoS2-C sputtered coating with high hardness. Appl Surf Sci 2015;331:66–71. doi:10.1016/j.apsusc.2015.01.057.

[111] Xu J, He TF, Chai LQ, Qiao L, Wang P, Liu WM. Growth and characteristics of self-assembled MoS2/Mo-S-C nanoperiod multilayers for enhanced tribological performance. Sci Rep 2016;6:1–10. doi:10.1038/srep25378.

[112] Xu J, Chai L, Qiao L, He T, Wang P. Influence of C dopant on the structure, mechanical and tribological properties of rf-sputtered MoS2/aC composite films. Appl Surf Sci 2016;364:249–56. doi:10.1016/j.apsusc.2015.12.152.

[113] Wu Y, Liu Y, Yu S, Zhou B, Tang B, Li H, et al. Influences of Space Irradiations on the Structure and Properties of MoS2/DLC Lubricant Film. Tribol Lett 2016;64:1–10. doi:10.1007/s11249-016-0759-7.

[114] Cai S, Guo P, Liu J, Zhang D, Ke P. Friction and Wear Mechanism of MoS 2 / C Composite Coatings Under Atmospheric Environment. Tribol Lett 2017;65:1–12. doi:10.1007/s11249-017-0862-4.

[115] Wang C, Hausberger A, Nothdurft P, Lackner JM, Schwarz T. The potential of tribological application of DLC/MoS2 coated sealing materials. Coatings 2018;8.

doi:10.3390/coatings8080267.

[116] Duan Z, Zhao X, Nai Z, Qiao L, Xu J, Wang P, et al. Mo-S-Ti-C Nanocomposite Films for Solid-State Lubrication. ACS Appl Nano Mater 2019;2:1302–12. doi:10.1021/acsanm.8b02184.

[117] Li L, Lu Z, Pu J, Wang H, Li Q, Chen S, et al. The superlattice structure and self-adaptive performance of C–Ti/MoS2 composite coatings. Ceram Int 2020;46:5733–44. doi:10.1016/j.ceramint.2019.11.022.

[118] Nossa A, Cavaleiro A. The influence of the addition of C and N on the wear behaviour of W-S-C/N coatings. Surf Coatings Technol 2001;142–144:984–91. doi:10.1016/S0257-8972(01)01249-X.

[119] Nossa A, Cavaleiro A, Carvalho NJM, Kooi BJ, De Hosson JTM. On the microstructure of tungsten disulfide films alloyed with carbon and nitrogen. Thin Solid Films 2005;484:389–95. doi:10.1016/j.tsf.2005.02.018.

[120] Evaristo M, Nossa A, Cavaleiro A. Tribological behaviour of reactive and co-sputtered W-S-C coatings. Ciência Tecnol Dos Mater 2006;18:21–6.

[121] Polcar T, Evaristo M, Cavaleiro A. The tribological behavior of W-S-C films in pin-on-disk testing at elevated temperature. Vacuum 2007;81:1439–42. doi:10.1016/j.vacuum.2007.04.010.

[122] Polcar T, Evaristo M, Cavaleiro A. Friction of self-lubricating W-S-C sputtered coatings sliding under increasing load. Plasma Process Polym 2007;4:541–6. doi:10.1002/ppap.200731402.

[123] Evaristo M, Polcar T, Cavaleiro A. Tribological behaviour of C-alloyed transition metal dichalcogenides (TMD) coatings in different environments. Int J Mech Mater Des 2008;4:137–43. doi:10.1007/s10999-007-9034-2.

[124] Koch T, Evaristo M, Pauschitz A, Roy M, Cavaleiro A. Nanoindentation and nanoscratch behaviour of reactive sputtered deposited W-S-C film. Thin Solid Films 2009;518:185–93. doi:10.1016/j.tsf.2009.06.027.

[125] Polcar T, Gustavsson F, Thersleff T, Jacobson S, Cavaleiro A. Complex frictional analysis of self-lubricant W-S-C/Cr coating. Faraday Discuss 2012;156:383.

doi:10.1039/c2fd00003b.

[126] Pimentel J V., Polcar T, Evaristo M, Cavaleiro A. Examination of the tribolayer formation of a self-lubricant WSC sputtered coating. Tribol Int 2012;47:188–93. doi:10.1016/j.triboint.2011.10.021.

[127] Nyberg H, Sundberg J, Särhammar E, Gustavsson F, Kubart T, Nyberg T, et al. Extreme friction reductions during initial running-in of W–S–C–Ti low-friction coatings. Wear 2013;302:987–97. doi:10.1016/j.wear.2013.01.065.

[128] Sundberg J, Nyberg H, Särhammar E, Gustavsson F, Kubart T, Nyberg T, et al. Influence of Ti addition on the structure and properties of low-friction W-S-C coatings. Surf Coatings Technol 2013;232:340–8. doi:10.1016/j.surfcoat.2013.05.032.

[129] Zekonyte J, Cavaleiro A, Polcar T. Frictional properties of self-adaptive chromium doped tungsten-sulfur- carbon coatings at nanoscale. Appl Surf Sci 2014;303:381–7. doi:10.1016/j.apsusc.2014.03.010.

[130] Tomastik C, Tomala A, Pauschitz A, Roy M. The influence of carbon content on the microtribological performance of W-S-C films. J Eng Tribol 2014;228:745–55. doi:10.1177/1350650114529753.

[131] Zekonyte J, Polcar T. Friction Force Microscopy Analysis of Self-Adaptive W-S-C Coatings: Nanoscale Friction and Wear. ACS Appl Mater Interfaces 2015;7:21056–64. doi:10.1021/acsami.5b05546.

[132] Cao H, Wen F, Hosson JTM De, Pei YT. Instant WS2 platelets reorientation of self-adaptive WS2/a-C tribocoating. Mater Lett 2018;229:64–7. doi:10.1016/j.matlet.2018.06.111.

[133] Cao H, De Hosson JTM, Pei Y. Self-healing of a pre-notched WS2/a-C coating. Mater Res Lett 2019;7:103–9. doi:10.1080/21663831.2018.1561538.

[134] Amontons G. Memoires de l'Academie Royale des Sciences; Chez Gerard Kyuper. 1699.

[135] Gao J, Luedtke WD, Gourdon D, Ruths M, Israelachvili JN, Landman U. Frictional forces and Amontons' law: From the molecular to the macroscopic scale. J Phys Chem B 2004;108:3410–25. doi:10.1021/jp036362l.

[136] Polcar T, Evaristo M, Stueber M, Cavaleiro A. Synthesis and structural properties of Mo-Se-C sputtered coatings. Surf Coat Technol 2008;202:2418–22. doi:10.1016/j.surfcoat.2007.08.019.

[137] Polcar T, Evaristo M, Colaço R, Silviu Sandu C, Cavaleiro A. Nanoscale triboactivity: The response of Mo-Se-C coatings to sliding. Acta Mater 2008;56:5101–11. doi:10.1016/j.actamat.2008.06.029.

[138] Polcar T, Evaristo M, Stueber M, Cavaleiro A. Mechanical and tribological properties of sputtered Mo-Se-C coatings. Wear 2009;266:393–7. doi:10.1016/j.wear.2008.04.010.

[139] Kelly P. J, Arnell R. D. Magnetron sputtering: a review of recent developments and applications. Vacuum 2000;56:159–72. doi:10.1016/S0042-207X(99)00189-X.

[140] Swann S. Magnetron sputtering. Phys Technol 1988;19:67–75. doi:10.1088/0305-4624/19/2/304.

[141] Safi I. Recent aspects concerning DC reactive magnetron sputtering of thin films: a review. Surf Coatings Technol 2000;127:203–18. doi:10.1016/S0257-8972(00)00566-1.

[142] Oliver WC, Pharr GM. An improved technique for determining hardness and elastic modulus using load and displacement sensing indentation experiments. J Mater Res 1992. doi:10.1557/JMR.1992.1564.

[143] Todd MJ. Spin division and estimation of Coulomb torque in angular contact ball bearings. Tribol Lubr Wear Fifty Years On 1987;2:933–44.

[144] Hiraoka N. Wear life mechanism of journal bearings with bonded MoS2 film lubricants in air and vacuum. Wear 2001;249:1014–20. doi:10.1016/S0043-1648(01)00845-6.

[145] Fernandes F, Yaqub TB, Cavaleiro A. Influence of Ag additions on the structure , mechanical properties and oxidation behaviour of Cr-O coatings deposited by HiPIMS. Surf Coat Technol 2018;339:167–80. doi:10.1016/j.surfcoat.2018.02.025.

[146] Gangopadhyay S, Acharya R, Chattopadhyay AK, Paul S. Effect of substrate bias voltage on structural and mechanical properties of pulsed DC magnetron sputtered

TiN – MoS x composite coatings. Vaccum 2010;84:843–50. doi:10.1016/j.vacuum.2009.11.010.

[147] Weise G, Mattern N, Hermann H, Teresiak A, Ba I, Bru W. Preparation, structure and properties of MoSx films. Thin Soli 1997;298:98–106. doi:10.1016/S0040-6090(96)09165-1.

[148] Grigoriev SN, Fominski VY, Gnedovets AG, Romanov RI. Experimental and numerical study of the chemical composition of WSex thin films obtained by pulsed laser deposition in vacuum and in a buffer gas atmosphere. Appl Surf Sci 2012;258:7000–7. doi:10.1016/j.apsusc.2012.03.153.

[149] Evaristo M, Polcar T, Cavaleiro A. Synthesis and properties of W-Se-C coatings deposited by PVD in reactive and non-reactive processes. Vacuum 2009;83:1262–5. doi:10.1016/j.vacuum.2009.03.030.

[150] Fominski VY, Nevolin VN, Romanov RI, Smurov I. Ion-assisted deposition of MoSx films from laser-generated plume under pulsed electric field. J Appl Phys 2001;89:1449–57. doi:10.1063/1.1330558.

[151] Sunu SS, Prabhu E, Jayaraman V, Gnanasekar KI, Seshagiri TK, Gnanasekaran T. Electrical conductivity and gas sensing properties of MoO3. Sensors Actuators, B Chem 2004;101:161–74. doi:10.1016/j.snb.2004.02.048.

[152] Dupin J-C, Gonbeau D, Vinatier P, Levasseur A. Systematic XPS studies of metal oxides, hydroxides and peroxides. Phys Chem Chem Phys 2000;2:1319–24. doi:10.1039/a908800h.

[153] Moulder JF, Chastain J. Handbook of x-ray photoelectron spectroscopy : a reference book of standard spectra for identification and interpretation of XPS data. Physical Electronics Division, Perkin-Elmer Corp; 1992.

[154] Paolicelli G, Ferrer S, Comin F. Separation of the sp3 and sp2 components in the C 1s photoemission spectra of amorphous carbon films 1996;54:8064–9. doi:10.1103/PhysRevB.54.8064.

[155] Schaidle JA, Lausche AC, Thompson LT. Effects of sulfur on Mo2C and Pt/Mo2C catalysts: Water gas shift reaction. J Catal 2010;272:235–45. doi:10.1016/J.JCAT.2010.04.004.

[156] Abdallah WA, Nelson AE. Characterization of MoSe2 (0001) and ion-sputtered MoSe2 by XPS. J Mater Sci 2005;40:2679–81. doi:10.1007/s10853-005-2104-7.

[157] Terrones H, Del Corro E, Feng S, Poumirol JM, Rhodes D, Smirnov D, et al. New First Order Raman-active Modes in Few Layered Transition Metal Dichalcogenides. Sci Rep 2014;4:1–9. doi:10.1038/srep04215.

[158] Tonndorf P, Schmidt R, Böttger P, Zhang X, Börner J, Liebig A, et al. Photoluminescence emission and Raman response of monolayer MoS2, MoSe2, and WSe2. Opt Express 2017;21:1–536. doi:10.1201/9781315113722.

[159] Voevodin AA, Zabinski JS. Laser surface texturing for adaptive solid lubrication. Wear 2006;261:1285–92. doi:10.1016/j.wear.2006.03.013.

[160] Ferrari AC, Robertson J. Interpretation of Raman spectra of disordered and amorphous carbon. Phys Rev B 2000;61:95–107. doi:10.1103/PhysRevB.61.14095.

[161] Yaqub T Bin, Vuchkov T, Evaristo M, Cavaleiro A. DCMS Mo-Se-C solid lubricant coatings – Synthesis, structural, mechanical and tribological property investigation. Surf Coat Technol 2019. doi:10.1016/j.surfcoat.2019.124992.

[162] Betz G, Wehner GK. Sputtering of Multicomponent Materials. Sputtering by Part. Bombard. II. Top. Appl. Phys., Berlin, Heidelberg: Springer; 1983, p. 11–90. doi:10.1007/3-540-12593-0_2.

[163] Tan S, Zhang X, Wu X, Fang F, Jiang J. Comparison of chromium nitride coatings deposited by DC and RF magnetron sputtering. Thin Solid Films 2011;519:2116–20. doi:10.1016/j.tsf.2010.10.067.

[164] Mutafov P, Evaristo M, Cavaleiro A, Polcar T. Structure, mechanical and tribological properties of self-lubricant W-S-N coatings. Surf Coat Technol 2015;261:7–14. doi:10.1016/j.surfcoat.2014.11.074.

[165] Rasamani KD, Alimohammadi F, Sun Y. Interlayer-expanded MoS 2. Mater Today 2017;20. doi:10.1016/j.mattod.2016.10.004.

[166] Panigrahi PK, Pathak A. Aqueous Medium Synthesis Route for Randomly Stacked Molybdenum Disulfide. J Nanoparticles 2013. doi:10.1155/2013/671214.

[167] Sekine T, Izumi M, Nakashizu T, Uchinokura K, Matsuura E. Raman scattering and infrared reflectance in 2H-MoSe2. J Phys Soc Japan 1980;49:1069–77. doi:10.1143/JPSJ.49.1069.

[168] Musil J, Kunc F, Zeman H, Poláková H. Relationships between hardness, Young's modulus and elastic recovery in hard nanocomposite coatings. Surf Coat Technol 2002;154:304–13. doi:10.1016/S0257-8972(01)01714-5.

[169] Charitidis CA, Logothetidis S. Effects of normal load on nanotribological properties of sputtered carbon nitride films. Diam Relat Mater 2005;14:98–108. doi:10.1016/j.diamond.2004.07.022.

[170] Kano M, Yasuda Y, Mabuchi Y, Ye J, Konishi S. Ultra-low friction properties of DLC lubricated with ester-containing oil - Part 1: Pin-on-disc & SRV friction tests. Tribol Ser 2003;43:689–92. doi:10.1016/s0167-8922(03)80096-2.

[171] Prasad S, Zabinski J. Super slippery solids. Nature 1997;387:761. doi:10.1038/42820.

[172] Voevodin AA, Neill JPO, Zabinski JS. Tribological performance and tribochemistry of nanocrystalline WC / amorphous diamond-like carbon composites. Thin Solid Films 1999;342:194–200. doi:10.1016/S0040-6090(98)01456-4.

[173] Cao H, Wen F, Kumar S, Rudolf P, De Hosson JTM, Pei Y. On the S/W stoichiometry and triboperformance of WS x C(H) coatings deposited by magnetron sputtering. Surf Coatings Technol 2018. doi:10.1016/j.surfcoat.2018.04.040.

[174] Yaqub T Bin, Vuchkov T, Sanguino P, Polcar T, Cavaleiro A. Comparative Study of DC and RF Sputtered MoSe2 Coatings Containing Carbon—An Approach to Optimize Stoichiometry, Microstructure, Crystallinity and Hardness. Coatings 2020;10:133. doi:10.3390/coatings10020133.

Annex A

T. Bin Yaqub, T. Vuchkov, M. Evaristo, A. Cavaleiro, *DCMS Mo-Se-C solid lubricant coatings – Synthesis, structural, mechanical and tribological property investigation***, Surf. Coat. Technol. (2019).**

DCMS Mo-Se-C solid lubricant coatings – Synthesis, structural, mechanical and tribological property investigation

Talha Bin Yaqub[a,b,*], Todor Vuchkov[a,b], Manuel Evaristo[b], Albano Cavaleiro[a,b]

[a] IPN - LED & MAT - Instituto Pedro Nunes, Laboratory of Tests, Wear and Materials, Rua Pedro Nunes, 3030-199, Coimbra, Portugal
[b] SEG-CEMMPRE, Department of Mechanical Engineering, University of Coimbra, Rua Luís Reis Santos, 3030-788, Coimbra, Portugal

ABSTRACT

Mo-Se-C is a very less explored subset of carbon-based transition metal dichalcogenide (TMD-C) nanocomposite coatings but a potential candidate as solid lubricant coatings in aerospace and automotive industries due to excellent frictional stability both in humid air and vacuum conditions. The present work aims at the development and investigation of dc magnetron co-sputtered Mo-Se-C coatings using separate C and $MoSe_2$ targets, as a first step for industrial up-scaling. By varying the applied C power, a carbon content of 44 to 60 at. % was achieved. 50 at. % C was selected for the deposition of coatings with negative substrate bias of 50, 70 and 90 V dc voltage and, for the latter, pulsed dc bias was also applied. Maximum Se/Mo ratio of 1.88 was evaluated by wavelength dispersive spectroscopy (WDS) analysis. After the application of substrate bias, the deposition rate and Se/Mo ratio decreased while higher compactness was observed by scanning electron microscopy (SEM). Mo-Se-C coatings displayed broad amorphous grazing incidence X-ray diffraction patterns. Transmission electron microscopy (TEM) showed $MoSe_2$ platelets randomly oriented in amorphous carbon matrix. X-ray photoelectron spectroscopy (XPS) was not conclusive towards the presence of Mo-C bonds while Raman analysis showed the presence of $MoSe_2$ crystalline peaks. Nano-indentation tests showed an increase in the hardness of coatings deposited under negative substrate bias. Tribological tests were performed in humid air and dry nitrogen. 400C(90V) coating displayed the highest frictional stability in both environments, while the lowest friction coefficient of 0.025 and specific wear rate of 2.4×10^{-8} mm^3/Nm were achieved for tests in dry nitrogen.

1. Introduction

Solid lubrication has emerged as a potential solution to replace conventional lubrication procedures in machining and tribological operations. Liquid lubrication is mostly used for friction reduction, but it has very adverse environmental and economic impacts [1,2]. Therefore, the transition towards solid lubricant coatings is governed by the urge to pave way for the manufacturing of products with superior quality, cost-effective production and more environment-friendly industrial system. In recent times, various coating systems have been developed to provide easy shear properties/mechanisms in tribological contacts and thus may help to overcome problems of liquid lubrication especially in aerospace, tool manufacturing and automotive industries. Mainly, solid lubricant coatings include, soft metals (such as Ag, In, Sn, and Au) [1], metal oxides (PbO, B_2O_3, MoO_3, and NiO) [3,4], DLCs (diamond like carbon) [5–7], transition metal dichalcogenides [8], Ag doped chromium nitride [9,10] and tungsten carbide with carbon (WC/C) [11]. High temperature oxidation and poor cyclic environment

performance are some of the limitations of these coating systems [7,12,13]. For instance, DLCs and other carbon-based materials are the choices for low friction applications in humid environments but they are unable to provide satisfactory results in vacuum [13,14]. Oxide coatings on the other hand, become brittle at low temperatures, resulting in abrasive wear debris and increased friction [15]. Growing economic needs, urge the demand for coating operability in both humid and high vacuum conditions especially in case of satellites and aerospace applications. Therefore, any lubricant system operable in both earth and space environments, coupled with low wear and friction would be considered a breakthrough in the aerospace industry.

TMD compounds have been under research for the past few decades. The use of TMDs for aerospace components by NASA dates back to the early 60's for dry and vacuum applications [16]. TMDs have a general formula of X-M-X, where M is a transition metal atom and X are the chalcogenides. In a typical TMD structure, each metal atom is surrounded by 6 chalcogenide atoms and each chalcogenide is bonded to 3 metal atoms. Bonding structure of TMDs is unique with strong covalent

bonding within X-M-X sandwich while between sandwiches, there are weak Van der Waals bonds that provide many beneficial properties in tribological applications (such as easy shear layers) [17]. Pure sputtered TMD coatings are porous with low hardness and weak adhesion to the substrates along with very low load bearing capacity, attributed to a very high porosity. All these drawbacks make pure TMDs inappropriate for most applications submitted to high contact loads [12,18,19]. Furthermore, the tribological performance of TMDs deteriorate significantly in the presence of moisture and oxygen (COF = 0.1-0.2) [20]. Heating may remove moisture and water vapours but this cannot be possible in every case/application area. In order to overcome these limitations, structural modifications were done by alloying TMDs with different metals (Ti, Au, Pb, Zr and Cr) [21–29] and non-metals (N and C) [30,58]. These approaches resulted in improved microstructure and mechanical properties without compromising the low friction performance but long-term stability is still a question mark.

Among all previously alloyed elements, carbon has been widely studied as it showed promising results. Carbon not only increases the mechanical properties of TMDs due to better compactness of coatings, but also provides oxidation resistance along with chameleon behavior (self-adaptation properties according to working conditions) in cyclic environments. The formation of tribolayers in TMD-C coatings, in accordance with environmental surroundings, allows maintaining low friction in different humidity levels.

MoS_2 and WS_2 are the two most studied members of the TMD family, however, their tribological performance in humid environments is poor. $MoSe_2$ is an excellent lubricant in dry air or vacuum environment and shows relatively low friction in the humid air. In dry air, the wear rate of MoS_2 is lower as compared to $MoSe_2$ while in humid air $MoSe_2$ shows better results. $MoSe_2$ also has better oxidation resistance despite having lower activation energy than MoS_2 [31,32]. As mentioned earlier, combinations with C improved the density, mechanical and tribological properties of TMDs. Although less explored, Mo-Se-C can present interesting tribological behavior. Polcar et al. [33–36] studied in detail the Mo-Se-C system deposited using rf magnetron sputtering of a carbon target with $MoSe_2$ pellets placed in the erosion zone, and achieved some good results. However, this deposition procedure is not suitable for upscaling at an industrial level due to either working with rf power supplies or using composite targets. The sputter deposition with individual targets has not been reported yet. This is more industrially acceptable way of depositing thin coatings by sputtering, having the main advantage of the easy control of the coating composition by varying the applied power to both targets. To our knowledge, dc magnetron sputtering of low friction Mo-Se-C coatings (by co-sputtering 2 individual targets) has not been carried out yet.

Here, we present the effects of the carbon concentration and substrate bias on the properties of Mo-Se-C coatings deposited by direct current magnetron sputtering (DCMS) from two individual targets ($MoSe_2$ + graphite). The main objective is to shed some light on the chemical composition, microstructure, crystal structure, bonding structure, and mechanical properties of the deposited system. The research will also include the tribological performance investigation in humid air and dry nitrogen atmospheres. Special attention will be paid on to the effects of substrate bias voltage on the coating properties and performance. This research can pave way towards the industrial implementation of Mo-Se-C coatings in areas involving components sliding in inert and humid atmospheres.

2. Experimental procedure

DC magnetron sputtered Mo-Se-C coatings were deposited in Ar gas atmosphere in a Hartec deposition unit, equipped with 2 targets, graphite (150 mm × 150 mm) and $MoSe_2$ (139 mm × 139 mm). Polished (111) silicon wafer substrates (for chemical composition, cross-sectional and surface morphology, coating thickness measurement, structural evolution, chemical bonding and mechanical properties

evaluation), high speed steel substrates AISI M2, Ø20 × 3 mm (for critical adhesion load evaluation) and AISI 52100, Ø25 × 7 mm (for reciprocating tribological tests) were used. Steel substrates were first ground in steps using emery papers from P180 down to P1200 grit sizes and then fine polished using diamond suspension (6, 3 and 1 μm respectively). Polishing resulted in a roughness (Ra) less than ~ 0.02 μm. Prior to placement in the deposition chamber, all substrates were ultrasonically cleaned in acetone and ethanol for 15 min each. The samples were placed on a rotating substrate holder (18 rev/min) positioned at 100 mm from each target. Before the depositions, sputter cleaning of the substrates and targets was carried out in Ar gas atmosphere by maintaining a pressure of 0.5 Pa. The cleaning of the substrates and targets was proceeded in a systematic way. First $MoSe_2$ target was sputter cleaned for 15 min with a dc power (P = 200 W) and shutter in front, to avoid cross-contamination. Meanwhile, etching of substrates was also done with pulsed dc power (ENI RPG 50) by applying V = 400 V, f = 250 kHz, and pulse-on time = 1600 ns. Power on $MoSe_2$ target was turned off after 15 min and the dc power to C was switched on (P = 150 W). The shutter was moved in front of C target. Conditions for substrate etching were kept the same. After 15 min, sputter cleaning of C and etching of substrates was terminated and then the depositions were carried out at the same pressure of 0.5 Pa in Ar gas atmosphere. The power to $MoSe_2$ target was kept constant for all depositions while the power applied to C target was varied to achieve a series of depositions with different C contents. The effects of dc and pulsed dc substrate bias on the coating properties were also studied by depositing a set of coatings with different applied substrate bias voltage and were compared to the coatings deposited without substrate bias. A list of all deposited coatings, as well as the main deposition parameters are shown in Table 1. From now onwards, the coatings will be named as presented in Table 1.

Wavelength dispersive spectroscopy (WDS-Oxford Instruments) was used to determine the chemical composition of the coatings. The surface and fractured cross-sectional morphologies were analysed using field emission scanning electron microscopy (SEM-Zeiss Merlin). The coating thickness was measured by SEM from the cross-sectional images. X-ray diffraction (X′ Pert Pro MPD diffractometer) operated in grazing (3⁰) mode utilizing copper $K_{α1}$ radiation (λ = 1.5406 Å), was used for the crystal structure analysis and to check the presence of $MoSe_2$ and Mo-C nanocrystals in the C matrix. High-resolution transmission electron microscopy images were acquired on the thin films deposited on copper TEM grids. The deposition time for thin films was set to 1.5 min in order to achieve a thickness of 25-40 nm. The observation was performed in a Jeol JEM 2100 using 200 kV excitation voltage.

Raman and X-ray photoelectron spectroscopies (XPS) were used for the chemical bonding analysis. Raman spectroscopy was performed in a wave number range of 100 to 1800 cm⁻¹ using 532 nm laser (XploRA, Horiba). Care was taken in selecting the laser power and acquisition time to avoid coating damage. XPS was performed using Kratos Axis

Table 1
Main Deposition parameters used for depositing Mo-Se-C Coatings.

Coatings	MoSe₂ Power (W)	Carbon Power (W)	Bias (V)	Time (min)	Thickness (μm)	Deposition Rate (nm/min)
Pure MoSe₂	200	-	-	60	2.3	38.3
330C	200	330	-	90	1.6	17.8
400C	200	400	-	90	1.9	21.1
500C	200	500	-	120	2.5	20.8
400C(50V)	200	400	50	120	2.0	16.7
400C(70V)	200	400	70	120	1.8	15
400C(90V)	200	400	90	120	2.2	18.3
400C Pulsed 90V	200	400	p-90	120	2.3	19.2

Ultra HAS with monochromatic Al Kα X-rays (hν = 1486.6 eV). The power of the X-ray source was set to 90 W and a charge neutralizer was used during measurements. The survey spectra were obtained by setting the pass energy at 80 eV with a step of 1 eV and a dwell time of 200 ms. The high-resolution spectra of the regions of interest were obtained using a pass energy of 40 eV with a step of 0.1 eV and a dwell time of 600 ms. Sputter etching was performed using Ar^+ ion gun operated at 2.2 keV and current density of $2.2 \mu A/cm^2$. The data acquisition was done at pressures lower than 10^{-6} Pa. The data analysis was done using the CasaXPS software. The baselines of the spectra were obtained using the Shirley method and peak fitting was done using Gaussian-Lorentzian functions.

The hardness measurements were performed by nanoindentation (Micro Materials Nano Test platform), with a Berkovich diamond indenter and based on the method developed by Oliver and Pharr [37]. The load (5 mN) was selected to avoid the influence of the substrate since indentation depth remained less than 10 % of the coating thickness. A total of 32 indentations were performed at two different positions and the average was calculated. The coating adhesion on the M_2 steel substrates was evaluated in a scratch-testing apparatus (CSM Revetest). The specimens were scratched as the normal force was progressively increased from 2-50 N, using a Rockwell indenter (tip radius = 0.2 mm), a scratch speed of 10 mm/min and a loading rate of 100 N/min. The critical loads were determined by analysing scratches by optical microscopy. The coating adhesive properties were quantified using the critical load value corresponding to the load for which the first exposure of the substrate occurred.

The tribological testing was performed in an Optimol SRV friction and wear equipment under reciprocating sliding conditions against a 100Cr6 steel ball of 10 mm diameter. Before testing, both disc and ball were ultrasonically cleaned in acetone for 15 min. The tests were performed at 25 °C in humid atmosphere (relative humidity ~35-45 %) as well as in dry nitrogen atmosphere. The reciprocating frequency and stroke length were set to 25 Hz and 2 mm respectively, resulting in a sliding speed of 0.1 m/s under 30 N applied load (initial Hertzian contact stress ~1.48 GPa). The test duration was set at the maximum sliding distance of 180 m, resulting in 90000 cycles. The experiments were repeated twice to ensure repeatability. The wear profiles were then taken by stylus profilometer (Surftest SJ-500) and the wear track images and elemental maps were acquired using SEM. Specific wear rates were later calculated using the wear volume, applied load and sliding distance.

3. Results and discussion

3.1. Chemical composition and deposition rate

The chemical composition of the deposited coatings measured by WDS is shown in Table 2, along with Se/Mo ratios. All coatings present a small amount of residual oxygen that may have accumulated in growing coatings from the residual atmosphere of the chamber or from contamination in the porous $MoSe_2$ target [35,38]. With the increase in the power applied to C target, the percentage of C in the coatings

increased. The pure $MoSe_2$ coating displayed the highest deposition rate of ~38 nm/min (Table 1) due to its highly porous and columnar morphology (see Fig. 1). When the C target was sputtered in the chamber, to deposit Mo-Se-C nanocomposite coatings, the deposition rate decreased to ~18 nm/min for 330C coating (330 W power), as compared to the pure $MoSe_2$ coating. This decrease is related to the higher compactness and the lower porosity of the coating. With increasing C target power, the additional sputtered C atoms made the deposition rate to increase up to ~21.1 nm/min. Further increase in the power to 500 W (for 500C coating) resulted in a small decrease of the deposition rate down to ~20.8 nm/min which may be related to the increase in the voltage on the C target from 530 V for 400C coating to 560 V for 500C coating. With the increase in voltage, more energetic Ar neutrals are produced and, thus, enhancement of the re-sputtering of atoms from the growing coating can occur.

Carbon content around 50 at. % (400C coating) was selected to deposit coatings with substrate bias. With the application of substrate bias, there was no specific trend for the carbon percentage in the coatings. The deposition rate showed a decrease after the application of substrate bias, which may be related to the re-sputtering of atoms from the growing coatings due to the progressive increase of Ar ions bombardment of the growing coatings. The substrate bias also helps to increase the compactness due to an easier ad-atom mobility effect [39]. Increased ion bombardment also resulted in a decrease of the Se/Mo ratio (see Table 2). The Se/Mo ratio decreased from 1.88 in the coating without substrate bias (400C) down to 1.44 in the 90 V pulsed bias one. The lower Se/Mo ratio can also be related to the preferential re-sputtering of Se from the growing coating as explained in literature for different TMDs. When sputtering a compound, the lighter element, here Se, is preferentially sputtered [35]. The effect of ion bombardment on the Se/Mo ratio was enhanced in the pulsed substrate bias deposition. With pulsed dc 90 V, the plasma was more confined near the substrate enhancing ion bombardment and thus leading to higher re-sputtering of Se. However, overall, the Se/Mo ratio was much closer to stoichiometry as compared to other TMD-C nanocomposite coatings reported, in particular WS_2, WSe_2 and MoS_2 [30,40–42]. In all these compounds the atomic mass of the elements is much more different than in $MoSe_2$, reducing the preferential sputtering rate of the lighter element in $MoSe_2$ [43]. In our previous work on Mo-Se-C coatings deposited by rf sputtering from composite C target with $MoSe_2$ pellets, we have reported Se/Mo ratio around 1.45 for a coating with 50 at. % C [35,36] as compared to 1.88 achieved in this study for the same carbon content (400C coating), both coatings deposited without substrate bias. Again, this result can be understood by the higher plasma density close to the substrate existing in rf discharges [44,45]. Therefore, by dc co-sputtering of separate $MoSe_2$ and C targets it is easier to keep the Se/Mo ratio close to stoichiometry, with the consequent advantages of either allowing to use higher bombardment of the growing coating (more compact coatings) or having higher Se/Mo ratios, known to induce a better friction behavior [14].

Table 2
Chemical composition and adhesion critical loads of the deposited coatings.

Coatings	C (at. %)	Mo (at. %)	Se (at. %)	O (at. %)	Se/Mo	Lc$_3$ – Critical Load (N)
Pure MoSe$_2$	5 ± 0.2	29 ± 0.1	64 ± 0.3	2 ± 0.1	2.2	-
330C	44 ± 0.6	19 ± 0.2	34 ± 0.3	3 ± 0.1	1.79	9.2 ± 0.4
400C	50 ± 0.4	16 ± 0.3	30 ± 0.3	4 ± 0.2	1.88	13 ± 0
500C	60 ± 0.3	13 ± 0.2	24 ± 0.2	3 ± 0.1	1.85	17 ± 0
400C(50V)	55 ± 0.3	15 ± 0.4	25 ± 0.5	5 ± 0.3	1.67	19.2 ± 0.4
400C(70V)	51 ± 0.5	17 ± 0.1	28 ± 0.3	4 ± 0.1	1.64	12.5 ± 0.7
400C(90V)	51 ± 0.2	18 ± 0.2	28 ± 0.2	3 ± 0.1	1.56	23 ± 0.4
400C(p-90V)	55 ± 0.4	18 ± 0.2	26 ± 0.2	1 ± 0.2	1.44	16 ± 0.4

3.2. Cross-section and surface morphology

Surface and fractured cross-sectional morphologies were analysed using field emission scanning electron microscopy (SEM-Zeiss Merlin). The coating thickness was also measured by SEM from the cross-sectional images. Selected cross-sectional and surface morphology micrographs are displayed in Fig. 1. Pure MoSe$_2$ depicted a columnar cross-sectional morphology with significant porosity, which is a typical feature of sputtered pure TMD coatings. Their sponge-like and highly porous surface morphology agrees with the cross-section. With the introduction of C, the columnar structure persisted but with a fairly dense morphology (Fig. 1c). The length of the columns decreased as well, and the growth occurred in a dendritic way. The surface of this coating showed fine grains with compact morphology (Fig. 1d). Further increase of the C content led to an increase of the compactness with less amount of spaces between columns up to negligible porosity and voids were left. This is in accordance with previous literature on C based TMD nanocomposite coatings [14].

With the application of substrate bias to the 400C coating (50 at. % C), the compactness further increased from the 400C(50V) coating having a dense structure with small contributions of dendritic grain growth up to morphology with no columns for the -70 V substrate bias coating. The coatings with -90 V (Fig. 1 e)) and pulsed -90 V substrate bias were the densest and the smoothest ones. With the application of the substrate bias, progressively more and more ions collide with the growing coating with higher energies resulting in the removal of impurities and more atomic coverage. The surface morphology was granular cauliflower-like for -50 V substrate bias coating and displayed no significant features with further increase of substrate bias (Fig. 1f). As expected, the surface roughness decreased with the application of substrate bias and topographical details almost disappeared. Literature states that the densification and compactness of the coatings improves the adhesion, the mechanical and the sliding properties (like resistance to environmental attacks) [14,30].

3.3. Structural analysis

XRD patterns of the deposited coatings in grazing incidence angle mode are shown in Fig. 2. Here, only selected patterns have been displayed as all other coatings (with and without substrate bias) showed similar patterns. Pure MoSe$_2$ displayed peaks related to typical sputtered and crystalline TMD coating structure (ICCD n^0 087-2419). The broad peak at 2Θ = 30-40^0 corresponds to a turbostrating stacking of 10L planes (L = 1,2,3 ….) as explained by Weise et al. [40]. The combined peaks at 2Θ = 55-55.5^0 correspond to (110) peak of MoSe$_2$ and Si (311) peak from the substrate as denoted in Fig. 2. The (002) peak at 2Θ = 13^0 related to parallel orientation of the basal planes of MoSe$_2$ crystals showed very low intensity. This is because the TMD coatings usually grow initially with basal planes parallel to the substrate, which changes progressively as the coating thickens.

With the introduction of C, the structure became X-ray amorphous, displaying only broad peaks (except 2Θ = 55^0 peak corresponding to Si (311) substrate). XRD of dc and pulsed dc substrate bias coatings gave rise to a pattern similar to those of the coatings without substrate bias (see 400C(90V) as an example in Fig. 2). These coatings, highly compact, as observed by SEM, are X-ray amorphous in nature. No evidence of the presence of nanocrystals of Mo-C were found. Although XRD has limitations with phases having very low grain sizes, if existing, nanograins should be very small to be detected by XRD analysis. Similarly, the patterns, on one hand, clearly correspond to amorphous carbon but the coatings have very small nanocrystals of MoSe$_2$ (in broad peak region) whose presence is clearly evident from TEM and Raman analysis.

A TEM micrograph of the 400C coating is shown in Fig. 3 (left). Platelets/nanograins of the (002) basal planes of MoSe$_2$ phase in an amorphous carbon matrix can be clearly seen. The platelets are randomly oriented in the matrix resembling wires [33]. The length of the

platelets and distance between the (002) planes were measured at various areas; average values less than 10 nm and 0.65-0.7 nm, respectively, were calculated. The platelets were smaller in size and not properly grown as an ordered structure. When MoSe$_2$ and C were sputtered together, C restricts the growth and ordering of crystalline MoSe$_2$, thus decreasing the platelet length and increasing the distance between the planes. This smaller size and the random orientation of the platelets may be the reasons why MoSe$_2$ peaks were not detected in XRD analysis.

Fig. 3 (right), shows that although with the application of substrate bias, the compactness (section 3.2) and hardness (section 3.5) of the coating increased but the microstructure remained the same; thus, no difference in the easy shear properties of the coatings is expected. (002) basal planes again formed platelets/nanograins of MoSe$_2$ in the amorphous carbon matrix. (002) planes interplanar distance was in the range of 0.6-0.7 nm.

3.4. Chemical bonding analysis

XPS spectra were obtained for the coating with ~50 at. % of carbon deposited with and without substrate bias (400C and 400C(90V)). Due to the presence of C in the coatings, charge correction for the binding energies was carried out using the oxygen O1s peak originating from MoO3. After the charge correction, the Mo3d$_{5/2}$ peak originating from Mo-O bonds in MoO$_3$ (not shown) was identified at BE (binding energy) of 232.5 eV which is in good agreement with the literature [46,47]. The high resolution XPS spectra of the regions of interest, obtained after sputter cleaning are shown in Fig. 4. The presence of Se 3s photoemission peak at binding energy of 232 eV (Mo3d region of interest) and LMM Auger lines at 287 eV (C1s region of interest) [48] can complicate the interpretation of the Mo and C spectra obtained. To better understand the effect of these features, high resolution XPS spectra were also obtained from a selenium pellet (99.9 % purity, Testbourne Ltd) sputter cleaned for 60 min in the spectrometer. The same acquisition parameters were used as for the coatings analysed. The spectra obtained from the selenium pellet are shown in Fig. 5. The Se 3s photoemission peak was observed at BE of 231 eV (see Fig. 5a), and considering a chemical shift of ~1 eV towards lower binding energy, as a result of Se-Mo bonding, which was identified in the coatings, a contribution of this photoemission peak at ~230 eV is expected in the spectra of the coatings. The scan done for the pure Se pellet, at the C1s region of interest (Fig. 5b) showed the L$_3$M$_{33}$M$_{45}$ (^{1}P) and L$_3$M$_{33}$M$_{45}$ (^{3}P) Se Auger lines at ~297.7 and ~285.5 eV, respectively. The position of the Auger lines at 285.5 eV can clearly contribute towards the intensity of the C1s spectra obtained from the coating as its position is close to the location of the binding energies for C-C bonding of sp2 (BE = 284.5 eV) and sp3 type (BE = 285.4 eV) [49]. Considering these features, no reasonable fitting could be achieved for the Mo3d and C1s regions of interest. Partial fitting was done for the Mo3d peaks with focus on the strongest features of the spectra and no fitting was attempted for the C1s region.

The Mo3d spectra of the coatings 400C and 400C 90V obtained after etching are shown in Fig. 4 a) and 4 c), respectively. The peaks were fitted using separation of the binding energies between the Mo3d$_{5/2}$ and Mo3d$_{3/2}$ peaks set to 3.1 eV with their peak area ratios set to 3/2 [48]. As Se and C have the same electronegativity (2.55), identification of Mo-C bonds from the Mo3d spectra can be very difficult. The Mo3d$_{5/2}$ BE location for Mo-C bonds presented in the literature is in the range 228.2-228.7 eV [50] which is at the same location as Mo-Se bonding identified in MoSe$_2$ which is located at 228.4-228.7 eV [51]. Fitting of the spectra obtained before etching (not shown) was performed using 4 doublets. The first doublet was located at 228.5 eV for the coating deposited without substrate bias and 228.3 eV for the coating deposited with substrate bias, values which represent Mo-Se bonding in MoSe$_2$ and are in agreement with the literature [51]. The slightly lower value obtained for the coating deposited with substrate bias can be the result

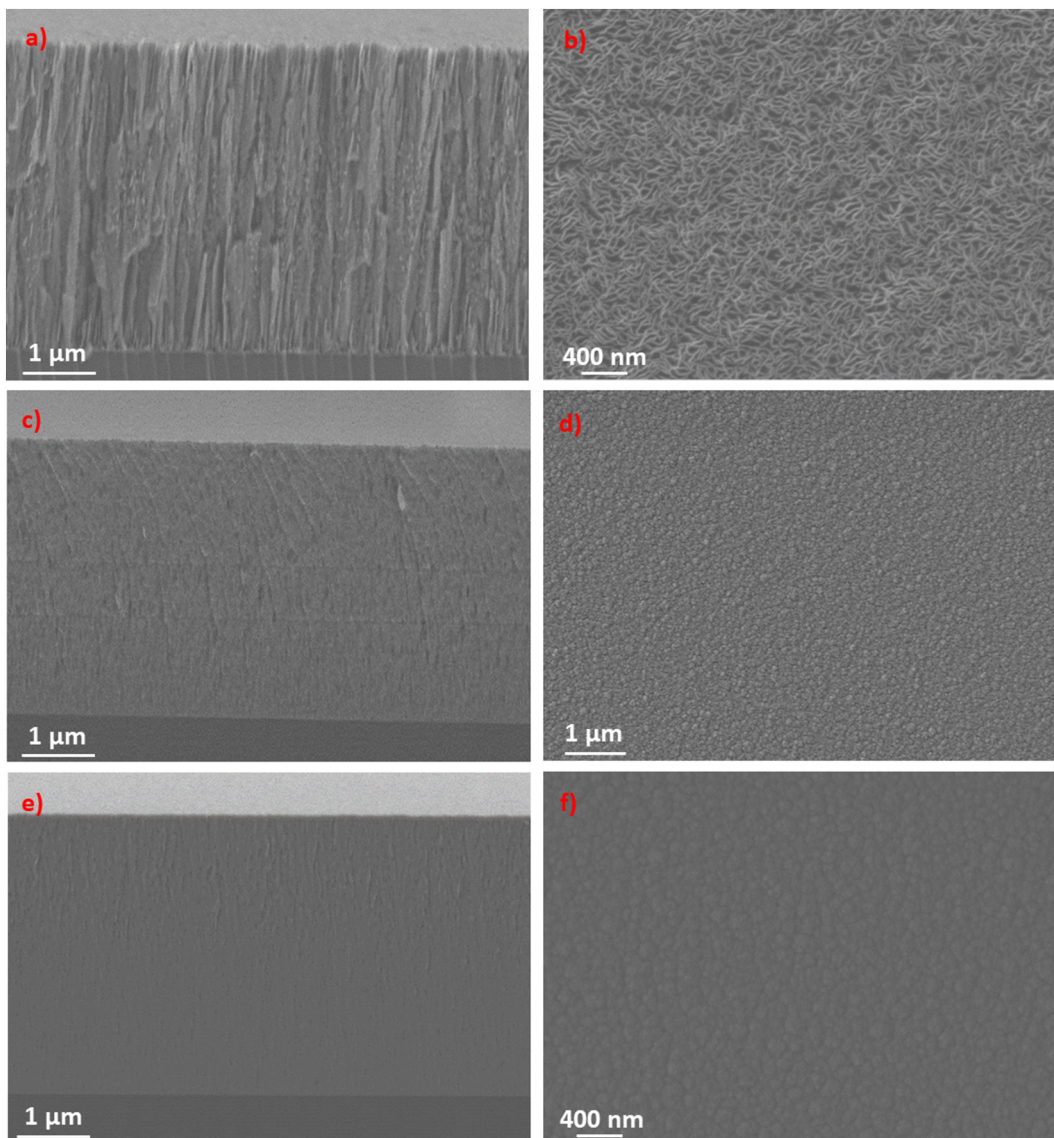Fig. 1. SEM cross-section images-a)Pure MoSe$_2$, c)400C, e)400(90V bias) and surface morphology images-b)Pure MoSe$_2$, d)400C, f)400(90V bias) of the coatings.
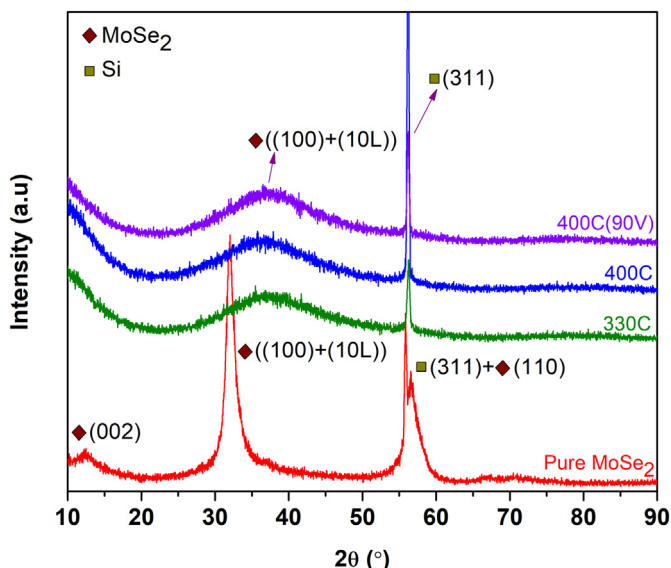

Fig. 2. X-ray diffraction patterns of the coatings.

of a lower Se/Mo ratio. The additional doublets used for fitting were located at the same positions for both coatings and they were identified as Mo-O bonds where Mo has different oxidation state (see Fig. 4). The Mo3d spectrum after Ar$^+$ ion etching has shown narrower main peaks and fitting was done using 2 doublets which were located at the same location for both coatings. The first doublet was positioned at 228.5 (Mo3d$_{5/2}$) which is considered to represent Mo-Se bonds in MoSe$_2$. The second doublet was located at BE of 229.2 eV and is representing Mo 4 + oxidation state in MoO$_2$. The Se 3d peaks obtained after etching showed no significant difference compared to the spectra obtained on the as deposited coatings. The peaks were fitted using a separation of 0.86 eV between the binding energies of the 3d$_{5/2}$ and 3d$_{3/2}$ peaks. Fitting of the Se3d spectra before and after sputter cleaning was performed with 2 doublets for both the coatings. The first doublet was located at 3d$_{5/2}$ BE of 54.2 eV representing Se-Mo bonding which is in good agreement with previous studies and reference values [48,51]. The second doublet needed to complete the fitting was positioned at 55.2 eV (not shown) and this peak was assigned to Se-Se bonding [48].

C1s photoelectron spectra is shown in Fig. 4 b). Considering the presence of the Se L$_3$M$_{23}$M$_{45}$ (^{3}P) Auger line (compare Figs. 4b) and Fig. 5 b), fitting of the spectra was not attempted. However, the main peak from these spectra has the same location for both coatings with no
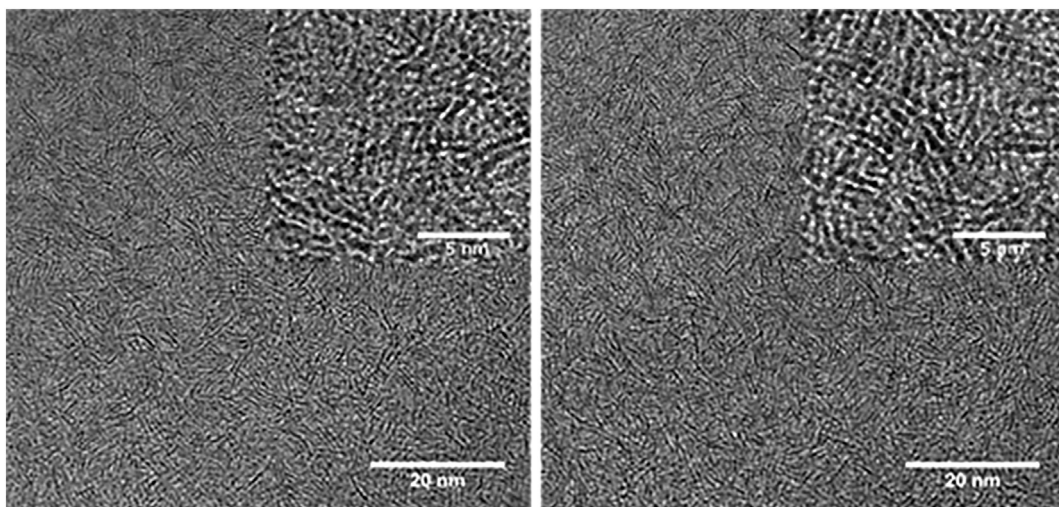
Fig. 3. TEM images of the coatings: 400C - left and 400C(90V) - right.
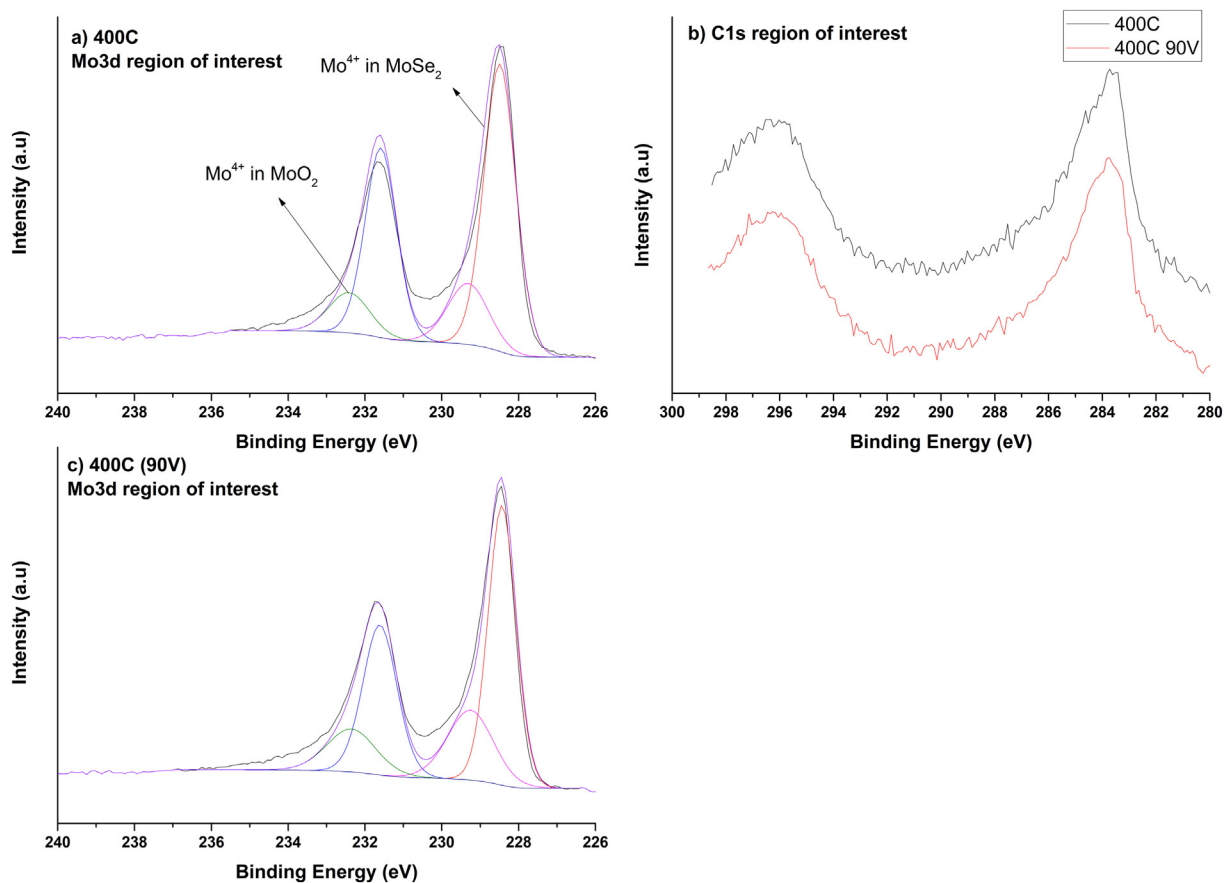
Fig. 4. XPS spectra acquired obtained after sputter cleaning a) Mo3d region of interest for 400C b) C1s region of interest for 400C and 400C(90V) c) Mo3d region of interest for 400C(90V).

significant difference between them. From the XPS measurements done, no significant difference could be observed for the coatings deposited with and without substrate bias. The Mo3d spectra revealed Mo-O bonds, indicating oxidation of the pristine coating surfaces. Nevertheless, these features disappeared after the sputter cleaning process for both coatings. Depiction of Mo-C bonds, which would be indicative of the existence of nanocrystals of Mo-C was very difficult. The chemical shifts in the Mo spectra are very similar for both Mo-Se and Mo-C bonding types. On the other hand, it was shown that there is severe

interference between the C1s and Se Auger LMM peak, making the identification of the bonding types from the C1s peak unreliable.

The Raman spectra of pure $MoSe_2$, 400C and 400C(90V) coatings are presented in Fig. 6. The spectrum for these coatings can be divided into three main regions.

I A group of sharp $MoSe_2$ peaks around 200 cm^{-1}
II Mo-O peaks at 700-900 cm^{-1} region
III D and G peaks belonging to amorphous carbon (1300-1600 cm^{-1}).
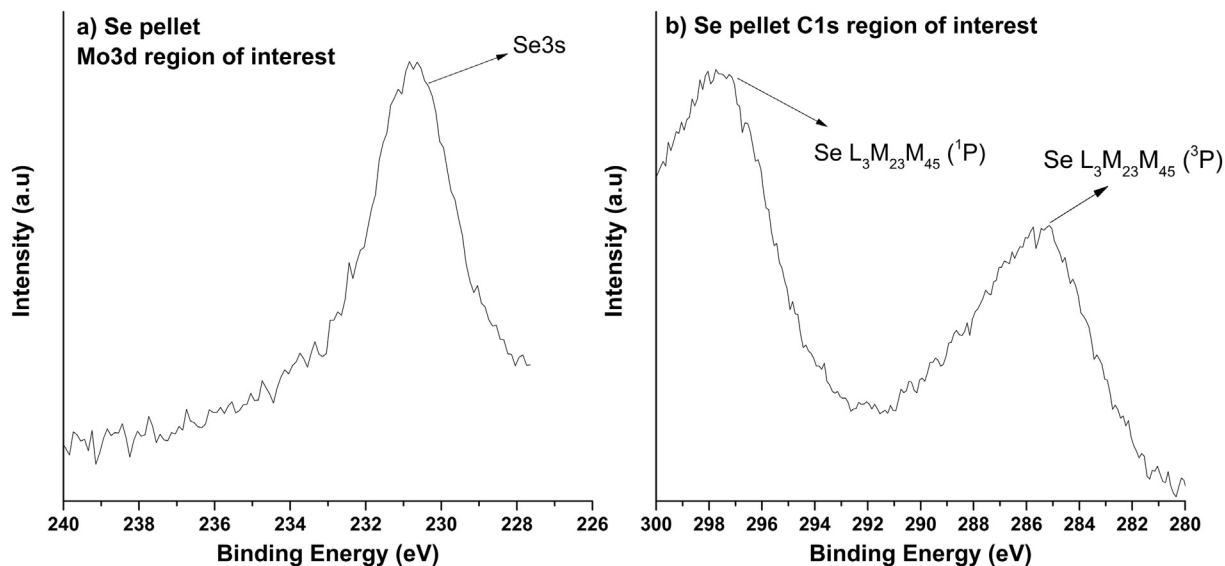
Fig. 5. XPS spectra of the Se pellet: a) Mo3d region of interest, b) C1s region of interest.

The group of peaks belonging to crystalline $MoSe_2$ is due to the splitting of E_{1g}, A_{1g} and E_{2g} modes (correspond to different in-plane and out of plane phase shifts whenever more than one $MoSe_2$ layers are present in the sample). The detail can be found in Refs. [52,53]. The important thing to be noted is that for 400C and 400C(90V) coatings, the obtained spectra clearly depict narrow peaks showing the existence of crystalline $MoSe_2$, in the amorphous carbon matrix, in agreement with TEM observations. It is observed that the sharpness and intensity of the peaks decreased in the Mo-Se-C coatings in comparison with pure $MoSe_2$. The introduction of carbon in the coatings, disturbed the growth of $MoSe_2$ crystals, thus promotes the formation of these platelet-shaped crystals with just one to two layers thickness. This was the reason why $MoSe_2$ crystallinity was not detected by XRD analysis, where only a broad peak appeared. The low-intensity broad peaks (at 700-900 cm-1) were identified as oxides, in particular MoO_3 [54] which can come either from the contamination during the deposition or the exposure to the atmosphere. D and G peaks clearly show the amorphous nature of the C, in accordance with X-ray and TEM results and thus confirming the establishment of a nanocomposite structure of $MoSe_2$ platelets embedded in an amorphous C matrix. For the analysis of D and G peaks of carbon, deconvolution was performed using a Breit-Winger-Fano asymmetric line for G-peak and Lorentz line for D-peak [55]. For 400C coating, D and G peaks were located at 1389 and 1563 cm^{-1} respectively while for 400C(90V) the peak centres moved to 1387 and 1560 cm^{-1} respectively. ID/IG ratios calculated using peak heights were 1.22 and 1.34 for 400C and 400C(90V) respectively. No significant quantity of sp3 C-C bonds is expected in the coatings due to the high ID/IG ratios [36]. Despite 90 % filter application, strong oxide peaks as well as the D and G peaks have been observed for pure $MoSe_2$ coating due to the high sensitivity of the coating to the laser. The laser power density, laser filter and exposure time to laser beam strongly affects the resulting spectrum for pure $MoSe_2$ coatings.

3.5. Hardness behaviour and adhesion

The hardness of deposited Mo-Se-C coatings was measured by nano-indentation and the results are shown in Fig. 7. Owing to the porous morphology, pure $MoSe_2$ coating showed a very low hardness of 0.2 GPa. As it has already been discussed, the density and compactness of Mo-Se-C coatings increased with C, thus more than one order of magnitude increase of the hardness for C-containing coatings has been observed.

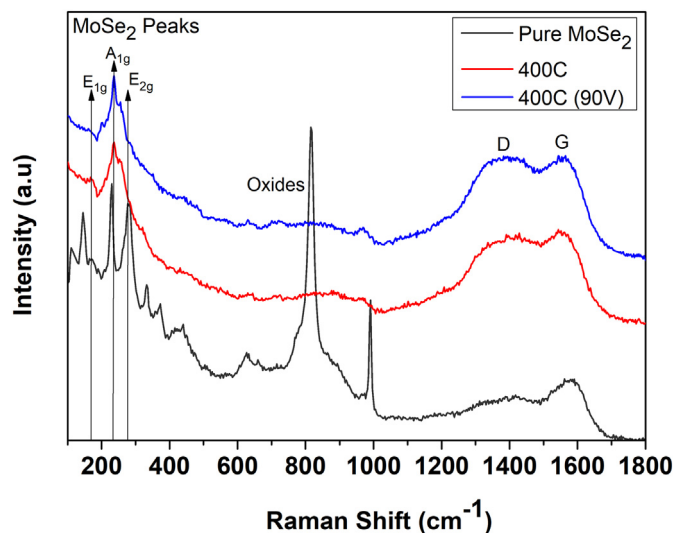The increase in hardness of Mo-Se-C coatings, as compared to the

Fig. 6. Raman spectra of the coatings.

pure $MoSe_2$ coating, can be explained by the increase in compactness and the decrease in the porosity. On the other hand, the nanocomposite structure, i.e. a combination of softer crystalline $MoSe_2$ nanoparticles embedded in amorphous carbon matrix can also contribute for this increase. C-based coatings deposited in similar conditions by magnetron sputtering show hardness much higher than the pure $MoSe_2$ (typically higher than 10 GPa). Therefore, knowing that an important part of the coatings is the amorphous C hardness, a significant increase in the hardness for Mo-Se-C coatings should be expected as, in fact was observed.

330C, 400C and 500C coatings showed almost identical hardness. The hardness value in this work for the coating with 50 at. % was superior to that achieved in previous studies for rf sputtered Mo-Se-C coatings, even if Se/Mo is higher [35,36]. With the application of substrate bias, the coatings show even better mechanical properties due to either the enhanced density and compactness as explained above, or the lower Se/Mo ratio.

It can also be noted from Fig. 7, higher the Se/Mo, the lower is the hardness, confirming the importance of this ratio on the overall mechanical behavior of this type of coatings. Same was observed for Mo-S-C coatings in literature [56]. Other studies also suggested that the
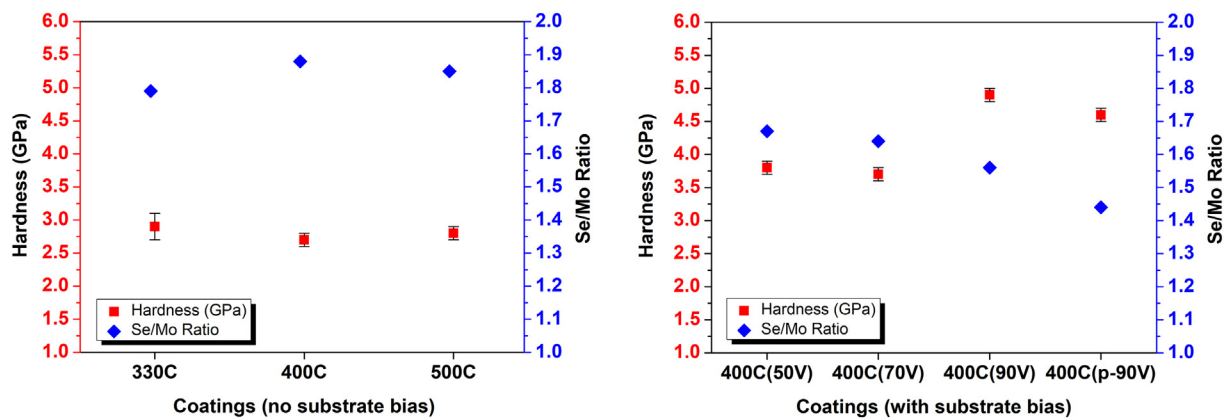
Fig. 7. Hardness and Se/Mo ratios as a function of carbon power and applied substrate bias.
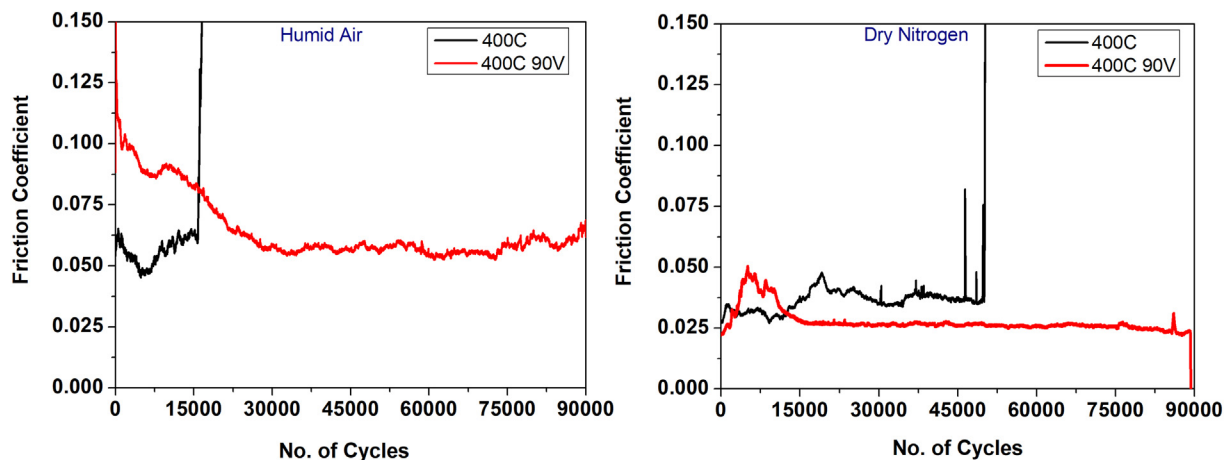

Fig. 8. Tribological behavior of reciprocating tests performed in humid air and dry nitrogen atmospheres.
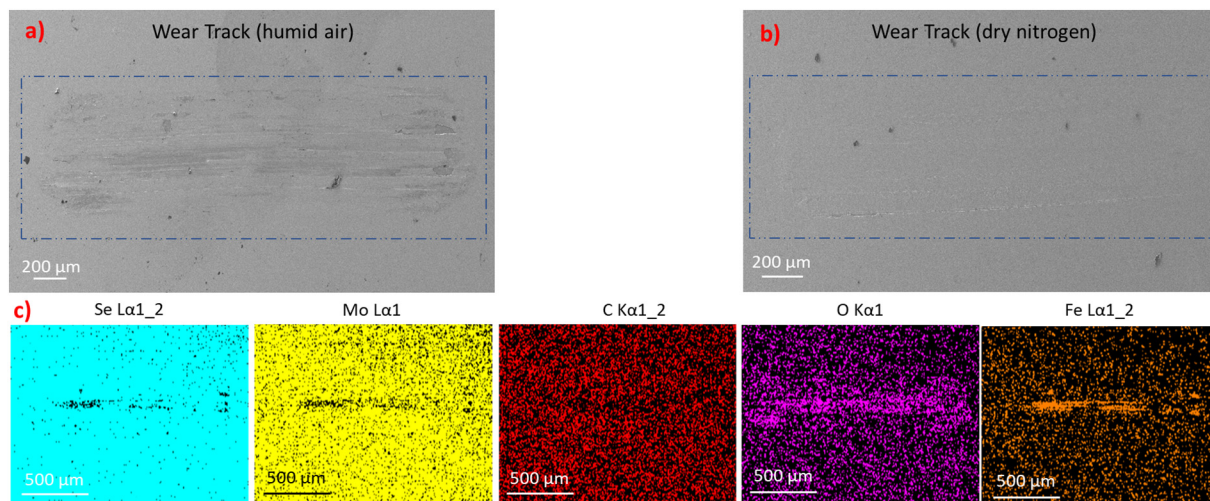

Fig. 9. 400C(90V) coating reciprocating test wear track: a) and b) SEM images of sliding in humid air and dry nitrogen respectively, while c) the elemental map distribution of wear track after sliding in humid air.

presence of hard metal-C nanocrystals, which can also be related with a lower chalcogenide/transition metal ratio, could contribute for the hardness of TMD-C sputtered coatings [57], but no clear evidences of Mo-C bonds have been observed in this work. Maximum hardness was observed for 400C(90V) dc substrate bias coating (4.9 Pa) which is better than the values reported in the literature for Mo-Se-C coatings, irrespective of the C percentage.

The coating adhesion to the M2 steel substrates was evaluated by scratch-test (see Table 2). The 330C coating showed the lowest adhesion critical load value with Lc_3 around 9 N. The 400C coatings deposited with 90 V dc substrate bias, out-performed others and showed Lc_3 of 23 N. All coatings were found to fail by Lc_3 failure mode.

3.6. Tribological behavior

The literature for TMD-C coatings reports that coatings displayed best tribological properties with ~50 at. % carbon content [14]. Tribological tests were performed on 400C coating displaying 50 at. % C and the maximum Se/Mo ratio while 400C(90V) was selected as it displayed the best mechanical properties. Fig. 8 shows the friction curves for tests performed in both humid air and dry nitrogen atmospheres. For 400C coating, the COF started with a lower value of 0.06 and after ~16200 cycles, the coating failed. This can be related to the lower hardness of the coatings leading to high wear. Specific wear rate calculated was ~3.0×10^{-6} mm^3/Nm. On the other hand, when 400C(90V) coating was tested, a steady drop of the friction coefficient was observed during the first 30000 cycles, which is due to the running-in period consisting of asperity deformation and formation of an easy shear tribofilm. A steady-state behavior with COF of around 0.06 was observed during the remaining time of the test. Periodic drops and increments of the friction coefficient to values closer to 0.05 and 0.07 respectively, were observed. The wear of this coating was very less with the specific wear rate close to ~2.65×10^{-7} mm^3/Nm with an average COF value was 0.065 which is similar to 400C coating. Overall, the frictional response of 400C(90V) was quite stable throughout the selected test duration/cycles (unlike 400C coating).

When the same coatings were tested in dry nitrogen, much improved tribological results were achieved owing to the absence of moisture affecting MoSe$_2$ properties. 400C coating displayed an initial COF of 0.03, slightly increasing thereafter and fluctuating around 0.04 until ~50000 cycles were reached. Close to this value, the COF increased instantaneously and the coating failed. Unlike tests in humid air, the coating survived for longer number of cycles with a specific wear rate of ~5.1×10^{-7} mm^3/Nm. On the other hand, for the 400C(90V) coating, the COF displayed a maximum value of 0.05 at ~5000 cycles and then decreased as the test progressed. This running-in period can be related to the formation of a MoSe$_2$ tribolayer. From ~15000 cycles until the end of the test, the COF was highly stable with an average value of 0.025. Unlike humid air test, no peaks or fluctuations were observed after reaching the steady-state, revealing the harmful effect of moisture on the friction performance of these coatings. 400C(90V) coating again displayed long-term stability. The average COF of the whole test was 0.027 and the wear was also very low with a specific wear rate of ~2.4×10^{-8} mm^3/Nm.

The application of substrate bias not only improved compactness, hardness and adhesion but also contributed for improvement of tribological properties. These coatings show COF and specific wear rates better than the previous studies on the Mo-Se-C system in humid air and dry nitrogen environments. In humid air, Polcar et al. [33] reported COF of 0.05 and specific wear rate of 2.6×10^{-6} mm^3/Nm for 51 at. % carbon under 30 N applied load and 500 cycles. While in dry nitrogen, the literature reports tests performed under 2 N, 5 N and 10 N loads and 157 m sliding distance for a coating containing 47 at. % C. The lowest reported COF 0.04 and the wear rate was 2.5×10^{-7} mm^3/Nm in case of test performed under 10 N applied load, values underperforming those we achieved in this work [35].

The wear tracks of the coatings deposited with substrate bias were analysed in SEM. In humid air, there were delaminated parts but such trend was not observed in dry nitrogen tests, as the coating looked smooth and intact (Fig. 9a) and b) respectively), which can justify its better performance. Fig. 9c) shows the elemental maps of the wear scar in humid air test. No significant changes in the intensities of the elements can be observed inside and outside of the wear track, excepting the detection of Fe and O in the central part, which can indicate that substrate was reached in that zone. As it was demonstrated before [35], the low friction performance is attributed to the formation of a thin MoSe$_2$ tribolayer at the top contact during sliding, which occurs when randomly distributed MoSe$_2$ platelets reorient parallel to the sliding, under the applied load.

For the harder coating (400C(90V)), the friction and wear responses are much better than for the softer coating (400C), although the latter has more MoSe$_2$ content. High hardness contributes for a higher wear resistance retarding the material loss. On the other hand, the harder coating also has a higher Young's modulus (70.6 GPa against 57.5 GPa for 400C coating). Therefore, the contact area will be lower and, for the same applied normal load, the contact stresses are higher. The reorientation process of the MoSe$_2$ platelets is facilitated with higher shear stresses and, so, the formation of tribofilm is easier with the consequent beneficial effect on the frictional behaviour. Once the tribofilm is formed after aggregation of smaller MoSe$_2$ crystals into larger ones, it provides easy shear properties and low COF persists. The tribofilm thus dominates the sliding role.

4. Conclusions

DC magnetron sputtered Mo-Se-C coatings were deposited using two separate targets of graphite and MoSe$_2$. The effects of increasing carbon power and the application of substrate bias on the properties of the deposited coatings were explored. Increasing carbon power led to an increase in the carbon content of the coatings in the range from 44 at. % to 60 at. %. The maximum Se/Mo ratio of 1.88 was achieved for coating deposited without bias and the ratio decreased as the substrate bias was increased. Pure MoSe$_2$ coating was highly porous and columnar while adding carbon or/and increasing the substrate bias led to a more compact morphology. Pure MoSe$_2$ coating showed a crystalline structure while all the other coatings were X-ray amorphous. No strong evidence of the presence of Mo-C nanocrystals was evident from X-ray diffraction studies. However, TEM analysis showed the presence of MoSe$_2$ platelets with (002) basal planes randomly dispersed in an amorphous carbon matrix. XPS analysis of C1s spectrum was not conclusive about evidence of Mo-C bonds and Raman spectra displayed clear peaks of MoSe$_2$ nanocrystals. The hardness of all coatings without substrate bias was almost similar but after applying substrate bias an increase in the hardness of the coatings was observed. The coatings containing ~50 at. % carbon deposited with dc 90 V substrate bias displayed hardness results better than those reported in literature. This hardness increase can be related to their higher compactness with the application of substrate bias voltage. The Mo-Se-C coating deposited with 90 V substrate bias showed excellent sliding properties in different atmospheres. The tribological results achieved with sputtering of two targets are quite impressive and the current study seems to be a successful first step to the direct industrial upscaling of the system for applications on the components sliding in inert and humid atmospheres.

References

[1] E.C. Fitch, Fluid chemical stability, Proactive Maint. Mech. Syst. Elsevier, U.K, 1992, pp. 99–126, , https://doi.org/10.1016/B978-1-85617-166-3.50005-6.
[2] J.M. Herdan, Lubricating oil additives and the environment—an overview, Lubr. Sci. 9 (1997) 161–172, https://doi.org/10.1002/ls.3010090205.
[3] T.W. Scharf, S.V. Prasad, Solid lubricants: a review, J. Mater. Sci. 48 (2013) 511–531, https://doi.org/10.1007/s10853-012-7038-2.
[4] S.V. Prasad, N.T. McDevitt, J.S. Zabinski, Tribology of tungsten disulfide-nanocrystalline zinc oxide adaptive lubricant films from ambient to 500°C, Wear 237 (2000) 186–196, https://doi.org/10.1016/S0043-1648(99)00329-4.
[5] A. Grill, Diamond-like carbon: state of the art, Diam. Relat. Mater. 8 (1999)

428–434, https://doi.org/10.1016/S0925-9635(98)00262-3.

[6] A. Erdemir, O.L. Eryilmaz, G. Fenske, Synthesis of diamondlike carbon films with superlow friction and wear properties, J. Vac. Sci. Technol. A Vacuum, Surfaces, Film. 18 (2000) 1987–1992, https://doi.org/10.1116/1.582459.

[7] C. Donnet, A. Erdemir, Tribology of Diamond-like Carbon Films: Fundamentals and Applications, Springer Science & Business Media, 2007, https://doi.org/10.1007/978-0-387-49891-1.

[8] C. Muratore, A.A. Voevodin, Molybdenum disulfide as a lubricant and catalyst in adaptive nanocomposite coatings, Surf. Coat. Technol. 201 (2006) 4125–4130, https://doi.org/10.1016/j.surfcoat.2006.08.014.

[9] C.P. Mulligan, D. Gall, CrN-Ag self-lubricating hard coatings, Surf. Coat. Technol. 200 (2005) 1495–1500, https://doi.org/10.1016/j.surfcoat.2005.08.063.

[10] C.P. Mulligan, T.A. Blanchet, D. Gall, CrN-Ag nanocomposite coatings: effect of growth temperature on the microstructure, Surf. Coat. Technol. 203 (2008) 584–587, https://doi.org/10.1016/j.surfcoat.2008.06.052.

[11] J. Esteve, G. Zambrano, C. Rincon, E. Martinez, H. Galindo, P. Prieto, Mechanical and tribological properties of tungsten carbide sputtered coatings, Thin Solid Films 373 (2000) 282–286, https://doi.org/10.1016/S0040-6090(00)01108-1.

[12] A.A. Voevodin, C. Muratore, S.M. Aouadi, Hard coatings with high temperature adaptive lubrication and contact thermal management: Review, Surf. Coat. Technol. 257 (2014) 247–265, https://doi.org/10.1016/j.surfcoat.2014.04.046.

[13] C. Donnet, A. Erdemir, Historical developments and new trends in tribological and solid lubricant coatings, Surf. Coat. Technol. 181 (2004) 76–84, https://doi.org/10.1016/j.surfcoat.2003.10.022.

[14] T. Polcar, A. Cavaleiro, Review on self-lubricant transition metal dichalcogenide nanocomposite coatings alloyed with carbon, Surf. Coat. Technol. 206 (2011) 686–695, https://doi.org/10.1016/j.surfcoat.2011.03.004.

[15] J. Sanders, J. Zabinski, J. Nainaparampil, S. Prasad, Lubrication using a micro-structurally engineered oxide: performance and mechanisms, Tribol. Lett. 8 (2000) 103–116, https://doi.org/10.1023/A:1019187202237.

[16] R.L. Fusaro, Effect of substrate surface finish on the lubrication and failure mechanisms of molybdenum disulfide films, ASLE Trans 25 (1982) 141–156, https://doi.org/10.1080/05698198208983076.

[17] T. Polcar, A. Nossa, M. Evaristo, A. Cavaleiro, Nanocomposite coatings of carbon-based and transition metal dichalcogenides phases: a review, Rev. Adv. Mater. Sci. 15 (2007) 118–126.

[18] M.R. Hilton, Fracture in MoS2 solid lubricant films, Surf. Coat. Technol. 68–69 (1994) 407–415, https://doi.org/10.1016/0257-8972(94)90194-5.

[19] D.-Y. Wang, C.-L. Chang, W.-Y. Ho, Microstructure analysis of MoS2 deposited on diamond-like carbon films for wear improvement, Surf. Coat. Technol. 111 (1999) 123–127, https://doi.org/10.1016/S0257-8972(98)00712-9.

[20] A.A. Voevodin, J.S. Zabinski, Nanocomposite and nanostructured tribological materials for space applications, Compos. Sci. Technol. 65 (2005) 741–748, https://doi.org/10.1016/j.compscitech.2004.10.008.

[21] N.M.U. Renevier, J. Hamphire, V.C. Fox, J. Witts, T. Allen, D.G. Teer, Advantages of using self-lubricating, hard, wear-resistant MoS 2 -based coatings, Surf. Coat. Technol. (2001) 67–77, https://doi.org/10.1016/S0257-8972(01)01108-2.

[22] A. Savan, M.C. Simmonds, Y. Huang, C.P. Constable, Effects of temperature on the chemistry and tribology of co-sputtered MoS x -Ti composite thin films, Thin Solid Films 489 (2007) 137–144, https://doi.org/10.1016/j.tsf.2005.04.078.

[23] T.W. Scharf, A. Rajendran, R. Banerjee, F. Sequeda, Growth, structure and friction behavior of titanium doped tungsten disulphide (Ti-WS2) nanocomposite thin films, Thin Solid Films 517 (2009) 5666–5675, https://doi.org/10.1016/j.tsf.2009.02.103.

[24] H. Chien, K. Ma, S.V.P. Vattikuti, C. Kuo, C. Huo, C. Chao, Tribological behaviour of MoS 2/Au coatings, Thin Solid Films 518 (2010) 7532–7534, https://doi.org/10.1016/j.tsf.2010.05.040.

[25] J.R. Lince, Tribology of co-sputtered nanocomposite Au/MoS 2 solid lubricant films over a wide contact stress range, Tribol. Lett. 17 (2004) 419–428, https://doi.org/10.1023/B:TRIL.0000044490.03462.6e.

[26] K.J. Wahl, D.N. Dunn, I.L. Singer, Wear Behavior of Pb – Mo – S Solid Lubricating Coatings, Wear (1999) 175–183, https://doi.org/10.1016/S0043-1648(99)00100-3.

[27] M. Ye, G. Zhang, Y. Ba, T. Wang, X. Wang, Z. Liu, Microstructure and tribological properties of MoS 2 + Zr composite coatings in high humidity environment, Appl. Surf. Sci. 367 (2016) 140–146, https://doi.org/10.1016/j.apsusc.2016.01.163.

[28] B. Deepthi, H.C. Barshilia, K.S. Rajam, M.S. Konchady, D.M. Pai, J. Sankar, A.V. Kvit, Structure, morphology and chemical composition of sputter deposited nanostructured Cr-WS2 solid lubricant coatings, Surf. Coat. Technol. 205 (2010) 565–574, https://doi.org/10.1016/j.surfcoat.2010.07.050.

[29] V. Rigato, G. Maggioni, D. Boscarino, L. Sangaletti, L. Depero, V.C. Fox, D. Teer, C. Santini, A study of the structural and mechanical properties of Ti-MoS2coatings deposited by closed field unbalanced magnetron sputter ion plating, Surf. Coat. Technol. 116–119 (1999) 176–183, https://doi.org/10.1016/S0257-8972(99)00312-6.

[30] T. Polcar, A. Cavaleiro, Self-adaptive low friction coatings based on transition metal dichalcogenides, Thin Solid Films 519 (2011) 4037–4044, https://doi.org/10.1016/j.tsf.2011.01.180.

[31] T. Kubart, T. Polcar, L. Kopecký, R. Novák, D. Nováková, Temperature dependence of tribological properties of MoS2 and MoSe2 coatings, Surf. Coat. Technol. 193 (2005) 230–233, https://doi.org/10.1016/j.surfcoat.2004.08.146.

[32] W.A. Brainard, The Thermal Stability and Friction of Disulfides, Diselenides, and Ditellurides of Molybdenum and Tungsten in Vacuum (10-9 to 10-6 Torr), NASA, Washington, D.C., 1969.

[33] T. Polcar, M. Evaristo, R. Colaço, C. Silviu Sandu, A. Cavaleiro, Nanoscale tri-boactivity: the response of Mo-Se-C coatings to sliding, Acta Mater. 56 (2008) 5101–5111, https://doi.org/10.1016/j.actamat.2008.06.029.

[34] T. Polcar, M. Evaristo, M. Stueber, A. Cavaleiro, Mechanical and tribological properties of sputtered Mo-Se-C coatings, Wear 266 (2009) 393–397, https://doi.org/10.1016/j.wear.2008.04.010.

[35] F. Gustavsson, S. Jacobson, A. Cavaleiro, T. Polcar, Frictional behavior of self-adaptive nanostructural Mo-Se-C coatings in different sliding conditions, Wear 303 (2013) 286–296, https://doi.org/10.1016/j.wear.2013.03.032.

[36] T. Polcar, M. Evaristo, M. Stueber, A. Cavaleiro, Synthesis and structural properties of Mo-Se-C sputtered coatings, Surf. Coat. Technol. 202 (2008) 2418–2422, https://doi.org/10.1016/j.surfcoat.2007.08.019.

[37] W.C. Oliver, G.M. Pharr, An improved technique for determining hardness and elastic modulus using load and displacement sensing indentation experiments, J. Mater. Res. (1992), https://doi.org/10.1557/JMR.1992.1564.

[38] F. Fernandes, T.B. Yaqub, A. Cavaleiro, Influence of Ag additions on the structure, mechanical properties and oxidation behaviour of Cr-O coatings deposited by HiPIMS, Surf. Coat. Technol. 339 (2018) 167–180, https://doi.org/10.1016/j.surfcoat.2018.02.025.

[39] S. Gangopadhyay, R. Acharya, A.K. Chattopadhyay, S. Paul, Effect of substrate bias voltage on structural and mechanical properties of pulsed DC magnetron sputtered TiN – MoS x composite coatings, Vaccum 84 (2010) 843–850, https://doi.org/10.1016/j.vacuum.2009.11.010.

[40] G. Weise, N. Mattern, H. Hermann, A. Teresiak, I. Ba, W. Bru, Preparation, structure and properties of MoS x films, Thin Solid Films 298 (1997) 98–106, https://doi.org/10.1016/S0040-6090(96)09165-1.

[41] S.N. Grigoriev, V.Y. Fominski, A.G. Gnedovets, R.I. Romanov, Experimental and numerical study of the chemical composition of WSex thin films obtained by pulsed laser deposition in vacuum and in a buffer gas atmosphere, Appl. Surf. Sci. 258 (2012) 7000–7007, https://doi.org/10.1016/j.apsusc.2012.03.153.

[42] S. Dominguez-Meister, A. Justo, J.C. Sanchez-Lopez, Synthesis and tribological properties of WSex films prepared by magnetron sputtering, Mater, Chem. Phys. 142 (2013) 186–194, https://doi.org/10.1016/j.matchemphys.2013.07.004.

[43] M. Evaristo, T. Polcar, A. Cavaleiro, Synthesis and properties of W-Se-C coatings deposited by PVD in reactive and non-reactive processes, Vacuum 83 (2009) 1262–1265, https://doi.org/10.1016/j.vacuum.2009.03.030.

[44] P.M. Martin, Handbook of Deposition Technologies for Films and Coatings: Science, Applications and Technology, Elsevier Inc., 2009.

[45] V.Y. Fominski, V.N. Nevolin, R.I. Romanov, I. Smurov, Ion-assisted deposition of MoSx films from laser-generated plume under pulsed electric field, J. Appl. Phys. 89 (2001) 1449–1457, https://doi.org/10.1063/1.1330558.

[46] S.S. Sunu, E. Prabhu, V. Jayaraman, K.I. Gnanasekar, T.K. Seshagiri, T. Gnanasekaran, Electrical conductivity and gas sensing properties of MoO3, Sens. Actuators B Chem. 101 (2004) 161–174, https://doi.org/10.1016/j.snb.2004.02.048.

[47] J.-C. Dupin, D. Gonbeau, P. Vinatier, A. Levasseur, Systematic XPS studies of metal oxides, hydroxides and peroxides, Phys. Chem. Chem. Phys. 2 (2000) 1319–1324, https://doi.org/10.1039/a908800h.

[48] J.F. Moulder, J. Chastain, Handbook of X-Ray Photoelectron Spectroscopy : a Reference Book of Standard Spectra for Identification and Interpretation of XPS Data, Physical Electronics Division, Perkin-Elmer Corp, 1992.

[49] G. Paolicelli, S. Ferrer, F. Comin, Separation of the Sp3 and Sp2 Components in the C 1s Photoemission Spectra of amorphous carbon films vol. 54, (1996), pp. 8064–8069, https://doi.org/10.1103/PhysRevB.54.8064.

[50] J.A. Schaidle, A.C. Lausche, L.T. Thompson, Effects of sulfur on Mo2C and Pt/Mo2C catalysts: water gas shift reaction, J. Catal. 272 (2010) 235–245, https://doi.org/10.1016/J.JCAT.2010.04.004.

[51] W.A. Abdallah, A.E. Nelson, Characterization of MoSe2 (0001) and ion-sputtered MoSe2 by XPS, J. Mater. Sci. 40 (2005) 2679–2681, https://doi.org/10.1007/s10853-005-2104-7.

[52] H. Terrones, E. Del Corro, S. Feng, J.M. Poumirol, D. Rhodes, D. Smirnov, N.R. Pradhan, Z. Lin, M.A.T. Nguyen, A.L. Elías, T.E. Mallouk, L. Balicas, M.A. Pimenta, M. Terrones, New first order Raman-active modes in few layered transition metal dichalcogenides, Sci. Rep. 4 (2014) 1–9, https://doi.org/10.1038/srep04215.

[53] P. Tonndorf, R. Schmidt, P. Böttger, X. Zhang, J. Börner, A. Liebig, M. Albrecht, C. Kloc, O. Gordan, D.R.T. Zahn, S.M. de Vasconcellos, R. Bratschitsch, Photoluminescence emission and Raman response of monolayer MoS2, MoSe2, and WSe2, Opt. Express. 21 (2017) 1–536, https://doi.org/10.1201/9781315113722.

[54] A.A. Voevodin, J.S. Zabinski, Laser surface texturing for adaptive solid lubrication, Wear 261 (2006) 1285–1292, https://doi.org/10.1016/j.wear.2006.03.013.

[55] A.C. Ferrari, J. Robertson, Interpretation of Raman spectra of disordered and amorphous carbon, Phys. Rev. B. 61 (2000) 95–107, https://doi.org/10.1103/PhysRevB.61.14095.

[56] L. Gu, P. Ke, Y. Zou, X. Li, A. Wang, Amorphous self-lubricant MoS2-C sputtered coating with high hardness, Appl. Surf. Sci. 331 (2015) 66–71, https://doi.org/10.1016/j.apsusc.2015.01.057.

[57] C. Tomastik, A. Tomala, A. Pauschitz, M. Roy, The influence of carbon content on the microtribological performance of W-S-C films, J. Eng. Tribol. 228 (2014) 745–755, https://doi.org/10.1177/1350650114529753.

[58] T. HudecMarián Mikula, Leonid Satrapinskyy, Tomáš Roch, Martin Truchlý, Peter Švec, Teodor Huminiuc, Tomáš Polcar, Structure, mechanical and tribological properties of Mo-S-N solid lubricant coatings, Applied Surface Science 486 (2019) 1–14, https://doi.org/10.1016/j.apsusc.2019.03.294 In this issue.

Annex B

T. Bin Yaqub, T. Vuchkov, P. Sanguino, T. Polcar, A. Cavaleiro, *Comparative Study of DC and RF Sputtered MoSe₂ Coatings Containing Carbon—An Approach to Optimize Stoichiometry, Microstructure, Crystallinity and Hardness*, Coatings. 10 (2020) 133.

Comparative Study of DC and RF Sputtered MoSe$_2$ Coatings Containing Carbon—An Approach to Optimize Stoichiometry, Microstructure, Crystallinity and Hardness

Talha Bin Yaqub [1,2,*], Todor Vuchkov [1,2], Pedro Sanguino [2], Tomas Polcar [3,4] and Albano Cavaleiro [1,2]

1   IPN—LED & MAT—Instituto Pedro Nunes, Laboratory of Tests, Wear and Materials, Rua Pedro Nunes, 3030-199 Coimbra, Portugal; todor.vuchkov@ipn.pt (T.V.); albano.cavaleiro@dem.uc.pt (A.C.)
2   SEG-CEMMPRE, Department of Mechanical Engineering, University of Coimbra, Rua Luís Reis Santos, 3030-788 Coimbra, Portugal; pesang@hotmail.com
3   Department of Control Engineering, Faculty of Electrical Engineering, Czech Technical University in Prague, Technická 2, 6 Prague, Czech Republic; T.Polcar@soton.ac.uk
4   nCATS, University of Southampton, University Road, Southampton SO17 1BJ, UK
*   Correspondence: talha.yaqub@ipn.pt

Abstract: Low stoichiometry, low crystallinity, low hardness and incongruencies involving the reported microstructure have limited the applicability of TMD-C (Transition metal dichalcogenides with carbon) solid-lubricant coatings. In this work, optimized Mo–Se–C coatings were deposited using confocal plasma magnetron sputtering to overcome the above-mentioned issues. Two different approaches were used; MoSe$_2$ target powered by DC (direct current) or RF (radio frequency) magnetron sputtering. Carbon was always added by DC magnetron sputtering. Wavelength dispersive spectroscopy displayed Se/Mo stoichiometry of ~2, values higher than the literature. The Se/Mo ratio for RF-deposited coatings was lower than for their DC counterparts. Scanning electron microscopy showed that irrespective of the low carbon additions, the Mo–Se–C coatings were highly compact with no vestiges of columnar growth due to optimal bombardment of sputtered species. Application of substrate bias further improved compactness at the expense of lower Se/Mo ratio. X-ray diffraction, transmission electron microscopy, and Raman spectroscopy confirmed the presence of MoSe$_2$ crystals, and (002) basal planes. Even very low carbon additions led to an improvement of the hardness of the coatings. The work reports a comparison between RF and DC sputtering of MoSe$_2$ coatings with carbon and provides a guideline to optimize the composition, morphology, structure, and mechanical properties.

Keywords: transition metal dichalcogenides; optimized; stoichiometry; crystallinity; microstructure; magnetron sputtering

1. Introduction

Tribology is the field of science that plays a vital role in the everyday use of small machinery or large industrial setups. Friction and wear of interacting bodies must be overcome to have highly efficient machines and industrial systems [1]. Solid lubricant coatings are under research for the past few decades, yet there are still many issues that need to be solved. In industries such as aerospace, automobile, tooling or power plants, the working conditions can change very frequently from very dry to a highly humid atmosphere, or from room temperatures to around 350–400 °C [2]. Thus,

the solid lubricant coatings must be capable of working in diverse environments without losing their efficient sliding properties. Various systems have been developed consisting of single-component coatings [3], multicomponent coatings [4], super-lattice and nanostructured coatings [5], and smart self-adaptive coatings [6,7]. Among these, self-adaptive solid lubricant coatings represent a domain of smart materials with high potential. TMDs have been combined with different metals [8–17], non-metals [18–21] and compounds [22,23] to enhance their microstructural, mechanical, and sliding properties. The most widely studied are the TMDs with carbon; it is an interesting combination of materials providing self-adaptive behavior in dry atmospheres and quite acceptable performance in humid conditions as well. TMDs alone show excellent low frictional behavior in dry atmosphere and vacuum environments owing to their layered structure [24]. The sliding performance is affected by moisture as it can increase the coefficient of friction (COF) from 0.001 in dry and vacuum conditions [25] to 0.1–0.2 [24] in humid environments. Moisture and oxygen target the dangling bonds of TMDs and degrade its tribological efficiency. The pure sputtered TMD coatings are columnar and highly porous, which leads to low hardness and weak adhesion to the substrates. The low mechanical properties restrict the application of pure TMD coatings in industries due to reduced load-bearing capacity and high wear [26–28]. On the other hand, amorphous carbon coatings provide high hardness but are not suitable for applications that work in dry atmospheres. Therefore, a combination of carbon and TMDs was explored by various authors [18,29–36], with the main idea to harvest the best properties of both materials and prepare the ultimate solid lubricant that will be able to reduce friction in diverse environments.

The issues related to low hardness and low load-bearing capacity were solved, to some extent, by carbon addition. However, an increase in carbon content typically led to chalcogen depletion, often below required threshold to provide effective solid lubrication. For TMDs, the closer the stoichiometry of the compound, the better the frictional response of the coatings. Besides, the literature reports many incongruencies regarding the microstructure; sometimes TMD nanoparticles/crystals are present in TMD-C coatings, while, in other cases the coatings are amorphous. In our previous studies, we observed that carbon-based $MoSe_2$ nanocomposite coatings performed better in a humid atmosphere, exhibiting higher stoichiometry compared to other TMDs [20,37]. The low hardness of Mo–Se–C coatings is still an issue as a combination of lower hardness and higher Se/Mo ratio results in higher wear of the coatings. The application of substrate bias can improve the hardness but has an adverse effect on the stoichiometry [37].

This study is focused on the optimization of the deposition parameters of Mo–Se–C coatings to achieve a microstructure and morphology giving an optimal Se/Mo ratio together with a high degree of $MoSe_2$ crystallinity without compromising high compactness and hardness. Two different target-power supply combinations (RF and DC) were used to identify the main deposition parameters, and to further compare the properties of the coatings achieved by both methods. Previously, our research group deposited Mo–Se–C coatings by RF sputtering of a composite target [20,25,38], and DC sputtering of 2 separate targets [37]; the latter study showed much improved properties when compared to other reports on TMD-C systems. Also, better control of the coating properties could be achieved while working with separate targets as it grants freedom to vary the applied power to the targets. DC power supply provides higher deposition rates at lower costs when compared to RF sputtering. On the other hand, we noticed in our previous study that DC sputtering was hindered by plasma instabilities at the $MoSe_2$ target, which was attributed to charge accumulation on the surface of the target [37]. Thus, RF sputtering of $MoSe_2$ might improve stability of the deposition. In this work, sputtering was performed in a top-down configuration; cathodes were mounted at an angle to the substrate normal, leading to a more concentrated and convergent plasma to the substrates. The influence of power supply, RF, or DC, and the carbon content on the coating stoichiometry, the crystallinity of $MoSe_2$, as well as the compactness and hardness, were studied. The effects of substrate bias voltage on coating properties were also investigated.

2. Materials and Methods

Mo–Se–C solid lubricant coatings were deposited by balanced magnetron sputtering using ATC-Orion 8 (from AJA INTERNATIONAL, US) deposition chamber equipped with 4 targets. Two different setups of targets and power supplies were used. In case 1, DC power supply was connected to two carbon targets (99.99%) and one $MoSe_2$ target (99.99%) while the fourth target was powered by RF power supply and assigned to Cr (99.99%). In case 2, DC power supply was connected to two carbon targets (99.99%) and one Cr target (99.99%) while the RF power supply target was assigned to the $MoSe_2$ target (99.99%). Two carbon targets were selected since carbon has a very low sputtering yield. The Cr target was used for the deposition of an interlayer and gradient layers to enhance the adhesion of the coatings. Each target had a diameter of 50.2 mm. The target to substrate distance was ~80 mm and the targets were tilted 30^0 with respect to the substrate normal to enhance the deposition rate, homogeneity of coatings and to provide continuous sputtering on to the substrates. The substrate holder was rotated at a speed of 10 rpm to enhance the homogeneity in the coatings. The chemical composition, thickness, morphology, microstructure, and mechanical properties of the coatings were analyzed using polished (111) silicon substrates. The substrates were each ultrasonically cleaned for 20 min in acetone and ethanol before being placed in the deposition chamber, which was then pumped down to a base pressure of 5×10^{-5} Pa. Before deposition, sputter cleaning of the targets and etching of the substrates were carried out in an Ar atmosphere, for 30 min, by maintaining an overall chamber pressure of 1.33 Pa, with shutters in front of the targets. A power of 250 W was applied to carbon, $MoSe_2$ and Cr targets for cleaning while 40 W RF power was used for substrate etching.

After cleaning, the pressure was decreased to 0.5 Pa for underlayers and final coating deposition. The total time for the interlayer, gradient layer, and final Mo–Se–C coating deposition for case 1 and case 2 was 110 and 210 min, respectively, to achieve a coating thickness of ~2 μm. Power applied to the $MoSe_2$ target was kept constant in all cases, while the composition was varied by applying different powers to the carbon targets. In the case of interlayer, 250 W power was applied to Cr target for 10 min and then for the next 10 min Cr target power was gradually decreased to 0 W, while power to each carbon target was progressively increased to 250 W. For the last 5 min of the gradient layer, power to $MoSe_2$ was also progressively increased to 250 W to have different gradient layer compositions. Eventually, the power to Cr target was turned off and the power to the other targets was adjusted as shown in Table 1. For the coatings deposited with substrate bias, an RF voltage of -50 V was applied. In case of DC and RF sputtered pure $MoSe_2$ coatings, the deposition time was 60 min and 120 min, respectively, since the sputtering rate of the RF power supply is lower. For pure coatings, Cr interlayers were not deposited. Instead, substrate bias was applied initially for 2 min, in order to have a Mo rich interlayer. The coatings will be denominated as shown in Table 1.

Table 1. Main deposition parameters, thickness and deposition rates of the coatings.

Coating	$MoSe_2$ Power (W)	Carbon Power (W)	Bias (V)	Time (min)	Thickness (μm)	Deposition Rate (nm/min)
Case 1						
DC Pure $MoSe_2$	270	-	-	60	1.9	32
DC324	270	324	-	110	2.4	22
DC540	270	540	-	110	2.3	21
DC676	270	675	-	110	2.6	24
DC540(50V)	270	540	50	110	2.2	20
Case 2						
RF Pure $MoSe_2$	270	-	-	120	2.3	19
RF170	270	170	-	170	2.5	15
RF270	270	270	-	210	2.6	13
RF340	270	340	-	170	2.6	15
RF270(50V)	270	270	50	170	1.9	11

The chemical composition of the deposited coatings was determined using wavelength dispersive spectroscopy (WDS, Oxford Instruments, High Wycombe, UK). Morphologies of the fractured cross-section and the top surface of the coatings were analysed by field emission scanning electron microscopy (SEM-Zeiss Merlin, Oberkochen, Germany). Cross-section images were used to measure the thickness of the coatings. The crystal structure of the deposited coatings was analyzed by X-ray diffraction (X'Pert Pro MPD diffractometer, PANalytical B.V., Almelo, Netherlands) operating in grazing incidence (3°) mode utilizing copper $K_{\alpha 1}$ (λ = 1.5406 Å) radiation. The nanostructure of the coatings was analyzed by TEM (Jeol JEM 2100, Akishima, Tokyo) using an accelerating voltage of 200 kV. For TEM analysis, 25–35 nm thick coatings were deposited on copper TEM grids. Raman spectroscopy was performed using 532 nm laser (XploRA, Horiba, Kyoto, Japan), from 100 to 1800 cm^{-1} wave number range. Filter and acquisition time were selected in a way to avoid the coating damage. Nanoindentation (Micro Materials Nano Test Platform, Wrexham, UK) hardness measurements were performed using Berkovich diamond indenter under 3 mN load. A total of 32 indentations were made at two different locations. The indentation load was selected (after some preliminary trials) to keep indentation depth of less than 10% of the coating thickness to avoid influence of the substrate effect. The analysis was performed based on the Oliver and Pharr method [39].

3. Results

3.1. Chemical Composition, Deposition Rate, and Thickness

Table 2 shows the chemical composition of deposited coatings measured by wavelength dispersive spectroscopy (WDS). As expected, the application of power to carbon targets resulted in an increase of carbon content in the coatings and a very small decrease in Se/Mo ratio. The carbon content is almost similar for corresponding coatings in cases 1 and 2, but Se/Mo ratios are different since RF sputtering produces higher plasma density near the substrate [40,41]. Thus, the higher bombardment of Ar ions can be expected, increasing the preferential re-sputtering of the chalcogen atoms. In both cases, the application of substrate bias led to a significant drop of Se/Mo ratio. Substrate bias results in increased ion bombardment leading to higher preferential re-sputtering of the lighter Se element. The ratio decreased from 1.96 (DC540) to 1.77 (DC540 (50V)) for case 1 and similarly from 1.81 (RF270) to 1.07 (RF270(50V)) for case 2; the latter has the highest sub-stoichiometry (1.07) of all coatings. Overall, for the coatings without the substrate bias, the achieved Se/Mo ratio was ~2, unlike previous studies on other TMD-C coatings [19,42–44], which were sub-stochiometric. Although the preferential sputtering rate of chalcogen atoms is very low in MoSe$_2$, due to the small atomic mass difference [45] when compared to other TMDs such as MoS$_2$ or WS$_2$, there is an additional reason for improvement: here, the carbon content was kept only up to 25 at.%. In other studies, the carbon content was much higher and thus led to a decrease in the stoichiometry, which occurs because by increasing the carbon target power (for higher carbon content), the current and voltage on the target also increase. As a consequence, the energy and number of the Ar neutrals reflected at the target are higher. Reflected neutrals additionally bombard the growing coating, causing further preferential re-sputtering of lighter Se element. Even in this study, any additional increments of carbon beyond 25 at.% would further reduce Se/Mo ratio as suggested by the small but noticeable decrease in the Se/Mo ratio with increasing carbon content from 0 to 25 at.%. Previously, the effort was focused on high carbon content to achieve denser microstructures. The carbon content of 50 at.% was considered an optimum compromise between mechanical properties and solid lubrication [19]. We will show later that we can achieve enhanced mechanical properties without compromising the stoichiometry. The oxygen content measured by WDS was negligible considering unavoidable residual contamination of the chamber atmosphere and porosity of MoSe$_2$ target [7].

Deposition rates and thickness of the coatings are shown in Table 1. In both cases, pure MoSe$_2$ was highly porous; the deposition rate calculated as a thickness per time is thus the highest. RF sputtered pure coating displayed lower deposition rates (19 nm/min vs. 32 nm/min for DC sputtered MoSe$_2$),

which is in agreement with the literature [40,46]. With the introduction of carbon in the chamber, more sputtered species formed the coating, but the deposition rate for Mo–Se–C coatings (in both cases) decreased in comparison to the pure MoSe$_2$ coatings. Such behavior is attributed to the compactness of the coatings with the addition of carbon (Figures 1 and 2).

Considering only Mo–Se–C coatings, the deposition rate increased a little with increasing the carbon power but overall, there was not much of a difference as the values were in the error range. Within each case, the deposition time was kept almost constant for all the Mo–Se–C coatings deposited with or without substrate bias. The deposition rate with bias was always lower due to enhanced Ar$^+$ ion bombardment resulting in higher material removal from the growing coating along with higher density and compactness. DC sputtered Mo–Se–C coatings also show higher deposition rates than our recent work [37], due to confocal sputtering resulting in continuous arrival of sputtered species on the substrates. In previous work the arrival was intermittent as the substrates were passing in front of the targets one by one.

Table 2. Chemical composition and Se/Mo of the coatings.

Coatings	C (at.%)	Mo (at.%)	Se (at.%)	O (at.%)	Se/Mo
Case 1					
DC324	17.7 ± 0.4	27.1 ± 0.2	54.2 ± 0.3	1.0 ± 0.2	2.00
DC540	21.4 ± 0.3	26.2 ± 0.1	51.3 ± 0.2	1.1 ± 0.1	1.96
DC676	25.1 ± 0.5	25.2 ± 0.2	48.4 ± 0.4	1.3 ± 0.1	1.92
DC540(50V)	27.2 ± 0.4	26.1 ± 0.5	46.2 ± 0.5	0.5 ± 0.1	1.77
Case 2					
RF170	17.9 ± 0.3	28.2 ± 0.2	52.4 ± 0.4	1.5 ± 0.1	1.86
RF270	21.7 ± 0.3	27.3 ± 0.1	49.4 ± 0.2	1.6 ± 0.1	1.81
RF340	24.7 ± 0.4	26.6 ± 0.2	47.7 ± 0.2	1.0 ± 0.2	1.79
RF270(50V)	35.2 ± 0.6	30.9 ± 0.4	33.1 ± 0.6	0.8 ± 0.2	1.07

3.2. Fractured Cross-Section and Surface Morphology

Figures 1 and 2 show the fractured cross-section and surface morphologies of cases 1 and 2 coatings, respectively, analysed by SEM. For MoSe$_2$ coatings, Cr interlayers were not applied. The denser region near the substrate corresponds to the initial few minutes of deposition with the substrate bias leading to high preferential re-sputtering of Se and increased Mo content in this compact adhesion layer. In case 1, the sputtered MoSe$_2$ coating (Figure 1a) displayed a columnar and porous cross-sectional morphology, with columns extending down to the Mo-rich layer. The porous nature of the MoSe$_2$ coating was also evident from the sponge-like surface morphology (Figure 1f). When carbon was co-sputtered, the coatings became compact and columns disappeared (Figure 1b). Surface morphology micrographs corroborate the cross-sectional results: the sponge-like and porous surface features were replaced by a compact cauliflower type morphology after carbon addition (Figure 1g), due to limited surface mobility influencing the coating growth. No changes in the top and cross-sectional surface morphologies were observed after a further increase in the carbon content. The substrate bias contributed to a slight smoothening of the surface (Figure 1j), due to increased bombardment of growing coatings and thus providing increased adatom mobility and higher atomic coverage. The higher adatom mobility and, in turn, the increase of compactness is also facilitated by the elevated temperature at the surface of the growing film due to the substrate bias.

In case 2, the MoSe$_2$ coating was again porous (Figure 2a) but it showed a strong contribution of dendritic growth as compared to DC sputtered one. Also, surface morphology did not show sponge-like features; instead, much wider features and grown-up crystals were observed (Figure 2f), which are related to the higher atomic mobility and low deposition rate of RF sputtering, thus allowing more time for the grains to nucleate at favorable sites and grow in size [47]. As expected, the addition of carbon led to an increase in compactness and a decrease of porosity similar to the case 1 coatings. For RF170, the sudden decrease of power to carbon targets after gradient layer deposition (500 W to

170 W), resulted in the formation of a visible layer in the fractured cross-section image (Figure 2b). For the biased coating (Figure 2j), smoothening of the surface was also observed as in case 1 coatings.

Our previous works [25,38], showed columns/dendrites in Mo–Se–C coatings. In this study, the lack thereof is related to the higher homogeneity achieved, very likely due to a continuously optimal bombardment of the growing coating with energetic particles. Furthermore, continuous confocal sputtering enhanced the substrate temperature, which is also contributing to the densification of the coatings [48]. With these conditions, even low carbon content addition to TMD coatings can give rise to a compact morphology (without columns). Globally comparing both DC and RF deposited coatings, similar morphologies and compactness were displayed. Based on the experience and reported literature [19,20], the enhanced compactness with high Se/Mo ratios achieved in this study can be ideal for mechanical and tribological properties.
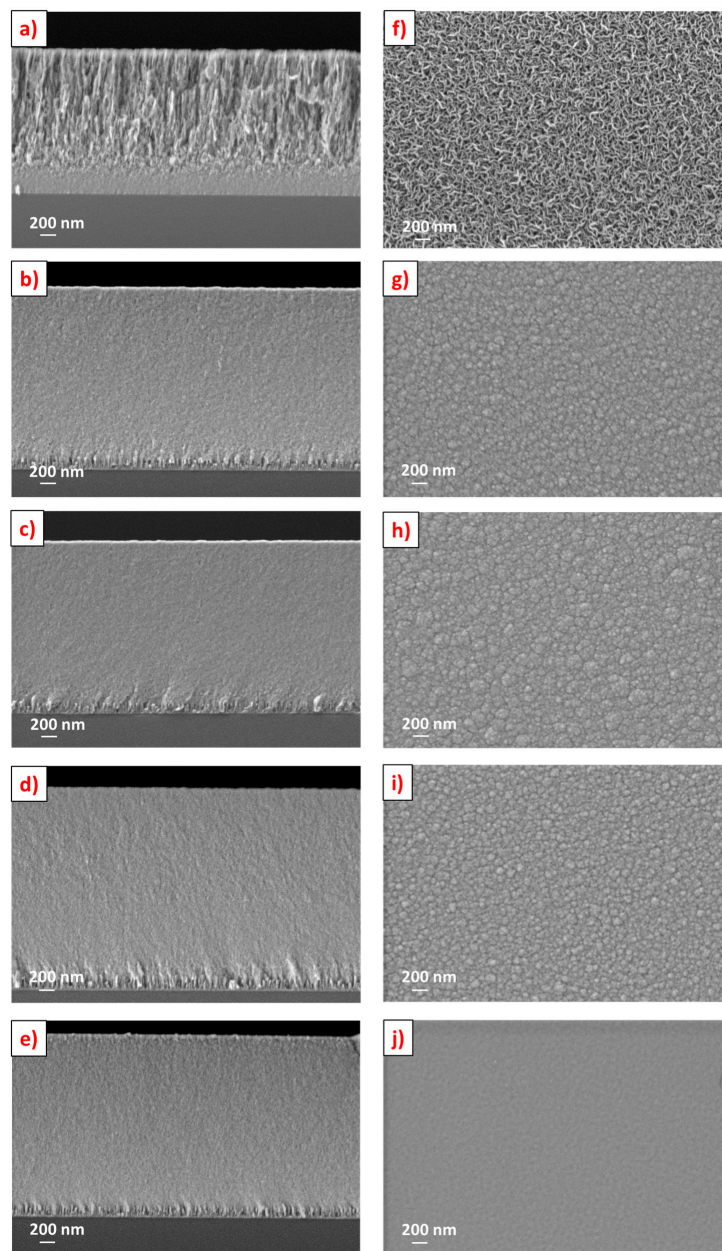
Figure 1. Scanning electron microscopy micrographs of the cross-section morphologies: (**a**) Pure MoSe$_2$, (**b**) DC324, (**c**) DC540, (**d**) DC676, (**e**) DC540(50V) and their respective top surface morphologies: (**f**) Pure MoSe$_2$, (**g**) DC324, (**h**) DC540, (**i**) DC676, (**j**) DC540(50V).
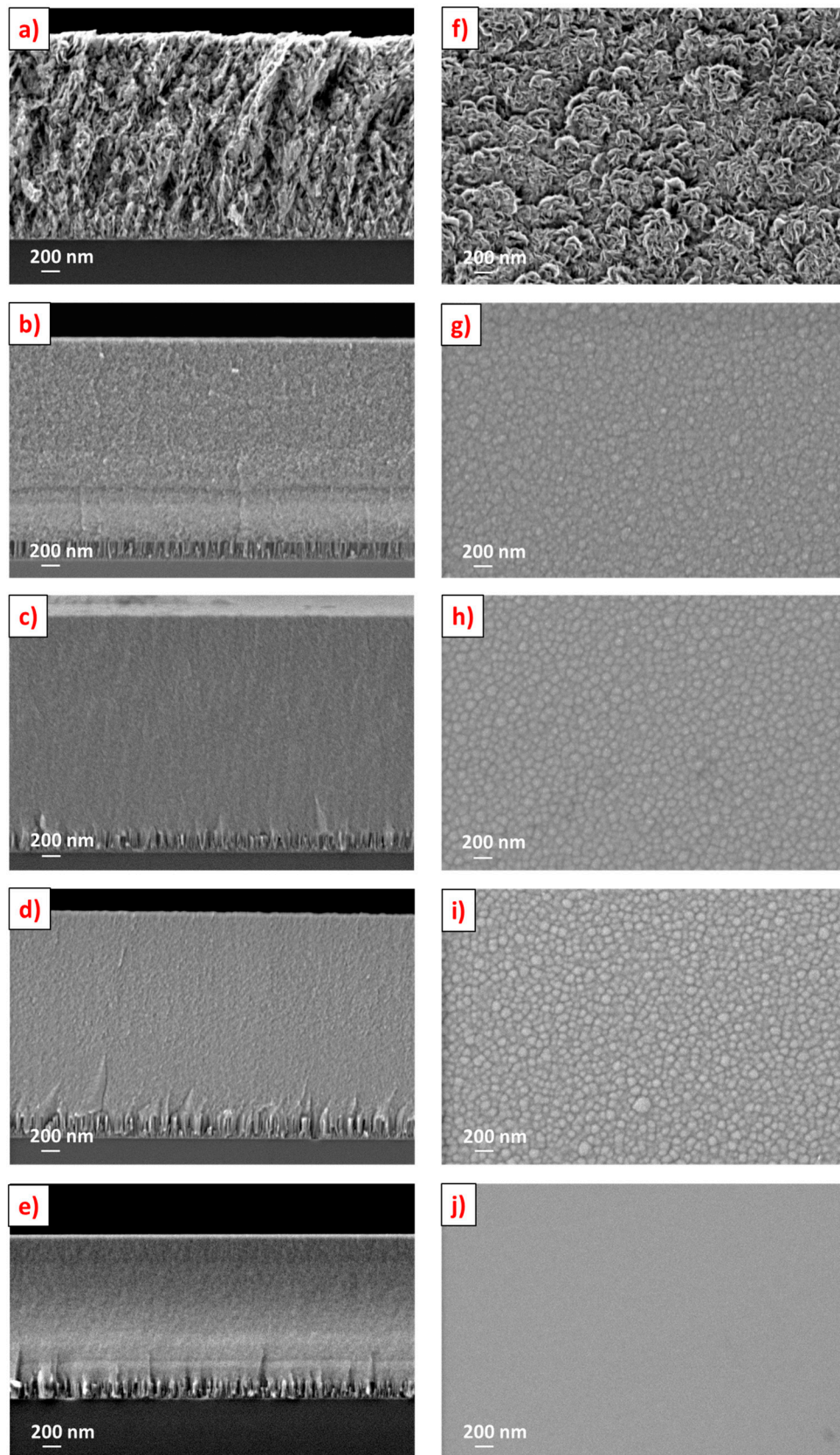
Figure 2. Scanning electron microscopy micrographs of the cross-section morphologies: (**a**) Pure MoSe$_2$, (**b**) RF170, (**c**) RF270, (**d**) RF340, (**e**) RF270(50V) and their respective top surface morphologies: (**f**) Pure MoSe$_2$, (**g**) RF170, (**h**) RF270, (**i**) RF340, (**j**) RF270(50V).

3.3. Crystal Structure

3.3.1. X-ray Diffraction

Grazing incidence X-ray diffraction analysis was used to assess the crystal structure of the coatings. Well-defined crystalline peaks typical of pure sputtered TMDs were visible in both XRD patterns for the pure $MoSe_2$ coatings ICCD n° 087-2419 (Figure 3). Working in grazing incidence (3°), the peaks detected at ~13° correspond to the (002) planes inclined 5° in relation to the surface, which are closely parallel to the surface. These planes play a vital role in the easy shear properties of TMDs during sliding. At 30°–50°, peaks with an extended shoulder related to the (100) and (10 L) planes were observed. This feature was reported by Weise et al. [42], and is related to the turbostratic stacking of the (10 L) planes (L = 1, 2, 3, 4, ...). The TMD peaks at ~13° and ~30°–50° were sharper and more well-defined in pure RF $MoSe_2$ coating than for DC one, showing the higher degree of crystallinity of the former. In RF $MoSe_2$ coating, (002) basal planes were dominant compared to (100) and (10 L) while, in DC, the inverse was observed. As the only main differences in the deposition of both coatings were the low deposition rates and the more ions impinging the growing coating in RF deposition—more time and enhanced adatom mobility and surface diffusion exists, allowing the atoms to relax at more favorable states, i.e., (002) preferential orientation [47]. More (002) contribution in RF sputtered $MoSe_2$ is also in agreement with work of Muratore [49], who explained for MoS_2 that the deposition rates of ~15 nm/min are required for achieving (002) basal planes and, in spite of the low desorption energies of (002) than (100), the former orientation can be achieved if there is some energetic ion bombardment (as it is in RF sputtering). It was further reported that having a deposition rate closer to ~15 nm/min provided an increased burial rate of the 2nd layer as compared to the desorption rates of the first layer thus promoting the (002) orientation. Muratore [49] added that an increase in (002)/(100) ratio enhanced the tribological properties. So, we expect that the pure RF coatings will provide better sliding properties then DC ones.
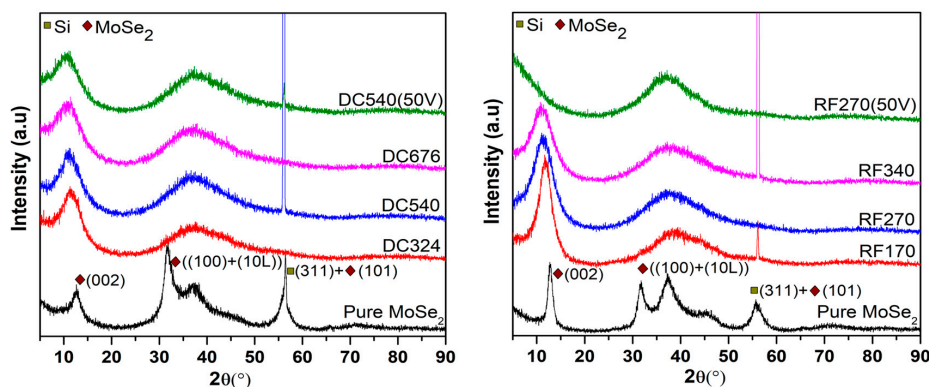
Figure 3. X-ray diffraction patterns of the coatings (case 1-left and case 2-right).

In both cases, carbon addition leads to structural changes and reduced crystallinity. Therefore, a broad peak at ~30°–50°, related to (100) and (10 L) planes of $MoSe_2$ nanocrystals (<10 nm) appeared. Unlike other works on TMD-C coatings [20], (002) peaks were also detected for Mo–Se–C coatings, which can tentatively be explained by the lower percentage of carbon content and the higher Se/Mo ratio. Mutafov [50] claimed in his work on WSN coatings that (002) peaks were observed due to very low (i.e., less than 1.2) S/W ratio, but our results contradict that, as the decrease in Se/Mo ratio resulted in the vanishing of (002) peak (RF270(50V). Regardless, these peaks reveal the interesting presence of (002) planes with a possible positive impact on the tribological behavior of the coatings. As compared to pure coatings, the (002) peak in Mo–Se–C coatings is broader (in both cases), suggesting smaller sizes of $MoSe_2$ crystallites (in agreement with TEM results shown later). Carbon disturbs the growth and impedes the formation of well-defined $MoSe_2$ crystals. The addition of carbon, and the consequent decrease of Se/Mo ratio, also results in an increase in the interplanar distance confirmed

by the (002) peak shift to lower angles (the shift is more evident in case 1 coatings). The decrease in Se/Mo ratio cannot explain the peaks shifts to a lower angle; however, carbon can become entrapped in the basal planes [51], causing the c lattice constant to increase. The increase in interplanar distances due to the incorporation of a 3rd element in the lattice has been reported by Rasamani [51] and Panigrahi [52], which is in agreement with our observations. The interplanar distances calculated from XRD diffractograms increased from ~0.69 nm (DC MoSe$_2$) to ~0.75 nm (DC324) and from ~0.67 nm (RF MoSe$_2$) to ~0.73 (RF170) in cases 1 and 2, respectively. Further increase in the carbon content increased this broadening of the peaks, shifts in (002) peaks position to lower angles, and an increase in the interplanar distances. The latter may reduce the Vander Waals forces between the basal planes and add a positive impact on the easy shearing properties of MoSe$_2$. With the application of substrate bias, no effect on the X-ray diffraction patterns was observed in case 1 coatings. In case 2, (002) peaks were absent, very likely due to very low Se/Mo ratios (1.77 for DC540(50V) vs. 1.07 for RF270(50V)). Just like pure MoSe$_2$ coatings, by similar reasons, the (002) peaks are more intense and sharper in C based MoSe$_2$ (Mo–Se–C) RF coatings than in DC Mo-Se-C coatings, despite their lower Se/Mo ratio.

3.3.2. TEM Analysis

Transmission electron microscopy analysis was performed to investigate the shape and size of MoSe$_2$ structures embedded in the carbon matrix (Figure 4). Although only selected HR-TEM images are shown for both cases, they are representative of all the coatings. Additionally, HR-TEM image of pure MoSe$_2$ coating has been shown for microstructural comparison. The pure coatings depicted well-defined crystals of MoSe$_2$ having long range ordering with crystal sizes much greater than C based coatings. Planes having orientation other than (002) basal planes were also detected, agreeing with XRD results. After the introduction of carbon, the micrographs in both cases showed MoSe$_2$ nanoplatelets/nanograins randomly dispersed in the form of wires, separated by an amorphous phase. A total of 20 readings were taken for each sample at different locations to measure the average distance between the planes and the average number of stacked planes. The average distances were 0.691 ± 0.007 nm and 0.689 ± 0.009 nm for DC540 and RF270 coatings, respectively (a bit lower than the one from XRD i.e., 0.76 nm), which corresponds to the (002) planes of MoSe$_2$ phase. Similarly, the average number of stacked planes were 4.6 ± 0.2 for DC540 coating and 4.0 ± 0.3 for RF270 coating, respectively. The length of the nanoplatelets was calculated at various regions with an average value of less than 10 nm, unlike pure coatings. Such small dimensions reflect the structural disturbance induced by the carbon incorporation in the pure coatings, hindering a suitable organization of the atoms during growth. TEM results agree with XRD observation (Section 3.3.1) concerning the small size of the crystals, which was the reason for the (002) XRD peak broadening for Mo–Se–C coatings. The interplanar distances measured from XRD and TEM are slightly different which can be probably explained by the very low thickness of TEM samples (25–30 nm) when compared to those analysed by XRD (~2 μm), leading to less stresses in the TEM samples in comparison to XRD ones.
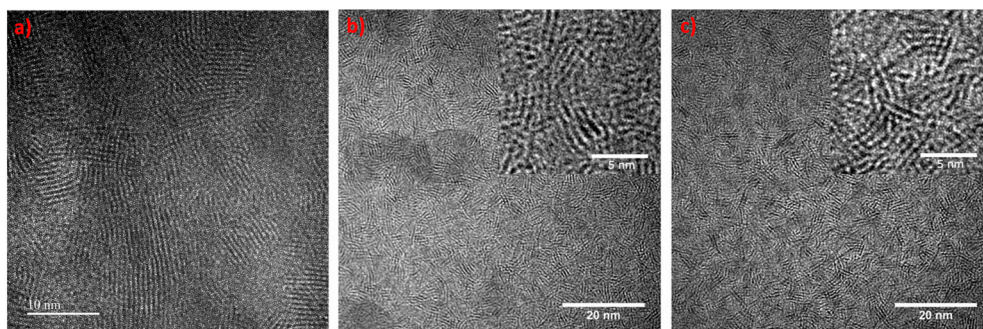

Figure 4. Transmission electron microscopy images of the (**a**) Pure MoSe$_2$, (**b**) DC540 and (**c**) RF270 coatings.

3.4. Chemical Bonding

Raman spectroscopy was performed on samples from cases 1 and 2 (Figure 5) to further study the phases present in the coatings, specially carbon. Well-defined peaks in positions typical of $MoSe_2$ were obtained in all coatings, confirming XRD and TEM results. Furthermore, as expected, the addition of carbon resulted in a decrease in the intensity and an increase in the broadness of $MoSe_2$ peaks.
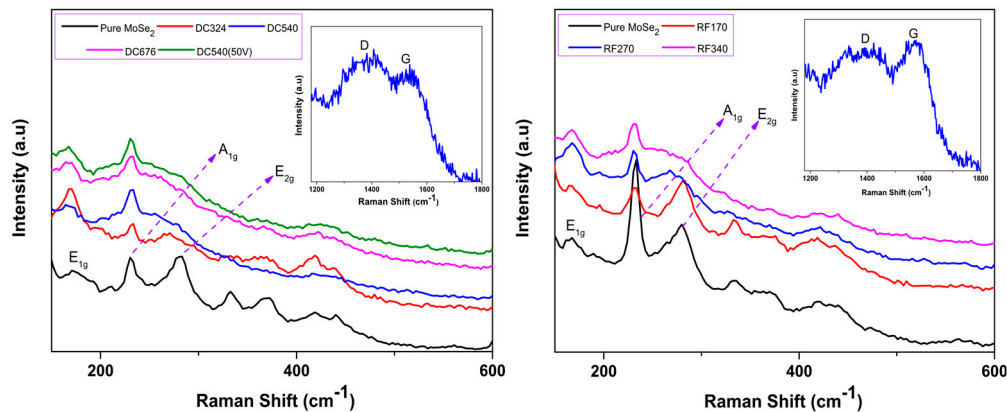

Figure 5. Raman spectra of coatings from case 1 (left) and case 2 (right)-inset in left figure is showing D and G peaks.

Generally, for $MoSe_2$ coatings, different in-plane (E_{1g} and E_{2g}) and out of the plane (A_{1g}) vibrational modes appear [53]. In the deposited pure coatings, the E_{2g} mode were significantly higher than the carbon-based coatings. The E_{2g} mode became Raman inactive and the peak disappeared with the increments of carbon, due to the structural disturbance and decrease of crystallite size of $MoSe_2$. These observations agreed with XRD and TEM results where the (100) and (10 L) peaks disappeared and crystallite sizes decreased. Moreover, carbon addition also restricted the $MoSe_2$ bond vibrations due to increased compactness of the coating (Section 3.2), thus influenced the Raman response. Some other broad and barely visible peaks around ~350 and ~445 cm^{-1} corresponding to $MoSe_2$ peaks were also observed. The E_{2g} peak was also overlapping with the oxides (Mo-oxide) positioned at ~289 cm^{-1} [54,55].

Finally, the nature of the carbon phase was observed by analyzing D and G peaks. D peak was deconvoluted using the Lorentz line while for G peak Breit-Winger-Fano asymmetric line was used [56]. The peak positions after deconvolution indicated the presence of an amorphous carbon phase. It was also observed that the increase of carbon and decrease of Se/Mo ratio resulted in an increase in the intensity of the peaks related to amorphous carbon. ID/IG increased from 0.57 to 1.24 for DC324 to DC676 coatings, respectively and from 0.45 to 1.23 for RF170 to RF340 coatings, respectively. Only DC540(50V) was analyzed to study the influence of substrate bias on ID/IG ratio and peak positions; minor differences were observed. D and G peaks of only one Raman spectra from each case (having 22 at.% C) has been shown to be a representative of all coatings.

3.5. Mechanical Properties

Hardness and reduced modulus (E*) values of the coatings are shown in Figure 6. DC and RF pure $MoSe_2$ coatings displayed hardness values of 1.4 GPa and 1.0 GPa, respectively. After carbon addition, all the coatings show higher hardness than $MoSe_2$ due to the denser morphology, increased compactness, and presence of the carbon phase. Generally, in this study, the case 1 sputtered coatings outperformed case 2 ones due to more (002) crystallinity of the latter. Presence of higher number (002) planes, in the case 2 coatings, resulted in easy shearing properties and low hardness. Regardless, despite lower carbon content, all coatings showed higher hardness values than those achieved in previous works [20,37,38]. A hardness of ~3.2 GPa was reported for single target RF sputtered $MoSe_2$

coatings deposited with 61 at.% of carbon [38], while here, a hardness of 4.6 GPa and 4.3 GPa was achieved for case 1 (DC676) and case 2 (RF340), respectively, with only ~25 at.% of carbon. In our recent study of separate target DC sputtering, we reported ~2.8 GPa for 50 at.% C coating deposited without substrate bias [37].
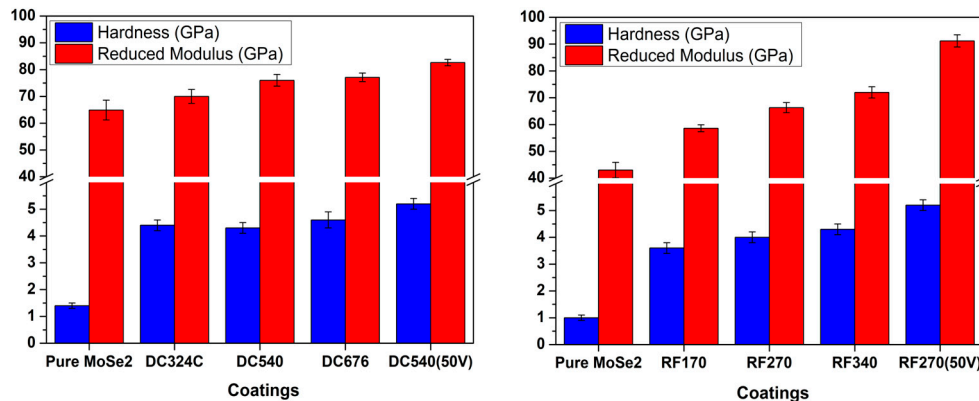

Figure 6. Hardness and reduced modulus of the coatings (case 1-left and case 2-right).

Moreover, the application of RF substrate bias resulted in the reduction of the Se/Mo ratio and the enhancement of density and compactness, resulting in the highest hardness (i.e., 5.2 GPa) for both DC540(50V) and RF270(50V) coatings; however, it must not be forgotten that the latter had very low Se/Mo ratio, which is not desirable.

It should be remarked that higher hardness values were achieved despite a much higher Se/Mo ratio (more contribution of the softer phase). Although the opposite trend was found in all works, i.e., the higher contribution of the softer phase reduces the hardness. The achieved results negate the claims of the literature [25,57], that ~50 at.% C is required for superior mechanical properties. The results also do not support the hypothesis of Mutafov et al. [50] which states that the presence of (002) planes parallel to the surface enhances the hardness, since the indenter applies load perpendicular to the parallel planes. If this was true, case 1 coatings should not show higher hardness than case 2 ones, since the latter presents higher crystallinity and higher (002) preferential orientation. We suggest that the high hardness is predominantly due to the higher compactness, the absence of columnar morphology, and the homogeneity of the coatings.

In both cases, the reduced elastic modulus followed similar trends as hardness, i.e., values increase for higher carbon contents. Parameters related to the elastic strain to failure H/E* [58] and fracture toughness H^3/E^{*2} [59] are shown in Figure 7. These values are often related to the elastic energy storage and the wear resistance of the materials, with higher values considered to be beneficial for the final tribological performance [60].
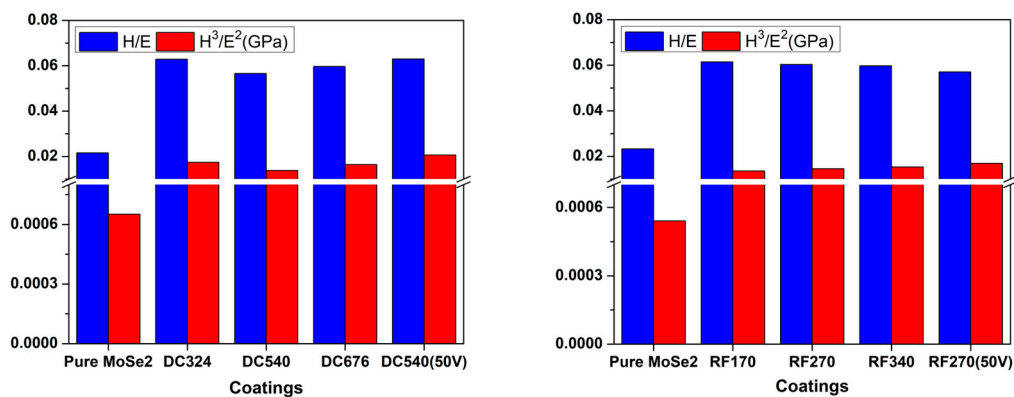
Figure 7. H/E* and H^3/E^{*2} of the coatings (case 1-left and case 2-right).

4. Conclusions

This study provides solutions to optimize the synthesis and properties of Mo–Se–C coatings. Magnetron sputtered Mo–Se–C solid lubricant coatings were deposited by using different combinations of DC and RF magnetron sputtering. Low carbon content (~18 at.% to ~25 at.%) resulted in stoichiometric coatings, i.e., Se/Mo close to 2. The carbon addition and the application of substrate bias resulted in a slight reduction of the Se/Mo ratio with the exception of substrate biased RF coating. Only in the case of $MoSe_2$ were differences in the morphology of DC and RF coatings achieved; with the addition of carbon and the application of substrate bias, both cases showed similar morphologies with a significant increase of the compactness and density. Unlike previous studies, and due to the continuous confocal sputtering, no columns or dendrites were observed in any of the Mo–Se–C coatings. Thus, this angled sputtering will be an interesting alternative to be explored for coating 3D parts. Also, differing from the literature, the (002) basal planes of $MoSe_2$ phase were observed in the XRD diffractograms, even after carbon additions. The addition of carbon increased the (002) interplanar distances, which are expected to decrease the Vander Waals forces and enhance the easy shearing properties of $MoSe_2$. HR-TEM images showed the presence of $MoSe_2$ nanocrystals, with a dimension lower than 10 nm, embedded in an amorphous phase. Raman analysis confirmed the presence of $MoSe_2$ crystalline material and detected an amorphous carbon phase. Mechanical properties of the coatings were enhanced after carbon additions due to the very high compactness to the coatings in the literature, despite the low carbon contents and high stoichiometry. In short, the results achieved with this deposition approach were much better than the literature and solved the issues of achieving a combination of low stoichiometry, high crystallinity, high hardness, and microstructure optimization for TMD-C solid lubricant coatings.

References

1. Stachowiak, G.; Batchelor, A.W. *Engineering Tribology*; Butterworth-Heinemann: Oxford, UK, 2013.
2. Aouadi, S.M.; Luster, B.; Kohli, P.; Muratore, C.; Voevodin, A.A. Progress in the development of adaptive nitride-based coatings for high temperature tribological applications. *Surf. Coat. Technol.* **2009**, *204*, 962–968. [CrossRef]
3. Bhushan, B. *Modern Tribology Handbook*; CRC Press: Boca Raton, FL, USA, 2001.
4. Jehn, H.A. Multicomponent and multiphase hard coatings for tribological applications. *Surf. Coat. Technol* **2000**, *131*, 433–440. [CrossRef]
5. Vepřek, S. The search for novel, superhard materials. *J. Vac. Sci. Technol. Vac. Surf. Film* **1999**, *17*, 2401–2420. [CrossRef]
6. Voevodin, A.A.; O'Neill, J.P.; Zabinski, J.S. WC/DLC/WS2 nanocomposite coatings for aerospace tribology. *Tribol. Lett.* **1999**, *6*, 75–78. [CrossRef]
7. Fernandes, F.; Yaqub, T.B. A Cavaleiro, Influence of Ag additions on the structure, mechanical properties and oxidation behaviour of Cr-O coatings deposited by HiPIMS. *Surf. Coat. Technol.* **2018**, *339*, 167–180. [CrossRef]
8. Renevier, N.M.U.; Hamphire, J.; Fox, V.C.; Witts, J.; Allen, T.; Teer, D.G. Advantages of using self-lubricating, hard, wear-resistant MoS_2 -based coatings. *Surf. Coat. Technol.* **2001**, *142*, 67–77. [CrossRef]

9.   Savan, A.; Simmonds, M.C.; Huang, Y.; Constable, C.P. Effects of temperature on the chemistry and tribology of co-sputtered MoSx-Ti composite thin films. *Thin Solid Films* **2007**, *489*, 137–144. [CrossRef]

10.   Scharf, T.W.; Rajendran, A.; Banerjee, R.; Sequeda, F. Growth, structure and friction behavior of titanium doped tungsten disulphide (Ti-WS2) nanocomposite thin films. *Thin Solid Films* **2009**, *517*, 5666–5675. [CrossRef]

11.   Chien, H.; Ma, K.; Vattikuti, S.V.P.; Kuo, C.; Huo, C.; Chao, C. Tribological behaviour of MoS 2/Au coatings. *Thin Solid Films* **2010**, *518*, 7532–7534. [CrossRef]

12.   Lince, J.R. Tribology of co-sputtered nanocomposite Au/MoS 2 solid lubricant films over a wide contact stress range. *Tribol. Lett.* **2004**, *17*, 419–428. [CrossRef]

13.   Wahl, K.J.; Dunn, D.N.; Singer, I.L. Wear behavior of Pb—Mo—S solid lubricating coatings. *Wear* **1999**, *230*, 175–183. [CrossRef]

14.   Ye, M.; Zhang, G.; Ba, Y.; Wang, T.; Wang, X.; Liu, Z. Microstructure and tribological properties of MoS 2 + Zr composite coatings in high humidity environment. *Appl. Surf. Sci.* **2016**, *367*, 140–146. [CrossRef]

15.   Deepthi, B.; Barshilia, H.C.; Rajam, K.S.; Konchady, M.S.; Pai, D.M.; Sankar, J.; Kvit, A.V. Structure, morphology and chemical composition of sputter deposited nanostructured Cr-WS2 solid lubricant coatings. *Surf. Coat. Technol.* **2010**, *205*, 565–574. [CrossRef]

16.   Rigato, V.; Maggioni, G.; Boscarino, D.; Sangaletti, L.; Depero, L.; Fox, V.C.; Teer, D.; Santini, C. A study of the structural and mechanical properties of Ti-MoS2coatings deposited by closed field unbalanced magnetron sputter ion plating. *Surf. Coat. Technol.* **1999**, *116*, 176–183. [CrossRef]

17.   Teer, D.G.; Hampshire, J.; Fox, V.; Bellido-Gonzalez, V. The tribological properties of MoS2/metal composite coatings deposited by closed field magnetron sputtering. *Surf. Coat. Technol.* **1997**, *94*, 572–577. [CrossRef]

18.   Voevodin, A.A.; O'Neill, J.P.; Zabinski, J.S. Nanocomposite tribological coatings for aerospace applications. *Surf. Coat. Technol.* **1999**, *116*, 36–45. [CrossRef]

19.   Polcar, T.; Cavaleiro, A. Self-adaptive low friction coatings based on transition metal dichalcogenides. *Thin Solid Films* **2011**, *519*, 4037–4044. [CrossRef]

20.   Polcar, T.; Cavaleiro, A. Review on self-lubricant transition metal dichalcogenide nanocomposite coatings alloyed with carbon. *Surf. Coat. Technol.* **2011**, *206*, 686–695. [CrossRef]

21.   Hudec, T.; Mikula, M.; Satrapinskyy, L.; Roch, T.; Truchlý, M.; Jr, P.Š.; Huminiuc, T.; Polcar, T. Structure, mechanical and tribological properties of Mo-S-N solid lubricant coatings. *Appl. Surf. Sci.* **2019**, *486*, 1–14. [CrossRef]

22.   Prasad, S.V.; McDevitt, N.T.; Zabinski, J.S. Tribology of tungsten disulfide-nanocrystalline zinc oxide adaptive lubricant films from ambient to 500 °C. *Wear* **2000**, *237*, 186–196. [CrossRef]

23.   Characterization of air-annealed, pulsed laser deposited ZnO-WS2 solid film lubricants bt transmission electron microscopy. *Thin Solid Films* **1997**, *305*, 130–143. [CrossRef]

24.   Voevodin, A.A.; Zabinski, J.S. Nanocomposite and nanostructured tribological materials for space applications. *Compos. Sci. Technol.* **2005**, *65*, 741–748. [CrossRef]

25.   Polcar, T.; Evaristo, M.; Cavaleiro, A. Comparative study of the tribological behavior of self-lubricating W-S-C and Mo-Se-C sputtered coatings. *Wear* **2009**, *266*, 388–392. [CrossRef]

26.   Voevodin, A.A.; Muratore, C.; Aouadi, S.M. Hard coatings with high temperature adaptive lubrication and contact thermal management: Review. *Surf. Coat. Technol.* **2014**, *257*, 247–265. [CrossRef]

27.   Hilton, M.R. Fracture in MoS2 solid lubricant films. *Surf. Coat. Technol.* **1994**, *68*, 407–415. [CrossRef]

28.   Wang, D.-Y.; Chang, C.-L.; Ho, W.-Y. Microstructure analysis of MoS2 deposited on diamond-like carbon films for wear improvement. *Surf. Coat. Technol.* **1999**, *111*, 123–127. [CrossRef]

29.   Cao, H.; de Hosson, J.T.M.; Pei, Y. Effect of carbon concentration and argon flow rate on the microstructure and triboperformance of magnetron sputtered WS2/a-C coatings. *Surf. Coat. Technol.* **2017**, *332*, 142–152. [CrossRef]

30.   Cao, H.; Wen, F.; Kumar, S.; Rudolf, P.; de Hosson, J.T.M.; Pei, Y. On the S/W stoichiometry and triboperformance of WSxC(H) coatings deposited by magnetron sputtering. *Surf. Coat. Technol.* **2018**, *365*, 41–51. [CrossRef]

31.   Gu, L.; Ke, P.; Zou, Y.; Li, X.; Wang, A. Amorphous self-lubricant MoS2-C sputtered coating with high hardness. *Appl. Surf. Sci.* **2015**, *331*, 66–71. [CrossRef]

32.   Cai, S.; Guo, P.; Liu, J.; Zhang, D.; Ke, P. Friction and Wear Mechanism of MoS 2 / C Composite Coatings Under Atmospheric Environment. *Tribol. Lett.* **2017**, *65*, 1–12. [CrossRef]

33. Xu, J.; Chai, L.; Qiao, L.; He, T.; Wang, P. Influence of C dopant on the structure, mechanical and tribological properties of rf-sputtered MoS2/aC composite films. *Appl. Surf. Sci.* **2016**, *364*, 249–256. [CrossRef]

34. Donnet, C.; Erdemir, A. Historical developments and new trends in tribological and solid lubricant coatings. *Surf. Coat. Technol.* **2004**, *181*, 76–84. [CrossRef]

35. Gustavsson, F.; Jacobson, S. Diverse mechanisms of friction induced self-organisation into a low-friction material—An overview of WS2tribofilm formation. *Tribol. Int.* **2016**, *101*, 340–347. [CrossRef]

36. Polcar, T.; Gustavsson, F.; Thersleff, T.; Jacobson, S.; Cavaleiro, A. Complex frictional analysis of self-lubricant W-S-C/Cr coating. *Faraday Discuss.* **2012**, *156*, 383. [CrossRef] [PubMed]

37. Bin, T.; Yaqub, T.; Vuchkov, M.; Evaristo, A. Cavaleiro, DCMS Mo-Se-C solid lubricant coatings—Synthesis, structural, mechanical and tribological property investigation. *Surf. Coat. Technol.* **2019**, *378*, 124992. [CrossRef]

38. Polcar, T.; Evaristo, M.; Stueber, M.; Cavaleiro, A. Synthesis and structural properties of Mo-Se-C sputtered coatings. *Surf. Coat. Technol.* **2008**, *202*, 2418–2422. [CrossRef]

39. Oliver, W.C.; Pharr, G.M. An improved technique for determining hardness and elastic modulus using load and displacement sensing indentation experiments. *J. Mater. Res.* **1992**, *7*, 1564–1583. [CrossRef]

40. Martin, P.M. *Handbook of Deposition Technologies for Films and Coatings: Science, Applications and Technology*; Elsevier Inc.: Oxford, UK, 2009.

41. Fominski, V.Y.; Nevolin, V.N.; Romanov, R.I.; Smurov, I. Ion-assisted deposition of MoSx films from laser-generated plume under pulsed electric field. *J. Appl. Phys.* **2001**, *89*, 1449–1457. [CrossRef]

42. Weise, G.; Mattern, N.; Hermann, H.; Teresiak, A.; Ba, I.; Bru, W. Preparation, structure and properties of MoSx films. *Thin Soli.* **1997**, *298*, 98–106. [CrossRef]

43. Grigoriev, S.N.; Fominski, V.Y.; Gnedovets, A.G.; Romanov, R.I. Experimental and numerical study of the chemical composition of WSex thin films obtained by pulsed laser deposition in vacuum and in a buffer gas atmosphere. *Appl. Surf. Sci.* **2012**, *258*, 7000–7007. [CrossRef]

44. Dominguez-Meister, S.; Justo, A.; Sanchez-Lopez, J.C. Synthesis and tribological properties of WSex films prepared by magnetron sputtering. *Mater. Chem. Phys.* **2013**, *142*, 186–194. [CrossRef]

45. Betz, G.; Wehner, G.K. Sputtering of Multicomponent Materials. In *Sputtering by Particle Bombardment II*; Springer: Berlin/Heidelberg, Germany, 1983; pp. 11–90. [CrossRef]

46. Swann, S. Magnetron sputtering. *Phys. Technol.* **1988**, *19*, 67–75. [CrossRef]

47. Tan, S.; Zhang, X.; Wu, X.; Fang, F.; Jiang, J. Comparison of chromium nitride coatings deposited by DC and RF magnetron sputtering. *Thin Solid Films* **2011**, *519*, 2116–2120. [CrossRef]

48. Kelly, P.J.; Arnell, R.D. Magnetron sputtering: A review of recent developments and applications. *Vacuum* **2000**, *56*, 159–172. [CrossRef]

49. Muratore, C.; Voevodin, A.A. Control of molybdenum disulfide basal plane orientation during coating growth in pulsed magnetron sputtering discharges. *Thin Solid Films* **2009**, *517*, 5605–5610. [CrossRef]

50. Mutafov, P.; Evaristo, M.; Cavaleiro, A.; Polcar, T. Structure, mechanical and tribological properties of self-lubricant W-S-N coatings. *Surf. Coat. Technol.* **2015**, *261*, 7–14. [CrossRef]

51. Rasamani, K.D.; Alimohammadi, F.; Sun, Y. Interlayer-expanded MoS 2. *Mater. Today* **2017**, *20*, 83–91. [CrossRef]

52. Panigrahi, P.K.; Pathak, A. Aqueous Medium Synthesis Route for Randomly Stacked Molybdenum Disulfide. *J. Nanoparticles.* **2013**, *23*, 1–10. [CrossRef]

53. Tonndorf, P.; Schmidt, R.; Böttger, P.; Zhang, X.; Börner, J.; Liebig, A.; Albrecht, M.; Kloc, C.; Gordan, O.; Zahn, D.R.T.; et al. Photoluminescence emission and Raman response of monolayer MoS2, MoSe2, and WSe2. *Opt. Express* **2017**, *21*, 4908–4916. [CrossRef]

54. Gustavsson, F.; Jacobson, S.; Cavaleiro, A.; Polcar, T. Frictional behavior of self-adaptive nanostructural Mo-Se-C coatings in different sliding conditions. *Wear.* **2013**, *303*, 286–296. [CrossRef]

55. Sekine, T.; Izumi, M.; Nakashizu, T.; Uchinokura, K.; Matsuura, E. Raman scattering and infrared reflectance in 2H-MoSe2. *J. Phys. Soc. Jpn.* **1980**, *49*, 1069–1077. [CrossRef]

56. Ferrari, A.C.; Robertson, J. Interpretation of Raman spectra of disordered and amorphous carbon. *Phys. Rev. B.* **2000**, *61*, 95–107. [CrossRef]

57. Polcar, T.; Evaristo, M.; Cavaleiro, A. The tribological behavior of W-S-C films in pin-on-disk testing at elevated temperature. *Vacuum* **2007**, *81*, 1439–1442. [CrossRef]

58. Leyland, A.; Matthews, A. On the significance of the H/E ratio in wear control: A nanocomposite coating approach to optimised tribological behaviour. *Wear* **2000**, *246*, 1–11. [CrossRef]

59. Musil, J.; Kunc, F.; Zeman, H.; Poláková, H. Relationships between hardness, Young's modulus and elastic recovery in hard nanocomposite coatings. *Surf. Coat. Technol.* **2002**, *154*, 304–313. [CrossRef]

60. Charitidis, C.A.; Logothetidis, S. Effects of normal load on nanotribological properties of sputtered carbon nitride films. *Diam. Relat. Mater.* **2005**, *14*, 98–108. [CrossRef]

Annex C

T. Bin Yaqub, S. Bruyere, J. François Pierson, T. Vuchkov, A. Cavaleiro, *Insights into the wear track evolution with sliding cycles of carbon-alloyed transition metal dichalcogenide coatings*. **Surf Coat Technol 2020;403:126360.**

Insights into the wear track evolution with sliding cycles of carbon-alloyed transition metal dichalcogenide coatings

Talha Bin Yaqub[a,b,*], Stéphanie Bruyere[c], Jean-François Pierson[c], Todor Vuchkov[a,b], Albano Cavaleiro[a,b]

[a] IPN - Instituto Pedro Nunes, LED & MAT - Laboratory of Tests, Wear and Materials, Rua Pedro Nunes, 3030-199 Coimbra, Portugal
[b] SEG-CEMMPRE, Department of Mechanical Engineering, University of Coimbra, Rua Luís Reis Santos, 3030-788 Coimbra, Portugal
[c] Institut Jean Lamour (UMR CNRS 7198), Université de Lorraine, 2 allée André Guinier, Campus Artem BP50840, 54011 Nancy, France

ABSTRACT

This study is aimed towards a better understanding of the tribological performance of the optimized Mo-Se-C dry lubricant coatings. The coatings are deposited with a lower carbon content (< 30 at. %), as compared to the literature. The detailed analysis of the wear track and the tribolayer evolution as a function of the C content and the number of sliding cycles is discussed, using Raman spectroscopy, scanning electron microscopy (SEM) and high-resolution transmission electron microscopy (HRTEM) analyses. The coatings are highly compact, homogeneous, with (002) basal planes parallel to the surface as observed by X-ray diffraction (XRD) studies. In unidirectional tests, under ambient conditions, the friction coefficient and the specific wear rate decrease with the number of sliding cycles. After 25,000 cycles, the wear tracks are not fully covered with $MoSe_2$ tribolayer, instead displayed zones of the tribolayer as well as the as-deposited coating. After 100,000 cycles, the wear track is covered by a thick $MoSe_2$ tribolayer. Scanning-TEM (STEM) chemical composition mapping also confirms that $MoSe_2$ tribolayer is dominating during sliding in ambient air. Reciprocating sliding tests are also performed in ambient air, dry N_2, and at 200 °C. The transition metal dichalcogenide (TMD) phase is always governing the low friction, with coatings not showing the chameleon behavior claimed in the literature for C-containing TMD coatings.

1. Introduction

Solid lubricant coatings are under research for the past few decades. They are potential candidates for applications involving aerospace, tool manufacturing and automotive industries [1–4]. Transition metal dichalcogenides (TMD) lie among the most developed classes of solid lubricant coatings [5]. TMDs in their pure sputtered form are porous, with columnar cross-section morphology that makes them very soft. This causes very low load-bearing capacities and low adhesion to the substrate, leading to poor tribological properties. One other major drawback of pure sputtered TMDs is their low resistance to moisture and oxidation. The dangling bonds in TMDs can react with moisture and increase the interlamellar interactions, thus affecting the low frictional properties [6]. These issues of pure TMD coatings can be solved by doping/combining with other elements that can either react with TMDs to form metal compounds or support them by forming nanocomposite coatings. The most common doping elements include metals e.g. Ti, Au, Pb, Zr and Cr [7–11] or non-metals e.g. C and N [12–16].

Among these elements, carbon is considered one of the most promising elements for achieving stable nanocomposite TMD coatings intended for low friction applications in diverse environments.

Voevodin et al. [17] were among the first researchers to introduce TMD-C nanocomposite coating consisting of WS₂/WC/DLC. According to the authors, carbon was governing the frictional properties when sliding in ambient air and WS₂ was playing a dominant role in the vacuum and the dry conditions, which was called at that moment as a "chameleon behavior". Following their works, many other researchers published works on TMD-C coatings [6,18–20]. In some cases, the results contradicted the findings of Voevodin et al. [17] and it was claimed that whether it is dry, vacuum or ambient atmosphere, TMD phases were playing the main role in easy shear tribological properties [6,21,22]. This will be discussed in this work for Mo-Se-C coatings. The usage of $MoSe_2$ as a TMD phase in nanocomposite coatings is rarer, as compared to MoS_2 or WS_2. The interest for the Mo-Se-C system relies on the scarce literature available, which shows that the $MoSe_2$ phase is less sensitive to humidity [23]. An additional advantage of the $MoSe_2$ is the

---

smaller difference in the atomic mass of the chemical elements of the compound when compared to, e.g. WS_2 [24]. This is important for the synthesis of the coatings by magnetron sputtering as the scattering behavior of the species will be more similar. Moreover, the preferential re-sputtering of the chalcogen atom due to the bombardment of the growing film with energetic species will be attenuated. In this context, the Se/Mo ratio, which is very important for TMD containing films, can be more easily controlled. Also, in our recent work [25], we reported the optimization of the compositional, morphological, structural and mechanical properties of Mo-Se-C coatings as compared to either other TMD-C systems or previous works on these coatings. This study is mainly focused on the ambient air tribological performance of the optimized coatings.

Most of the literature studies only deal with short duration tests which are not the best indication of the long-term performance [26–31]. Also, in the literature, the changes in the coefficient of friction (COF) with the number of sliding cycles have been reported without a very precise explanation [21,32]. Likewise, the literature on TMD-C coatings lacks the TEM investigation of the (evolution of) wear tracks achieved after different number of sliding cycles in ambient air. Based on the shortcomings of literature, in this work: i) the tribological performance has been tested at different sets of sliding cycles (5000, 25,000 and 100,000 cycles) to analyze the difference between the running-in and the steady-state stages during the tribological test. This will also unfold the ability of the coatings for long-duration sliding / long-term applicability. ii) Another important domain of focus is the exploration of the role of sliding cycles on the evolution of the wear track composition and the mechanism behind the wear track coverage by tribolayer. The study of the wear tracks composition and tribolayer evolution using SEM, Raman spectroscopy and HRTEM will reveal the science behind the decrease of the COF with an increasing number of sliding cycles as well as the mechanism of tribolayer formation. iii) Finally, the sliding performance of the coatings in diverse environments has been studied to reveal whether the Mo-Se-C coatings display or not, a chameleon character.

2. Experimental procedure

The coatings were deposited using four cathodes mounted at an angle of 30° to the substrate normal to converge the sputtered species on to the rotating substrate holder (rpm ~ 10) in balanced magnetron sputtering unit, ATC-Orion 8 (from AJA INTERNATIONAL, US). DC power supplies were connected to two carbon targets (99.99%) and one $MoSe_2$ target (99.99%) while the fourth target was supplied by RF power and was connected to Cr (99.99%). Polished (111) Si, M2 steel (Ø50 × 3 mm) and AISI 52100 steel (Ø25 × 7 mm) were used as substrates. The total deposition time was adjusted to obtain a final coating thickness in the range from 2 to 2.5 μm. Only the power applied to carbon targets was varied to have variations in chemical composition. The detailed deposition procedure can be found in Ref. [25] — only for coatings deposited by case 1. Selected coatings (pure MoSe2, 324C, 540C and 540C(50V)) deposited by direct current magnetron sputtering (DCMS) from Ref. [25] were tested. For simplicity, the coatings names were changed: Pure $MoSe_2$ as C1, 324C as C2, 540C as C3 and 540(50V) as C4. Only C4 was deposited with an RF substrate bias voltage of -50V.

The chemical composition of the coatings was determined using wavelength dispersive spectroscopy-WDS (Oxford Instruments). Surface morphologies, fractured cross-section morphologies and thicknesses of the coatings were assessed with a field emission scanning electron microscopy (SEM-Zeiss Merlin). Grazing incidence (3°) mode utilizing copper $K_{\alpha1}$ (λ = 1.5406 Å) radiation was used to access the crystal structure of the coatings (X'Pert Pro MPD diffractometer).

Unidirectional tribological tests were performed using a home-built pin on the disk tribometer. Three different sets of tribological tests with varying number of sliding cycles (5000, 25,000 and 100,000) were performed in ambient air. A 100Cr6 steel ball with a 10 mm diameter

was used as the counter body. Tests were performed at room temperature in relative humidity of 35–45 %. A load of 10 N was used, resulting in an initial maximum Hertzian contact stress of ~1.03 GPa. Experiments were repeated three times (except 100,000 cycle tests, where two repetitions were performed). The wear track profiles of the coatings were taken using stylus profilometer (Surftest SJ-500) and then specific wear rates were calculated. To calculate the specific wear rates of the counter body, the wear profiles were obtained using a 3D optical profilometer (Alicona Infinite Focus). All coating's wear tracks and counter body wear scar imaging was done using optical microscopy (DM4000 M LED). Wear tracks of selected coating samples were analyzed in SEM. Elemental mapping of the wear track was also carried out using energy dispersive spectroscopy (EDS). Raman spectroscopy (LabRam HR Horiba Jobin Yvon) of the wear tracks was performed using 488 nm Ar laser. For the high-resolution transition electron microscopy (HRTEM) analysis of the wear track in cross-sections (to access the sliding contact interface), lamellae were prepared by a focused ion beam (SEM-FIB, Helios Nanolab 600i) using Ga^+ ions. To protect the surface from damage during ion etching, a protective layer of Pt and C was first deposited. Ion beam energy was varied from 3 kV to 30 kV for thinning various regions but in the end, the energy of 1 kV was used to minimize the sample damage. For HRTEM imaging and scanning TEM (STEM) EDS mapping, JEOL ARM 200F (cold field emission gun) was used. Beam size in STEM mode was less than 1 nm.

To analyze the sliding behavior in dry N_2 and at 200 °C, reciprocating sliding tests (Optimal SRV friction and wear equipment) on selected specimens were performed in ambient air (relative humidity ~35–45 %), dry nitrogen (relative humidity less than 5%) and at high temperatures (200 °C). The tests were carried out for 25,000 cycles under 10 N applied load (maximum Hertzian contact stress ~1.03 GPa) and 10 mm 100Cr6 steel ball as the counter body. Wear track images that were observed in SEM. The wear profiles of the coatings and counter body were taken using a 3D optical profilometer (Alicona Infinite Focus), and later the specific wear rates were calculated.

3. Results and discussion

3.1. Main characteristics of the deposited coatings

The chemical composition in Fig. 1d) shows that the Se/Mo ratio was almost stoichiometric (Se/Mo ~ 2). Se/Mo ratio decreases linearly with increasing the carbon content in the coatings, unlike RF sputtering of Mo-Se-C from a composite target [33]. Substrate bias further decreased the Se/Mo ratio due to the enhanced re-sputtering of the chalcogen atoms from the growing coating. The reported maximum achieved values of Se/Mo, for Mo-Se-C coatings, are not more than 1.88 for DC magnetron sputtering [20]. So, this deposition approach resulted in coatings having a relatively high Se/Mo ratio. The columnar and porous cross-sections and surface morphologies of the pure coating (Fig. 1a) became very compact with either the addition of carbon (C3 coating — Fig. 1b) or the application of substrate bias (Fig. 1c). No columns or porosity were observed even for the lowest carbon content coating. The XRD diffractogram of pure $MoSe_2$ coating displayed peaks almost similar to the typical sputtered TMDs (Fig. 1e). The well-defined XRD peaks at ~30–45° in pure coating were replaced by broad amorphous peaks after carbon additions. Unlike other TMD-C coatings and also previous studies on Mo-Se-C coatings, the (002) peaks were still observed. The small shift of (002) peak position to lower angles is related to the increase in the interplanar distances of basal planes due to carbon entrapment/incorporation in the lattice, as explained in [34]. This further reduces the van der Waals forces of attraction. Anticipating the achieved landmarks, such as the improved Se/Mo ratios, higher compactness and non-columnar morphology, despite the higher $MoSe_2$ content than the ones found in the literature [6], the existence of (002) planes, closely parallel to the surface, and the increase in d-spacing can facilitate the sliding of $MoSe_2$ crystals with an increased tribological
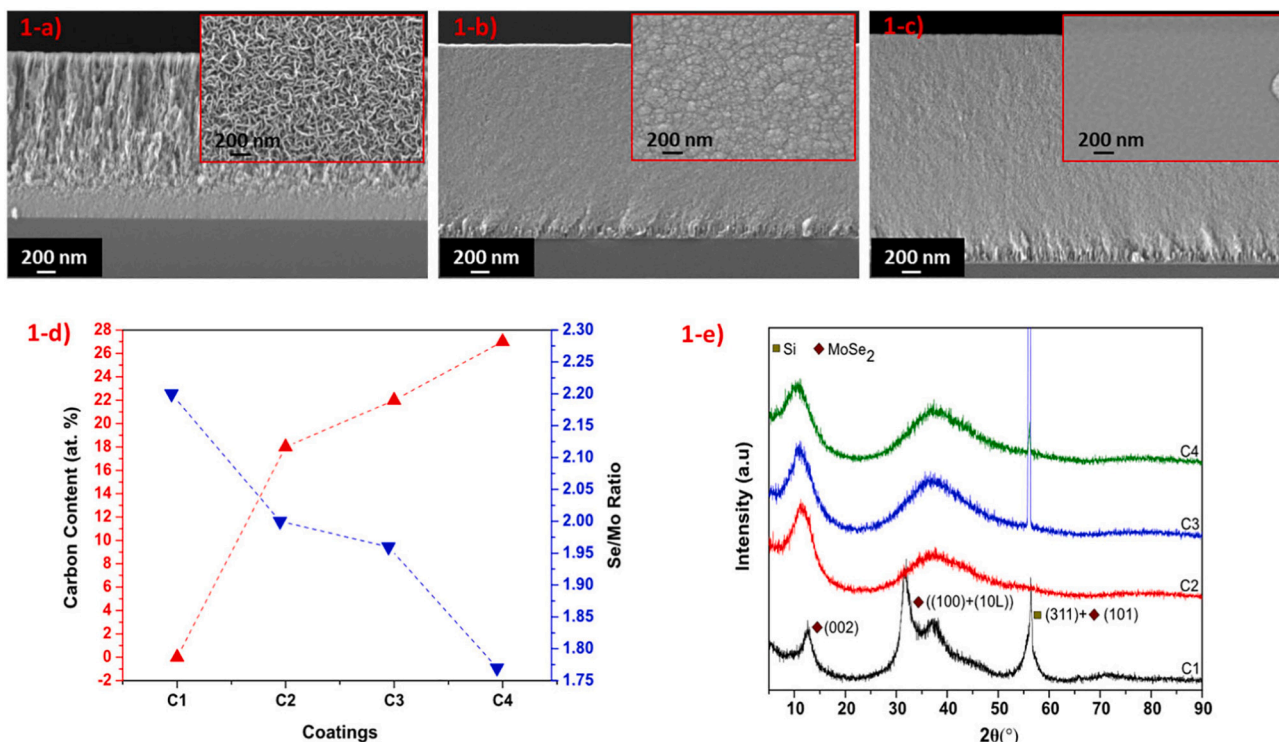
Fig. 1. SEM cross-section and surface morphology (inset) micrographs (a) C1 (Pure MoSe$_2$), (b) C2(18%C), (c) C4 (27%C, 50 V bias), (d) Carbon content vs. Se/Mo ratios and (e) X-ray diffraction patterns of the coatings.

performance. Therefore, much lower COF than the literature is expected. A more detailed analysis of the main characterization of these coatings can be found in case 1 of Ref. [25].

3.2. Tribological analysis

3.2.1. Ambient air unidirectional tests
3.2.1.1. Short duration tests. For the tests performed for 5000 cycles, the pure coating (C1) failed after a few hundred cycles with extensive delamination, probably due to its low load-bearing capacity attributed to the columnar and porous morphology [6]. For all other coatings, a progressive increase in the COF was observed with increasing C content (Fig. 2), from an average value (value taken from the whole test) of 0.025 for the lowest C content coating (C2), up to 0.064 for C4 coating

Fig. 2. Unidirectional sliding COF results of all coatings at different cycles.

deposited with the application of substrate bias. In the latter two coatings (C3 and C4), the steady-state region was not reached until the end of this test. The increase in the running-in period with C content can be explained by the increased difficulty in forming the tribolayer which will be responsible for the low friction, as it will be shown and discussed later. The higher mechanical strength of the coatings (increase of the hardness), due to either the higher content of the C-phase or the increase in the density and compactness of the coatings, makes tribolayer formation process more difficult. Moreover, as the low friction tribolayer is mainly composed of (002) aligned MoSe$_2$ crystals, the lower amount of this phase, with increasing C content, enlarges the running-in period. The mechanical strength seems also directly related to the specific wear rates (Fig. 3). The C2 coating displayed much higher values than the C3 and C4 coatings, due to excess of softer MoSe$_2$ phase and lower hardness. The soft phase could not resist the rapid material removal during the initial stages of sliding processes and, therefore, some delaminated regions were also observed in this coating (Fig. 4b). The other coatings resisted the wear efficiently due to their high compactness and hardness. Furthermore, they also have higher Young's modulus (C3 = 75 GPa, C4 = 82 GPa). A combination of high hardness and high Young's modulus contributes to wear resistance, thus, increasing the running-in period and tribolayer formation cycles/ duration.

Specific wear rates of the counter bodies were very low, more than two orders of magnitude lower than those from the disk (Fig. 3). No detectable wear was observed on C2 coating as its lower hardness gives rise to a lot of material transfer to the counter body from the beginning of the test, protecting it from wear. The counter bodies tested against the other coatings displayed minor specific wear rates.

3.2.1.2. Medium duration tests. By increasing the testing cycles from 5000 to 25,000 the running-in period was overcome and all coatings reached the steady-state sliding condition with the formation of tribolayers which were easily detected in the wear tracks (Fig. 4). As it would be expected, the lowest C content coating (C2) displayed minor
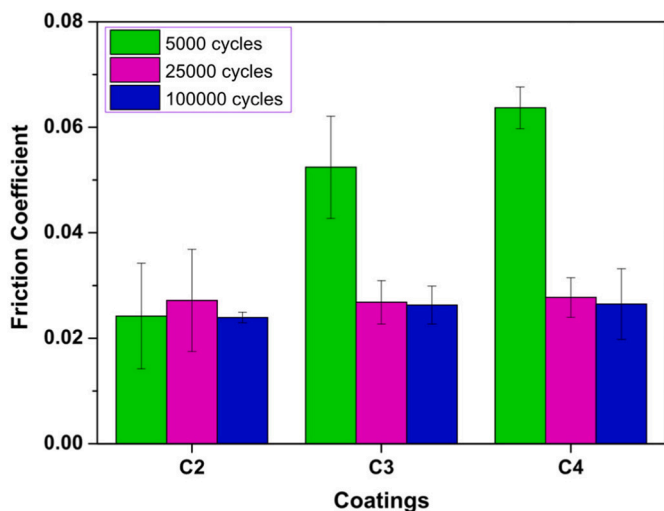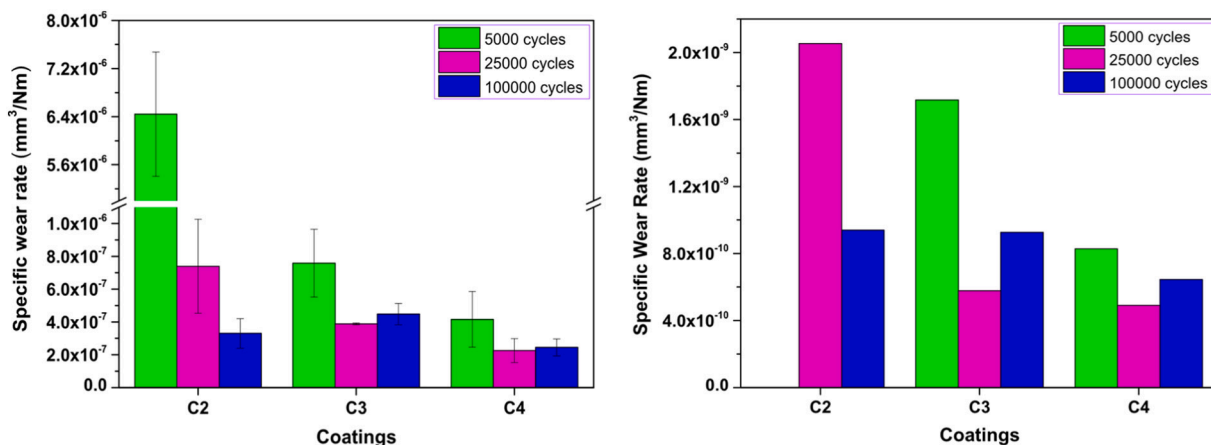
Fig. 3. Specific wear rates of the disk/coatings (left) and counter bodies (right) at different sliding cycles.

changes in COF, since the tribolayer formation had already achieved; the steady-state average value was ~0.028. For the C3 and C4 coatings, the steady-state was reached with an average COF of ~0.026 and ~0.027, respectively. Such behavior suggests that, for these coatings, the low friction tribolayer was also formed.

All coatings displayed a decrease in the wear rate. The decrease was more substantial for the low C coating, attributed to the much higher wear during the running-in period. It is important to remark that C2 coating showed less zones of delamination in this test (Fig. 4d), suggesting that replenishing of those zones occurred with the wear debris created in the sliding contact and transfer layer on the counter body.

For the test with 25,000 cycles, wear was then observed for C2 coating's counter body (Fig. 3). The irregularities created by the delamination acted as abrasive features for the ball, thus, increasing the wear of the counter body. Specific wear rates of the other counter bodies decreased since the coatings were sliding in the steady-state condition under the influence of the tribolayer, which protects both elements of the sliding pair from wear. C4 coating and its counter body outperformed the rest in terms of COF and specific wear rates in this test.

3.2.1.3. Long duration tests. As the sliding cycles were increased to 100,000, stable friction curves were obtained despite minor worn-through zones observable in some wear tracks. As per Fig. 3, all coatings showed similar COF values, suggesting that the sliding mechanism is similar in all of them. When the specific wear rates were calculated for both the balls and the disks (Fig. 3), no significant differences in the values were found among the tested samples. C4 film showed a slightly smaller value, particularly due to its slightly better mechanical strength. These lower values were achieved because either the tribolayer in the wear track or the protective transferred layer to the ball supports the sliding in the steady-state region, avoiding material removal.

After considering COF and specific wear rates of the coatings and the counter bodies in all tests, C4 displayed superior results.

3.2.1.4. Wear track and counter body analysis. Although with some minor differences, the overall tribological behavior of all C-containing coatings is very similar. Therefore, a detailed analysis of the wear tracks was performed just in one of them. Since C4 coating was the one presenting the best combination of high hardness, low friction and high
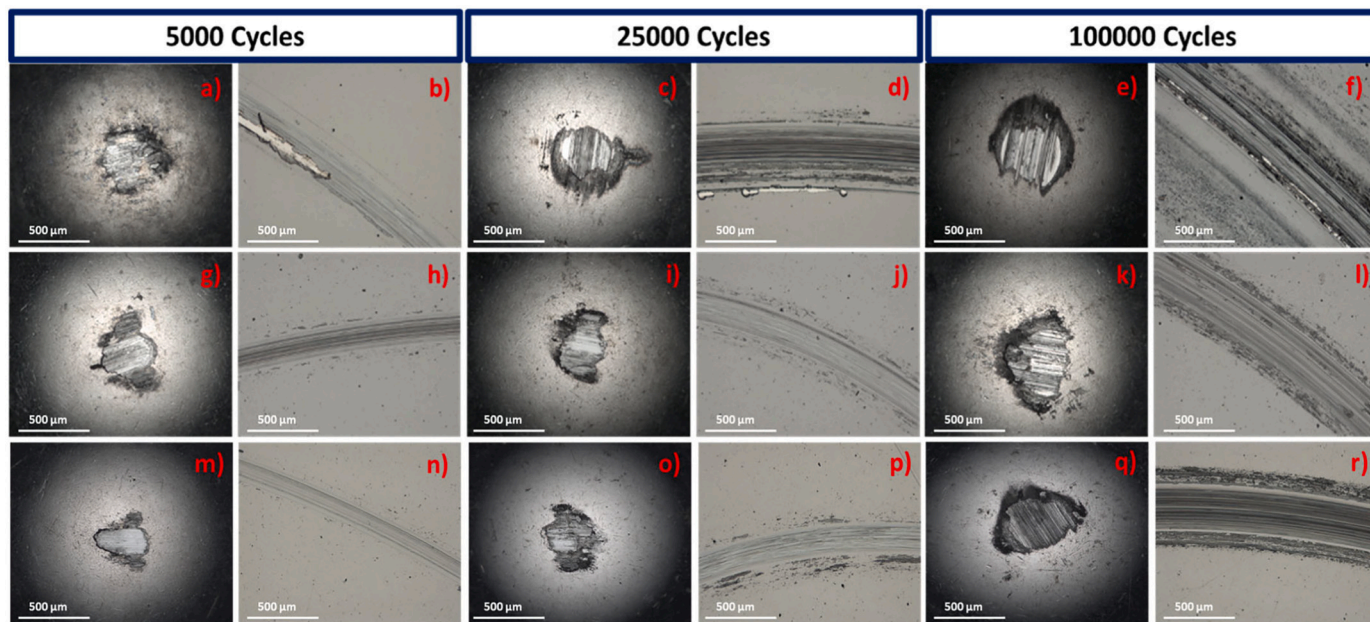

Fig. 4. Optical microscopy images of the wear tracks and counter bodies after 5000 cycles: a) and b)—C2 coating, g) and h)—C3 coating, m) and n)—C4 coating; 25,000 cycles: c) and d)—C2 coating, i) and j)—C3 coating, o) and p)—C4 coating; 100,000 cycles: e) and f)—C2 coating, k) and l)—C3 coating, q) and r)—C4 coating.
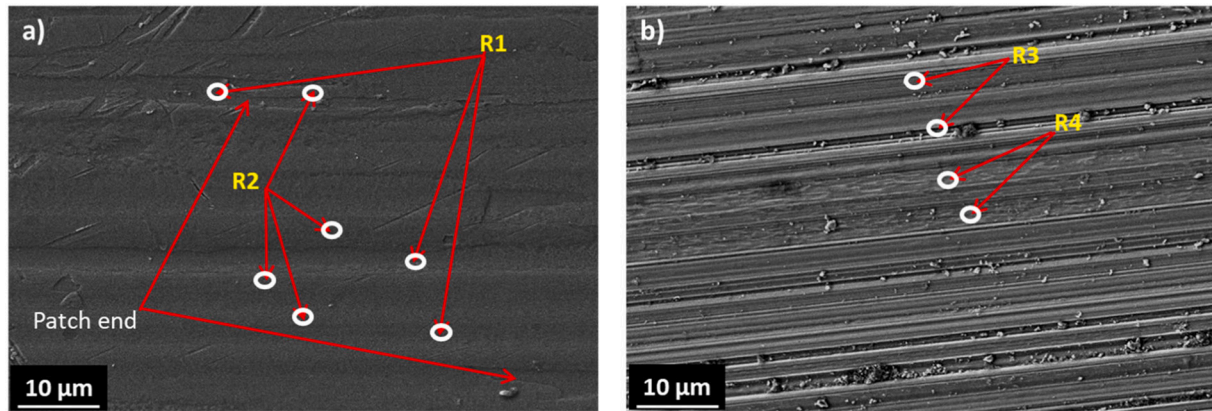
Fig. 5. SEM micrographs of the wear tracks of C4 coating: a) 25,000 cycles and b) 100,000 cycles.

wear resistance for both the coating and the counter body, it was selected for the analysis. The wear tracks were first observed in SEM (Fig. 5). After 5000 cycle test, wear tracks were quite smooth, with very small regions comprising of thin patches. Increasing cycles to 25,000 resulted in broad patchy regions separated by valleys. For the 100,000 cycles test, almost the whole of the track was covered with patches with very minor valleys in between.

Raman analysis (Fig. 6) of the regions highlighted in Fig. 5, confirmed this trend with the wear tracks having regions corresponding to tribolayer of $MoSe_2$ (R2) and as-deposited regions (R1) after 25,000 cycles while completely covered $MoSe_2$ transformed layer after 100,000 cycles (R3 and R4). Despite topographical features on the wear track surface due to sliding, no vestiges of as-deposited regions or patches without $MoSe_2$ tribolayer were detected after 100,000 cycles. Raman spectroscopy showed the presence of crystalline $MoSe_2$ and also a high contribution of Mo-oxides in the wear debris. Major Mo-oxide peaks lie between 600 and 1000 cm^{-1} while small quantities might also be present at ~289 cm^{-1} along with crystalline MoSe2 [20,35,36]. Moreover, a high contribution of C was detected in wear debris as compared to R2, R3 and R4 regions (Fig. 6b). The observed decrease of COF with an increasing number of sliding cycles can be understood by the progressively increased presence of TMD tribolayers, as observed by SEM and Raman analysis.

Additionally, elemental mapping for the highest duration test wear track (of C4 coating), i.e. after 100,000 cycles, is shown in Fig. 7. This picture is representative of all of the wear track. Except for some dispersed wear debris containing high contents of C or O, the wear track surface was quite uniform. No significant signal related to Fe and Cr

was observed, confirming that the coating is still present, without worn through areas.

To confirm the formation and importance of the tribolayer, FIB lamellas were prepared from the wear tracks in cross-section and, then, analyzed by transmission electron microscopy. The cross-sections were cut perpendicular to the sliding direction. Only one selected HRTEM image, representative of most of the wear track after 25,000 cycles and 100,000 cycles test (each), is shown in Fig. 8. The observation revealed lattice fringes with the distance between them of ~0.64 nm. This is the distance between the basal (002) planes in $MoSe_2$. The $MoSe_2$ crystals are well aligned with the sliding direction. The average interplanar distance calculated from various regions was ~0.64 nm, agreeing well with (002) $MoSe_2$ basal planes. So, TEM analysis of wear tracks also confirmed that $MoSe_2$ tribolayers are the reason behind the low COF achieved. After 25,000 cycles test, the tribolayer was patchy i.e., showed both as-deposited and oriented material zones (Fig. 8a) and not covering the whole wear track. Regions resembling as-deposited coatings, without tribolayer were evident (Fig. 8b). On the other hand, the tribolayer after 100,000 cycles test (Fig. 8c) was thicker than for 25,000 cycles and covered the whole wear track, without any vestiges of as-deposited regions. TEM results agreed well with SEM and Raman observations.

Another important remark which showed that the tribolayer is mainly formed by a well-crystallized $MoSe_2$ phase is the higher Se/Mo ratio in the tribolayer. Fig. 9 shows the STEM-EDS elemental maps from a lamella of the wear track cross-section. The edge of the arrowhead in the bright field images shows the start of the tribolayer. Clearly, an increase of the Se/Mo ratio in the tribofilm can be observed from the
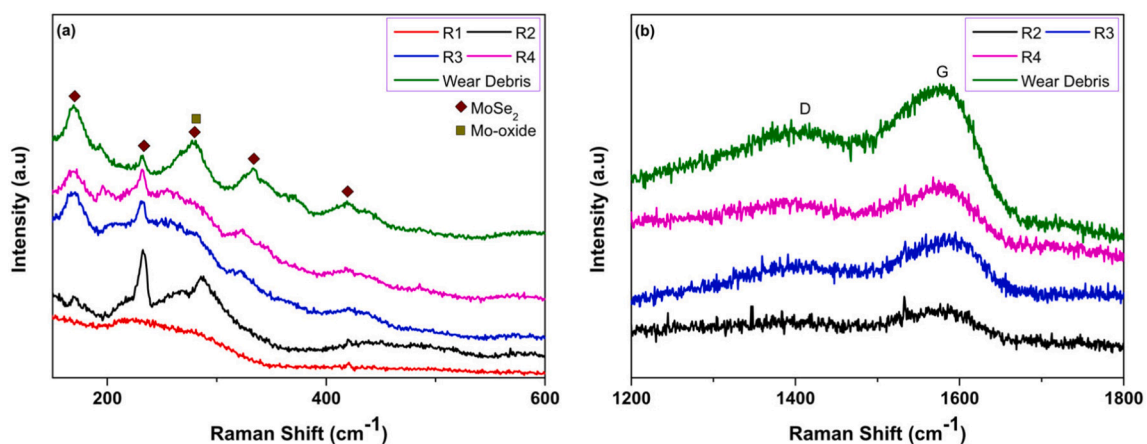

Fig. 6. Raman spectra showing (a) MoSe2 peaks and (b) C peaks obtained from different regions of C4 coating wear tracks and wear debris — the regions are highlighted in Fig. 5.
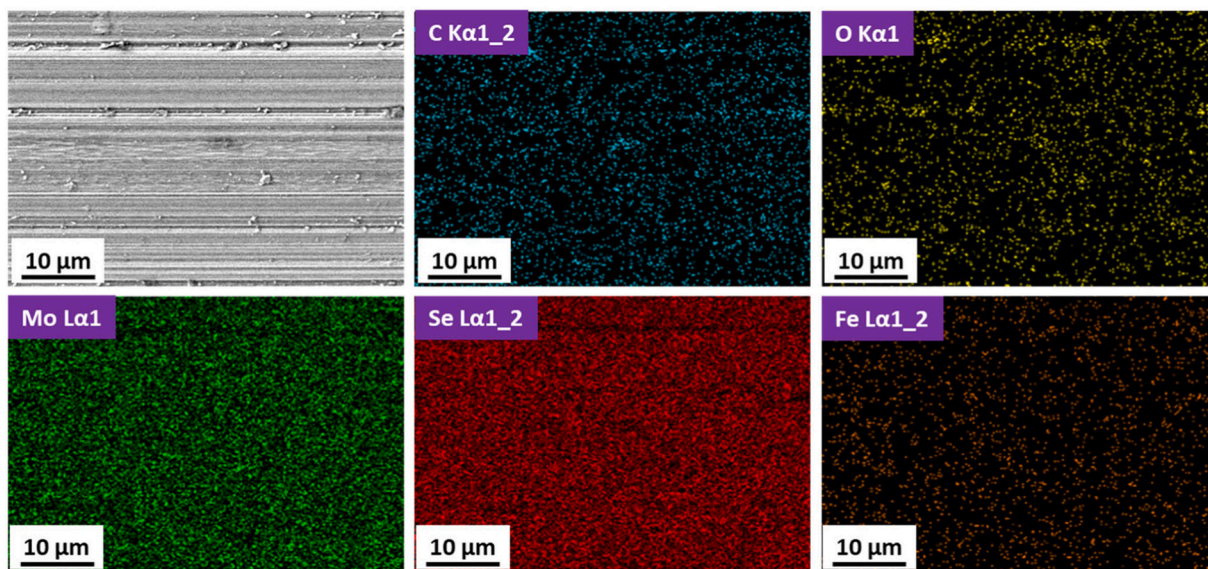
Fig. 7. EDS elemental maps for C4 coating's wear track after 100,000 cycles test.

map. Besides, a compositional analysis using EDS was also performed in both zones (as-deposited and tribolayer): the tribolayer presented composition closer to the stoichiometry of $MoSe_2$ (Se/Mo = ~2 in tribofilm vs. ~1.8 inside the coating), showing that the tribolayer was mainly composed of this phase.

After comparing with the literature, it can be said that the achieved values are superior to those of other TMD-C coatings (tested in ambient air) with respect to COF, specific wear rates, and sliding cycles. For instance, literature reports that under $10\,N$ applied load, COF ~ 0.15 and specific wear rate of ~10^{-6} have been achieved for W−S−C coatings tested under 50% relative humidity [37]. Polcar et al. [6] reported sliding results of W−S−C, W−Se−C, Mo−S−C and Mo-Se-C coatings (under $10\,N$ applied load): the COF was ~0.07 for W−Se−C and Mo−S−C while W−S−C and Mo-Se-C coating systems showed ~0.1. Moreover, COF of 0.12 and 0.08 have been reported, at 35–40 % relative humidity, for Mo-Se-C coatings with 29 at.% C and 68 at.% C, respectively [33]. In another study [35], a Mo-Se-C coating with 47 at. % C displayed ~0.1 COF and ~$2.5 \times 10^{-6}\,mm^3$/Nm specific wear rate, under $10\,N$ load at 55% relative humidity. The values decreased to ~0.05 COF and ~$2 \times 10^{-7}\,mm^3$/Nm specific wear rate when the C content was increased to 61 at.%. In these studies, the trend was to use higher C contents to increase the compactness and the hardness of the coatings to achieve sufficient environmental resistance for improved tribological properties. In this study, we have found COF lower than 0.03 for coatings with only 18 at.% of C. So, it has been concluded that

if the deposition procedure is properly optimized: higher Se/Mo ratio, compactness, hardness, lower COF and specific wear rate than literature, can be achieved, despite a maximum C content of ~27 at.% as compared to 50 at.% (advised by literature) [6]. It is even expected that the deposited coatings, especially C4 coating, might run for much longer durations than tested.

In short, these unidirectional tribological tests and in-depth wear track studies are a big advancement towards clarifying ambiguities about ambient air tribological performance of less explored C-alloyed $MoSe_2$ coatings and also the role of C and $MoSe_2$ in the tribological behavior. It is expected that the excellent ambient air stability will open new domains for the research and implementation of $MoSe_2$ coatings in industries as a replacement of other TMDs which show considerably high friction and wear in ambient conditions [6,19,30].

3.2.2. Diverse environment reciprocating tests

The tribological analysis was further extended by testing the performance of C3 (no substrate bias) and C4 (biased) coatings in different environments. These coatings were shortlisted owing to their excellent performance in unidirectional pin on disk tests. Reciprocating sliding tests in ambient air (relative humidity ~35–45 %), dry nitrogen (relative humidity < 5 %) and high temperature (200 °C, ambient air) were performed for 25,000 cycles. The reciprocating tests were selected as an alternative to the unidirectional pin on disk since this equipment was not able to provide a controlled environment. The standard
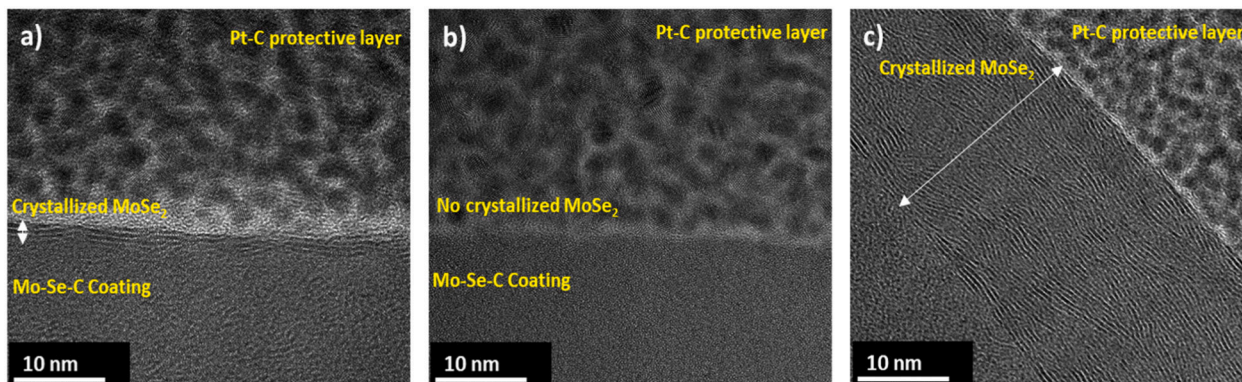

Fig. 8. TEM micrographs of the C4 coating's wear tracks after sliding tests: a) 25,000 cycles with tribolayer b) 25,000 cycles with no indication of tribolayer and c) 100,000 cycles.
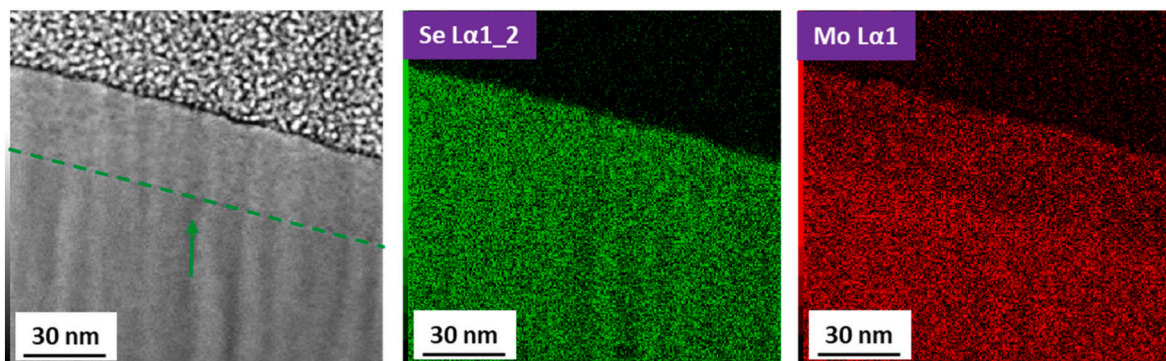
Fig. 9. STEM-EDS elemental maps of wear track after 100,000 cycles test.
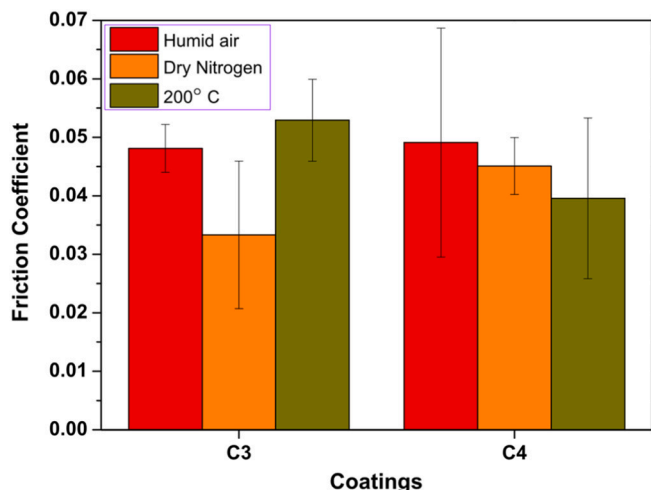

Fig. 10. Reciprocating sliding COF values of C3 and C4 coatings in diverse environments.

ambient air tests were repeated for a better comparison between results. The COF and the specific wear rates in all three environments are shown in Figs. 10 and 11, respectively.

For ambient air sliding, the steady-state COF was ~0.05 for both C3 and C4 coatings, with wear tracks showing minor delaminated areas. Based on the EDS mapping, the coatings delaminated in the interface between the Cr interlayer and the coating since an increased Cr signal was observed in the delaminated zones (Fig. 12). Relating to the reasons previously discussed, a lower hardness can be associated with the higher wear rate. It is confirmed in Fig. 11 where C3 coating shows a higher wear rate compared to the C4 coating due to its low hardness.

On the other hand, this difference in the hardness of both coatings is reflected in the wear rate of the counter body which, when sliding against the C3 coating, showed less wear compared to the one sliding against the C4 coating. Overall, the observed trends of COF and specific wear rates of reciprocating sliding tests were similar to the unidirectional sliding tests. The slightly higher measured values can be explained as the SRV device calculates a cycle average COF taking into consideration the higher friction during stroke reversal [38].

Predictably, due to sliding in an inert environment, the COF and specific wear rates decreased in relation to the values achieved in room conditions. The steady-state average COF was ~0.033 and ~0.045 for C3 and C4 coatings, respectively. It is well known that TMDs perform better in dry and vacuum atmospheres [2,39]. C3 coating with a high Se/Mo ratio performed slightly better when compared to C4 coating, which had lower Se/Mo ratio, behavior which can be attributed to the easier formation of the low shear strength tribolayer responsible for the low friction behavior of these types of coatings.

For tests performed at 200 °C, the COF showed minor changes for both C3 and C4 coatings, as compared to ambient air and dry nitrogen tests, although in opposite directions i.e., increasing for the former and decreasing for the latter. With the increase of the temperature, moisture is removed from the atmosphere surrounding the sample but, on the other hand, the probability of oxidation of $MoSe_2$ above 150 °C is enhanced [33]. Therefore, the higher Se/Mo ratio in C3 coating promotes its likelihood for high-temperature oxidation, resulting in higher COF compared to the C4 coating. In terms of specific wear rates, the values were comparable to the ones obtained for the C3 coating during sliding in the ambient air atmosphere.

Minor fluctuations in COF were observed by changing the sliding environments. If the range of error values is considered in all tests, the differences are even less important. This minor difference in values suggests that the mechanism controlling the friction performance
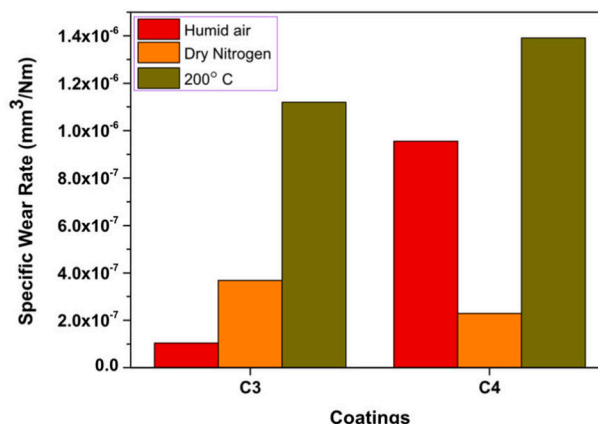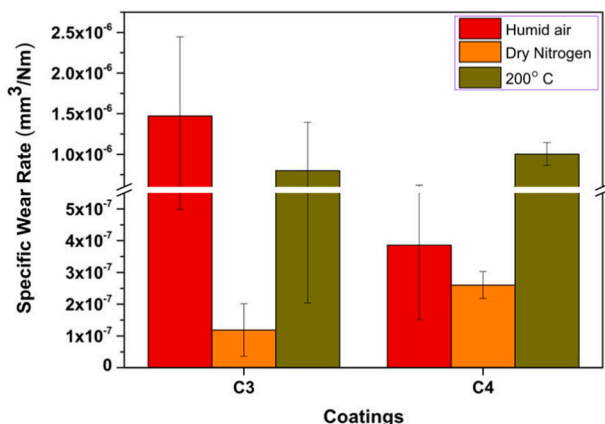

Fig. 11. Reciprocating sliding specific wear rates of C3 and C4 disk/coating (left) and (right) counter bodies in diverse environments.
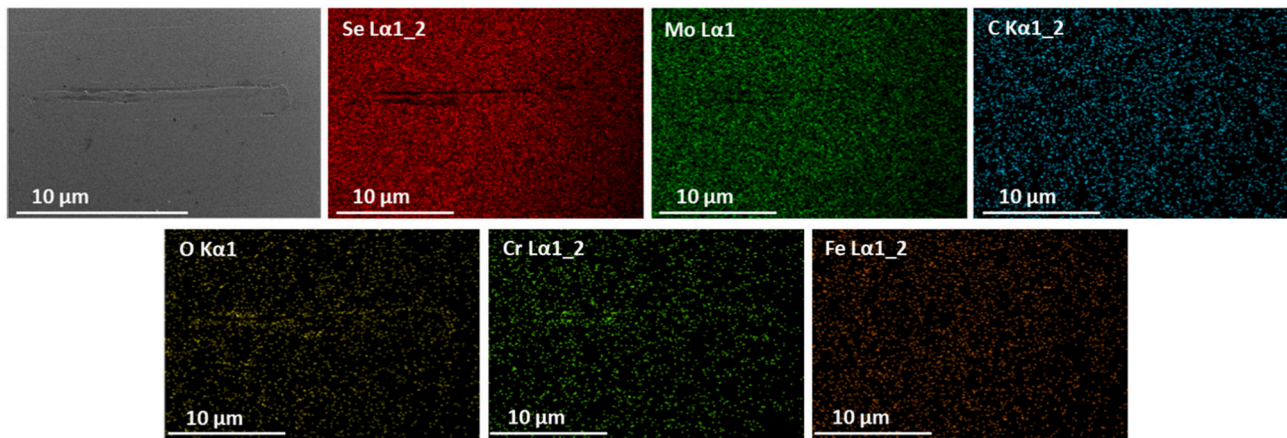
Fig. 12. EDS elemental maps for C3 coating wear track after reciprocating sliding in ambient air.

should be similar, i.e., as found in unidirectional tests: the formation of a lubricious phase based on a stacking of basal planes of $MoSe_2$ is responsible for the friction and wear reduction. C only played a role in the improvement of the mechanical properties, as non-hydrogenated carbon phases are unable to provide friction reduction in inert environments like dry nitrogen [40]. Therefore, considering the similarity in frictional response during the testing in different environments, these coatings do not show a chameleon behavior, i.e. the frictional response is always governed by the $MoSe_2$ phase. So, it is safe to say that all TMD-C coatings do not show chameleon behavior, conflicting with what is frequently reported in the literature. This is very likely due to the lower carbon content, and the good crystallinity of the TMD phase. Thus, the tribological response is dependent on the carbon content and the ratio between the chalcogen atoms and transition metal atoms (Se/Mo ratio). Having a coating with a good crystallinity of the TMD phase (related to the Se/Mo ratio), and relatively higher amount of TMD phase (carbon content of less than 30 at.%) are the most probable conditions that need to be fulfilled for the tribological response to be governed by the TMD phase in all sliding environments.

4. Conclusions

Optimized Mo-Se-C coatings were deposited by the confocal DCMS technique. Low C contents, in the range form ~18 up to ~27 at.% were used. Porous and columnar $MoSe_2$ pure coatings became compact even with the lowest C additions of ~18 at.%. The addition of C disturbed the structural arrangement inducing less crystalline coatings. However, the low C content and Se/Mo values close to the stoichiometry of $MoSe_2$ resulted in a structure with the presence of (002) $MoSe_2$ basal planes, which could play a vital role in the easy shearing properties during sliding. Raman spectroscopy confirmed the structural results from XRD analysis. Unidirectional tribological tests in ambient air showed low COF and specific wear rates, with values as low as ~0.027 and 2×10^{-7} mm^3/Nm, respectively. As a general trend, increasing C increased the running-in period, while, an increase in the number of cycles decreased the COF as coatings entered from running-in to steady-state sliding regime. SEM and Raman showed that a $MoSe_2$ tribolayer forms initially in patches and partially covers the wear track, but with the increase in sliding cycles, it covers the whole wear track. TEM cross-sections also confirmed that the tribolayer solely consists of well-oriented $MoSe_2$ and these observations were further reinforced by EDS analysis of wear tracks. COF and specific wear rates only showed minor fluctuations when the sliding environment was changed, unlike the literature on other TMD coatings. Considering the similarities in the tribological response, it can be said that $MoSe_2$ was playing the dominant role in the wear track to reduce friction and wear in all environments. This allowed us to conclude that Mo-Se-C coatings with a high

Se/Mo ratio (e.g. higher than 1.7) and a relatively low carbon content (less than 30 at.%) do not show chameleon behavior. The coatings display excellent ability to be used as solid-lubricant in diverse environments and for equipment that needs longer durations between inspections, like satellites.

CRediT authorship contribution statement

Talha Bin Yaqub: Conceptualization, Methodology, Writing - original draft, Visualization, Formal analysis, Investigation. **Stéphanie Bruyere:** Formal analysis, Investigation, Resources, Supervision. **Jean-François Pierson:** Formal analysis, Investigation, Resources. **Todor Vuchkov:** Investigation, Data curation, Formal analysis. **Albano Cavaleiro:** Conceptualization, Methodology, Writing - review & editing, Resources, Supervision, Funding acquisition.

Declaration of competing interest

The authors declare that they have no known competing financial interests or personal relationships that could have appeared to influence the work reported in this paper.

References

[1] F. Fernandes, T.B. Yaqub, A. Cavaleiro, Influence of Ag additions on the structure, mechanical properties and oxidation behaviour of Cr−O coatings deposited by HiPIMS, Surf. Coat. Technol. 339 (2018) 167–180, https://doi.org/10.1016/j.surfcoat.2018.02.025.
[2] A.A. Voevodin, J.S. Zabinski, Nanocomposite and nanostructured tribological materials for space applications, Compos. Sci. Technol. 65 (2005) 741–748, https://doi.org/10.1016/j.compscitech.2004.10.008.
[3] T. Bin Yaqub, K. Hebbar Kannur, T. Vuchkov, C. Pupier, C. Héau, A. Cavaleiro, Molybdenum diselenide coatings as universal dry lubricants for terrestrial and aerospace applications, Mater. Lett. 275 (2020) 128035, , https://doi.org/10.1016/j.matlet.2020.128035.
[4] A. AL-Rjoub, A. Cavaleiro, F. Fernandes, Influence of Ag alloying on the morphology, structure, mechanical properties, thermal stability and oxidation resistance of multilayered TiSiN/Ti(Ag)N films, Mater. Des. 192 (2020) 108703, ,

https://doi.org/10.1016/j.matdes.2020.108703.

[5] T.W. Scharf, S.V. Prasad, Solid lubricants: a review, J. Mater. Sci. 48 (2013) 511–531, https://doi.org/10.1007/s10853-012-7038-2.

[6] T. Polcar, A. Cavaleiro, Review on self-lubricant transition metal dichalcogenide nanocomposite coatings alloyed with carbon, Surf. Coat. Technol. 206 (2011) 686–695, https://doi.org/10.1016/j.surfcoat.2011.03.004.

[7] N.M.U. Renevier, J. Hamphire, V.C. Fox, J. Witts, T. Allen, D.G. Teer, Advantages of using self-lubricating, hard, wear-resistant MoS₂-based coatings, Surf. Coat. Technol. (2001) 67–77, https://doi.org/10.1016/S0257-8972(01)01108-2.

[8] J.R. Lince, Tribology of co-sputtered nanocomposite Au/MoS₂ solid lubricant films over a wide contact stress range, Tribol. Lett. 17 (2004) 419–428, https://doi.org/10.1023/B:TRIL.0000044490.03462.6e.

[9] M. Ye, G. Zhang, Y. Ba, T. Wang, X. Wang, Z. Liu, Microstructure and tribological properties of MoS₂ + Zr composite coatings in high humidity environment, Appl. Surf. Sci. 367 (2016) 140–146, https://doi.org/10.1016/j.apsusc.2016.01.163.

[10] B. Deepthi, H.C. Barshilia, K.S. Rajam, M.S. Konchady, D.M. Pai, J. Sankar, A.V. Kvit, Structure, morphology and chemical composition of sputter deposited nanostructured Cr-WS₂ solid lubricant coatings, Surf. Coat. Technol. 205 (2010) 565–574, https://doi.org/10.1016/j.surfcoat.2010.07.050.

[11] D.G. Teer, J. Hampshire, V. Fox, V. Bellido-Gonzalez, The tribological properties of MoS₂/metal composite coatings deposited by closed field magnetron sputtering, Surf. Coat. Technol. 94–95 (1997) 572–577, https://doi.org/10.1016/S0257-8972(97)00498-2.

[12] T. Hudec, M. Mikula, L. Satrapinskyy, T. Roch, M. Truchlý, P. Švec Jr., T. Huminiuc, T. Polcar, Structure, mechanical and tribological properties of Mo−S−N solid lubricant coatings, Appl. Surf. Sci. 486 (2019) 1–14, https://doi.org/10.1016/j.apsusc.2019.03.294.

[13] K.H. Kannur, T. Bin Yaqub, T. Huminiuc, T. Polcar, C. Pupier, C. Héau, A. Cavaleiro, Synthesis and structural properties of Mo−S−N sputtered coatings, Appl. Surf. Sci. 527 (2020) 146790, , https://doi.org/10.1016/j.apsusc.2020.146790.

[14] T. Vuchkov, M. Evaristo, T. Bin Yaqub, T. Polcar, A. Cavaleiro, Synthesis, microstructure and mechanical properties of W−S−C self-lubricant thin films deposited by magnetron sputtering, Tribol. Int. 150 (2020) 106363, , https://doi.org/10.1016/j.triboint.2020.106363.

[15] T. Vuchkov, T. Bin Yaqub, M. Evaristo, A. Cavaleiro, Synthesis, microstructural, and mechano-tribological properties of self-lubricating W−S−C(H) thin films deposited by different RF magnetron sputtering procedures, Coatings 10 (2020), https://doi.org/10.3390/coatings10030272.

[16] H. Cao, J.T.M. De Hosson, Y. Pei, Effect of carbon concentration and argon flow rate on the microstructure and triboperformance of magnetron sputtered WS₂/a-C coatings, Surf. Coat. Technol. 332 (2017) 142–152, https://doi.org/10.1016/j.surfcoat.2017.06.087.

[17] A.A. Voevodin, J.P. O'Neill, J.S. Zabinski, Nanocomposite tribological coatings for aerospace applications, Surf. Coat. Technol. 116–119 (1999) 36–45, https://doi.org/10.1016/S0257-8972(99)00228-5.

[18] J. Zekonyte, T. Polcar, Friction Force Microscopy Analysis of Self-adaptive W−S−C Coatings: Nanoscale Friction and Wear, (2015), pp. 1–11, https://doi.org/10.1021/acsami.5b05546.

[19] H. Cao, F. Wen, S. Kumar, P. Rudolf, J.T.M. De Hosson, Y. Pei, On the S/W stoichiometry and triboperformance of WS × C(H) coatings deposited by magnetron sputtering, Surf. Coat. Technol. (2018), https://doi.org/10.1016/j.surfcoat.2018.04.040.

[20] T. Bin Yaqub, T. Vuchkov, M. Evaristo, A. Cavaleiro, DCMS Mo-Se-C solid lubricant coatings — synthesis, structural, mechanical and tribological property investigation, Surf. Coat. Technol. (2019), https://doi.org/10.1016/j.surfcoat.2019.124992.

[21] J.V. Pimentel, T. Polcar, M. Evaristo, A. Cavaleiro, Examination of the tribolayer formation of a self-lubricant WSC sputtered coating, Tribol. Int. 47 (2012) 188–193, https://doi.org/10.1016/j.triboint.2011.10.021.

[22] T. Polcar, A. Cavaleiro, Self-adaptive low friction coatings based on transition metal dichalcogenides, Thin Solid Films 519 (2011) 4037–4044, https://doi.org/10.1016/j.tsf.2011.01.180.

[23] T. Kubart, T. Polcar, L. Kopecký, R. Novák, D. Nováková, Temperature dependence of tribological properties of MoS₂ and MoSe₂ coatings, Surf. Coat. Technol. 193 (2005) 230–233, https://doi.org/10.1016/j.surfcoat.2004.08.146.

[24] M. Evaristo, T. Polcar, A. Cavaleiro, Synthesis and properties of W−Se−C coatings deposited by PVD in reactive and non-reactive processes, Vacuum 83 (2009) 1262–1265, https://doi.org/10.1016/j.vacuum.2009.03.030.

[25] T. Bin Yaqub, T. Vuchkov, P. Sanguino, T. Polcar, A. Cavaleiro, Comparative study of DC and RF sputtered MoSe₂ coatings containing carbon—an approach to optimize stoichiometry, microstructure, crystallinity and hardness, Coatings 10 (2020) 133.

[26] M. Evaristo, T. Polcar, A. Cavaleiro, Tribological behaviour of C-alloyed transition metal dichalcogenides (TMD) coatings in different environments, Int. J. Mech. Mater. Des. 4 (2008) 137–143, https://doi.org/10.1007/s10999-007-9034-2.

[27] J. Noshiro, S. Watanabe, T. Sakurai, S. Miyake, Friction properties of co-sputtered sulfide/DLC solid lubricating films, Surf. Coat. Technol. 200 (2006) 5849–5854, https://doi.org/10.1016/j.surfcoat.2005.08.147.

[28] T. Polcar, M. Evaristo, A. Cavaleiro, The tribological behavior of W−S−C films in pin-on-disk testing at elevated temperature, Vacuum 81 (2007) 1439–1442, https://doi.org/10.1016/J.VACUUM.2007.04.010.

[29] H. Nyberg, J. Sundberg, E. Särhammar, F. Gustavsson, T. Kubart, T. Nyberg, U. Jansson, S. Jacobson, Extreme friction reductions during initial running-in of W−S−C−Ti low-friction coatings, Wear 302 (2013) 987–997, https://doi.org/10.1016/j.wear.2013.01.065.

[30] L. Gu, P. Ke, Y. Zou, X. Li, A. Wang, Amorphous self-lubricant MoS₂−C sputtered coating with high hardness, Appl. Surf. Sci. 331 (2015) 66–71, https://doi.org/10.1016/j.apsusc.2015.01.057.

[31] Y. Wu, H. Li, L. Ji, L. Liu, Y. Ye, J. Chen, H. Zhou, Structure, mechanical, and tribological properties of MoS₂/a-C:H composite films, Tribol. Lett. 52 (2013) 371–380, https://doi.org/10.1007/s11249-013-0216-9.

[32] T. Polcar, M. Evaristo, A. Cavaleiro, Comparative study of the tribological behavior of self-lubricating W−S−C and Mo-Se-C sputtered coatings, Wear 266 (2009) 388–392, https://doi.org/10.1016/j.wear.2008.04.011.

[33] T. Polcar, M. Evaristo, M. Stueber, A. Cavaleiro, Mechanical and tribological properties of sputtered Mo-Se-C coatings, Wear 266 (2009) 393–397, https://doi.org/10.1016/j.wear.2008.04.010.

[34] K.D. Rasamani, F. Alimohammadi, Y. Sun, Interlayer-expanded MoS₂, Mater. Today 20 (2017), https://doi.org/10.1016/j.mattod.2016.10.004.

[35] F. Gustavsson, S. Jacobson, A. Cavaleiro, T. Polcar, Frictional behavior of self-adaptive nanostructural Mo-Se-C coatings in different sliding conditions, Wear 303 (2013) 286–296, https://doi.org/10.1016/j.wear.2013.03.032.

[36] T. Sekine, M. Izumi, T. Nakashizu, K. Uchinokura, E. Matsuura, Raman scattering and infrared reflectance in 2H−MoSe₂, J. Phys. Soc. Jpn. 49 (1980) 1069–1077, https://doi.org/10.1143/JPSJ.49.1069.

[37] T. Polcar, A. Nossa, M. Evaristo, A. Cavaleiro, Nanocomposite coatings of carbon-based and transition metal dichalcogenides phases: a review, Rev. Adv. Mater. Sci. 15 (2007) 118–126.

[38] M. Kano, Y. Yasuda, Y. Mabuchi, J. Ye, S. Konishi, Ultra-low friction properties of DLC lubricated with ester-containing oil — part 1: pin-on-disc & SRV friction tests, Tribol. Ser. 43 (2003) 689–692, https://doi.org/10.1016/s0167-8922(03)80096-2.

[39] S. Prasad, J. Zabinski, Super slippery solids, Nature 387 (1997) 761, https://doi.org/10.1038/42820.

[40] J. Andersson, R.A. Erck, A. Erdemir, Friction of diamond-like carbon films in different atmospheres, Wear 254 (2003) 1070–1075, https://doi.org/10.1016/S0043-1648(03)00336-3.

Annex D

T. Bin Yaqub, K. Hebbar Kannur, T. Vuchkov, C. Pupier, C. Héau, A. Cavaleiro,
*Molybdenum diselenide coatings as universal dry lubricants for terrestrial and aerospace applications***, Mater. Lett. 275 (2020) 128035. doi:10.1016/j.matlet.2020.128**

Molybdenum diselenide coatings as universal dry lubricants for terrestrial and aerospace applications

Talha Bin Yaqub [a,b,*], Kaushik Hebbar Kannur [b,c], Todor Vuchkov [a,b], Christophe Pupier [c], Christophe Héau [c], Albano Cavaleiro [a,b]

[a] IPN - LED & MAT - Instituto Pedro Nunes, Laboratory of Tests, Wear and Materials, Rua Pedro Nunes, 3030-199 Coimbra, Portugal
[b] SEG-CEMMPRE, Department of Mechanical Engineering, University of Coimbra, Rua Luís Reis Santos, 3030-788 Coimbra, Portugal
[c] IREIS-HEF Group, Avenue Benoit Fourneyron, CS 42077-42162 Andrezieux-Boutheon, France

ABSTRACT

The hindrance behind large-scale application of carbon-alloyed transition metal dichalcogenide (TMD-C) coatings is the substantial variation of frictional response in ambient and dry atmosphere sliding. This study introduces less explored Mo-Se-C coatings as universal solid lubricants. Direct current (DC) and radio frequency (RF) sputtered coatings were tribologically tested, for the first time, under various contact pressure (CP) regimes, vacuum and ambient air (humidity: 35–45%) conditions, short and long sliding cycles and sliding speeds to simulate industrial requirements. No significant variations between performance was observed by changing the sliding conditions. In all conditions, nearly consistent friction coefficient range (0.02–0.06), and long-term endurance shows that these coatings can be an ideal candidate for low friction in the aerospace environment. Moreover, this system can also have an immense potential for other advanced applications.

© 2020 Elsevier B.V. All rights reserved.

1. Introduction

The aerospace industry governs transportation, networking, and space exploration domains, and depends largely on the efficiency of the working and lifetime of aircraft, satellites and space shuttles, etc. Friction and wear of sliding components are major sources of their performance degradation [1]. As the space machinery has to work in both terrestrial and non-terrestrial environments, liquid lubrication can have some limitations due to its contamination issues. On the other hand, problems like cold start, liquid replacements and environmental issues are also increasing demands for an alternative i.e., *solid lubricants* [2]. Various material combinations have been tried in the past few decades to develop solid lubricant coatings, which can operate in both ambient and vacuum atmosphere without degradation. Smart self-adaptive coatings are a very popular subset of solid lubricants having the ability to fulfil the requirements of the space industry. In this field, TMDs got quite high attention. Whether pure or combined with other elements or compounds, all the coatings displayed very low friction coefficient (COF) in vacuum/dry atmospheres (COF less than 0.03), but, as soon as the sliding environment changed to ambient air, the

COF increased very significantly to 0.1–0.15 or even more [2–4]. These large performance discrepancies are the major hindrance to their application in the aerospace industry, especially for satellites that endure coastal climate before being launched. Thus, an alternative system is required. Unfortunately, to date, none of the systems is stable enough to provide similar, or, nearly similar COF in both sliding environments. Therefore, the development of a coating system that can show similar performance in both atmospheres would be a notable achievement.

This work reports some novel and remarkable results for Mo-Se-C coatings as univeral solid lubricants for terrestrial and aerospace environments. The key features tested/reported in this study are:

1. Testing in vacuum atmospheres at low CP, and ambient air at both low and high CP – to date, no study can be found on the performance of Mo-Se-C coatings in vacuum and also at low CP in any environment.
2. The vacuum, CP and sliding speed were selected to replicate actual industrial conditions in diverse environments [5–7].
3. Finally, for the first time, COF comparison for MoSe$_2$ in combination with C, sputtered with DC magnetron sputtering vs. RF magnetron sputtering has been reported, for both environments.

* Corresponding author.
  E-mail address: talha.yaqub@ipn.pt (T.B. Yaqub).

2. Experimental Procedure:

Pure $MoSe_2$ coatings were deposited in an AJA International deposition unit using DC and RF magnetron sputtering while carbon was added by DC magnetron sputtering. More details concerning the deposition procedure and the substrates used can be found in the supplementary material and ref [8]. Only coatings deposited without substrate bias in ref [8] were studied here. The ambient air and vacuum tribological testing at low CP of ~ 85 MPa (typical value in journal bearings) was carried out in a linear reciprocating tribometer with 100Cr6 steel cylinder (10 mm × Ø10 mm) on flat arrangement. 5 mm stroke length and 2 mm/s sliding speed was selected as the parts move much slower in space [5]. A high vacuum condition (10^{-6} mbar) was used for the vacuum tests. Although, the initial CP mostly reported in the literature is above 600 MPa (claiming coatings are good for aerospace applications), in actual industrial applications the pressure can vary from those high values down to less than 100 MPa [6,7]. Thus, to further simulate earth environment tests and for parts that operate at high CP (e.g. ball bearings), unidirectional rotative ball-on-disk sliding tests in ambient air were carried out under 1010 MPa CP and 0.1 m/s sliding speed, against 100Cr6 steel ball (Ø10 mm). Low CP tests were carried out up to 10,000 cycles while 25,000 and 100,000 cycles were selected for high CP tests. In the latter case, the idea was to examine the coating stability for longer sliding durations. In all tests, the coatings were sliding under the steady-state regime. At least two repetitions were done for all tests.

3. Results and Discussion:

Pure $MoSe_2$ coatings were highly porous, irrespective of DC or RF power supplies. With the addition of C, coatings became compact in both cases with a minor decrease in Se/Mo composition. X-ray diffraction (XRD), transmission electron microscopy (TEM) and Raman spectroscopy showed that the coatings were polycrystalline with $MoSe_2$ embedded in amorphous carbon. The hardness increased with C, showing a maximum of 4.6 GPa for DC676 coating. The coatings names are related to their C content as: DC324-18% C, DC676-25% C, RF170-18% C and RF340-25% C. For further details about the properties of these coatings, see supplementary data and ref [8]. The results of all tribological tests performed in this work are shown in table 1.

The ranges of the resulting mean values have been reported based on the repeatability of the tests and for better comparison among all tribological testing conditions. The main tribological results are described as follows:

3.1. Low contact pressure Tests:

COF evolution of coatings after low CP tests are shown in Fig. 1. When analyzed in a global way, the friction curves have similar terms and values for all coatings, independently of the deposition technique and the environmental conditions. In the case of testing in ambient air, some coatings show a longer running-in period, which can be related to the time for the formation of the tribolayer [3]. However, the final values of all the low CP tests in all environments are remarkably very similar i.e., in the range of 0.02–0.06 for both ambient air and vacuum conditions. Significant deviation was observed for pure RF in vacuum to ambient air sliding. In ambient air, this coating shows a COF value higher than 0.06, which should be related to the partial delamination observed (see Fig. 2). The analysis of table 1 also allows to draw very similar conclusions about the wear rates. All coatings show approximately the same wear rate independently of the power supply used for the deposition as well as the testing environment (in the range [2–4 x10^{-6} mm^3/ Nm]) being the only exception, again, the pure RF coating in ambient air, due to the observed delamination. Therefore, globally it is possible to conclude that, differently from what can be found in literature for other TMD-based coatings, the friction and wear behaviour of Mo-Se-C coatings reported here are much less influenced by the deposition technique, C content and testing environment.

3.2. High contact pressure tests

COF evolution curves of coatings after high CP tests are shown in Fig. 3. Despite the different conditions in both tribological tests (low vs. high CP), the trends are very similar. Friction values in all cases are very close, in the range [0.01 – 0.04]. These values are remarkably low in comparison with the literature for pin-on-disk tests of TMD-based coatings tested in ambient air conditions [2–4]. Very often, values as high as 0.1–0.15 are referred [2,4,9]. As it would be expected, the friction curves for 25,000 and 100,000 cycles are almost similar, since the material and testing conditions are the same. This result clearly shows that the steady-state for 25,000 cycles test is kept constant for much higher duration tests. Similar results occur for the wear rates.

All coatings show values in the range [2–6 x10^{-7} mm^3/Nm], except DC676 and pure $MoSe_2$ deposited films. The DC pure coating completely failed with its total destruction during testing, whereas partial delamination is observed in RF sputtered film which gives rise to the higher measured values of its wear rate. The lower COF and specific wear rates in high-pressure tests can be attributed to the non-Amonton response of TMDs (as the applied load in these tests was higher) and the difference in sliding mechanisms between unidirectional and reciprocating tests [3,10]. However, globally, the values are very close to each other and within the same range of COF achieved for low CP in diverse environments.

Considering the reported CP used in industrial journal and ball bearings [6,7], our study shows COF and wear rate as optimum for such applications, irrespective of the sliding environment. Moreover, it is known that atomic oxygen adversely affects the

Table 1
Tribological results of the coatings under different testing conditions.

Coatings	Low contact pressure (Applied load 5 N, Hertzian contact stress 85 MPa)				High contact pressure (Applied load 10 N, Hertzian contact stress 1010 MPa)			
	Ambient air		Vacuum		Ambient air			
	COF	Specific wear rate mm^3/Nm	COF	Specific wear rate mm^3/Nm	COF (25000 cycles)	Specific wear rate mm^3/Nm	COF (100000 cycles)	Specific wear rate mm^3/Nm
DC $MoSe_2$	0.03–0.05	2–3 E-6	0.02–0.04	2–3 E-6	Failed-T.D.	NA	Failed-T.D.	NA
DC324	0.04–0.05	2–4 E-6	0.03–0.04	2–4 E-6	0.01–0.02	3–5 E-7	0.01–0.03	2–4 E-7
DC676	0.04–0.06	3–5 E-6	0.04–0.06	2–3 E-6	0.03–0.04	1–2 E-6	0.02–0.04	1–2 E-6
RF $MoSe_2$	0.06–0.07	1–2 E-5 (P.D.)	0.02–0.03	1–3 E-6	0.02–0.04	1–3 E-6 (P.D.)	0.02–0.03	7–10 E-7 (P.D.)
RF170	0.05–0.07	2–4 E-6	0.04–0.06	1–4 E-6	0.03–0.04	4–6 E-7	0.03–0.04	3–6 E-7
RF340	0.05–0.06	4–6 E-6	0.04–0.06	2–4 E-6	0.02–0.03	2–5 E-7	0.02–0.04	1–4 E-7

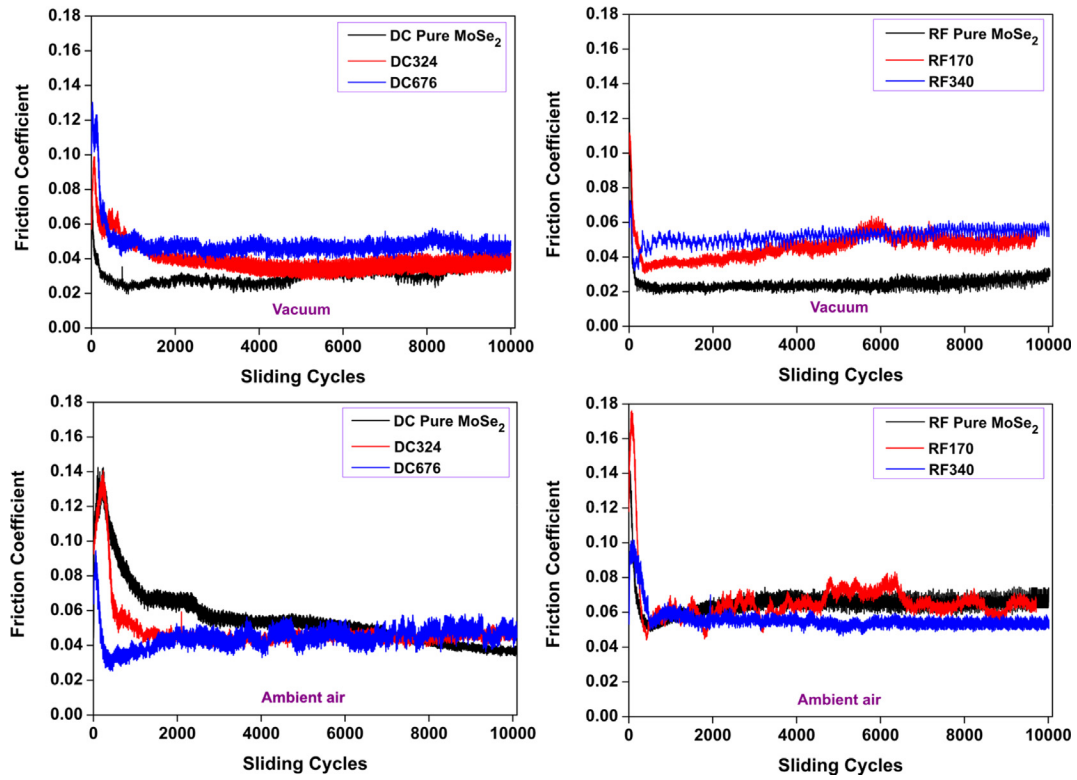**P.D. - Partial delamination, T.D. - Total delamination

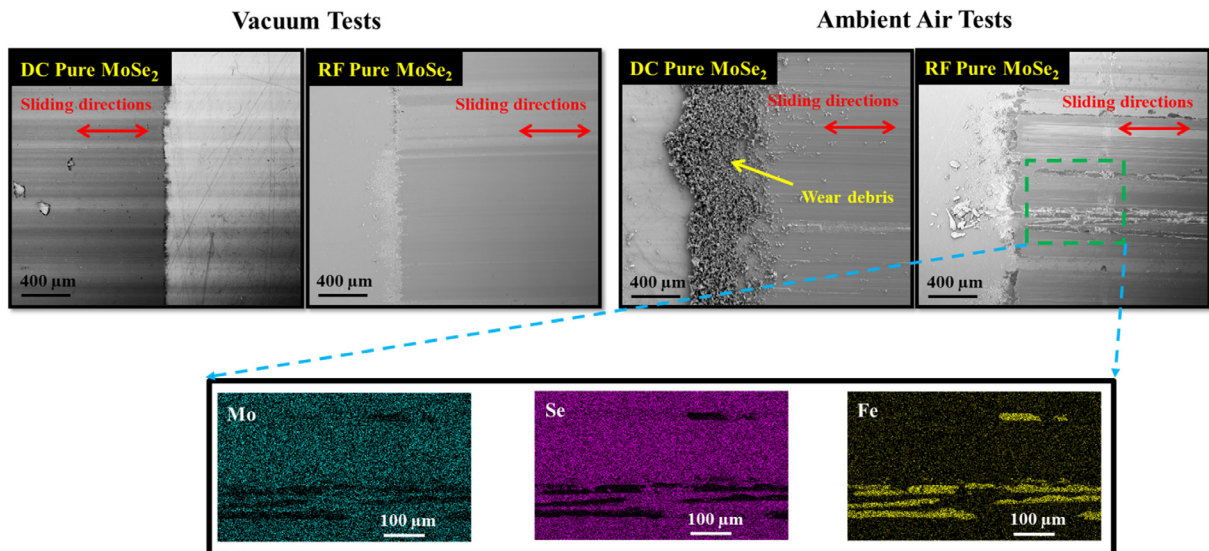**Fig. 1.** Friction curves after vacuum and ambient air tests at low contact pressure.

Fig. 2. Wear track morphologies of pure MoSe$_2$ coatings of Low contact pressure tests.

properties of MoS$_2$ coatings in space machinery due to the re-sputtering of S and the resulting MoO$_3$ formation [6]. This problem can be overcome using MoSe$_2$ due to a lower re-sputtering of Se, as compared to S [8], avoiding, then, the oxidation and degradation processes. Finally, the deposition by DC sputtering was shown to be similar to RF, the technique that has been used for the deposition of Mo-Se-C system. This is more industrially favorable and the results perfectly align with this demand.

4. Conclusions:

Pure and carbon-alloyed MoSe$_2$ coatings were deposited by both DC and RF sputtering. The coatings were tribologically tested in vacuum and ambient atmospheres under 85 MPa and 1010 MPa CP and sliding speeds for mimicking terrestrial and space applications. When shifting from low contact to extreme loading conditions, vacuum to ambient air atmospheres or DC
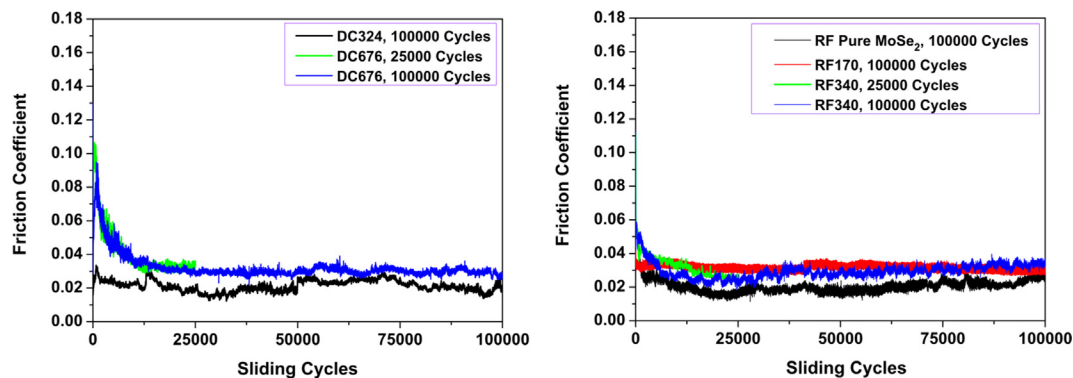
Fig. 3. Friction curves after 100,000 cycles in ambient air at high contact pressure. 25,000 cycles curves of only maximum C coatings are shown for reference.

to RF power sources, consistent low COF and wear rates were achieved, a breakthrough that has not been reported earlier for any solid lubricant system. Hence, Mo-Se-C coatings are of high importance for applications that demand solid lubricants for working independently of the surrounding environment and loading conditions. This research can guide towards resolving sustainable solid lubrication issues for aerospace and terrestrial machine components.

CRediT authorship contribution statement

Talha Bin Yaqub: Conceptualization, Methodology, Writing - original draft, Visualization, Formal analysis, Investigation. **Kaushik Hebbar Kannur:** Conceptualization, Methodology, Formal analysis, Investigation. **Todor Vuchkov:** Formal analysis, Investigation. **Christophe Pupier:** Resources. **Christophe Héau:** Resources. **Albano Cavaleiro:** Writing - review & editing, Resources, Supervision, Funding acquisition.

Declaration of Competing Interest

The authors declare that they have no known competing financial interests or personal relationships that could have appeared to influence the work reported in this paper.

Appendix A. Supplementary data

Supplementary data to this article can be found online at https://doi.org/10.1016/j.matlet.2020.128035.

References

[1] T.W. Scharf, S.V. Prasad, J. Mater. Sci. 48 (2013) 511–531.
[2] C. Donnet, A. Erdemir, Surf. Coat. Technol. 181 (2004) 76–84.
[3] T. Polcar, A. Cavaleiro, Surf. Coat. Technol. 206 (2011) 686–695.
[4] A.A. Voevodin, J.P.O. Neill, J.S. Zabinski, Tribol. Lett. 6 (1999) 75–78.
[5] M.J. Todd, Tribol. Lubr. Wear. Fifty Years On. 2 (1987) 933–944.
[6] E.W. Roberts, Tribol. Int. 23 (2) (1990) 95–104.
[7] N. Hiraoka, Wear. 249 (2001) 1014–1020.
[8] T. Bin Yaqub, T. Vuchkov, P. Sanguino, T. Polcar, A. Cavaleiro, Coatings. 10 (2020) 133.
[9] H. Cao, F. Wen, S. Kumar, P. Rudolf, J.T.M. De Hosson, Y. Pei, Surf. Coatings Technol. (2018).
[10] M. Kano, Y. Yasuda, Y. Mabuchi, J. Ye, S. Konishi, Tribol. Ser. 43 (2003) 689–692.